VOLUME 111 NUMBER 1

THE ASTROPHYSICAL JOURNAL

AN INTERNATIONAL REVIEW OF SPECTROSCOPY AND ASTRONOMICAL PHYSICS

JANUARY 1950

NEUTRAL OXYGEN IN STELLAR ATMOSPHERES . . . *P. C. Keenan and J. A. Hynek* 1
THE SPECTRUM OF THE NEBULOSITY SURROUNDING T TAURI . . . *George H. Herbig* 11
SPECTRA OF VARIABLE STARS IN THE ORION NEBULA . . . . . *George H. Herbig* 15
THE VARIABILITY OF THE SPECTRUM OF UPSILON SAGITTARII . . . *Jesse L. Greenstein* 20
THE VELOCITY-CURVE OF R CANIS MAJORIS . . . . . *O. Struve and Burke Smith* 27
Ca II EMISSION IN LAMBDA AND ZETA ANDROMEDAE . . . . . *Linio Gratton* 31
THE SPECTRUM OF COMET 1948I . . . . . *P. D. Jose and P. Swings* 41
THE BAND SPECTRUM OF CO^+. I. FIRST NEGATIVE SYSTEM ($B^2\Sigma - X^2\Sigma$) . . . . . *K. Narahari Rao* 50
THE DERIVATION OF VACUUM WAVE NUMBERS AND THE REDUCTION OF MEASURED WAVE LENGTHS TO STANDARD ATMOSPHERIC CONDITIONS . . . . . *Harold D. Babcock* 60
PHOTOELECTRIC STUDIES. I. COLOR-LUMINOSITY ARRAY FOR MEMBERS OF THE HYADES CLUSTER . . . . . *Olin J. Eggen* 65
PHOTOELECTRIC STUDIES. II. COLOR-LUMINOSITY ARRAY FOR MEMBERS OF THE PLEIADES CLUSTER . . . . . *Olin J. Eggen* 81
THE ILLUMINATION FROM THE SOLAR CRESCENT NEAR TOTALITY OF THE ECLIPSE OF MAY 20, 1947 . . . . . *R. A. Richardson and E. O. Hulburt* 99
A PHOTOGRAPHIC STUDY OF THE DRACONID METEOR SHOWER OF 1946 . . . . . *Luigi G. Jacchia, Zdeněk Kopal, and Peter M. Millman* 104
THE POYNTING-ROBERTSON EFFECT ON METEOR ORBITS . . . . . *Stanley P. Wyatt, Jr., and Fred L. Whipple* 134
ON THE INTEGRAL EQUATION GOVERNING THE DISTRIBUTION OF THE TRUE AND THE APPARENT ROTATIONAL VELOCITIES OF STARS . . . . . *S. Chandrasekhar and G. Münch* 142
EXACT CURVES OF GROWTH FOR THE FORMATION OF ABSORPTION LINES ACCORDING TO THE MILNE-EDDINGTON MODEL. II. CENTER OF THE DISK . . . . . *Marshal H. Wrubel* 157
THE THERMODYNAMIC STRUCTURE OF THE OUTER SOLAR ATMOSPHERE. I. THE GENERAL METHOD OF ANALYSIS AND PRELIMINARY RESULTS . . . . . *Richard N. Thomas* 165
PROTON-PROTON REACTIONS IN RED DWARF STARS . . . . . *Lawrence H. Aller* 173
FURTHER STUDIES ON THE ORIGIN OF THE SOLAR SYSTEM . . . . . *D. ter Haar* 179
NOTES
THE SPECTROSCOPIC BINARY CPD−61°669 . . . . . *J. Sahade and J. Landi Dessy* 191
SPECTROGRAPHIC OBSERVATIONS OF THE ECLIPSING VARIABLE UX MONOCEROTIS AT BOSQUE ALEGRE . . . . . *Jorge Sahade* 194
THE RADIAL VELOCITIES OF CPD−63°896 . . . . . *Jorge Sahade and Jorge Landi Dessy* 196
THE SPECTRUM OF NOVA SCUTI 1949 . . . . . *Attilio Colacevich* 197
NOTE ON THE SPECTRAL CLASSIFICATION OF CARBON STARS IN THE INFRARED . . . . . *J. J. Nassau and A. Colacevich* 199
THE SPECTRUM OF THE LIGHT OF THE NIGHT SKY DURING THE RECENT SUNSPOT MAXIMUM . . . . . *M. K. Vainu Bappu* 201
A HIGH-TEMPERATURE MODEL ATMOSPHERE . . . . . *Anne B. Underhill* 203
HYDRIDE EMISSION BANDS IN THE SPECTRUM OF THE NIGHT SKY . . . . . *A. B. Meinel* 207

THE UNIVERSITY OF CHICAGO PRESS
CHICAGO, ILLINOIS, U.S.A.

January 1950 Vol. 111, No. 1

THE ASTROPHYSICAL JOURNAL

AN INTERNATIONAL REVIEW OF SPECTROSCOPY AND ASTRONOMICAL PHYSICS

Edited by

W. W. MORGAN
Managing Editor
Yerkes Observatory of the University of Chicago

S. CHANDRASEKHAR

PAUL W. MERRILL
Mount Wilson Observatory of the Carnegie Institution of Washington

HARLOW SHAPLEY
Harvard College Observatory
Cambridge, Massachusetts

N. U. MAYALL
Lick Observatory
University of California

With the Collaboration of the American Astronomical Society

Collaborating Editors:

1949-50	1949-51	1950-51
CECILIA H. PAYNE-GAPOSCHKIN Harvard College Observatory	W. BAADE Mount Wilson Observatory	LYMAN SPITZER, JR. Princeton University Observatory
H. N. RUSSELL Princeton University	LEO GOLDBERG Observatory of the University of Michigan	A. N. VYSSOTSKY Leander McCormick Observatory
ANDREW McKELLAR Dominion Astrophysical Observatory, Victoria	G. HERZBERG National Research Council, Ottawa	ALBERT E. WHITFORD Washburn Observatory

The Astrophysical Journal is published bimonthly by the University of Chicago at the University of Chicago Press, 5750 Ellis Avenue, Chicago, Illinois, during July, September, November, January, March, and May. ¶The subscription price is $12.00 a year; the price of single copies is $3.00. Orders for service of less than a full year will be charged at the single-copy rate. ¶Postage is prepaid by the publishers on all orders from the United States and its possessions. No extra charge for countries in the Pan American Postal Union. ¶Postage is charged extra as follows: for Canada and Newfoundland, 42 cents on annual subscriptions (total $12.42); on single copies, 7 cents (total $3.07); for all other countries in the Postal Union, 96 cents on annual subscriptions (total $12.96), on single copies 16 cents (total $3.16). ¶Patrons are requested to make all remittances payable to The University of Chicago Press, in United States currency or its equivalent by postal or express money orders or bank drafts.

The following is an authorized agent:

For the British Empire, except North America and Australasia: The Cambridge University Press, Bentley House, 200 Euston Road, London, N.W. 1, England. Prices of yearly subscriptions and of single copies may be had on application.

Claims for missing numbers should be made within the month following the regular month of publication. The publishers expect to supply missing numbers free only when losses have been sustained in transit, and when the reserve stock will permit.

Business correspondence should be addressed to The University of Chicago Press, Chicago 37, Illinois.

Communications for the editors and manuscripts should be addressed to: W. W. Morgan, Editor of THE ASTROPHYSICAL JOURNAL, Yerkes Observatory, Williams Bay, Wisconsin.

Line drawings and photographs should be made by the author, and all marginal notes such as co-ordinates, wave lengths, etc., should be included in the cuts. It will not be possible to set up such material in type.

One copy of the corrected galley proof should be returned as soon as possible to the editor, Yerkes Observatory, Williams Bay, Wisconsin. Authors should take notice that the manuscript will not be sent to them with the proof.

The cable address is "Observatory, Williamsbay, Wisconsin."

The articles in this journal are indexed in the *International Index to Periodicals*, New York, N.Y.

Applications for permission to quote from this journal should be addressed to The University of Chicago Press, and will be freely granted.

Notice to subscribers: If you change your address, please notify us and your local postmaster immediately. The post office does not forward second-class mail.

Entered as second-class matter, July 31, 1940, at the Post-Office at Chicago, Ill., under the Act of March 3, 1879.
Acceptance for mailing at special rate of postage provided for in United States Postal Act of October 3, 1917, Section 1103, amended February 28, 1925.

[PRINTED IN U.S.A.]

THE ASTROPHYSICAL JOURNAL

AN INTERNATIONAL REVIEW OF SPECTROSCOPY AND ASTRONOMICAL PHYSICS

VOLUME 111 JANUARY 1950 NUMBER 1

NEUTRAL OXYGEN IN STELLAR ATMOSPHERES

P. C. KEENAN AND J. A. HYNEK

Perkins Observatory

Received September 21, 1949

ABSTRACT

Total absorptions of the lines of *O* I at λ 7774 and λ 8446 have been determined from grating spectrograms of fifty-six stars of early type.

The intensities of the oxygen lines increase rapidly through the later subdivisions of type B to a rather flat maximum in type A. They decline more slowly through type F and disappear in type G. The line λ 7774, especially, is very sensitive to absolute magnitude and, from B5 to G2, forms one of the most striking of the luminosity criteria for the separation of supergiants from other stars.

The abundance of oxygen relative to hydrogen has been found for five stars: α CMa, α CMi, α Per, γ Cyg, and δ CMa. The mean ratio is about one oxygen atom to every thousand hydrogen atoms in these atmospheres.

The tendency of the triplet lines, λ 8446, to go into emission more readily than do the quintet lines, λ 7774, has been explained by Bowen as due to the coincidence of the *O* I triplet 1025.77 with Lyman-β. Thus any departure from the normal absorption ratio of about 0.6 for 8446/7774 is an indicator of ultraviolet emission in Lyman-β.

I. OBSERVED EQUIVALENT WIDTHS

The study of oxygen in stellar atmospheres has been limited to spectra of stars of the first few subdivisions of type B,[1, 2] in which lines of ionized oxygen are present, and to the solar spectrum, in which forbidden faint neutral lines in the visible region and permitted neutral lines in the near infrared have been observed.[3, 4, 5]

Only relatively recently has it become possible, by the use of faster photographic emulsions for the infrared, to utilize the *O* I lines at λ 7774 and λ 8446 for an investigation of the behavior and abundance of oxygen in stars ranging in spectrum from the later subdivisions of type B to type G. These are the only lines of neutral oxygen which attain any considerable strength in the observable regions of stellar spectra.

The configuration of energy levels from which these lines arise is shown in Figure 1. The transition $3^5S^o - 3^5P$ gives rise, in all, to three lines at λλ 7771.90, 7774.18, and 7775.40, which on spectrograms of moderate dispersion are barely resolvable. Similarly, the transition $3^3S^o - 3^3P$ produces three lines (two of which are coincident) at λ 8446.35

[1] A. Unsöld, *Zs. f. Ap.*, **21**, 22, 1941 (τ Sco).

[2] L. H. Aller, *Ap. J.*, **104**, 347, 1946 (10 Lac).

[3] C. W. Allen, *M.N.*, **96**, 843, 1936.

[4] M. Minnaert, *Utrecht Photometric Atlas of the Solar Spectrum* (1940).

[5] I. S. Bowen, *Rev. Mod. Phys.*, **20**, 109, 1948.

and λ 8446.76. On our spectrograms these appear essentially as one line. The lines at λ 7774 and at λ 8446 appear in a very clear portion of the spectrum, and, except perhaps in the late F and G spectral types, no blending of any consequence interferes with their measurement.

As early as 1934, Merrill,[6] in his pioneer photographic infrared survey of stellar spectra, outlined the general behavior of these lines. In several respects they are similar to the lines of hydrogen, having excitation potentials only about 1 volt below that of the Balmer series. The lines at λ 8446 lie between P17 and P18 of the Paschen series, thus affording good opportunity for quantitative comparison. There are, however, significant differences in behavior between the lines of these two elements in stellar spectra. To define these more precisely was one of the aims of our investigation.

Spectrograms of fifty-four stars were taken on Eastman I-N plates, covering the range 7300–8700 A. The instrument was the grating spectrograph on the 69-inch reflector, giving a scale of about 48 A/mm. The stars are listed in Table 1, in which the total absorptions of the fifth and sixth columns are given to hundredths of an angstrom for lines measured on the microphotometer and to tenths of an angstrom for those estimated visually against a set of standard lines.

The variation of the intensity of the *O* I lines with spectral type is shown in Figure 2, where total absorptions of λ 7774 have been plotted separately for stars of four different luminosity classes. The gaps in the plots are due to the lack of suitable stars bright enough to be photographed in the infrared. Smoothed curves for the different luminosity classes are brought together in Figure 3, and, in spite of the considerable scatter of the original data, they are reasonably consistent in showing flat maxima between spectral types A0 and F0. There is some indication of a progressive shift of the *O* I maximum from A0 for main-sequence stars to nearly F0 for the brightest supergiants. The rise in intensity through the middle subdivisions of type B is more rapid than the falling-off through type F. On spectrograms of moderate scale the oxygen lines effectively disappear in the early G stars, but they persist further in the supergiants.

The oxygen lines are extremely sensitive to absolute magnitude, especially in the more luminous stars. This is shown by the curves of Figure 3 and even more strikingly by the reproductions in Figure 4 of F0 stars ranging from dwarf to supergiant. The only stars in which the effect is not pronounced are those of luminosity classes III and V, which are not clearly separated in Figure 3 for spectral classes earlier than about A5.

The intensity of λ 7774 forms one of the most sensitive criteria known for the recognition of supergiants of types B5–G0. The oxygen lines have proved of value in setting up accurate classes for the supergiants, though their usefulness is limited by the exposures required to photograph these white stars in the infrared. This difficulty is partly offset by the great strength of the lines in I*a* stars, such as ε Aur and α Cyg, where the total absorption of λ 7774 exceeds 2 A. Such lines can be detected even on small-scale spectrograms taken with fast cameras, where the presence or absence of λ 7774 will show whether a given star is a supergiant.

As a test of the visibility of λ 7774 on prismatic spectrograms of rather low dispersion, a series of I-N plates was taken with the Pα camera (scale about 250 A/mm at λ 7700) on the Perkins two-prism spectrograph. It was found that λ 7774 could just be detected when its total absorption reached about 0.5 A. The line could be clearly seen when $w = 0.7$ A and was conspicuous for total absorptions in excess of 1 A. Comparison of these results with Figure 3 makes it clear that supergiants can easily be detected throughout the range from B3 to G0 in spectral type. Even with this low dispersion, however, exposure times required for these early-type stars in the infrared remain longer than the exposures for the blue region on Eastman 103*a*-O plates when a scale of 120 A/mm at $H\gamma$ is used.

[6] *Mt. W. Contr.*, No. 486; *Ap. J.*, **79**, 183, 1934.

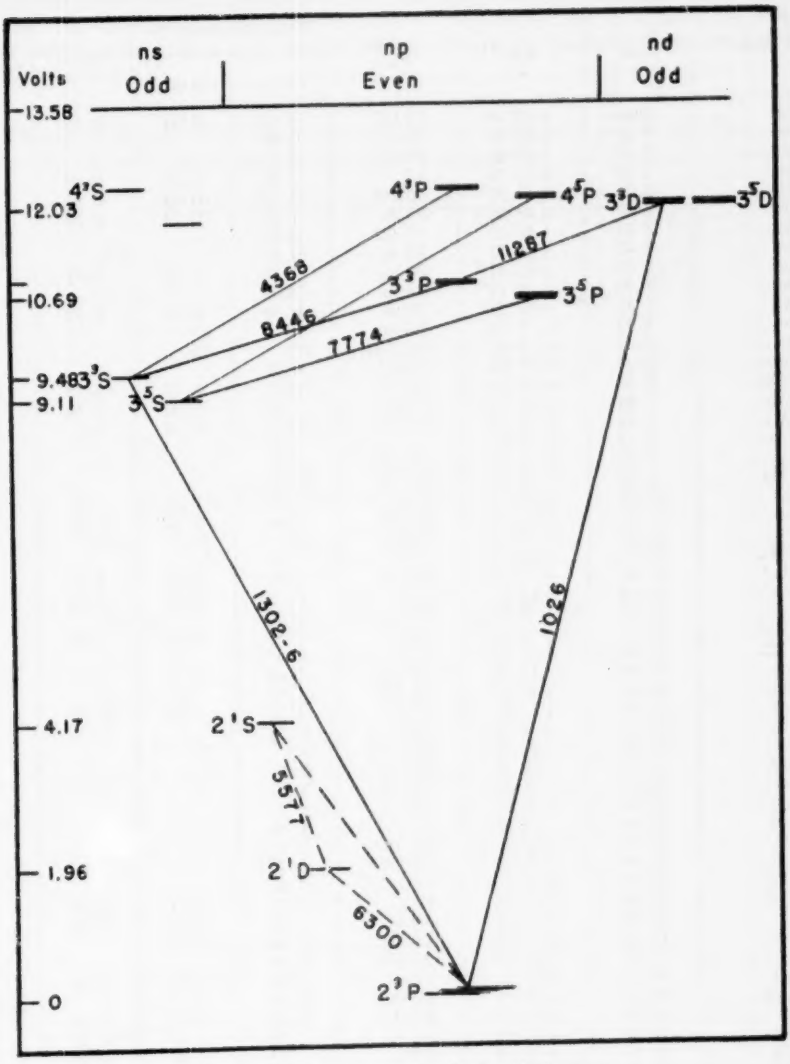

FIG. 1.—The lower energy levels of neutral oxygen

TABLE 1

TOTAL ABSORPTIONS OF *O* I LINES

Star	α_{1900}	δ_{1900}	MKK Type	Total Absorption (A)		Ratio	No. of Plates
				λ 7774	λ 8446		
β Cas	0h03m	+58° 36′	F2 III	0.96	0.53	0.55	.....
δ Cas	1 19	+59 43	A5 V	0.88	.....	.....	.....
α Tri	1 47	+29 06	F5 III	0.3±	.....	.....	.....
β Ari	1 49	+20 19	A5 V	0.88	0.61	0.69	.....
β Tri	2 03	+34 31	A5 III	0.74	0.40	0.54	.....
α Per	3 17	+49 30	F5 Ib	1.15	0.79	0.69	2
δ Per	3 35	+47 28	B5 III	0.66	.....	.....	2
ζ Per	3 47	+31 35	B1 Ib	(0.1)	.....	.....	.....
ε Aur	4 55	+43 41	F0 Ia	2.34	1.20	0.51	.....
β Ori	5 09	− 8 19	B8 Ia	(2.0)	.....	.....	.....
α Lep	5 28	−17 54	F0 Ib	0.96	0.55	0.57	.....
ε Ori	5 31	− 1 16	B0 Ia	(0)	(0)	.....	.....
ζ Ori	5 43	− 9 42	B0.5 Ib	(0)	(0)	.....	.....
ξ Gem	6 39	+13 00	F5 III	0.61	.....	.....	.....
α CMa	6 40	−16 35	A1 V	0.47	0.19	0.35	2
δ CMa	7 04	−26 14	F8 Ia	1.88	0.80	0.43	.....
α CMi	7 34	+ 5 29	F5 IV	0.43	0.32	0.74	3
δ Hya	8 32	+ 6 03	.....	0.80	.....	.....	.....
ε Hya	8 41	+ 6 47	G0 III	(0.1)	.....	.....	.....
θ UMa	9 26	+52 08	F6 III	(0.3)	.....	.....	.....
η Leo	10 01	+17 15	A0 Ib	1.84	1.25	0.68	.....
ζ Leo	10 11	+23 55	F0 III	0.64	0.36	0.56	.....
ρ Leo	10 27	+ 9 49	B1 Ib	(0)	(0)	.....	.....
β UMa	10 55	+56 55	A1 V	0.87	.....	.....	.....
δ Leo	11 08	+21 04	A4 V?	0.92	0.46	0.50	.....
β Leo	11 44	+15 08	A3 V	0.78	0.68	0.87	.....
β Vir	11 45	+ 2 20	F8 V	0.36	.....	.....	.....
γ Vir sf	12 36	− 0 54	F0 V	0.55	0.36	0.66	.....
η UMa	13 43	+49 49	B3 V	0.37	.....	.....	.....
η Boo	13 49	+18 54	G0 IV	0.49	.....	.....	.....
γ Boo	14 28	+38 45	A7 III	1.13	.....	.....	.....
α CrB	15 30	+27 03	A0 V	1.50	0.70	0.47	.....
λ Ser	15 41	+ 7 40	G2 V	(0.1)	.....	.....	.....
β Sco	15 59	−19 32	B0.5 IV	(0)	(0)	.....	.....
γ Her	16 17	+19 23	F0 III	(0.9)	.....	.....	.....
ξ Her	16 37	+31 47	G0 IV	(0.3)	.....	.....	.....
η Her	16 39	+39 07	G5 III	(0.3)	.....	.....	.....
ψ Oph	17 04	−15 36	A2 V	0.86	.....	.....	.....
β Dra	17 28	+52 23	G2 Ib	(0.5)	.....	.....	.....
α Oph	17 30	+12 38	A5 III	0.75	.....	.....	2
67 Oph	17 55	+ 2 56	B5 I–II	1.12	.....	.....	.....
45 Dra	18 30	+56 58	F6 Ib	0.74	0.51	0.68	.....
α Lyr	18 33	+38 41	A0 V	1.05	0.70	0.67	.....
γ Lyr	18 55	+32 33	B9 III	0.86	.....	.....	.....
δ Cyg	19 41	+44 53	A0 III	0.93	.....	.....	.....
γ Cyg	20 18	+39 56	F8 Ib	1.16	0.50	0.44	.....
41 Cyg	20 25	+30 02	F4 Ib	(1.2)	.....	.....	.....
β Del	20 32	+14 15	F5 III	0.68	0.40	0.59	.....
α Cyg	20 38	+44 55	A2 Ia	2.19	1.17	0.53	.....
σ Cyg	21 13	+39 59	B9 Ia	1.72	0.84	0.49	.....
β Aqr	21 26	− 6 01	G0 Ib	0.54	0.19	0.34	.....
9 Peg	21 39	+16 53	G5 Ib	(0.4)	.....	.....	.....
α Aqr	22 00	− 0 48	G1 Ib	(0.6)	.....	.....	.....
ι Peg	22 02	+24 51	F5 V	0.52	.....	.....	.....
ψ Peg	22 38	+29 42	G2 II–III	(0)	.....	.....	.....
ξ Peg	22 41	+11 40	F6 III–IV	(0.3)	.....	.....	.....

The behavior described above for the *O* I lines applies to stars that have normal spectra in the sense that they can be fitted into the usual two-dimensional scheme of classification. The anomalous weakness of the lines in the peculiar A-type stars is under separate investigation and will not be discussed in this paper. Emission-line stars are dealt with in Section III.

II. THE OXYGEN-HYDROGEN ABUNDANCE RATIO

The occurrence of the *O* I lines and the Paschen series of hydrogen with comparable intensity and in the same general region of the spectrum is a circumstance favoring a de-

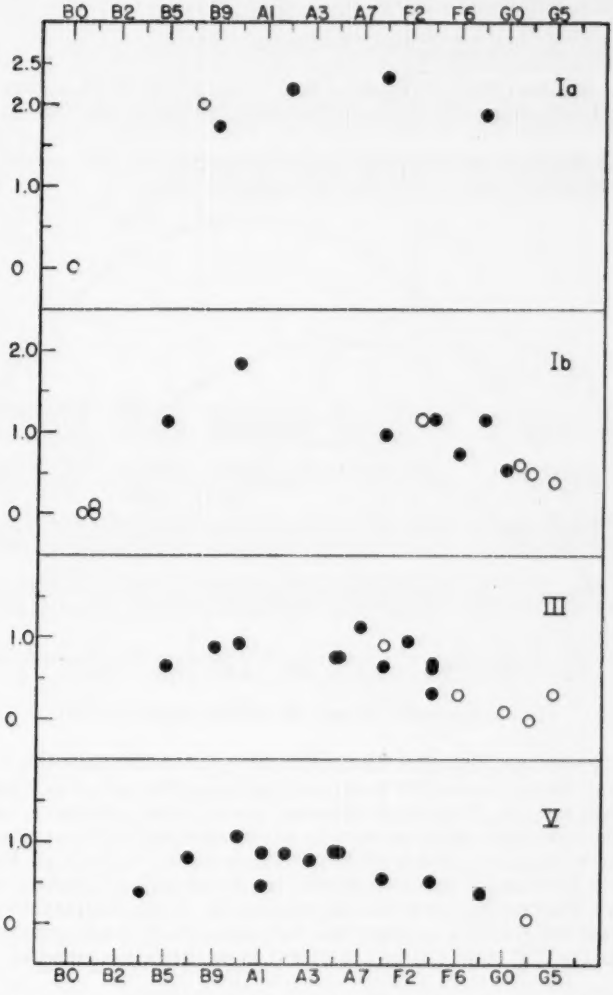

FIG. 2.—Variation of total absorption of λ 7774 with spectral type. The luminosity class of the group of stars is indicated in the upper right corner of each section.

termination of the abundance ratio of the two elements. For reasons indicated in Section III, the lines at λ 8446 are less suited to this purpose than the λ 7774 triplet, and we have made use of the latter only.

The three lines (see accompanying table) arise from a metastable quintet state. The

λ	Transition	Relative Strength
7771.96	$3^5S_2^o - 3^5P_3$	7
7774.18	$3^5S_2^o - 3^5P_2$	5
7775.40	$3^5S_2^o - 3^5P_1$	3

population of this level might be expected to be abnormal if the atoms were excited directly from the ground level by the forbidden resonance transition. The data of Table 1

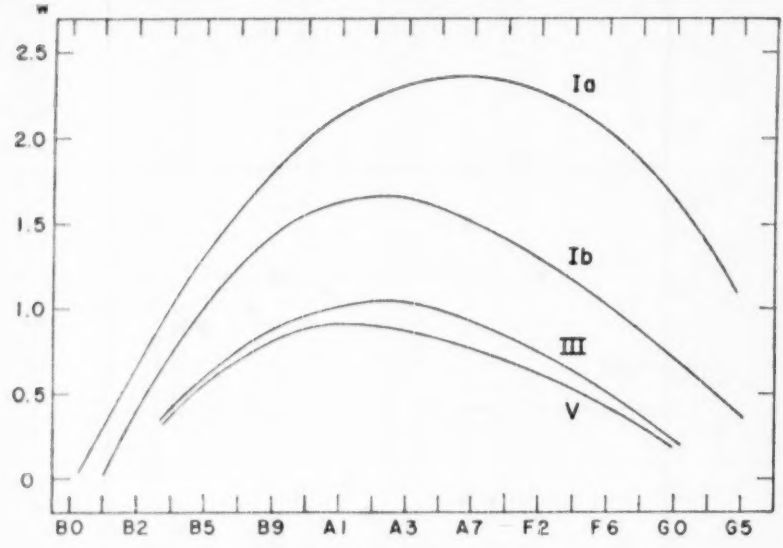

FIG. 3.—Luminosity effects in the total absorption of λ 7774.

(seventh col.), however, show that the relative strengths of the absorption lines from the normal 3^5S^o and the metastable 3^5S^o levels have just about the ratio, 3 to 5, predicted from their statistical weights, if the small difference in excitation potential is neglected. For the twelve giant and main-sequence stars for which measured ratios are given in Table 1, the mean ratio of equivalent widths of the two blends is 0.60 ± 0.04 (m.e.). Because of the position of the lines on the curve of growth, the actual ratio of numbers of transitions must be lower. Presumably, the levels are populated by recombinations of ionized atoms, but in any case the evidence suggests that the metastability is not important and that the atoms in the 3^5S^o state can be considered as in thermal equilibrium with the remainder.

The *f*-values for the three transitions of the λλ 7772–7775 lines have not been determined directly. The sum of these *f*-values cannot be far from 1, however, for the only

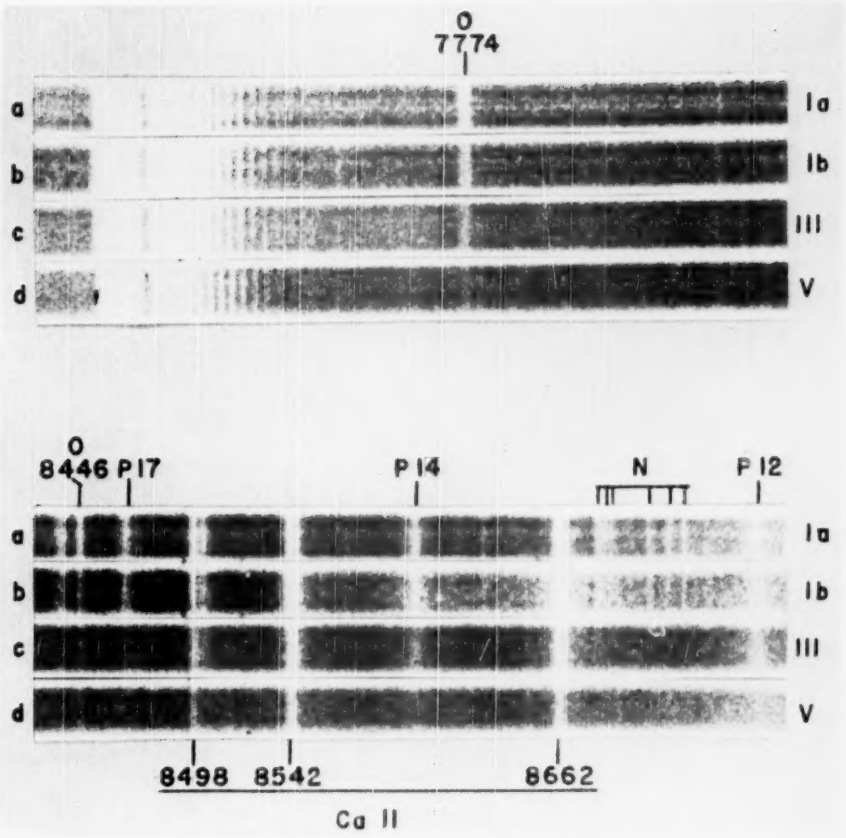

FIG. 4.—The oxygen lines in stars of type F0:

a)	ϵ Aur	*Ia*
b)	α Lep	*Ib*
c)	ζ Leo	III
d)	γ Vir	V

permitted series of absorption lines from the 3^5S^o level go to the n^5P levels, and the second multiplet in this series, 3^5S^o—4^5P at 3947 A, has never been observed in a stellar spectrum with sufficient strength to be positively identified, even in a star such as ϵ Aur, which shows λ 7774 in tremendous strength. Adopting $\Sigma f = 1$ for the λ 7774 multiplet and knowing that, for the three lines, $f1:f2:f3 = 7:5:3$, we arrive at the individual f-values: 0.47, 0.33, and 0.20.

With high dispersion the three lines are well separated, with no appreciable overlapping of wings, as can be seen on the tracings of the *Utrecht Atlas of the Solar Spectrum*. Consequently, each of the lines leads to an independent value of the population of the 3^5S^o level in the sun. For this number, N_3, Bowen[5] found 4.9×10^{11} from the Utrecht data.

TABLE 2

RELATIVE ABUNDANCE OF OXYGEN AND HYDROGEN

STAR	TYPE	ADOPTED TEMP. (° K)	ξ (KM/SEC)	OXYGEN		HYDROGEN			OXYGEN ABUNDANCE
				N_3	N_0	N_{01}	N_{02}	N_0	
α CMa..	A1 V	8000	1.9*	1.2×10^{13}	1.2×10^{19}	8.8×10^{14}	1.8×10^{16}†	7.4×10^{21}	1.6×10^{-3}
α CMi..	F5 IV	6300	2.3‡	2.8×10^{12}	1.0×10^{20}	.....	1.8×10^{16}†	5.8×10^{23}	1.7×10^{-4}
α Per...	F5 Ib	5800	3.7‡	7.2×10^{13}	1.1×10^{22}	2.0×10^{15}	2.6×10^{16}†	3.4×10^{24}	3.2×10^{-3}
γ Cyg...	F8 Ib	5500	7.6§	5.3×10^{13}	2.2×10^{22}	8.2×10^{14}	2.9×10^{16}†	1.1×10^{25}	2.0×10^{-3}
δ CMa..	F8 Ia	5300	5.5‖	2.2×10^{14}	1.8×10^{23}	1.3×10^{15}	.....	3.9×10^{25}	4.6×10^{-3}
Sun....	G2 V	5200#	0.9‡	4.9×10^{11}#	6.1×10^{20}#	.....	.....	1.05×10^{24}**	5.8×10^{-4}

* L. H. Aller, *Ap. J.*, **96**, 321, 1942.

† S. Günther, *Zs. f. Ap.*, **7**, 106, 1933.

‡ K. O. Wright, *J.R.A.S. Canada*, **40**, 183, 1946; also *Pub. Dom. Ap. Obs. Victoria*, Vol. **8**, No. 1, 1948.

§ Wright, *J.R.A.S. Canada*, **40**, 183, 1946; and *Pub. Dom. Ap. Obs. Victoria*, Vol. **8**, No. 1, 1948; Sahade and Cesco, *Ap. J.*, **104**, 133, 1946.

‖ Wright, *J.R.A.S. Canada*, **40**, 183, 1946; and *Pub. Dom. Ap. Obs. Victoria*, Vol. **8**, No. 1, 1948; H. R. Steel, *Ap. J.*, **102**, 429, 1945.

I. S. Bowen, *Rev. Mod. Phys.*, **20**, 109, 1948.

** M. Minnaert, *B.A.N.*, **10**, 339, 399, 1948.

For the stars observed with moderate dispersion, the lines are only partly resolved, and we measure the total absorption, w, of the blend. Since the blending is entirely instrumental, we know that

$$w = w_{7771} + w_{7774} + w_{7775} .$$

We must apply the curve of growth to each line separately in order to find N_3, for we cannot assume that the lines lie on the linear part of the curve. If we could make that assumption, we should have

$$w_{7771} : w_{7774} : w_{7775} = 0.47 : 0.33 : 0.20 ;$$

but, actually, the lines lie well on the flat portion of the curve and the ratios of the equivalent widths will be much closer to 1. The procedure followed here has been to enter the curve of growth successively until we find three values of the w's that yield Nf-values in the above ratio. Usually two or three approximations were sufficient, since the w's were never far from the proportion 10:9:8.

For the five stars listed in Table 2, curves of growth determined from lines of neutral metals were available. References to the sources are given in the fourth column of the table, containing the adopted turbulent velocity, which defines the upper part of the curve. Since these curves of growth are based upon lines of low excitation potential, their application to the high-level lines of the oxygen triplet is admittedly a possible source of

serious error; but, until more is known of the way in which the curve of growth depends upon excitation potential, the method must serve as a first approximation.

In Table 2 the fifth column gives for these five stars the values of N_3 found from the observed equivalent widths of Table 1. The sixth column gives N_0, the total number of neutral oxygen atoms above the photosphere, derived on the assumption that the distribution of atoms among the possible energy levels obeys the Boltzmann formula. Here the question of what temperatures should be inserted in the Boltzmann expression immediately arises. The most positive clue to the answer has been furnished by Bowen's work on oxygen in the sun.[8] He observed not only the infrared lines but also the forbidden lines involving the metastable 2^1D level and the normal 2^3P level (see Fig. 1). The observed populations of these three sets of levels, covering a range of more than 9 volts in excitation potential, provided a very accurate determination of the excitation temperature for oxygen in the sun's atmosphere. Bowen's value of 5200° lies about halfway between the sun's effective temperature and the considerably lower estimates that have been made of the excitation temperature for low-lying levels of metallic atoms. We have assumed that the same situation holds in the other stars observed and have adopted a temperature intermediate between the effective and the usual excitation temperatures in computing the Boltzmann factors. The temperatures actually used are given in the third column of Table 2.

It should be noted that, although the Boltzmann factors are very sensitive to temperature, the estimates of relative abundance of oxygen and hydrogen which will be discussed below are affected very little by the temperature adopted, since the observed lines of oxygen and hydrogen have similar excitation potentials.

We derive the relative abundance of oxygen to hydrogen as the ratio of the numbers of neutral atoms of the two elements. The ionized atoms can be neglected, since the ionization potentials of oxygen and hydrogen differ by only 0.02 volts and are both so high that relatively few of these atoms are ionized at the temperatures of the stars in Table 2.

For hydrogen, total absorptions of lines in two spectral regions are available; the measurements of the Balmer lines by Günther,[7] which lead to the numbers N_{02} (hydrogen atoms in the second quantum level) of the eighth column, and our measurements of Paschen 14 (λ 8598) and Paschen 17 (λ 8467), whence the values of N_{03} in the seventh column are found. For both series it is assumed that the hydrogen lines are so greatly broadened that the linear relation between N_{0n} and w (total absorption in angstroms) can be applied.[8] Then

$$N_{0n} = \frac{m c^2}{\pi e^2 f \lambda^2} w = \frac{1.129}{f \lambda^2} w ,$$

where λ is given in centimeters.

For three stars the total numbers of neutral hydrogen atoms estimated from the lines of the two series can be compared. In Table 3 the vaules of N_0 derived from the Balmer lines average about twice as great as those from the Paschen lines. This would imply that the atmospheric opacity is greater at 8400 A than at 4300 A; but, since the infrared observations are made on only two rather high members of the Paschen series, they may lead to underestimates of N_0. The values of N_0 in Table 2 were averaged from both sets of data, with double weight given the Balmer-line data except in the case of γ Cyg, for which Günther measured the absorption of $H\gamma$ only.

In the case of the sun the best estimate for N_0 of hydrogen appears to be the mean value of 1.05×10^{24} obtained by Minnaert,[9] and this is the figure given in the ninth column of Table 2.[10]

[7] *Zs. f. Ap.*, **7**, 106, 1933.

[8] Cf. the discussion by Unsöld, *Physik der Sternatmosphären* (Berlin: Julius Springer, 1938), pp. 286–90.

[9] *B.A.N.*, **10**, 339 and 399, 1948.

[10] Actually, this does not differ widely from the value of 1.4×10^{24} obtained by Unsöld (*Zs. f. Phys.*, **59**, 353, 1930; *Zs. f. Ap.*, **24**, 314, 1948) from the intensities of the Balmer lines; but the agreement is partly fortuitous, since Unsöld adopted a higher excitation temperature.

For the sun the data of the table give 5.8×10^{-4} for the oxygen/hydrogen abundance ratio. This can be checked against the determination by Minnaert,[9] based on the fact that the intensity of any line in the solar spectrum can furnish a direct estimate of the abundance of the responsible element relative to hydrogen.[11] Minnaert found an oxygen/hydrogen ratio of 7×10^{-4}. The close agreement with our figure is mainly a check on the consistency of the arithmetic, since he also made use of Bowen's observational data for oxygen; but it does show that, if Minnaert had derived the number of hydrogen atoms from the oxygen data alone, he would have arrived at about the same answer that he found from the lines of all the metallic ions and neutral atoms.

TABLE 3

ESTIMATES OF NUMBERS OF NEUTRAL HYDROGEN ATOMS

Star	N_0	
	Balmer Series (Günther)	Paschen Series (Perkins)
α CMa	1.1×10^{22}	0.4×10^{22}
α Per	4.3×10^{24}	1.6×10^{24}
γ Cyg	1.4×10^{25}	1.0×10^{25}

TABLE 4

COLLECTED VALUES OF OXYGEN/HYDROGEN ABUNDANCE RATIO

Star	Type	Source	$N_{\text{Oxygen}}/N_{\text{Hydrogen}}$
10 Lac	O9 V	Aller	0.5×10^{-3}
τ Sco	B0 V	Unsöld	1×10^{-3}
α CMa	A1 V	Perkins	2×10^{-3}
α CMi	F5 IV	Perkins	0.2×10^{-3}
α Per	F5 Ib	Perkins	3×10^{-3}
γ Cyg	F8 Ib	Perkins	2×10^{-3}
δ CMa	F8 Ia	Perkins	5×10^{-3}
Sun	G2 V	Minnaert, Perkins	0.6×10^{-3}
Planetary nebulae		Aller and Menzel	0.25×10^{-3}

Although the same objections to the use of hydrogen-line intensities to find relative abundances apply to some extent to all the stars included in Table 2, the method should be reasonably sensitive, and we can hope that the results have some significance. The only other measurements of oxygen abundance that are available for comparison are the data for two early-type stars in which the lines of *O* II and *O* III could be observed and compared with the Balmer lines of hydrogen. The star τ Sco was studied by Unsöld[1] and 10 Lac by Aller.[2] The results for all available stars, together with the data of Aller and Menzel[12] for planetary nebulae, are collected in Table 4.

The measured values of the oxygen-hydrogen abundance ratio cover a range of about

[11] This follows immediately from the argument of the preceding paragraph, as has been emphasized by Minnaert and others.

[12] *Ap. J.*, **102**, 239, 1945.

twenty-five times. In view of the large probable errors involved in reading abundances from the flat parts of curves of growth, as well as the possible systematic errors discussed above, there is no strong evidence of real variations from star to star. It is perhaps significant, however, that the three supergiant stars in Table 4 show oxygen abundances nearly four times greater than the mean for main-sequence stars. Taking the data as a whole, we can conclude that in stellar atmospheres there are about 1000 hydrogen atoms to every oxygen atom.

III. BEHAVIOR OF THE *O* I LINES IN STARS WITH EXTENDED ATMOSPHERES

There are ten supergiants for which measurements of the λ 8446 and λ 7774 lines are given in Table 1, and for these the mean ratio of the total absorptions is 0.54 ± 0.04. A departure from the ratio of 0.60 measured for giants and main-sequence stars is not clearly established, but the observations do suggest a slight relative weakening of λ 8446 in the spectra of supergiants.

As soon as we turn to stars that have spectra marked by emission lines, we find striking anomalies in the behavior of the oxygen lines. It has been noted by several observers that λ 8446, involving triplet levels, goes into emission more readily than does the quintet blend λ 7774. This was observed in P Cyg and γ Cas by Merrill,[6] and it was pointed out by Swings[13] that in P Cyg the absorption component of λ 7774 is much stronger than that of λ 8446, while the emission components of the two are comparable in strength. Similar anomalies have been noted for υ Sgr by Greenstein and Merrill[14] and in several other stars by Hiltner.[15] In some cases λ 8446 appears in emission while λ 7774 remains in absorption. Perkins spectra of ζ Tau and several other stars show this clearly.

If it were necessary to account for differences in absorption intensities only, the phenomena might be taken as examples of the well-known tendency for normal levels to be underpopulated in contrast to metastable levels in fields of dilute radiation. The emission effects show that a more particular mechanism is at work in the case of these oxygen lines, and there is little doubt that Bowen[16] has correctly explained the observations as examples of resonance excitation. The *O* I transition $2^3P_2 - 3^3D^\circ$ represents a line of wave length 1025.766, less than 0.05 A distant from Lyman-β at λ 1025.717. This is one of the closest known coincidences of important lines of two elements and was noticed originally by Hopfield.[17] Whenever Lyman-β is strongly in emission, resonance absorption should increase the population of the 3^3D° level of oxygen. Downward transitions will then give the emission lines λ 11286, λ 11287, $3^3P - 3^3D^\circ$, and thus overpopulate the 3^3P states—the upper levels for the emission of λ 8446 (see Fig. 1).

From this interpretation it follows that the appearance of emission at λ 8446 is an indicator of emission in the invisible Lyman series of hydrogen. Even before the oxygen emission is strong enough to produce a clear reversal of the line, the filling-in of the absorption line by incipient emission can be detected by an anomalous intensity ratio of λ 8446 to λ 7774.

Of particular interest is the observation by Hiltner that, in the shell star 28 Tau (Pleione), λ 8446 is a very strong absorption line. At first sight, this appears to be a contradiction, for 28 Tau is a Be star with *Hα* emission. Spectrograms of the visual region, however, show that in recent years, while *Hα* has been a strong double emission line, *Hβ* has remained mainly an absorption line. We interpret the infrared observations as indicating that in 28 Tau the Lyman series is behaving similarly to the Balmer series, without strong emission in Lyman-β.

[13] *Pub. A.S.P.*, **56**, 238, 1944.

[14] *Mt. W. Contr.*, No. 723; *Ap. J.*, **104**, 177, 1946.

[15] *Ap. J.*, **105**, 212, 1947.

[16] *Pub. A.S.P.*, **59**, 196, 1947.

[17] *Ap. J.*, **59**, 114, 1924.

THE SPECTRUM OF THE NEBULOSITY SURROUNDING T TAURI*

GEORGE H. HERBIG†
Yerkes and McDonald Observatories
Received August 26, 1949

ABSTRACT

The spectrum of the nebulosity immediately surrounding T Tauri was observed by placing the spectrograph slit in various position angles through the star. The spectrum of the nebula consists of emission lines of [*O* II], [*S* II], and *H*. The amount of light of T Tauri scattered or reflected in the nebula seems to be small. The outline of the nebula obtained from measurements of the extension of the emission lines is in agreement with that found from direct photographs.

Three distinct nebulous areas have been observed in the vicinity of the irregular variable star T Tauri.[1] The first of these, NGC 1555, was discovered by J. R. Hind in 1852 and is one of the best examples of a variable nebula. It lies about 45″ to the west of T Tauri. Another small nebula was discovered by O. Struve in 1868, about 4′ to the west of the variable star. This object is catalogued as NGC 1554. The third nebula was discovered visually in 1890 by S. W. Burnham[2] with the 36-inch Lick refractor. He described it as follows: "This star [T Tauri] is placed within a very small condensed nebula. It is somewhat elongated in the direction 151°.7. A rough reading of the wires gave 4″.4 for the length of the nebula in this direction. It is less extended on the opposite side of the star or nucleus, with a shorter diameter of perhaps half of that measured." This observation was corroborated a few nights later by Barnard. The object was re-examined by Barnard in 1895, with the surprising result that the small, very definite nebula surrounding T Tauri had disappeared and was replaced by a very faint, indefinite nebulous glow. The last observation published by Barnard was made in 1897 with the Yerkes 40-inch refractor, when he saw a very small nebulous patch very close to the variable, at a distance of 1″ or 2″, in the direction of the elongation of Burnham's elliptical nebula of 1890.

Photographs taken by W. Baade at Mount Wilson[3] have revealed, in addition to Burnham's nebula, a knoblike protuberance from the photographic image of T Tauri in p.a. 190°. It is with the nebulous features discovered by Burnham and by Baade that the present paper deals. I am greatly indebted to Dr. Baade for permitting me to inspect his direct photographs of the nebulosities at T Tauri.

Observation of the spectra of the close nebulosities at T Tauri is rendered difficult by their faintness and proximity to the variable star, which, at the time that the present observations were made, was of visual magnitude 10. A telescope of long focal length is required, as well as good seeing and careful guiding. The first attempt to secure spectrograms of the nebulae was made at the Lick Observatory in 1947 with the 36-inch refractor. The results obtained were of low weight because of the impossibility of guiding with sufficient accuracy. The problem was taken up again in the winter of 1948–49 with the 82-inch reflector of the McDonald Observatory. On three nights of very good seeing, it was found possible to obtain six spectrograms of the nebulosity which were apparently free from contamination by light from T Tauri. The procedure followed was to place the

* *Contributions from the McDonald Observatory, University of Texas*, No. 181.

† National Research Fellow.

[1] The early visual observations have been summarized by E. E. Barnard in *M.N.*, **55**, 442, 1895; **59**, 372, 1899. Photographic observations of NGC 1554 and 1555 have been described by H. D. Curtis (*Pub. A.S.P.*, **27**, 242, 1915), F. G. Pease (*Ap. J.*, **45**, 89, 1917), and C. O. Lampland (*Pub. A.S.P.*, **48**, 318, 1936).

[2] *M.N.*, **51**, 94, 1890; *Pub. Lick. Obs.*, **2**, 175, 1894.

[3] See *Ap. J.*, **102**, 171, Pl. XV, 1945.

slit of the Cassegrain spectrograph through the image of the star in various position angles and then hold the star fixed on the slit during the exposure by the aid of a cross-wire in the guiding eyepiece. The exposure times ranged from 10 to 85 minutes on Eastman IIa-0 film. The $f/1$ Schmidt camera was used with both glass prisms (dispersion 150 A/mm at $H\gamma$) and quartz prisms (330 A/mm at $H\gamma$). Figure 1 shows five spectrograms taken with the latter combination. The third, fourth, and fifth spectrograms of Figure 1, all obtained with an exposure of 60 minutes, show immediately that emission lines extend from the star to distances of about 8″ in p.a. 151° and 190° and to considerably lesser distances in the other orientations.

The strongest emission line in the nebula is λ 3726, λ 3729 of [*O* II], followed by the [*S* II] pair at λ 4068 and λ 4076, and the hydrogen lines. There is no possibility that this spectrum arises simply from light of T Tauri scattered in the instrument or by poor guiding, for the following reasons: The strongest emission lines in the nebula, those of [*O* II] and [*S* II], are much weaker in the star than H and K of *Ca* II. In the spectrum of the star, the [*S* II] lines are weaker than $H\delta$; in the nebula, the opposite is the case. Neither the *Ca* II lines nor the continuous spectrum of the star shows any extension in p.a. 151° such as would be present if instrumentally scattered light were responsible for the nebular spectrum. Furthermore, the outline of the nebula, as defined by the extension of the [*O* II], [*S* II], and *H* lines (see below), is consistent with its shape and dimensions as observed on direct photographs.

There is no indication of the presence of the [*O* III] lines at λ 4959, λ 5006, although the definition of the spectrograms is poor in that region and the stellar continuum very strong. R. F. Sanford has observed [*O* I] λ 6300 in emission in the spectrum of the star.[4] Because of the serious astigmatism of the spectrograph in the red, no attempt was made at McDonald to discover whether this line is actually due to the nebula.

The extensions of four representative emission lines from the center of the star spectrum, as well as the width of the overexposed stellar continuum, were measured on three plates of 60 minutes' exposure obtained with the 330 A/mm dispersion. The results are contained in Table 1 and are plotted in polar form in Figure 2. In order to demonstrate the amount of agreement between such measurements on different spectrograms, a few measurements (indicated by open circles and squares) made on two comparable negatives of 150 A/mm dispersion are also plotted in Figure 2. The limits of extension of the nebular lines in Figure 1 have been connected by dashed lines. These lines have been added simply to aid the eye and are not based on any additional information. A heavy circle has been drawn through the points marking the extension of the stellar continuum, which show the amount of spreading of the overexposed star image at the wave length of each line.

The outline of the nebula obtained from the extension of the [*O* II], [*S* II], and *H* lines shows the elliptical figure extended in p.a. 151° and the displacement of the star along the major axis in p.a. 331°, seen by Burnham and Barnard. The "protuberance" in p.a. 190° discovered by Baade is likewise evident. The dimensions of the nebula measured on the spectrograms have not been corrected for seeing and guiding errors and hence are undoubtedly larger than the true values of the extension of the nebula out to the surface brightness specified by the photographic threshold of these particular spectrograms. The symmetrical extension of the K line of *Ca* II in all directions except p.a. 190° may be due entirely to atmospherically or instrumentally scattered light of T Tauri. The K line certainly does not behave as do the other emission lines. Its absence in p.a. 151° demonstrates that that part of the nebula scatters or reflects very little direct starlight. The extensions of the H and K lines in p.a. 190° are faint, but look real. Their observation depends entirely upon one spectrogram, however.

According to Burnham, "On the night of November 1st [1890], Mr. Keeler examined

[4] *Pub. A.S.P.*, **59**, 134, 1947.

FIG. 1.—The spectrum of T Tauri and the surrounding nebulosity. These five spectrograms were obtained with quartz prisms and the *f*/1 Schmidt camera, giving a dispersion of 330 A/mm at $H\gamma$. The slit was placed through T Tauri in various position angles. The individual plate data are as follows: *a*, Q*f*/1 11794, slit in p.a. 151°, exposure 1 minute; *b*, Q*f*/1 11795, slit in p.a. 151°, exposure 10 minutes; *c*, Q*f*/1 11796, slit in p.a. 151°, exposure 60 minutes; *d*, Q*f*/1 11797, slit in p.a. 61°, exposure 60 minutes; *e*, Q*f*/1 11813, slit in p.a. 190°, exposure 60 minutes. In each case the position angle quoted is that toward the top of the page. Note the growth of the nebular emission lines at λ 3727 and λ 4068, λ 4076 as the exposure time is increased in the first three spectrograms.

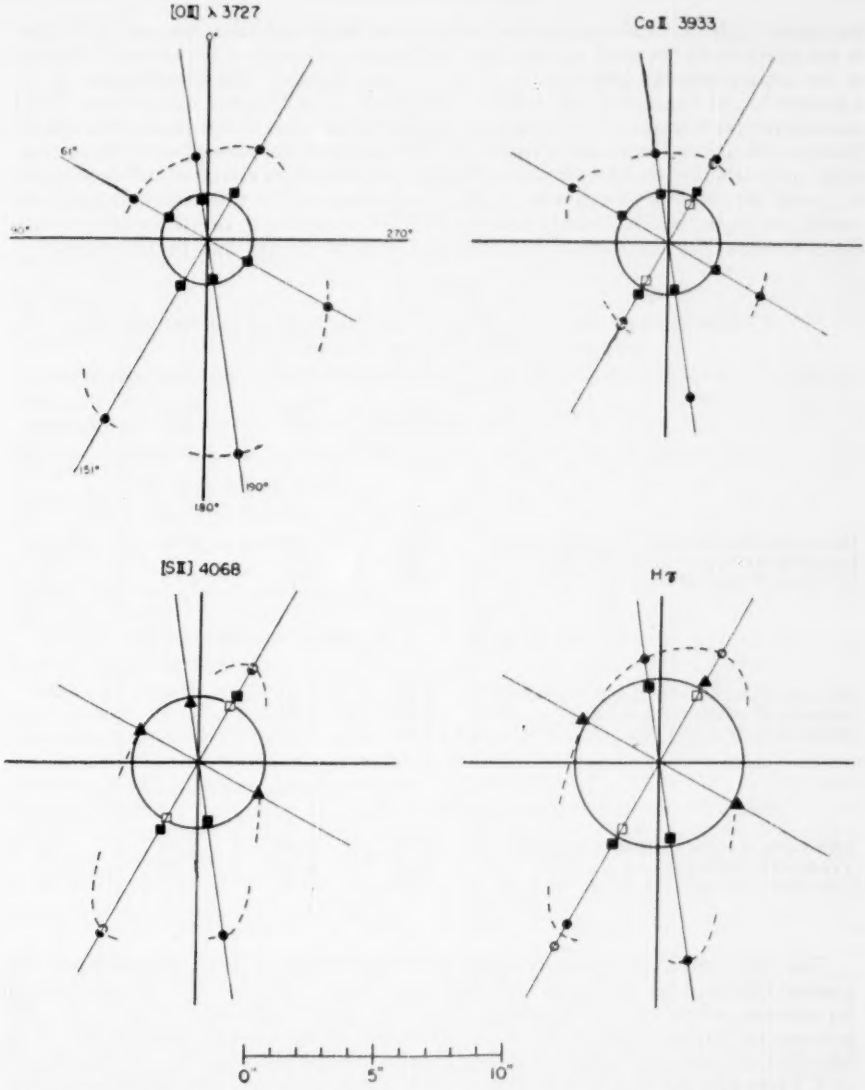

FIG. 2.—Polar diagram of the extension of the emission lines at T Tauri. Circles indicate the limit of extension of the emission lines. Squares represent the limit of extension of the overexposed continuous spectrum of T Tauri. Triangles indicate the limit of extension of the star spectrum when no extension of the emission lines was seen. Filled markings represent measures on Q $f/1$ spectrograms of exposure 60 minutes; open markings indicate measures on G $f/1$ negatives. The broken lines are intended to suggest the outline of the figure defined by the extension of the emission lines. The solid circles drawn through the squares and triangles represent the spread of the overexposed star image.

the nebula with the small spectroscope attached to the 36-inch telescope, and found that it was probably of the usual gaseous type, although on account of the extreme faintness of the nebula only the principal line at λ 5005 was visible."[2] The identification of the strongest bright line with [*O* III] λ 5006 is surprising, since that line has not been found on modern spectrograms of either star or nebula. No mention of this observation can be found in the original observing records of either Keeler or Burnham; hence it is not possible to say whether the identification is based on an actual measurement of wave length or is only the result of an estimate. Unless the spectrum of the nebula has changed, one would now be inclined to identify this line with *Hβ*. At any rate, this observation establishes Keeler as the discoverer of the emission nature of the spectrum of the nebula.

TABLE 1

EXTENSION OF THE EMISSION LINES AND THE STELLAR CONTINUOUS SPECTRUM FROM T TAURI, IN SECONDS OF ARC

	[*O* II] λλ 3726–29	*Ca* II λ 3933	[*S* II] λ 4068	$H\gamma$ λ 4340
	Q*f*/1 11796: Slit in p.a. 151°			
Half-width of stellar continuous spectrum	2".10	2".30	2".92	3".62
Extension of emission line in p.a. 151°	7.97	3.53	7.56	7.23
Extension of emission line in p.a. 331°	4.03	3.78	4.11	.....
	Q*f*/1 11797: Slit in p.a. 61°			
Half-width of stellar continuous spectrum	1.77	2.14	2.63	3.49
Extension of emission line in p.a. 61°	3.29	4.35	.....	.....
Extension of emission line in p.a. 241°	5.34	4.19	.....	.....
	Q*f*/1 11813: Slit in p.a. 190°			
Half-width of stellar continuous spectrum	1.56	1.89	2.34	3.00
Extension of emission line in p.a. 190°	8.46	6.16	6.80	7.80
Extension of emission line in p.a. 10°	3.29	3.53	.....	4.11

The spectrum of the nebulosity immediately surrounding T Tauri resembles that of a gaseous nebula of low ionization: sufficient to produce O^+ but not O^{++}. The existence of an emission nebula apparently excited by a dG5 star is surprising. It may be that the primary mechanism responsible for the production of the nebular emission lines is not identical with that operating in ordinary gaseous nebulae but arises from the interaction of T Tauri with the dark nebula upon which it is seen projected. The close nebulosity at T Tauri is unique, so far as is known at the present time, among the emission-line objects associated with dark nebulae. However, very few other stars of this type have been adequately examined for such nebulosity.

I am indebted to Dr. G. P. Kuiper and Dr. O. Struve for placing the facilities of the Yerkes and McDonald observatories at my disposal, to Mr. J. F. Chappell of the Lick Observatory for preparing Figure 1, and to the National Research Council for the award of a Fellowship for 1948–49.

SPECTRA OF VARIABLE STARS IN THE ORION NEBULA*

GEORGE H. HERBIG†
Yerkes and McDonald Observatories
Received October 25, 1949

ABSTRACT

Slit spectrograms of nineteen variable stars in the Orion nebula were obtained with the 82-inch reflector. Eleven of these stars had not previously been observed spectroscopically. Emission lines, usually of *H* and *Ca* II, appear in the spectra of eleven of the stars observed and possibly in one more. Those variables whose absorption spectra could be classified were of types G and K. No objects were found with rich emission spectra like those of the variables RW Aurigae, XZ Tauri, and Barnard 100, which are associated with the Taurus dark clouds.

The spectra of variable stars in the Orion nebula have been observed by J. L. Greenstein and O. Struve[1] and by the writer.[2] In all, sixteen stars were examined in these investigations, but only one (AN Orionis) was found (by Greenstein and Struve) to exhibit line emission in the photographic region. The absence of stars with spectacular emission spectra, such as are found associated with the dark nebulae in Taurus-Auriga-Orion and in Scorpio-Ophiuchus, was surprising. Suggestions were made that the presence of the high-luminosity Trapezium stars might be responsible for the lack of stars in the Orion nebula with spectra like T Tauri or that the situation of the Orion variables with respect to the nebular material might somehow be different. The results to be described here show that emission-line stars of one variety actually are present in the Orion nebula and that these speculations consequently must be modified.

The present investigation was planned to extend the observations to more and, generally, fainter variable stars. Since reliable estimates of magnitudes of the stars in the nebula are difficult, especially on blue-sensitive plates, because of the interference of the nebula itself, some uncertainty was felt as to whether variability had been established beyond a doubt for all the stars regarded as variable by A. Brun[3] and L. Rosino.[4] To settle this question, an examination was made of some forty plates of the series of direct photographs of the Orion nebula obtained between 1905 and 1919 by J. A. Parkhurst with the 40-inch Yerkes refractor. These plates were exposed behind a yellow filter, which effectively suppressed the nebulosity except in the immediate vicinity of the Trapezium. The area covered was 32′ by 40′, centered near the Trapezium. Twenty-nine stars in this area which were considered to be variable either by Brun or by Rosino were examined for variability. It was possible definitely to confirm fifteen of these, while two more were regarded as probably variable. In addition, three new variables were discovered. This list of twenty stars formed the nucleus of the spectroscopic observing program. Because of the poor observing conditions during the winter of 1948–1949 and the faintness of some of the variables, spectrograms were obtained at the McDonald Observatory of only twelve stars on this list, but plates were taken, as well, of four other stars which were not in the region covered by the 40-inch plates and of three other stars whose variability had not been confirmed. The spectra of eleven of the nineteen stars observed have not been published before.

* *Contributions from the McDonald Observatory, University of Texas*, No. 183.

† National Research Fellow.

[1] *Pub. A.S.P.*, **58**, 366, 1946.

[2] Dissertation, University of California, 1948; *Pub. A.S.P.*, **60**, 256, 1948.

[3] *Pub. l'Obs. Lyon*, Vol. 1, Ser. I, Fasc. 12, 1935.

[4] *Pubb. dell'Oss. astr. U. Bologna*, **5**, 1, 1946.

The observations were made with the Cassegrain spectrograph of the 82-inch reflector. The glass prisms were used, in most cases with the 90-mm camera, which gives a dispersion of 150 A/mm at $H\gamma$. For AN and EZ Orionis and for one plate of Brun 467, the 180-mm camera was used. This combination produces a dispersion of 75 A/mm at $H\gamma$. Eastman II*a*-O film was used altogether. The spectra of the brighter variables were widened by drifting, but those of the fainter stars and of the variables located in areas where the nebula was bright enough to interfere seriously were usually not widened. The slit length

TABLE 1

OBSERVATIONS OF ORION NEBULA VARIABLE STARS

Star	Photographic Range*	Dates of Spectrograms (U.T.) and Estimated Visual Magnitudes	Notes
TU Orionis	12.6?–15.2	1948 Dec. 2 (13.0); 1949 Feb. 13 (12.5:)	1
YZ Orionis	15.0 –15.8	1949 Feb. 16 (14.3:)	3
AA Orionis	12.0 –14.1	1948 Dec. 28 (12.3:); 1949 Jan. 5	3
AD Orionis	14.0 –16.6*	1949 Feb. 17 (13.5:)	1
AG Orionis	12.0 –14.5	1949 Jan. 6 (13.5:)	1
AH Orionis	12.5 –13.9	1948 Dec. 1 (13.5:); 1949 Feb. 19 (13.3:)	1
AI Orionis	13.4 –15.2	1948 Dec. 30 (13.5)	1
AK Orionis	13.1 –14.6	1948 Dec. 28 (13.0)	1
AM Orionis	12.7 –15.3	1949 Feb. 16 (13.5)	2
AN Orionis	11.0?–12.0?	1948 Dec. 16 (11.5:)	2
AQ Orionis	13.6 –14.8	1949 Feb. 16 (13.7)	2
AR Orionis	13.9 –15.1	1949 Feb. 13 (14.0:)	3
AZ Orionis	12.8 –15.2	1948 Dec. 30 (12.6); 1949 Feb. 4 (12.8)	1
EZ Orionis	11.0 –13.0?	1948 Dec. 12 (11.2:)	3
Brun 340	13.3 –15.0	1948 Dec. 2 (12.9)	1
Brun 467	13.8 –15.5	1949 Jan. 3 (12.4:); 1949 Feb. 8 (12.4)	1
Brun 522	13.7 –14.5	1949 Feb. 4 (12.7:)	4
Brun 532	15.3 –16.5	1949 Feb. 18 (14.5:)	1
Anon.	13.3 –$\leq$16*	1948 Nov. 16; 1949 Feb. 17 (14.0:)	5

* The ranges are photographic, as observed by Rosino, except for AD Orionis and the new variable, for which the magnitudes are visual. The range given for AD Orionis is that of the *General Catalogue* of Kukarkin and Parenago. The maximum magnitude for the new variable was determined on the Yerkes plates, while the minimum magnitude was estimated from visual observations with the 82-inch reflector.

NOTES TO TABLE 1

1. Variability confirmed on 40-inch plates.
2. Variability not confirmed.
3. Outside area covered by 40-inch plates.
4. Probably variable.
5. New variable. The variability of this star was discovered on the 40-inch plates. It lies about 5″ southeast of Brun 786 (= BD −5°1328) and was probably not discovered earlier because of its proximity to that star. It seems to remain faint for a considerable part of the time. The maxima are broad: a well-observed one in 1911–1912 lasted at least 100 days. During that time the star varied in light by about 1 mag.

was generally such that an appreciable portion on either side of the stellar spectrum was exposed only to the nebular background, in order to be able to differentiate between stellar and nebular emission lines. The observations are summarized in Table 1. The estimated spectral types are given in Table 2. Classification of the absorption spectra is difficult because of the presence of the nebular emission lines on nearly all plates. On the spectrograms of TU, AD, and AK Orionis, the nebular continuum as well was strong enough to interfere seriously with classification. A type such as "K0 ±" means that the assigned spectral type may be as much as half a spectral class in error. A luminosity classification of "IV or V" means that the star is definitely fainter than class III.

FIG. 1.—The Orion nebula, with the variable stars observed spectroscopically at the McDonald Observatory marked. The stars TU, AD, and AK Orionis are in the overexposed region near the Trapezium, just above the center. The numbers refer to the catalogue of Brun. (Lick Observatory photograph.)

Emission lines appear in eleven of the nineteen stars observed, and possibly in one more. No emission lines were found on a plate of EZ Orionis taken at the Lick Observatory in 1945, but on the McDonald plate taken in 1948 the emission lines at H and K are fairly conspicuous. This may indicate that the presence or absence of emission cannot be considered a permanent characteristic of these stars. An effort has been made to make the estimated intensities of Table 2 an index of the strength of the emission lines with respect to the underlying stellar continuous spectra rather than simply of their appearance on the negatives; but this may not have been entirely successful because of the considerable variation in density of the individual spectra. The strongest stellar emission lines appearing in these stars are the hydrogen lines and H and K of *Ca* II. In those cases in which the

TABLE 2

SPECTRA OF ORION NEBULA VARIABLE STARS

Star	Spectral Type	Intensity of Stellar Emission Lines
TU Orionis	K0±	No emission observed
YZ Orionis	Nearly continuous*	Strong
AA Orionis	K±	No emission observed
AD Orionis	Not classifiable†	No emission observed
AG Orionis	Continuous	Very strong
AH Orionis	K0, V	No emission observed
AI Orionis	Not classifiable‡	No emission observed
AK Orionis	G	No emission observed
AM Orionis	Continuous	Very strong
AN Orionis	K0–K1, IV	Weak
AQ Orionis	K0±	No emission observed
AR Orionis	Not classifiable§, ‖	Strong
AZ Orionis	K3–K5, IV or V	Weak
EZ Orionis	G, V	Medium
Brun 340	Nearly continuous*	Strong
Brun 467	K0±	Medium
Brun 522	K0–K2, IV or V	Weak?
Brun 532	Not classifiable‡	Medium?
Anon.	Continuous	Moderately strong

* A late-type spectrum is faintly visible.
† Nebular spectrum too strong for classification of stellar spectrum.
‡ Spectrum too weak for classification.
§ Lunar spectrum prevents classification.
‖ AR Orionis has a companion about 2″ distant.

star appears superimposed on a bright nebular background, the nebular hydrogen emission completely masks the stellar hydrogen lines, and only at the K line can the stars be examined for emission. This is the case, in particular, for TU, AD, and AK Orionis. However, the bright K line, judging from those stars where nebular interference is not serious, is usually weaker than the lower Balmer lines. Therefore, some of the stars in which no emission line was found at K may very well possess hydrogen emission which would be observable if the nebular lines were not so intense.

The spectra of the stars exhibiting emission lines deserve description in slightly more detail.

YZ Orionis.—The hydrogen emission lines are narrow and are visible as far as *H*8; the K line of *Ca* II is quite faint. *He* I λ 4471 is present.

AG Orionis.—The hydrogen lines are strong and rather diffuse; the decrement is slow. They are easily seen under the nebular emission. The K line is weaker than H + *He*. The spectrum shows no absorption lines.

AM Orionis.—The hydrogen lines are very strong and can be seen as far as *H*8. The K line is somewhat weaker than H + *He*. *He* I λ 4471 is present. There is no sign of absorption lines.

AN Orionis.—A weak, sharp emission line is present near the center of the absorption K line.

AR Orionis.—The hydrogen lines are visible as far as *H*8. The bright K line is weaker than H + *He*.

AZ Orionis.—*Hβ* appears as a weak emission line, while absorption *Hγ* is filled in.

EZ Orionis.—Slightly diffuse emission lines are present in the centers of absorption H and K. *Hβ* is bright, and absorption *Hγ* is filled in by emission.

Brun 340.—The nebular emissions conceal the stellar hydrogen lines, but H and K are present in the star as very diffuse bright lines. Several weak *Fe* II lines appear, and a line is present at the position of [*Fe* II] λ 4243.

Brun 467.—H and K are bright, and possibly *He* I λ 4026 as well, but the hydrogen lines are masked by the strong nebular emission lines.

Brun 522.—Weak emission may be present in the H and K absorption lines.

Brun 532.—There is probably hydrogen emission in this star, but it is seen with difficulty because of the nebular lines.

Anon.—The hydrogen lines are bright from *Hβ* through *H*8, and K is slightly stronger than H + *He*. No absorption lines can be seen with certainty.

Neither the presence nor the intensity of emission lines in the Orion nebula variables seems to bear any obvious correlation with the brightness, light-range, or projected situation of the stars with respect to the bright nebulosity. It has been suggested that the intensity of the radiation field of the illuminating stars of the nebula at the variable in question, a measure of which is the brightness of the nebula at that point, might be an important factor in the appearance or nonappearance of emission lines in that particular star. If the local intensity of radiation is a *controlling* factor, the occurrence of variables with bright lines in their spectra in regions where the nebula is very faint (e.g., YZ, AR, AZ, and EZ Orionis) must mean that the appearance of emission is favored in those stars lying a considerable distance from the Trapezium. If this is the case, such emission-line stars as AG Orionis, Brun 340, and Brun 467 would be explained as being only projected upon bright nebulosity. The faint *Ca* II emission observed in AN Orionis may not arise from action of the nebular material but may rather be of the variety which is quite common among such late-type subgiants.[8]

Emission-line objects with spectra similar to the Orion nebula variables have been found in the Taurus-Auriga-Orion dark clouds. However, among these stars there exists a distinct group of objects which have not been observed in the nebula. These objects are typified by such variables as RW Aurigae, XZ Tauri, and Barnard 100, which possess, in addition to bright *H* and *Ca* II, rich emission spectra composed of lines of *Fe* II, *Ti* II, *Cr* II, *Fe* I, *Ca* I, etc. Since these variables are among the brightest of the Taurus emission objects, their absence in the Orion nebula does not seem to be explicable in terms of faintness. Certain of the Orion nebula variables exhibit a phenomenon observed in some of the Taurus emission objects. That is, in those variables having the strongest emission lines, either only a faint trace of absorption lines or no absorption at all is visible in the continuous spectrum. This phenomenon, which may be due to veiling by continuous emission, seems in greater or lesser degree to be a fairly common characteristic of bright-line stars in nebulosity.

The concentration of nebula variables in spectral types G and K is noteworthy. A considerable gap in spectral type seems to exist between T Orionis, type A3e*a*, and these faint variables. Published observations of variability have suggested two F-type stars

[8] I am indebted to Dr. O. J. Eggen for this last remark.

as possible members of the nebula group of variables. They are 625.1936 Orionis[6] and HD 36671.[7] It seems quite likely, however, that they are foreground objects. The F-type irregular variable RY Orionis has sometimes been considered a member of the group, but its distance from the Trapezium (2°.6) makes such an association doubtful.

Several spectrograms of the fifth and sixth stars in the Trapezium—θ^1 Orionis E and F—were obtained with 75 A/mm dispersion. The spectrum of E is composite. The G band, *Ca* I λ 4226, and the *Fe* I lines of a G-type star are present; but at the shorter wave lengths the wide Balmer lines of an early-type star become conspicuous under the nebular emission. A sharp K line, presumably that of the early-type star, is superimposed upon the broad line of the G-type star. The line *He* I λ 4026 is visible in absorption under the nebular line. The early-type star is about type B5 or B8. Scattered light from the near-by θ^1 Orionis A and the strong nebular emission lines make more accurate classification difficult. Star F can be classified, with considerably more confidence, as of type B8.

I am indebted to Drs. G. P. Kuiper and O. Struve for the opportunity to work at the Yerkes and McDonald observatories and to the National Research Council for the award of a Fellowship for 1948–1949.

[6] P. M. Ryves, *A.N.*, **261**, 9, 1936.

[7] J. Gallo, *Pop. Astr.*, **39**, 267, 1931; *Tacubaya Bol.*, No. 13, 1931. Although listed as of type B9 in the *Henry Draper Catalogue*, HD 36671 is a metallic-line star.

THE VARIABILITY OF THE SPECTRUM OF UPSILON SAGITTARII

JESSE L. GREENSTEIN
Mount Wilson and Palomar Observatories
Received September 1, 1949

ABSTRACT

Line intensities measured on high-dispersion spectra of υ Sagittarii obtained in the last ten years have been used to determine the possible variation of the spectrum during the radial-velocity cycle. After reduction of the equivalent widths for possible systematic plate errors, the lines of *Ti* II have been found to vary out of phase with those of the other elements. Most lines tend to be strong at phases from 10 to 80 days. No other general variation of excitation or ionization is found. The variation of *Ti* II is not due to change of temperature alone. No large reflection effects are found near eclipse of the visible star. The suspected negative-velocity components of the Balmer lines are weak or absent.

The absorption-line spectrum of the observable star (which we will call the "primary") in the spectroscopic binary system of υ Sagittarii (HD 181615, 6) is known to be subject to some variation.[1, 2, 3, 4, 5] Hydrogen emission lines with P Cygni absorptions occurred at several active epochs, and at other epochs the normally strong lines of the ionized metals are said to have been appreciably weakened with respect to the high-excitation lines of *He* I and *Mg* II. A series of high-dispersion coudé spectra (2.8 A/mm) has been obtained in the last ten years in the region $\lambda\lambda$ 3700–4900. All are provided with the regular step-slit spectral calibration. A journal of the observations is given in Table 1; it will be noted that different emulsions were used and that the exposure ratio (calibration/star) averaged about 0.07 on the older plates. Since the characteristic curve of a photographic plate is a function of exposure time, systematic errors in the equivalent widths may occur. However, since this ratio of exposure times varied only from 0.03 to 0.12 on the older plates, useful results on relative intensities can probably be obtained; the absolute values of the equivalent widths may not be systematically correct.

Inspection[4] of these high-dispersion spectra revealed pronounced changes in the contours of many lines and, on two occasions, clearly visible doubling of some lines of *Fe* II, *Cr* II, *Ti* II, but none of this series of plates showed the spectrum in a stage of great activity, as described by J. S. Plaskett[3] or W. P. Bidelman.[5] No P Cygni components or sharp, deep "shell" lines are found. The only emission lines in the blue-violet are very weak, broad lines of *Fe* II; $H\beta$ and $H\gamma$ show no observable emission.

In the absence of gross changes, the possible systematic variation of the spectrum around the cycle of the radial-velocity orbit has been studied. R. E. Wilson[6] found $P = 137^{d}9$, eccentricity $e = 0.087$, $\omega = 28°6$. Conjunctions of the stars occur at phases of approximately 20 and 96 days in Wilson's orbit. (This scale of phases is used in Table 1.) The visible spectrum belongs completely to the primary, which would be eclipsed near 20 days. S. Gaposchkin,[7] from estimates on Harvard patrol plates, believes the star to be a β Lyrae variable of small range (0.15 and 0.08 mag.) with the observed "primary" behind at *secondary* minimum. If this is true, the invisible component is of higher surface brightness than the primary is. It was suggested previously[4] that the secondary may be hot enough either to provide excess excitation for the primary's

[1] A. J. Cannon, *Harvard Ann.*, **56**, 108, 1912.
[2] A. C. Maury, *Harvard Bull.*, No. 824, 1925.
[3] J. S. Plaskett, *Pub. Dom. Ap. Obs. Victoria*, **4**, 1, 1927.
[4] Greenstein and Adams, *Mt. W. Contr.*, No. 738; *Ap. J.*, **106**, 339, 1947.
[5] W. P. Bidelman, *Ap. J.*, **109**, 544, 1949.
[6] *Lick Obs. Bull.*, **8**, 132, 1914.
[7] *A.J.*, **51**, 109, 1945.

atmosphere or to ionize a common envelope which provides diffused ultraviolet radiation. On the first hypothesis a large reflection effect would occur in the spectrum; on the second, a smaller one. The highest temperature should occur near 20 days. Bidelman[5] has made a similar suggestion and asserted that the rare P Cygni eruptions have occurred near this same phase.

SPECTROPHOTOMETRY

A spectral region near $H\gamma$ (λλ 4326–4353) and another, λλ 4461–4584, were chosen. The equivalent widths, W, of fifty-one substantially unblended lines were measured on thirteen plates. The measured equivalent widths, when classified by elements, gave data for separate discussions of groups of lines of *Fe* II, *Ti* II, and *Cr* II; all these lines arise from lower metastable levels. The measures of strong lines like $H\gamma$, λ 4471 *He* I, and λ 4481 *Mg* II are individually reliable. A few lines of *Mg* II, *S* II, *Cl* II, and *Si* III were available; these arise from highly excited normal lower levels. A differential intensity variation of the metastable and normal lines would be evidence for shell or envelope phenomena.

TABLE 1

JOURNAL OF OBSERVATIONAL MATERIAL

Plate Ce	Emulsion	Exposure (Cal/Star)	JD 2400000+	Phase (Days)	Plate Quality	Line Quality
2086	Hi-Speed	0.04	29500	58	Strong	Double
2132	103-O	.03	29536	94	Strong	.....
2784	103-O Bkd	.12	30484	77	Good	Sharp violet
2791	103*a*-O	.07	30509	102	Weak	Double ??
2799	103*a*-O	.10	30511	104	Very strong	Wide double
2815	103*a*-O	.07	30541	134	Good	Sharp violet
2835	103*a*-O	.08	30571	26	Very strong	.....
2871	103*a*-O	.07	30629	84	Strong	Sharp red
3779	103*a*-O Bkd	.07	31579	68	Good	Sharp red
3962	103-O Bkd	.07	31715	66	Weak	.....
5648	103-O	.53	33050	21	Good	.....
5731	II*a*-O Bkd	.75	33085	76	Good	.....
5736	II*a*-O Bkd	0.47	33086	77	Good	

Reduction of the spectrophotometric observations proved rather complex. Since small differential variations are looked for, the use of the intensities measured on each plate would introduce unnecessarily large scatter. It is quite common to find systematic deviations in equivalent widths of as much as 20 per cent between plates of the same star taken with the same instrument; even larger effects may be expected with the short calibration exposure times and the variety of emulsions. Further, the observed changes in line shape may reflect a true change in kinetic temperature and thus in the curve of growth and the equivalent widths. It was thought best to reduce all line intensities to a system corresponding to the mean of the thirteen plates. For each line, i, a gross mean over all plates, $\bar{W}_i$, was obtained. The ratio of the actual intensity, W_{ik}, on the kth plate to this mean was defined as α_{ik}. The mean ratio of all n lines on a given plate to their standard intensities was then found, as follows:

$$\beta_k = \frac{1}{n}\sum_{i=1}^{n} \alpha_{ik} . \qquad (1)$$

Now a β_k deviating from unity could represent either a systematic error of the equivalent widths due to errors in the spectrophotometric calibration or a true strengthening or

weakening of the average intensities of all the lines on a given plate. Figure 1, giving the observed β_k's, shows that there is considerable scatter of the mean measured line intensity. There is a slight trend for $\beta_k > 1$ for phases 80–110 days, but the scatter is large. Two plates taken two days apart, Ce 2791 and 2799, disagree badly ($\beta = 0.99$ and 1.29). Many lines are strongly doubled on Ce 2799 and may actually be enhanced in intensity; nevertheless, Ce 2086 also has double lines and $\beta = 0.96$. Lines with asymmetries longward or shortward (R and V in Fig. 1) scatter above and below $\beta = 1$. It seems probable that the photometric accuracy is not sufficient to establish the reality of systematic variations from plate to plate; the amplitude of the observed mean variations is 15 per cent or less. It is, of course, not certain that variations repeat from cycle to cycle.

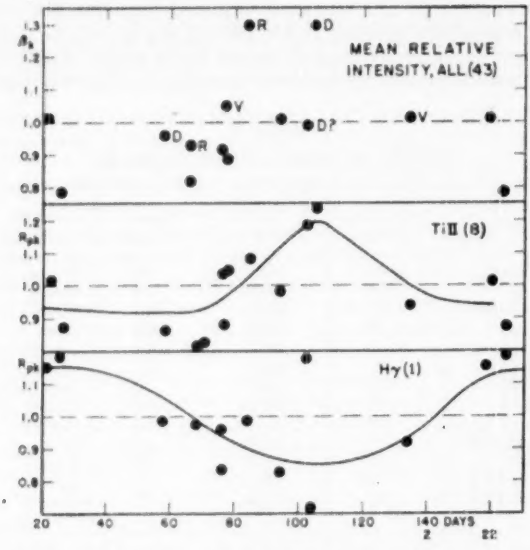

FIG. 1.—*Upper:* The mean relative intensity of all lines, β_k, on each plate. The symbol R means that the lines are sharp on the longward side, V shortward, D double. *Middle and lower:* The mean relative intensity R_{pk} for *Ti* II and $H\gamma$ on each plate, after correction by the factor $1/\beta_k$.

The variation of the intensity of one group of lines with respect to another group is detectable, even if of smaller amplitude, since possible systematic photometric errors may be removed. Define the relative intensity of a group of lines, p, on a given plate k as R_{pk}:

$$R_{pk} = \frac{1}{p\beta_k} \sum_{i=1}^{p} a_{ik} . \qquad (2)$$

The mean ratio in equation (2) should be unity when $p = n$; furthermore, the mean ratio over all values of k should be unity. Thus R_{pk} is a measure of the relative intensity which forces certain values to be greater than unity if others are less; it must either scatter or oscillate about $R = 1$. The relative intensities of the forty-three strongest lines have been computed and plotted in Figures 1 and 2. Smooth freehand curves were then drawn to give the best fit to the observed points. The equivalent widths ranged from 0.03 to 0.77 A; since the lines are intrinsically wide (i.e., about 0.5 A), the weak lines

are so shallow that their accuracy is low. The average deviation of R_{ik} for a single line from the mean of all lines of the given group, R_{pk}, on the given plate can be estimated from *Fe* II, where eighteen lines per group define a good mean R_{pk}. The deviation is found to be about ± 8 per cent. The average deviation of the plotted *Fe* II points from a smooth curve, if the latter represents a real systematic variation, should be about 2 per cent, which is close to the observed value. For *Ti* II we expect ± 3 per cent and for a single line like *Hγ* or *He* I, λ 4472, about ± 8 per cent. The actual scatter in the figures seems to be greater and may represent differences from cycle to cycle. Inspection of the data did not suggest any differences between strong and weak lines (which could result from a change of the curve of growth) but does suggest that the internal scatter within the group of *Ti* II lines on a plate is greater than in the *Fe* II group.

DISCUSSION

The ionization in *υ* Sagittarii is high, the metals and hydrogen being at least singly ionized. Thus an increase of temperature or a decrease of pressure might reduce the

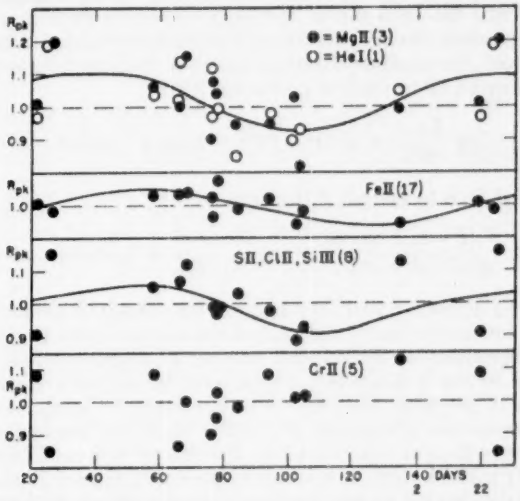

FIG. 2.—The corrected mean relative intensity, R_{pk}, for various elements in *υ* Sagittarii

effective numbers of singly ionized atoms. A differential effect will remain as a function of excitation potential (EP). The second ionization potentials (IP) of *Mg*, *Ti*, *Cr*, and *Fe* are 14.97, 13.6, 16.6, and 16.16 volts, respectively, while the excitation potentials of the lines used are about 10, 1, 4, and 3 volts. Thus differential ionization effects may be small, but excitation effects large. We would expect *H* and *Mg* II to behave similarly and *Ti* II , *Cr* II, and *Fe* II to form a separate group. A third group of high-excitation elements exists which has EP about 15 volts for *S* II and *Cl* II, 19 volts for *Si* III, and 21 volts for *He* I.

While considerable scatter remains in Figures 1 and 2, there is little doubt that *H*, *He* I, *Mg* II, *Fe* II, *S* II, *Cl* II, and *Si* III vary more or less in phase. Both high and low IP are represented in elements whose intensities, *R* (relative to their own respective mean intensities over the cycle), vary over the cycle but still preserve the same ratios to one another in any phase in the variation. This would appear visually as a general cyclic strengthening and weakening of these lines. The relative constancy of *Cr* II and *Fe* II is

noteworthy; it is clear that *Ti* II is the only representative of a variation with opposite phase. *Ti* II reaches a maximum near 105 days, while the other elements have minima near 112 days. (This coincidence of time is partly forced on the material by the averaging process used in the formation of the β_k's.) This phase corresponds to a time when the primary is receding from the earth between "eclipse" of the secondary and quadrature. The *Ti* II minimum and the maxima of the other elements near 40 days are roughly a half-cycle later. The primary eclipse should occur at 20 days, near to, but apparently not coincident with, the time of the *Ti* II minimum or the maxima of the other elements. It is fairly certain that the phase 20 days does not correspond to any outstandingly high intensity of lines of high excitation potential. The recent plate Ce 5648 was taken on the day of primary eclipse (21 days) and has an *R* of 1.01 for *Mg* II, 0.97 for *He* I, and 0.91 for the *S* II, *Cl* II, and *Si* III group—i.e., a normal spectrum for lines of high excitation. Thus we may exclude any large reflection effect in which the invisible, assumedly hot, secondary produces a "hot-spot" at the substellar point. Further, we cannot ascribe the low-excitation metallic lines to streams of matter between the stars, made visible near eclipse, since they should then show a strong maximum near 20 days.

We cannot describe the variation of *Ti* II with respect to *Fe* II as a simple temperature effect. Let us assume that *Fe* and *Ti* are dominantly doubly ionized.[8] If statistical weights are neglected, the number of excited atoms of the singly ionized element of second ionization potential IP in state of excitation EP is

$$\log \frac{N_{2,\,\mathrm{EP}}}{N_2} = \theta\,(\mathrm{IP} - \mathrm{EP}) - \tfrac{5}{2}\log T + \mathrm{const}\,. \tag{3}$$

The ratio of excited *Fe* II to excited *Ti* II yields

$$\log \frac{N\,(Fe\ \mathrm{II},\ 3\ \mathrm{volts})}{N\,(Ti\ \mathrm{II},\ 1\ \mathrm{volt})} = \log \frac{N_2\,(Fe)}{N_2\,(Ti)} + 0.56\,\theta + \mathrm{const}\,. \tag{4}$$

The variation of *Fe* II relative to *Ti* II has a semiamplitude of about 18 per cent, and these strong lines are on the nearly flat part of the curve of growth. Consequently, the variation in the logarithm of the relative number of atoms is about ± 0.3. Thus the change in θ should be nearly 0.5, which is impossibly large. The variation in, say, *Si* III, is not larger than 10 per cent; since its ionization change is small, this corresponds to an excitation temperature change of $\delta\theta < 0.01$. It is not impossible that the *Ti* II variation represents a type of departure from thermodynamic equilibrium in the ionization. The IP of *H* I is 13.54 volts, in near-coincidence with that of *Ti* II, 13.6 volts. Thus excessive Lyman continuous emission might have a particularly large ionizing effect on *Ti* II, without affecting *Fe* II and *Cr* II (16 volts). Further, *Mg* II, with IP = 15 volts, has a high excitation potential and need not reflect in its intensity variation merely an ionization change, since it is sensitive to excitation processes. This hypothesis as to the weakening of *Ti* II may be consistent with the earlier suggestion that both stars are moving in an ionized hydrogen envelope which is visible in the strong stationary *Hα* emission line.[9]

COMPONENTS OF THE BALMER LINES

It has been suggested[3, 5] that there existed outward-moving streams of hydrogen which produced several displaced absorption components of the Balmer lines. In a star described as hydrogen-poor[5] such streams would be of great interest. Plaskett[3] found components at -150, -200, and -300 km/sec to be present at all phases in the velocity-curve of the primary. This excludes their interpretation as streams moving from the

[8] J. L. Greenstein, *Ap. J.*, **91**, 438, 1940.

[9] Greenstein and Merrill, *Mt. W. Contr.*, No. 723; *Ap. J.*, **104**, 395, 1946.

primary to the secondary, since such streams would be visible only at primary eclipse, as is observed[10] in many "contact" binaries, e.g., β Lyrae. These streams are not clearly observed in the present set of plates, and their reality was doubted in earlier work[8] in the ultraviolet portion of the spectrum. In the region studied photometrically, only $H\gamma$ is available, and no shell or P Cygni structure is detectable. Since absorption lines do exist shortward of $H\gamma$ and other Balmer lines, a review of the present evidence as to the permanence of outward streaming is desirable. However, it can be safely asserted from

TABLE 2

POSSIBLE DISPLACED COMPONENTS OF THE BALMER AND *He* I LINES

Line	Predicted λ	Observed λ	Identification Ce 2132, 2815	Probable Identification
$H\beta$	58.92			
	58.11			
	56.49	56.18 (2)	*Cr* II .19 (20)	*Cr* II
$H\gamma$	38.30	38.72 (2)	*Fe* II .70 (p)	*Fe* II
	37.58	37.91 (5)	*Ti* II .92 (50)	*Ti* II
	36.13	36.70 (1)	*N* I .48 (5)	*
$H\delta$	99.73	99.99 (5)	*N* I .94 (9)	*N* I
	99.04			
	97.68	97.52 (3)	*Fe* II .51 (1), *N* III .31 (10)?	*Fe* II
$H\epsilon$	68.09	68.53 (8)	*Ca* II .47 (350)	*Ca* II
	67.42	67.51 (1-0)	*Fe* I .42 (8)	*Fe* I ?
	66.10	66.26 (2)	*Fe* II .43 (p)	*Fe* II+*He*?
3965	62.78	62.71 (1-0)		†
	62.12			
	60.80	60.93 (3)	*Fe* II .90 (3)	*Fe* II
3889	86.96	87.00 (0)	*Fe* I .05 (15)	*Fe* I
	86.31	86.29 (2)	*Fe* I .28 (40)	*Fe* I
	85.01	84.79 (2)	*V* II .85 (50)?	‡
$H\eta$	33.42	33.60 (2n)	*He* I .57 (1)	*He* I
	32.78	33.02 (1n)	*Fe* II .02 (p)	*Fe* II
	31.50	31.41 (1n)	*S* II .41 (3)	*S* II
$H\theta$	96.00	96.37 (1-0)	*Si* III .11 (4)	§
	95.37	95.47 (4)		‖
	94.11	94.34 (1)	*V* II .37 (50)	*V* II

* Not *N* I, but λ discrepant for *H* component.
† Possibly displaced *He* I?
‡ *V* II possible +(*H* + *He* I) component?
§ Not *Si* III alone but λ discrepant for *H* component.
‖ Too strong for *H* component.

Ce 5648, taken at primary eclipse (21 days), and Ce 2835 (25 days) that no enhancement of the lines shortward of $H\gamma$ occurred. We have no evidence as to whether sporadic outbursts or streams occur preferentially[5] at eclipse. Inspection of all thirteen plates showed no enhancements of lines shortward and close to $H\gamma$, $H\delta$, $H\epsilon$, and $H\zeta$.

Let us assume that streams occur at −150, −200, and −300 km/sec. Then Table 2 gives the predicted wave lengths of the displaced components and our measured[4] wave lengths (at phases 94 and 134 days) of near-by observed stellar lines. These measures have an average deviation of about ±0.03 A. Two metastable *He* I lines, λ 3889

[10] O. Struve, *Ap. J.*, **93**, 104, 1941.

(blended with $H\zeta$), and λ 3965, have been included, since these should be sensitive to the existence of dilution.

The remarks in the last column of Table 2 represent the most probable identification of the line at the measured stellar wave length. The results of the attempt to identify displaced components of *H* or *He* I in Table 2 are not encouraging. Since the spectra are poor near $H\beta$, failure of a component to appear there is not conclusive. For some of the other Balmer lines, possible components exist near each of the velocities given by Plaskett. Unfortunately, in no case is there a given velocity component near every Balmer line; for example, the component at −200 km/sec is absent in four lines. In general, the lines shortward of the hydrogen lines are well identified with metallic, *He* I, or *N* I lines, except perhaps λ 4336.70, which does not agree with the predicted position of an $H\gamma$ component; λ 3966.26, which may be blended with *Fe* II; and λ 3884.79, which is blended with *V* II. Thus there seems to be no positive evidence on our plates for the reality of the displaced hydrogen components; though not certainly excluded, they seem to be weak or absent at present (as well as in the 1939 McDonald series).

The sporadic variations of the line contours were previously[4] noted. In Figure 1 the nature of the line asymmetries or doublings is indicated; these are not simply correlated with phase in the orbit or with the general strength of the spectrum; on Ce 2799, where $\beta = 1.29$, all lines were, however, exceptionally strong. If the spectrum is intrinsically variable from cycle to cycle, it is quite possible that the intensity variations which we obtain are accidental features, not cyclic. For example, the *Ti* II enhancement on Ce 2791 and 2799 could result from the line doubling, which may indicate the presence of streams of metastable *Ti* II atoms in the upper atmosphere of the star. (Note that these are *not* streamings toward or away from the secondary, but nearly at right angles to it.) These sporadic streams have velocities of only ±12 km/sec and therefore are not related to the hydrogen components.

CONCLUSION

If we take the intensity variations shown in Figures 1 and 2 at their face value as the average behavior over many cycles, we find that the spectrum comes from one stellar atmosphere and has variations that do not exceed 15 per cent and are usually less than 10 per cent. The level of ionization and excitation is essentially constant. The metal with the lowest second ionization and excitation potentials, *Ti* II, tends to be weak when the visible star might be eclipsed and strongest half a cycle from that phase. No exact coincidence with eclipse times occurs. The total relative change of *Ti* II with respect to *He* I, *Mg* II, and *H* may attain 25 per cent. There is no phase at which the so-called F2 spectrum (actually about A0) disappears. The variation of this A0 spectrum involves a differential out-of-phase effect between *Ti* II and *Fe* II; the variation of *Fe* II with respect to the *He* I (or B3 spectrum) is small and in phase.

If the weakness of *Ti* II is considered to be due to increased second ionization, it is difficult to explain as normal thermal ionization. If superexcitation and ionization exist in υ Sagittarii, they are not caused by a simple reflection effect from an invisible hot companion, which would produce a systematic increase in ionization and excitation at phase 20 days. The high-excitation lines vary only slightly with phase; hence reflection cannot be dominant in the superexcitation. Either the system is enveloped in a nebulous envelope rich in ultraviolet emission, or chromospheric phenomena exist connected with a high kinetic temperature. Small variations in kinetic temperature around a cycle are possible if the star moves through a gaseous envelope at high speeds.

I am deeply indebted to Dr. Walter S. Adams for permission to use his long series of high-dispersion spectra and for valuable discussions of the variability of the spectra of shell stars.

THE VELOCITY-CURVE OF R CANIS MAJORIS*

O. STRUVE AND BURKE SMITH
Yerkes Observatory and McDonald Observatory
Received September 14, 1949

ABSTRACT

A new velocity-curve was obtained at the McDonald Observatory between November, 1948, and January, 1949. The elements resemble those obtained by Jordan in 1908–1912, but the amplitude is slightly greater, and the mass function is also greater. Nevertheless, the conclusions of Jordan and of Sitterly regarding the mass ratio of this system are confirmed.

The eclipsing binary R Canis Majoris, HD 57167, $\alpha = 7^h14^m.9$, $\delta = -16°12'$ (1900) has been observed by many photometric workers. S. Gaposchkin[1] has listed the following photometric elements: $A_1 = 0.56$ mag., $A_2 = 0.06$ mag., $L_b = 0.93$, $r_b = 0.25$, $k = 1.02$, $i = 76°.6$, Spec. = F0, ratio of surface brightness = 12.2. Dugan[2] found that the period had shortened abruptly in 1913–1914 and gave, as the elements,

$$\text{Principal minimum} = \text{JD } 2422030.6375 + 1^d.135939E\,.$$

TABLE 1

STAR LINES

λ	Element	λ	Element
3849.97	*Fe* I*	4215.52	*Sr* II†
3856.37	*Fe* I*	4226.73	*Ca* I
3878.58	*Fe* I*	4233.17	*Fe* II
3913.46	*Ti* II*	4250.79	*Fe* I
3933.66	*Ca* II*	4260.48	*Fe* I
3956.68	*Fe* I*	4290.03	*Cr* I+*Ti* II†
4005.25	*Fe* I	4299.24	*Fe* I†
4045.82	*Fe* I	4307.87	*Ti* II+*Fe* I†
4057.36	*Fe* I	4314.08	*Sc* II*
4063.60	*Fe* I†	4325.76	*Fe* I
4067.05	*Ni* II	4337.05	*Fe* I†
4071.74	*Fe* I	4340.47	*Hγ*
4077.71	*Sr* II*	4351.76	*Fe* II
4101.74	*Hδ*	4383.55	*Fe* I†
4118.55	*Fe* I*	4395.03	*Ti* II
4132.06	*Fe* I†	4404.75	*Fe* I†
4143.50	Fe I	4443.80	*Ti* II†
4167.27	*Mg* I†	4481.23	*Mg* II
		4528.62	*Fe* I†

* Indicates a line was measured only on CQ plates.
† Indicates a line was measured only on CG plates.

From observations with a photoelectric photometer, F. B. Wood[3] concluded that there was a further shortening of the period and adopted, as the light-elements,

$$\text{Principal minimum} = \text{JD } 2422030.6375 + 1^d.135938E\,.$$

* *Contributions from the McDonald Observatory, University of Texas*, No. 182.

[1] *Variable Stars* ("Harvard Observatory Monographs," No. 5 [Cambridge: Harvard College Observatory, 1938]), p. 68.

[2] *Contr. Princeton U. Obs.*, **6**, 49, 1924, and **19**, 34, 1939.

[3] *A.J.*, **48**, 185, 1940, and *Contr. Princeton U. Obs.*, **21**, 31, 1946.

He suggested that a period of 1.135937 days be used for predictions of minima during the next few years, as there were indications that the change in period was continuing. This value has been used in computing the phases of Table 2.

The star is of special interest not only because of the abrupt change in period but because of the low value obtained for the mass function. Spectrographic elements based on velocity-curves have been published by F. C. Jordan[4] and B. W. Sitterly.[5] The present results are based on forty-two spectrograms taken during the period November 17,

TABLE 2

RADIAL VELOCITIES OF R CANIS MAJORIS

Plate	Date	U.T.	Phase	Velocity (Km/Sec)	No. of Lines
	1948				
CQ 7178	Nov. 17	10:19	0.801	−17.9	25
7179	17	10:38	.813	−22.4	25
7304	Dec. 5	6:47	.518	−35.8	25
7306	5	8:17	.572	−36.4	24
7307	5	8:53	.594	−22.7	25
7308	5	9:38	.622	−23.7	25
7309	5	10:12	.643	−17.8	25
7310	5	10:50	.666	−20.3	24
7311	5	11:29	.689	−11.5	24
CG 7335	7	9:32	.379	−55.4	26
7336	7	9:58	.394	−59.7	25
7337	7	10:19	.408	−38.4	24
7338	7	10:39	.420	−49.1	25
7339	7	11:00	.432	−52.0	20
7340	7	11:20	.445	−50.8	23
7354	10	6:49	.920	−17.2	24
7355	10	7:07	.931	−29.1	25
7356	10	7:26	.943	−28.1	26
7357	10	7:42	.953	−25.6	25
7361	10	9:14	.009	−36.1	24
7362	10	9:37	.023	−56.9	23
7363	10	9:57	.035	−55.6	26
7364	10	10:21	.049	−49.9	28
7365	10	10:43	.063	−57.5	28
7379	11	6:05	.773	− 5.4	19
7382	11	8:49	.873	−20.6	27
7383	11	9:50	.911	−21.2	20
7399	15	6:40	.316	−70.9	26
7400	15	7:08	.333	−68.2	23
7401	15	7:40	.352	−62.6	29
7402	15	8:12	.372	−56.2	29
7403	15	9:01	.402	−48.6	26
7404	15	9:32	.421	−51.8	27
7405	15	10:04	.440	−46.1	28
7406	15	10:38	.461	−46.7	25
7407	15	11:25	.490	−48.0	23
7408	15	11:50	.505	−36.9	24
7425	20	9:44	.831	−18.0	25
7426	20	10:02	.842	−17.6	27
7427	20	10:22	.854	−20.1	26
7428	20	10:45	.868	−12.5	28
	1949				
7471	Jan. 2	6:28	0.154	−71.6	22

[4] *Allegheny Obs. Pub.*, **3**, 49, 1916.

[5] *A.J.*, **48**, 190, 1940.

1948, to January 2, 1949, with the 82-inch McDonald telescope equipped with the standard Cassegrain spectrograph. Nine spectrograms (CQ series), were taken with the 500-mm glass camera and quartz prisms, dispersion 55 A/mm at $H\gamma$, and thirty-three spectrograms (CG series), were taken with glass prisms, dispersion 26 A/mm at $H\gamma$. Only the spectrum of the brighter component is visible on these plates. Table 1 gives the wave lengths of the star lines used in determining the radial velocities. On the CG plates, only lines from λ 4005 to λ 4528 were measured, while with the CQ plates lines

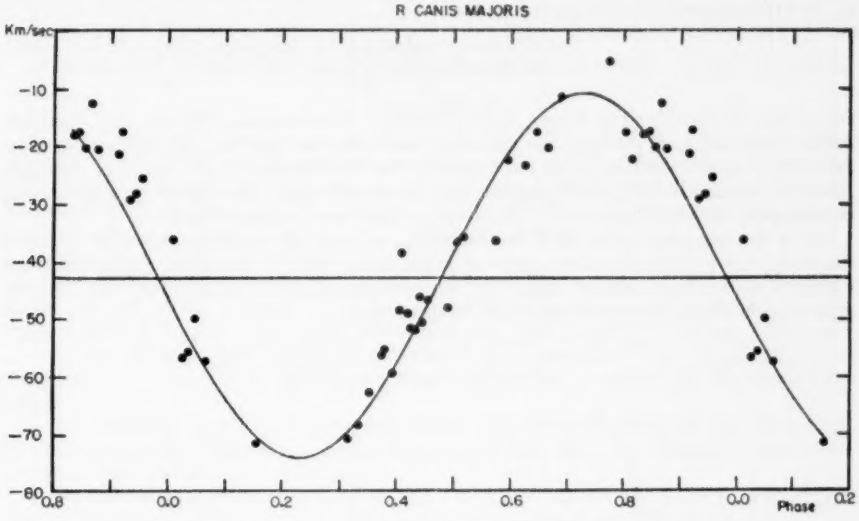

FIG. 1

TABLE 3

	Allegheny (1908–1912) (Jordan)	Mount Wilson (1929–1931) (Sitterly)	McDonald (1948–1949)
e	0.138	0.013	0.0
γ (km/sec)	−39.7	−34.8	−42.5
K (km/sec)	28.6	24.0	31.5
$a \sin i$ (km)	443,000	374,000	491,000
$f(m)\odot$	0.0027	0.0016	0.0037
No. of plates measured	49	22	42

from λ 3850 to λ 4481 were measured. There were found to be no systematic differences between velocities measured from lines near the violet end as compared to lines near the red end of the spectrum.

Table 2 gives the measured radial velocities, with the date, phase, and number of lines measured per plate. The velocities are plotted in Figure 1; the scatter is large, although the spectrum is not particularly poor. This large scatter is also apparent in the work of Jordan and of Sitterly.

Both Sitterly and Jordan adopted a small eccentricity, but Sitterly concluded, after discussion of the material, that e is equal to zero, or very small. Wood also states that his photometric observations give no indication of appreciable $e \cos \omega$. It is evident from Figure 1 that our observations give a value for e which is close to zero. In view of the large scatter, we have not undertaken a solution by least squares but have derived the circular elements shown in Table 3 for this curve.

It will be noted that our results are in better agreement with those of Jordan than with those of Sitterly. The most important difference seems to be in the semi-amplitude, K, and consequently in the mass function,

$$f(m) = \frac{m_2^3 \sin^3 i}{(m_1 + m_2)^2}.$$

Our value is considerably larger than Sitterly's. Nevertheless, Wood's and Jordan's earlier conclusions regarding the peculiar mass ratio in this system are not greatly affected. It is not possible, as yet, to conclude that the velocity-curve changes, although Sitterly's results in 1929–1931 suggest that the amplitude of the curve may have been considerably smaller than twenty years before and twenty years later.

With the assumed value of $P = 1^d.135937$ and with the velocity-curve as we have drawn it, the γ-axis crosses the curve at phase 0.48, which is 0.023 day earlier than the epoch of mid-eclipse derived from the photometric elements. One plate, CG 7361, at phase 0.009 shows the spectrum of the brighter star.

Ca II EMISSION IN LAMBDA AND ZETA ANDROMEDAE*

LIVIO GRATTON†
McDonald Observatory and Observatory of La Plata, Argentina
Received April 28, 1949

ABSTRACT

A discussion of the behavior of the calcium emission lines in λ And and ζ And is given, together with a discussion of other binary systems showing calcium emission lines.

There appears to be a period-luminosity relationship among late-type binaries having *Ca* II emission.

INTRODUCTION

It is well known that many stars of spectral types G, K, and M show a reversal of the H and K lines of *Ca* II on long-exposed spectrograms of sufficient dispersion. The case of α Boo has been known for a long time, and Adams and Joy[1] observed the reversal in several stars. Wellman measured the corresponding profiles[2] in α Boo and α Ori and gave a theory based upon Unsöld's interpretation of spectroheliograms.[3]

The emission lines of *Ca* II found in several late G- or early K-type binaries seem to have a different origin. Struve and Hiltner[4] have given good grounds for thinking that these lines are connected with the binary character of the stars and are limited to two regions near the bulges of the tidally distorted stars. The following facts favor this model:

a) These emission lines are much stronger than those observed in single late-type stars such as α Boo, being real emission lines rather than a reversal of the absorption lines.

b) The binaries which show *Ca* II emission lines are indifferently giants, subgiants, and dwarfs; apparently, there is no connection between the intensity of the lines and other physical characteristics.

c) In some eclipsing binaries, such as RZ Cnc,[5] RW UMa,[6] and RS CVn,[4] the *Ca* II emission exhibits an eclipse effect, which is difficult to understand without the hypothesis that it is isolated near the bulges of the distorted star.

d) There is only one single star, 56 Peg,[7] with *Ca* II emission of an intensity comparable to that of the binaries, but even this star has been suspected of possessing a variable radial velocity,[8] so that it might possibly be a binary of long period and small range.

In 1947 Hiltner[4] listed thirteen eclipsing binaries with *Ca* II emission. Apparently, he was not aware that a few spectroscopic binaries show the same phenomenon. These are rather bright stars and therefore may be studied in greater detail. Table 1 contains these additional stars; for completeness, 56 Peg is included, although its binary character needs confirmation.

λ ANDROMEDAE

Orbits of this spectroscopic binary were computed by Burns[9] from observations made at Lick and by Martin[10] from observations made by Henroteau at Ottawa. Both sus-

* *Contributions from the McDonald Observatory, University of Texas*, No. 185.

† Fellow of the Italian National Research Council.

[1] *Pub. A.S.P.*, **41**, 311, 1929; **43**, 407, 1931.

[2] *Zs. f. Ap.*, **19**, 236, 1939; **20**, 214, 1940.

[3] *Ap. J.*, **69**, 275, 1929.

[4] See Hiltner, *Ap. J.*, **106**, 481, 1947.

[5] W. A. Hiltner, *Pub. A.S.P.*, **58**, 166, 1947.

[6] O. Struve, *Ann. d'ap.*, **9**, 1, 1946.

[7] P. C. Keenan and J. L. Greenstein, *Ap. J.*, **96**, 309, 1942.

[8] W. W. Campbell, *Lick Obs. Bull.*, **6**, 149, 1911.

[9] *Lick Obs. Bull.*, **4**, 87, 1906; *Ap. J.*, **24**, 345, 1906.

[10] *Merate Contr.*, No. 4, 1928.

pected a variation in the elements,[6] but Luyten[11] showed that the Lick observations are consistent with constant elements; the Ottawa observations are of rather low accuracy. The *Ca* II emission was independently discovered at Merate in 1939 and at Victoria in 1938–1943, although λ Andromedae had been listed by Adams and Joy among stars showing H and K in emission.[1] The Victoria observers computed a new orbit, which represents the radial velocities measured at Lick and at Victoria[12] quite satisfactorily; details of this unpublished investigation were kindly communicated by Dr. Pearce. The following are the Victoria elements:

P,	$20^d.5215 \pm 0.0002$	γ,	$+6.88 \pm 0.13$ km/sec
T,	22758.626 ± 0.490	K,	6.65 ± 0.20 km/sec
e,	0.073 ± 0.028	$a \sin i$,	1,871,000 km
ω,	$311°.0 \pm 12.8$	$f(m)$,	0.0006

According to Dr. Pearce, the radial velocities from the emission lines agree perfectly with those from the absorption lines.

During my stay at the McDonald Observatory in 1948 I obtained thirty good spectra of this star with the Cassegrain spectrograph (two quartz prisms, 500-mm camera). Five spectra obtained at Merate in 1940 with a Zeiss glass spectrograph and a 48-cm

TABLE 1

SPECTROSCOPIC BINARIES WITH *Ca* II EMISSION

Star	Sp.	P (Days)	Reference
ζ And	G7	17.77	Emission discovered by writer; orbit, Spencer Jones, *Ann. Cape Obs.*, **10**, Part 8, 37, 1928
o Gem	K1p	19.60	Eberhard and Schwarzschild, *Ap. J.*, **88**, 292, 1938
HR 7428	cG6	108.6	Bidelman, private communication
56 Peg	cK0		Keenan and Greenstein, *Ap. J.*, **96**, 309, 1942
λ And	G7	20.52	Walker, *J.R.A.S. Canada*, **38**, 249, 1944; Gratton, *Merate Contr.*, Nuova serie, No. 17, 1944
Lal. 46867	G8p	6.72	Sanford, *Ap. J.*, **53**, 221, 1921

camera, giving a dispersion of some 30 A/mm at $H\gamma$, and seven spectra taken by H. Weaver at the McDonald Observatory in 1943 were also available. The latter were kindly lent to me for measurement. Table 2 shows the radial velocities from the absorption and the emission lines.

Table 3 contains the wave lengths used to reduce the McDonald spectrograms; they are somewhat different from the ones usually used for a K star, since the spectra were exposed for the H and K region.

The probable error derived from the internal agreement of plates taken on the same night is ± 1.4 km/sec for the absorption lines (14 lines) and ± 2.4 km/sec for the emission lines (2 lines). The 1940 observations are of higher accuracy; the usual error from a single plate of a star with lines as sharp as those in λ And is between ± 0.7 and ± 1.0; for the emission lines the corresponding probable error should be between ± 1.0 and ± 1.3.

The radial velocities from the absorption lines agree well with Pearce's elements, and no new determination of the orbit was thought necessary. The radial velocities from the emission lines agree with those from the absorption lines, on the average, but the individual values seem to differ rather more than would have been expected from the internal agreement of the measures. Moreover, by examining the plates in a comparator, it was

[11] *Pub. Minnesota Obs.*, Vol. 2, No. 1, 1934.

[12] E. C. Walker, *J.R.A.S. Canada*, **38**, 249, 1943.

found that the width of the emission lines varied slightly from one night to another in an irregular way. The decrease in width appeared asymmetrical, as if the lines were double, but at times the intensity of one of the components was much less than that of the other, causing a shift in the mean wave length. However, as this effect was not noticed by the observers at Victoria, too much importance cannot be given to this observation.

During a short visit to the Mount Wilson Observatory in July, 1948, through the courtesy of Dr. Merrill I was allowed to look at a plate of λ And taken with the coudé

TABLE 2

RADIAL VELOCITIES OF λ ANDROMEDAE

JD 2,400,000+	Phase	V_{abs}	V_{em}	JD 2,400,000+	Phase	V_{abs}	V_{em}
29942.33	1.18	+16.1	.....	32701.97	10.94	+ 0.9	− 2.5
54.31	13.16	− 0.2	+ 3.9	06.97	15.94	+ 3.0	+ 7.9
65.31	3.64	+13.0	+ 8.2	06.97	15.94	+ 4.3	+10.9
66.24	4.57	+13.4	+ 9.0	06.97	15.94	− 0.1	+ 7.9
67.22	5.55	+12.8	+ 6.8	06.97	15.94	+ 3.3	+ 4.9
30713.53	13.08	− 9.2	− 1.0	07.88	16.85	+ 5.5	+ 6.4
15.54	15.09	+ 5.5	− 4.3	07.88	16.85	+ 7.0	+ 9.4
16.54	16.09	+ 3.8	− 0.9	07.88	16.85	+ 5.2	+ 1.9
17.56	17.11	− 2.6	− 3.0	07.88	16.85	+ 3.7	− 0.1
18.56	18.11	+ 8.3	+ 6.4	12.96	1.41	+16.4	+15.6
19.53	19.08	+13.8	+ 8.8	12.97	1.42	+11.7	+18.6
25.55	4.58	+12.7	+14.9	12.97	1.42	+15.4	+14.1
32687.98	17.47	+ 7.1	+ 5.9	12.97	1.42	+12.8	+23.1
88.93	18.42	+ 9.4	+ 9.3	15.89	4.34	+12.9	+15.5
90.97	20.46	+13.0	+20.8	15.89	4.34	+ 9.5	+14.0
90.98	20.47	+10.7	+17.8	15.89	4.34	+10.2	+11.0
96.97	5.94	+ 8.0	+10.8	15.90	4.35	+ 6.7	+ 6.5
99.97	8.94	+ 3.5	+ 3.2	16.94	5.39	+11.4	+14.3
700.97	9.94	+ 6.6	+ 5.8	16.95	5.40	+ 9.8	+ 8.3
00.97	9.94	+ 6.7	+ 7.3	16.95	5.40	+11.6	+15.8
01.96	10.93	+ 3.5	+ 4.0	16.95	5.40	+14.9	+11.3

TABLE 3

WAVE LENGTHS FOR λ AND ζ ANDROMEDAE

λ	Element	λ	Element	λ	Element
3865.53	*Fe*	3953.88	*Fe, Co*	4018.11	*Mn, Fe*
3878.21	*Fe*	3956.68	*Fe*	4045.83	*Fe*
3895.66	*Fe*	3986.95	*Mg, Mn, Co*	4063.60	*Fe*
3902.96	*Fe, Cr*	3989.87	*Fe, Ti, Cr*	4071.75	*Fe*
3944.02	*Al*	4005.25	*Fe*		

dispersion (10 A/mm). On this plate the H and K lines appeared as very strong double emission lines superimposed on the ordinary broad absorption. With the same dispersion many other late-type stars showed H and K in emission, but the whole appearance of the lines was very different from that in λ And. In the majority of the stars examined the lines appeared triple, with one component stronger and more separated from the other.

In λ And the shape of the emission suggested two emission components of nearly the same intensity whose separation corresponded to a velocity of 28 km/sec. The phase of this plate according to Pearce's elements was 8.61 days. Among those stars which I could

examine at Mount Wilson, only 56 Peg had an emission structure similar to, although fainter than, λ And.

It is tempting to interpret the two observed components as originating in the two tidal bulges of the star; if such were the case, the difference in radial velocity would be a rotational effect. Assuming the period of rotation to be identical with the period of revolution, 20.5 days, and the stars to be elongated along the line joining the centers, we get for the distorted radius of the primary

$$R \sin i = 1.47 \times 10^7 \text{ km}.$$

According to Morgan, Keenan, and Kellman,[12] λ And is a subgiant of spectral type G8, and it is G7+ according to Mount Wilson; the trigonometric parallax is $+0''.037 \pm 0''.007$ and the spectroscopic parallax $0''.040$ (Mt. Wilson). We may assume $0''.038$ as a well-established mean value. The visual absolute magnitude, then, is +1.9 and the bolometric, +1.5; the mean radius should be 6.2 solar radii or 4.3×10^6 km. The inclination is unknown, but it is certainly small because of the very small value of the mass function. The value of $R \sin i$ from the supposed rotational effect is thus in strong disagreement with the expected mean radius of the star. The absorption lines of λ And are unusually sharp and cannot be reconciled with a large rotational velocity.

There is the possibility that the matter responsible for the emission is detached somewhat from the star and extends much farther than the chromosphere. But in this case the Victoria observers ought to have noticed the doubling of the emission at certain phases, and even on my spectra the appearance of the lines should show larger variations than those observed. We are left, therefore, with the conclusion that the observed doubling is due to a cause different from rotation. Probably a series of observations with high dispersion will be necessary to settle this point.

Dr. P. C. Keenan[14] observed this star in the infrared with the grating spectrograph of the Perkins Observatory and kindly communicated to me his results; he states that "the *Ca* II triplet is not in emission, but the lines are definitely weaker in absorption than in a normal G8 giant and look much as they usually do in an early G-type star. I suppose that they may be weakened by incipient emission and perhaps at other times the emission components could be seen."

ζ ANDROMEDAE

Orbits of ζ And were computed by J. B. Cannon from fifty-eight plates of the Dominion Observatory, Ottawa,[15] and by H. Spencer Jones from thirty-three plates of the Cape Observatory; Spencer Jones computed a definitive orbit by combining the Ottawa and Cape series of observations.[16] My own observations were made with the Cassegrain quartz spectrograph of the McDonald Observatory; the results are shown in Table 4.

Adding these new observations and five older determinations of the radial velocity from the Lick Observatory to those used by Spencer Jones, I computed differential corrections to his elements. I found it necessary to add a systematic correction of −2.3 km/sec to my velocities and one of +6.0 km/sec to the Ottawa determinations (also found by Spencer Jones). The corrections are small and probably only that to the period is significant. The velocity-curve is shown in Figure 1.

The corrected elements are found in Table 5, second column. The eccentricity is practically zero; therefore, a new solution was made, assuming a circular orbit and the previously determined period. The corresponding elements are shown in Table 5, third column; the epoch T is the time of zero orbital velocity on the ascending branch of the radial-velocity-curve.

[12] *An Atlas of Stellar Spectra* (Chicago: University of Chicago Press, 1943).

[14] Private communication.

[15] *Pub. Dom. Obs. Ottawa*, Vol. 2, No. 6, 1915. [16] *Ann. Cape Obs.*, Vol. 10, Part 8, 35, 1928.

The absorption lines of ζ And are diffuse and suggest a noticeable rotational velocity.

I discovered the emission lines on spectrograms taken at Merate; no previous mention of them has been found in the literature. Their radial velocity agrees reasonably well with that from the absorption lines. The intensity of the *Ca* II emission is a little less than in λ And and was found to be practically constant except on Plates 7050 and 7051, on which they were much fainter than average; these plates were taken near the γ-velocity

TABLE 4

RADIAL VELOCITIES OF ζ ANDROMEDAE

JD 2,400,000+	Phase (Days)	V_{abs}	V_{em}	JD 2,400,000+	Phase (Days)	V_{abs}	V_{em}
32716.98	9.85	−17.2	−17.2	32726.97	2.07	−37.8	−38.9
18.97	11.84	− 0.6	+ 7.3	27.97	3.07	−42.5	−56.5
18.97	11.84	+10.9	+ 8.8	27.97	3.07	−45.8	−46.8
19.97	12.84	− 1.9	+ 2.5	30.97	6.07	−44.5	−45.0
20.96	13.83	+ 4.8	+ 5.3	30.97	6.07	−42.8	−45.5
20.97	13.84	+ 6.6	+15.3	32.97	8.07	−28.3	−26.8
25.97	1.07	−21.4	−26.8	32.97	8.07	−31.3	−29.7
25.97	1.07	−28.9	−21.8	33.97	9.07	−21.6	−28.2
26.97	2.07	−43.1	−45.9	33.97	9.07	−21.9	−20.2

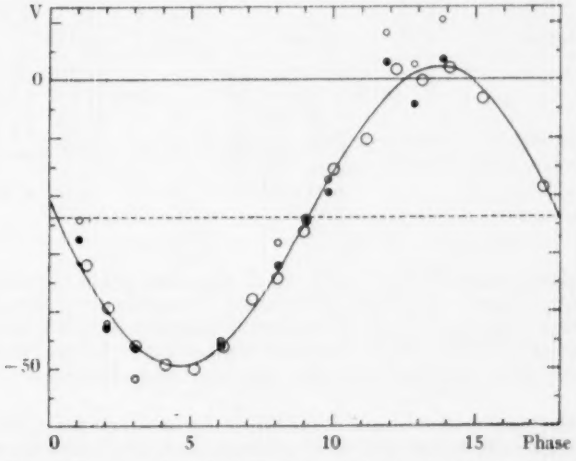

FIG. 1.—Radial-velocity-curve for ζ And. The large circles are the normal places used for computing the orbit. The small circles and dots are daily means of the McDonald radial velocities for emission and absorption lines, respectively. The velocities from absorption lines have been corrected by −2.3 km/sec.

on the descending branch, that is, at the time when the faint (unseen) companion was in front. This observation is confirmed by another plate taken on the preceding night, which, although unsuited for a radial-velocity determination, clearly shows the fainter H and K emission.

It is well known that ζ And is a variable of small amplitude. Stebbins[17] determined a photoelectric light-curve which agrees with the phases computed from the radial-velocity

[17] *Pub. Washburn Obs.*, 15, 29, 1928.

observations. He found that it was not possible to separate an eclipse effect from the ellipsoidal variation; the light-curve establishes an 8 per cent elongation of the brighter component.

From Stebbins' observations it is probable that the two stars are nearly in contact. This is consistent with my spectroscopic observations, if we interpret the fading of the emission lines as due to an eclipse effect.

We may put

$$R_1 + R_2 = (a_1 + a_2)\cos i\ ,$$

where R_1 and R_2 are the stellar radii and a_1 and a_2 the orbital radii for the bright and faint star, respectively. Practically, R_1 and R_2 are identical with the polar radii of the distorted stars; we shall take them equal to the radii of an average star of the same mass and luminosity.

Quite generally, expressing the period P in days, the masses $\mathfrak{M}_1$ and $\mathfrak{M}_2$ in solar masses, and the orbital radii in 10^6 km, we have

$$a_1 + a_2 = 2.93 P^{2/3} \mathfrak{M}_1^{1/3} (1 + r)^{1/3}, \qquad a_1 = 2.93 P^{2/3} \mathfrak{M}_1^{1/3} \frac{r}{(1 + r)^{2/3}},$$

where $r = \mathfrak{M}_2/\mathfrak{M}_1 = a_1/a_2$. ζ And is a G8 giant (Mt. Wilson); its trigonometric parallax is $+0''.034 \pm 0.006$, and the Mount Wilson spectroscopic parallax is $0''.014$. We shall

TABLE 5

ORBITS OF ζ ANDROMEDAE

Elements	I. Sol.	II. Sol.
P	$17^d.7692 \pm 0.0002$	$17^d.7692 \pm 0.0002$
T	2432476.128 ± 0.032	2432751.617 ± 0.001
γ (km/sec)	-23.79 ± 0.61	-23.71 ± 0.28
K (km/sec)	25.97 ± 0.38	26.33 ± 0.41
e	0.013 ± 0.068	0.00 assumed
ω	$80°.98 \pm 0.64$	
$a_1 \sin i$	6.34×10^6 km	6.43×10^6 km
$f(m)$	0.0323	0.0337

assume the weighted mean $0''.020 \pm 0.003$, which gives the visual absolute magnitude $+0.8 \pm 0.3$. Using Kuiper's empirically determined bolometric corrections,[18] we get the absolute bolometric magnitude $+0.3$. The effective temperature of a gG8 star is 4380°, and the corresponding radius is $R_1 = 12.6$ solar radii or 8.8×10^6 km. The most probable value of the mass, obtained from the empirical mass-luminosity relation,[19] is $\mathfrak{M}_1 = 2.7 \odot$.

Substituting the numerical values of P and $\mathfrak{M}_1$ in the equations for a_1 and $a_1 + a_2$, we get the values in Table 6, second and third columns, as a function of the mass ratio r.

Assuming $a_1 \sin i = 6.43 \times 10^6$ km, we obtain the values of the inclination i in the fourth column and of $R_1 + R_2$ in the fifth. As we already know R_1 and $\mathfrak{M}_1$, we obtain the values of R_2 and $\mathfrak{M}_2$ shown in the sixth and seventh columns.

From an inspection of this table it is seen that the best agreement with the mass-luminosity relation for normal stars is obtained with an r between 0.285 and 0.290. Taking, tentatively, $r = 0.29$, I find the orbital elements $a_1 = 6.8$, $a_1 + a_2 = 30.2$, $i = 71°$.

We next inquire whether these elements are consistent with Stebbins' light-curve. A detailed analysis would be difficult and would not be warranted by the many uncer-

[18] *Ap. J.*, **88**, 429, Table 9, 1938.

[19] G. P. Kuiper, *Ap. J.*, **88**, 472, 1938.

tainties in the data; we shall therefore satisfy ourselves with the following rather crude discussion.

The equipotential surfaces of the Roche model are given by

$$\frac{1}{1+r}\frac{1}{r_1}+\frac{r}{1+r}\frac{1}{r_2}+\frac{x^2+y^2}{2}=\text{Const.}$$

Here r_1 and r_2 are the distances from the centers of the two stars; x, y, and z are rectangular co-ordinates in a system with the origin at the center of gravity, the x-axis passing through the centers of the stars and the z-axis normal to the plane of the orbit.

TABLE 6

DATA FOR THE SYSTEM OF ζ ANDROMEDAE

r	a_1	a_1+a_2	i	R_1+R_2	R_2	$\mathfrak{M}_2$
0.270	6.39×10^6	30.0×10^6	.....	.....	.....	0.73
.275	6.49	30.1	82°	4.2×10^6	.....	0.74
.280	6.59	30.1	77	6.7	.....	0.76
.285	6.69	30.2	74	8.4	.....	0.77
.290	6.75	30.2	71	9.8	1.0×10^6	0.78
.30	6.98	30.3	67.0	11.9	3.1	0.81
.32	7.38	30.4	60.5	15.0	6.2	0.86
.35	7.95	30.7	54.0	18.1	9.3	0.94
.40	8.87	31.0	46.5	21.3	12.5	1.08
.45	9.74	31.4	41.3	23.6	15.8	1.2
.50	10.59	31.8	37.4	25.3	17.5	1.4
0.60	12.17	32.4	31.9	27.5	18.7	1.6

TABLE 7

PRINCIPAL RADII AND SURFACE GRAVITY FOR ζ ANDROMEDAE

	x_1	x_2	y	z
R	0.3002	0.2986	0.2958	0.2910
g	8.1059	8.3021	8.6129	9.2101

The co-ordinate system is supposed to be rotating with the stars, and the unit of length is $a_1 + a_2$. Assuming $r = 0.29$, we find that the surface of the primary is given by

$$\frac{0.775}{r_1}+\frac{0.225}{r_2}+\frac{x^2+y^2}{2}=2.9046,$$

if it coincides with an equipotential surface of the Roche model. Table 7 gives the corresponding radii in the x, y, and z directions, together with the values of the surface gravity (in arbitrary units); x_1 is directed toward the companion and x_2 in the opposite direction.

The brightness of the star at any instant is proportional to the projected surface area multiplied by the mean surface brightness. The ratio of the surface area at the times of the "eclipses" to that at the times of the maxima of the light-curve may be taken as equal to the ratio of the corresponding equatorial diameters,

$$\frac{R(x_1)+R(x_2)}{2R(y)}=1.0122$$

(it is actually smaller because of the inclination).

According to von Zeipel's theorem,[20] in a rotating star the surface brightness at any point is proportional to the local value of the gravity, g; we should therefore take a mean value of g over the visible surface of the star; but, as we are concerned only with orders of magnitude, we shall assume for g at the time of maxima the value along the y-axis; at the time of "primary eclipse" that corresponding to x_1; and at the "secondary eclipse" that corresponding to x_2. This approximation is better than one might think on account of the effect of limb darkening. However, we must take into account not the integrated light but that corresponding to the wave length of maximum sensitivity for Stebbins' photoelectric cell, viz., 4600 A. One easily obtains, for the ratio of the brightness,

$$\gamma_1 = 1 + \tau\left(1 - \frac{g_{x_1}}{g_y}\right) = 1.101\,, \qquad \gamma_2 = 1 + \tau\left(1 - \frac{g_{x_2}}{g_y}\right) = 1.064\,;$$

$$\tau = \frac{c_2}{4\lambda T\,(e^{-c_2/\lambda T} - 1)}\,,$$

where T is the mean temperature, 4380°, and $\lambda = 4600$ A. The corresponding Δm's for the two minima are then 0.104 and 0.067. Those obtained from the photoelectric light-curve are 0.10 and 0.07, respectively. The agreement shows that the adopted model works satisfactorily.

The rotational velocity of the bright component comes out to be 34 km/sec, which is consistent with the observed width of the absorption lines. The doubling of the emission lines near the maximum and minimum of the velocity-curve should amount to about 1 A, or 0.022 mm on our spectra; this is only a little below the resolving power of the equipment. Actually, at these phases the lines are distinctly wider than the lines of the comparison spectrum of the same photographic density and give a definite impression of being an unresolved pair.

Finally, one might ask whether a difference in g amounting to 6 per cent—or 4 per cent between the tidal bulges and the equatorial direction perpendicular to them—or a difference about twice as great between the bulges and the pole is sufficient to produce the temperature gradient necessary to cause the observed emission lines. I have given a formula[21] for the velocity of the currents to be expected in a rotating star because of the impossibility of fulfilling the conditions imposed by von Zeipel's theorem; a similar formula was given also by Eddington.[22] Applying this formula to the present case, I find that we should expect a velocity of the order of $10^{-12}/\rho$ km/sec near the bulges, ρ being the density of the atmospheric layers. This evaluation might be uncertain by a factor of 10 or even 100, so that we may conclude that the currents thus originated might be large enough to cause the local inversion of the thermal gradient which is required for explaining the emission lines. The currents are much stronger near the bulges, which may explain the localization of the observed emission.

A CORRELATION BETWEEN PERIOD AND LUMINOSITY FOR BINARIES SHOWING *Ca* II EMISSION

If the emission lines are connected with the tidal distortion of the stars, we must expect the giants showing emission to have longer periods than the dwarfs. We might, in fact, expect all stars with a tidal distortion larger than a given value to show the emission lines; if we neglect the variation of the mass, this leads to the condition

$$\frac{R}{a_1 + a_2} > k$$

[20] See, e.g., Z. Kopal, *Eclipsing Variables* (Cambridge, Mass.: Harvard College Observatory, 1946).

[21] *Merate Contr.*, Nuova serie, No. 19, 1945. [22] *M.N.*, **90**, 54, 1929.

for emission lines, where e is a constant and R the radius of the star. This is seen to be equivalent to

$$\frac{R}{P^{2/3}} > k_1 ,$$

where k_1 is a new constant. If we consider only stars of the same spectral type, R is proportional to the square root of the luminosity. In an absolute-magnitude-period diagram, all the binaries showing emission lines will thus lie above the line

$$0.3M + \log P = \text{Const} .$$

TABLE 8

ABSOLUTE MAGNITUDES OF BINARIES SHOWING *Ca* II EMISSION LINES

Star	Sp.	P (Days)	π_{tr}	M_{ap}	Luminosity	M_{ad}	Component Showing Emission
ζ And	G8	17.77	+0″034± 6	+0.4	g	+0.8±0.3	.....
RZ Eri	F5+G8	39.28	+ 12±11	+3	subg	+2 ±2	Secondary
SS Cam	gG1+dF5	4.82	.....	.....	d	.....	Secondary
AR Mon	K0	21.21	− 2±10	.....	g or c	0 ±1	Primary
σ Gem	K1p	19.60	+ 18± 6	+0.5	.....	+0.5±0.3	.....
RU Cnc	F9+G9	10.17	.....	.....	d?	.....	Secondary
RZ Cnc	K2+K5	21.64	.....	.....	g	+1.5±2	Primary
RW UMa	dF9+G9	7.33	.....	.....	subg	+2.5±2	Secondary
RS CVn	F4p+dG8	4.80	+ 48±12	+4.5	d	+6.0±1	Secondary
SS Boo	dG5+dG6	7.61	.....	.....	d	+5 ±2	Secondary
WW Dra	G2+K0	3.50	.....	+2.1	subg	+2.0±1	Secondary
Z Her	F2+F2	3.99	.....	.....	.....	.....	Secondary
AW Her	K2+G4	8.80	.....	.....	.....	.....	Secondary
HR 7428	cG6	108.58	.....	−1	c	−1 ±1	.....
RT Lac	G9+K1	5.07	+ 23±6	.....	subg	+4 ±1	Both
AR Lac	G5+K0	1.98	.....	.....	.....	.....	K star
56 Peg	cK0	Unknown	.....	−1.6	c	.....	.....
λ And	G7	20.52	+ 37± 7	+2.3	subg	+2.0±0.3	.....
Lal. 46867	G8p	6.72	+ 33± 5	+5.2	d	+5.0±0.3	.....

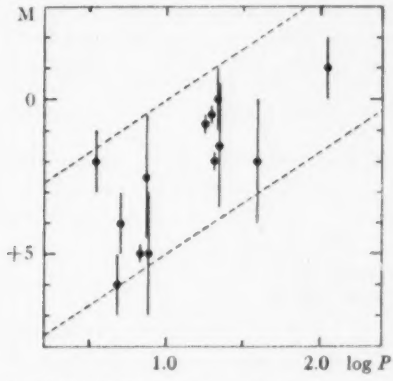

FIG. 2.—Correlation between M and P for binaries showing *Ca* II emission. The points refer to individual stars, the length of each line being equal to twice the estimated error of the absolute magnitude. The two dotted lines correspond to the equations $0.3\ M + \log P = 1.0$ and $0.3\ M + \log P = 2.5$, respectively.

We would not expect to find stars much above the limit, because the distortion would be too great and might cause instability; it may be shown that stars above the line $0.3M + \log P = 1.0$ are practically in physical contact.

Table 8 contains the data for nineteen binaries showing *Ca* II emission. The adopted absolute magnitudes result from a discussion of the data of the preceding columns, the probable errors being an estimate of the uncertainty. In all cases the adopted absolute magnitude is that of the component showing the emission lines.

TABLE 9

MEAN PERIODS OF BINARIES WITH *Ca* II EMISSION

	P (Days)	No. of Stars		P (Days)	No. of Stars
Supergiants	108	1	Subgiants	15	5
Giants	20	4	Dwarfs	6	4

Excluding SS Cam and Z Her on account of their spectral types, 56 Peg because the period is unknown (if it is a binary), and AW Her and AR Lac for want of data concerning their absolute magnitudes, we obtain the mean periods given in Table 9.

The individual values are shown in Figure 2, RU Cnc also being excluded on account of the uncertainty in the magnitude. It is seen that there is a definite correlation between M and P; we may tentatively take as the limiting line

$$0.3M + \log P = 2.5 .$$

Although the results from λ And are somewhat inconclusive, the discussion contained in the present paper seems to favor Struve and Hiltner's model of emission confined to a limited region near the bulges of the tidally distorted star.

THE SPECTRUM OF COMET 1948I*

P. D. JOSE AND P. SWINGS
McDonald Observatory
Received July 5, 1949

ABSTRACT

Eight spectrograms of Comet 1948I, covering the range of heliocentric distances from 0.65 to 2.21 A.U., have been obtained. Sodium emission is observed at $r = 0.73$ and $r = 0.79$ A.U. At large heliocentric distances ($r = 2.21$) only CN and the λ 4050 group are observed. The CN bands show the usual complex structure due to the fluorescence excitation by solar radiation. The behavior of CH and that of CH_2 are compared. Unidentified features are present within and between the Swan bands, as well as in the yellow-red region.

Progress in cometary physics depends to a great extent on the solution to the following problems:

a) Is the λ 4050 group really and exclusively due to CH_2? Recent laboratory work by A. Monfils and B. Rosen,[1] Mme R. Herman,[2] and others and observational work by C. Fehrenbach[3] and B. Rosen[4] have definitely raised the question.

b) Is the λ 6300 group really and exclusively due to NH_2? The cometary observations by Swings, McKellar, and Minkowski,[5] J. Dufay,[6] C. Fehrenbach,[7] and Swings and Page,[8] combined with numerous laboratory investigations,[9] indicate that the cometary emission in the visual region is probably not due entirely to NH_2.

c) What are the molecules responsible for the emissions observed[10] in various comets within and between the Swan sequences of C_2?

d) What is the physical relation between the CH_2 and CH molecules?

Actually, the answers to questions *a*, *b*, and *c* also have a direct bearing on our knowledge of the stars of the latest types. Recent work by McKellar and Swings[11] has led to the tentative identification of CH_2 in the N stars. The NH_2 bands may be expected in the latest M or N stars. As for the molecules responsible for the unidentified emissions in the region of the Swan bands, they may be of interest in relation with the unidentified absorptions found in the N stars, as discussed most recently by V. Hase and G. Shajn.[12]

The bright Comet 1948I provided an opportunity for securing additional observational material pertaining to the above-mentioned questions. Eight spectrograms were obtained during the period from November 14, 1948, to February 2, 1949, using various types of spectrographs attached to the Cassegrain focus of the McDonald reflector. All

* *Contributions from the McDonald Observatory, University of Texas*, No. 176.

[1] *Nature*, **164**, 713, 1949, and private communication.

[2] *C.R.*, **223**, 221, 1946; **227**, 962, 1948; **228**, 1691, 1949.

[3] *C.R.*, **227**, 519, 1948.

[4] Private communication.

[5] *Ap. J.*, **98**, 142, 1943.

[6] *C.R.*, **222**, 51, 1946.

[7] Private communication.

[8] *Ap. J.*, **108**, 526, 1948.

[9] See references in Swings, McKellar, and Minkowski (n. 5).

[10] N. T. Bobrovnikoff, *Ap. J.*, **99**, 173, 1944, and *Pub. Lick Obs.*, **17**, 436, 1931; Swings and Page, *loc. cit.*

[11] A. McKellar, *Ap. J.*, **108**, 453, 1948; P. Swings and A. McKellar, *Ap. J.*, **108**, 458, 1948; P. Swings and K. N. Rao, unpublished.

[12] *Pub. Crimean Ap. Obs.*, Vol. **2**, 1948.

these spectrograms are of good quality, except that of December 30, which is a little weak. They cover the region λλ 3300–6600. The heliocentric distances extend over the unusually wide range from $r = 0.65$ to $r = 2.21$ A.U. The comet had passed perihelion on October 27.4, the perihelion distance being relatively small, 0.14 A.U. All the spectroscopic observations were thus made after perihelion passage, as in the case of the previous bright Comet 1947n.[8] The absolute magnitude of Comet 1948l is approximately $M = 5.9$, hence almost equal to that of the preceding bright Comet 1947n ($M = 6.2$). These two objects are of only average luminosity, since absolute magnitudes from 0 to 15 have been observed; they owed their temporary high brightness to their proximity to the sun. The essential observational data are summarized in Table 1

TABLE 1

SPECTROGRAMS OF COMET 1948l OBTAINED AT THE McDONALD OBSERVATORY

Date (U.T.)	Heliocentric Distance, r (In A.U.)	Radial Velocity Relative to Sun (dr/dt in Km/Sec)	Camera	Dispersion in A/Mm at			Projected Slit-Width in A at			Emulsion	Exposure Time (Minutes)
				λ 3880	λ 4700	λ 6000	λ 3880	λ 4700	λ 6000		
1948											
Nov. 14.506	0.648	46.7	CQ	38	70	.....	0.95	1.75	.....	103*a*-O	32
17.496	0.728	44.8	*Qf*/2	115	216	450	2.07	3.90	8.10	103*a*-E	70
19.503	0.778	43.2	*Gf*/2	45	104	247	0.81	1.87	4.45	103*a*-E	80
24.500	0.900	40.6	*Gf*/2	45	104	247	0.81	1.87	4.45	103*a*-E	90
28.507	0.999	39.3	*Gf*/1	89	208	490	1.21	2.81	6.61	103*a*-E	70
Dec. 2.500	1.081	37.5	*Gf*/1	89	208	490	1.21	2.81	6.61	103*a*-E	60
30.354	1.634	31.1	*Qf*/1	230	432	900	3.11	5.83	12.3	103*a*-E	60
1949											
Feb. 2.266	2.209	27.3	*Qf*/1	230	432	.....	4.14	7.76	.....	103*a*-O	120

GENERAL DESCRIPTION OF SPECTRUM AND BEHAVIOR WITH HELIOCENTRIC DISTANCES

All the spectrograms were taken by guiding as accurately as possible on the nucleus, which had a stellar appearance. It is thus possible to obtain a picture of the distribution of the different emitting molecules within the head. The solar spectrum reflected by the nucleus is strong on all exposures. Comet 1948l is not so favorable as several others for the detection of emissions localized near the nucleus.

The D doublet of sodium appears clearly on the spectrograms of November 17 ($r = 0.73$) and 19 ($r = 0.78$). On November 17, the D emission is long, partly due to twilight, but is strongly enhanced in the nucleus. On November 19 the emission is purely nuclear; its double character could be measured accurately. The D emission does not appear at heliocentric distances greater than 0.78

No spectrogram covers the region of the *OH* band. The *NH* band appears on the spectrogram of November 17 ($r = 0.73$), but is unusually weak. The (1, 0) band of the violet system of *CN* is not seen with certainty on any spectrogram. On two strong exposures ($r = 0.73$ and $r = 0.78$) the $^2\Sigma \rightarrow {}^2\Pi$ system of *CH* appears clearly as nuclear emission on the longward side of the strong *CN* band at λ 3880. On account of the intense solar spectrum, no conclusive evidence is found for CH^+, although λ 4254 seems to be present for $r = 0.73$ and $r = 0.78$.

As appears clearly in Figure 1, the *CN* emission extends into the head much farther

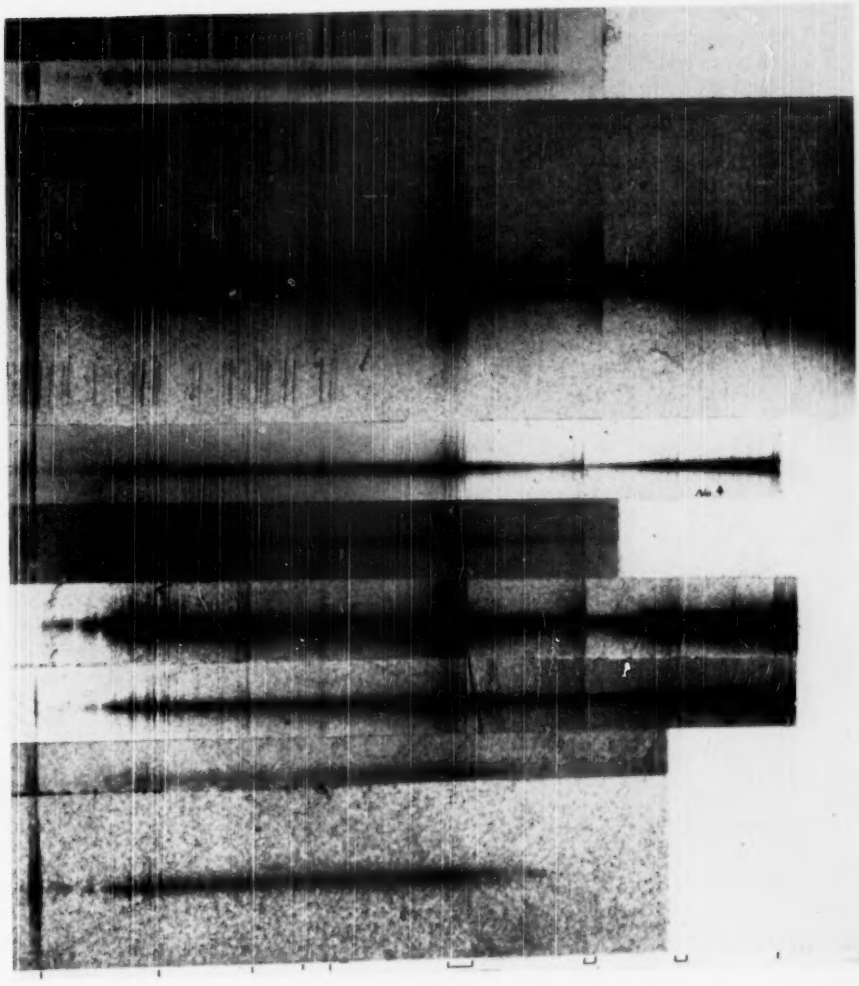

FIG. 1.—General evolution of the spectrum of Comet 1948I

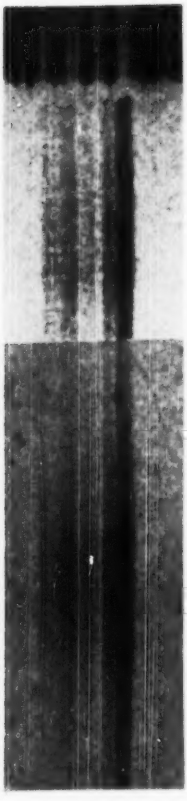

FIG. 2.—Structure of the (0, 0) band of *CN*

than does C_2. Actually, the intensity gradient along a *CN* line (as a function of distance from the nucleus) is smoother than along a C_2 band; this appears especially well on the spectrograms taken at $r = 0.73$ and $r = 0.78$. The intensity of C_2 decreases steadily, relative to *CN*, when r decreases. At $r = 0.78$ the head of the (0, 0) band of C_2 has, near the nucleus, approximately the same intensity as does the head of the (0, 0) band of *CN*. The strongest C_2 bands have practically disappeared at $r = 1.63$, and no trace of the (1, 0) band is left at $r = 2.21$.

At large heliocentric distances the only remaining conspicuous features in the region λλ 3800–5000 of the spectrum are *CN* and the λ 4050 group (see spectrogram at $r = 2.21$; cometary spectra have rarely been obtained at such large heliocentric distances). As has been emphasized in previous papers, the λ 4050 group increases steadily in intensity relative to all other molecules (except possibly the λ 6300 group)[13] when r increases. The present observations show that this intensity increase of the λ 4050 group takes place to $r = 2.21$ at least. At this large heliocentric distance λ 4052 is about as strong as the *R* branch of *CN* (0, 0) in the nuclear region. The considerable extension of *CN* stands in conspicuous contrast to the shortness of λ 4052 at $r = 2.21$.

The relative intensity behavior of *CH* and CH_2 is also clearly illustrated in Figure 1. For $r \leqslant 0.78$, λ 4313 *CH* is as strong as, or stronger than, λ 4052. The intensity ratio of *CH* and CH_2 declines steadily with increasing r; *CH* is still very weakly present for $r = 1.63$ but has practically disappeared for $r = 2.21$.

A similar comparison applies to C_2 and CH_2 or to *CN* and CH_2. For $r = 1.00$, λ 5165 C_2 is still stronger than λ 4052 but becomes weaker for $r > 1.0$. Similarly, the (0, 1) band of *CN* is stronger than λ 4052 for $r \leqslant 0.78$ but has become very weak compared with λ 4052 for $r = 2.21$.

The guiding was accurate enough for obtaining estimates of the extensions of the head in different molecules. However, the slit was not long enough to cover all the *CN* emission, so that only minimum values are obtained for this molecule. Measures made on the spectrograms of November 24, 1949 ($r = 0.90$), and February 2, 1949 ($r = 2.21$), give the following figures.

For $r = 0.90$: Diameter of $CN > 62{,}000$ km;
Diameter of $CH_2 \simeq 4140$ km.
For $r = 2.21$: Diameter of $CN > 166{,}000$ km;
Diameter of $CH_2 \simeq 22{,}000$ km.

The ratio of the diameters of CH_2 emission at $r = 2.21$ and $r = 0.90$ is 5.3, which is close to the square of the ratio of the heliocentric distances $(2.21/0.9)^2 = 6.03$. The contraction of the CH_2 zone, as the comet approached the sun, was proportional to r^2, as is required by Wurm's theory.[14] The preceding figures also illustrate the fact that the zone of CH_2 emission has a volume of the order of 3×10^{-4} that of the zone of *CN* emission or less.

STRUCTURE OF THE VIOLET CYANOGEN BANDS

The best spectrograms in the *CN* region, i.e., at $r = 0.65$ and $r = 0.78$, have been measured directly at the comparator and also on microphotometer tracings. The projected slit widths at λ 3880 are, respectively, 0.95 A for $r = 0.65$, and 0.81 A for $r = 0.78$. For $K'' > 11$ the separations between the rotational lines of the *R* branch are larger than 0.81 A, so that individual rotational lines should be observable.[15] Moreover, certain rotational lines may be reduced in intensity on account of Fraunhofer absorptions in the exciting solar radiation; this helps in bringing out individual rotational lines of the *R*

[13] The spectrogram obtained at $r = 1.63$ has poor definition in the red; for $r = 2.21$ the visual region was not covered.

[14] *Mitt. Hamburger Sternw. Bergedorf*, **8**, No. 51, 74, 1943, and references indicated in this paper.

[15] For a still higher resolution of the *CN* band see A. McKellar, *Ap. J.*, **99**, 162, 1944.

branch. Of course, the lines of the P branch are too closely packed to be separated ($\Delta\lambda <$ 0.54 A).

The measurements of the two spectrograms are in excellent agreement, although slight differences in the profiles are present. Since the radial velocity of the comet relative to the sun varies but slightly from $r = 0.65$ to $r = 0.78$, bringing about a shift of only 0.04 A in the exciting radiation, the change in the intensity distribution must be essentially due to a change in the rotational temperature of the CN molecules.

Figure 1 shows how strikingly the CN profile varies from $r = 0.65$ to $r = 2.21$. While some effect of the radial velocity certainly takes place over the wide range of heliocentric distances (from $r = 0.65$ to $r = 2.21$ the exciting radiation shifts by about 0.25 A), the main systematic variation in profile of CN is due to the decrease in rotational temperature. This point has been dwelt upon at length on previous occasions and will not be considered here again. Figure 2 shows the structures of the (0, 0) band of CN at $r = 0.65$ and $r = 0.78$. The results of the measurements are collected in Table 2.

The strongest feature is the part of the P branch from $P(9)$ to $P(22)$. Next in intensity is the group from $P(3)$ to $P(6)$, which is separated from the blend $P(9)$ to $P(22)$ by a deep minimum centered at $P(7)$. In the R branch several maxima and minima are due to blends, but there are also sharp individual rotational lines, for example, $R(13)$ and $R(16)$. Fairly high values of K'' (at least $K'' = 19$) are observed in the R branch, as is customary at small heliocentric distances. As a comparison, consider the case of Comet 1942g in which McKellar observed a maximum value of $K'' = +14$; the heliocentric distance was approximately 1.4 A.U. On our spectrogram for $r = 2.21$ the maximum K'' must be approximately 10 or even less.

While there is no doubt that the P branch is exclusively due to the (0, 0) transition of CN, a contribution of the (1, 1) transition is not excluded within the R branch of (0, 0). The origin of (1, 1) is at λ 3863.0. If, as is likely, the general rotational intensity distribution within the P and R branches of (1, 1) is the same[16] as within (0, 0), the maximum of the $P(1, 1)$ branch should arise around λ 3869, that of $R(1, 1)$ around λ 3857. It has been customary to neglect the possible effect of (1, 1), which doubtless is rather minor on account of the low vibrational temperature of the violet system of CN. However, it is not certain that the weaker features observed to the violet of λ 3859 are not partly due to (1, 1). The P branch of (1, 1) may also fill in the region around λ 3869 with a weak background of emission.

One may gather some information regarding the intensity of the hypothetical (1, 1) band by considering the (1, 0) transition at λ 3590. This (1, 0) band is not clearly present on any spectrogram of Comet 1948l, but it has been observed previously, for example, in Comet Cunningham.[17] The intensity ratio of the (1, 0) and (1, 1) transitions which arise from the same excited level should remain constant and equal to the ratio of the emission transition probabilities.[18] The theoretical[19] and laboratory[20] values of these probabilities agree to give to the (1, 1) band an intensity of from five to nine times that of the (1, 0) band.

It appears likely that the weak shortward intensity of the CN emission is due to the R branch of (1, 1), possibly with some contribution added by R lines of high K number

[16] Not considering the sharp minima due to the solar absorption lines.

[17] Swings, Elvey, and Babcock, *Ap. J.*, **94**, 320, 1941; P. Swings, *Ap. J.*, **95**, 270, 1941.

[18] Similarly, the (0, 0) and (0, 1) bands have a definite intensity ratio. But direct intensity comparisons between (0, 0) and (1, 0) or (1, 1) are precarious because the excited levels are not the same and the vibrational temperature plays an important role.

[19] Computed by A. McKellar and W. Buscombe, *Pub. Dom. Ap. Obs. Victoria*, **7**, 361, 1948, from theory developed by E. Hutchisson, *Phys. Rev.*, **36**, 410, 1930.

[20] Ornstein and Brinkman, *Proc. Kon. Akad. Wetensch., Amsterdam*, **34**, 33, 1931. In Pearse and Gaydon's *The Identification of Molecular Spectra* (London: Chapman Hall, Ltd., 1941), p. 76, the estimated intensities do not differ greatly: (1, 0), int. 8; (1, 1), int. 9.

($K'' = 20$–27) of (0, 0). At any rate, the (1, 1) transition is certainly very weak compared with (0, 0). A similar result has been obtained for Comet Cunningham,[21] in which weak lines measured at λλ 3852.0, 3854.0, and 3857.7 were attributed to the $R(7)$–$R(15)$ lines of the (1, 1) transition.

The two separate emissions at λ 3867.1 and λ 3869.2, which are blends of several R lines, arise on account of the effect of the solar absorption lines on the fluorescence pattern.[22] The whole space between λ 3867.1 and λ 3869.2 contains some weaker emission. On one plate the line at λ 3869.2 seems to show two maxima, at λ 3868.2 and

TABLE 2

STRUCTURE OF THE (0, 0) BAND OF CN

Int.	λ	Identification Notation		Remarks
1 from	3851.0			Wide weak emission with structure
1 to	3854.2	$R(20)$–$R(27)$ of (0, 0) *plus*		
0-1	3857.69	$R(7)$ –$R(16)$ of (1, 1)		Separation difficult
1-0	3858.35			
1	3859.40	$R(19)$	59.67	
Minimum	3860.60	$R(18)$	60.63	$R(17)$ is also weak
3s	3862.41	$R(16)$	62.49	Individual rotational line
5	3863.40	$R(15)$	63.38	Wider than λ 3862.4 and λ 3865.1
Minimum	3864.22	$R(14)$	64.30	
4s	3865.07	$R(13)$	65.15	Individual rotational line
Minimum	3865.89	$R(12)$	65.99	
4n	3867.12	$R(11)$	66.82	
		$R(10)$	67.62	
6n	3869.21	$R(9)$	68.41	
		$R(8)$	69.18	
		$R(7)$	69.92	
Minimum	3871.17	$R(6)$	70.67	
		$R(5)$	71.37	
3n	3872.12	$R(4)$	72.06	Some contribution of $R(5)$ and $R(3)$
4n	3873.50	$R(2)$	73.36	Some contribution of $R(3)$
		$R(1)$	74.00	
Deep min	3875.16	Origin	75.20	
7 from	3876.5			
		$P(4)$	77.35	Contributions of $P(3)$, $P(5)$, $P(6)$
to	3878.4			
Minimum	3878.87	$P(7)$	78.75	Also $P(8)$
from	3879.6	$P(9)$	3879.58	
to	3883.0	$P(22)$	3882.99	
Max. 10n	3880.46	$P(11)$	80.33	Contributions from $P(9)$–$P(22)$
Min	3881.62	$P(14)$	81.32	
		$P(15)$	81.59	
		$P(16)$	81.88	
Max. 15s	3882.02	$P(17)$	82.10	

λ 3869.7, respectively; these correspond to $R(9)$ and $R(7)$, respectively. In the emission at λ 3872.1, $R(3)$ and $R(5)$ contribute; $R(3)$ may also contribute in the emission appearing at λ 3873.5. All these contributions are affected by the profile of the exciting solar radiation.

The observed intensity distribution among the rotational lines is in complete agreement with the fluorescence mechanism.[22] The intensity minima in the R branch at $K'' =$

[21] P. Swings, *Lick Obs. Bull.*, **19**, 131, 1941

[22] *Ibid.*, and *M.N.*, **103**, 86, 1943; A. McKellar, *Rev. Mod. Phys.*, **14**, 179, 1942.

14, 12, and 6 + 5 correspond, as they should, to the minima at $K'' = 16$, 14, and 8 + 7 in the P branch. They are due to absorption lines in the exciting solar radiation shifted appreciably by radial velocity.

On one of the spectrograms the (0, 1) band shows a doubling of the P head, of the same type as in the (0, 0) band. The two intensity maxima correspond roughly to the same values as K'' as in the (0, 0) transition. Actually, all the rotational intensity distributions appear similar, although such a comparision is difficult and somewhat precarious on account of the considerable difference in intensity between (0, 0) and (0, 1). This is in agreement with the fluorescence theory, according to which the rotational intensity distributions arise from the population distributions among the excited rotational levels, as due to absorption of the complex solar radiation. The (0, 0) and (0, 1) bands have the same upper levels, hence should reveal similar rotational intensity distributions.

THE λ 4050 GROUP

The emission lines around λ 4050 definitely are not so sharp as are the individual *CH* or *CN* lines; they are not individual rotational lines of a molecule but, rather, narrow bands or blends. The emission lines have been measured on the best spectrograms; the wave lengths are in perfect agreement with those previously listed. The doubling of λ 4052 which McKellar observed in Comet 1942g (λ 4050.43 and λ 4051.75) cannot be seen clearly on our present spectrograms; this doubling corresponds to the two laboratory emissions measured by Mme R. Herman at λ 4049.9 and λ 4051.9. On one of our spectrograms we suspect a satellite, 1.2 A to the red of the strong λ 4043 line; however, the presence of a strong solar spectrum makes such a detection difficult and uncertain. Since Herzberg's work[23] it has been customary to attribute the λ 4050 group to the triatomic CH_2 radical, and there are excellent astronomical reasons favoring such an identification.[24] However, Herzberg[25] himself occasionally mentioned that the identification of CH_2 is still hypothetical and that some other molecule, such as C_2H, may also be considered possible.

The most recent laboratory work by A. Monfils and B. Rosen[1] on the fine structure of the main λ 4052 band leads to a moment of inertia which is too high for a molecule such as CH_2. This experimental investigation does not exclude the possibility that two different molecules[26] may take part in the emission around λ 4050.[27]

Fehrenbach[3] has suggested that λ 4013 and λ 4067 are too strong in Comet 1948g, compared with the laboratory, and that an emission other than CH_2 overlaps in the same region. The spectrograms of Comet 1948l do not seem to necessitate such an additional emission; λ 4013 and λ 4067 are not very strong (Fig. 3). It should be borne in mind that the profile of the CH_2 emission may, like that of *CN*, *CH*, *OH*, or *NH*, be sensitive to heliocentric distance and radial velocity. It may be understandable that different intensity distributions within the λ 4050 group could be present in different comets, or in the same comet at different heliocentric distances. For example, the intensity ratio of λ 4074 and λ 4043 may be influenced by the strong *Fe* I solar lines, in different degrees according to the radial velocity. Yet in Comet 1948l no striking difference is observed between the CH_2 profiles at $r = 0.7$ and $r = 2.2$, when proper account of the different resolutions is taken.

It is possible that a systematic examination of the intensity distribution within the

[23] *Ap. J.*, **96**, 314, 1942.

[24] P. Swings, *Rev. Mod. Phys.*, **14**, 190, 1942; *M.N.*, **103**, 86, 1943

[25] Private communication; see McKellar, *Ap. J.*, **108**, 456, 1948; T. L. Page, *Pub. A.S.P.*, **60**, 249, 1948.

[26] However, it remains true that the previously considered molecules, such as *NaH*, OH^+, *CH*, etc., are excluded for the interpretation of the λ 4050 group.

[27] In the present paper we have assumed that the λ 4050 group is due to CH_2.

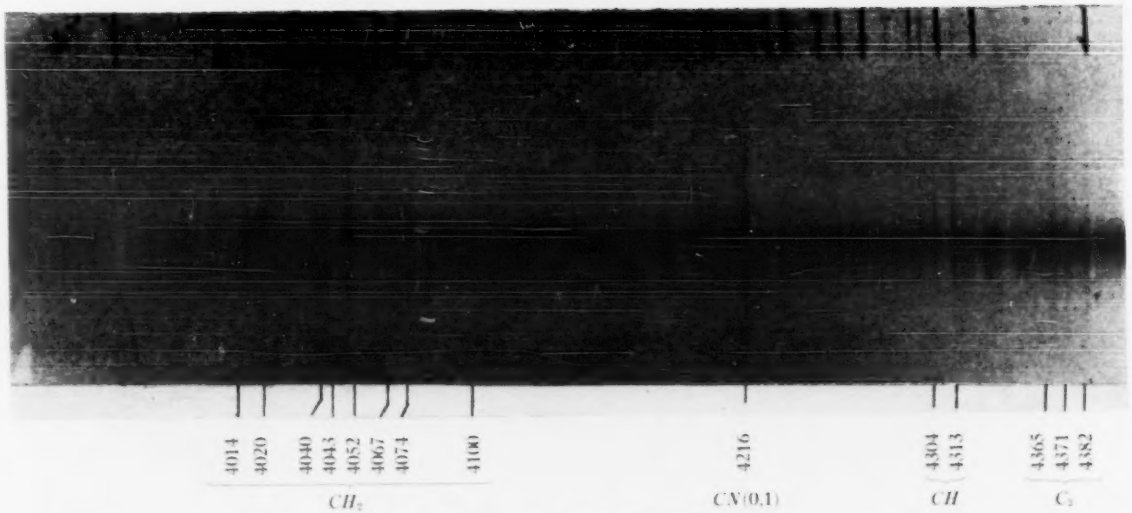

FIG. 3.—Region of the CH_2 and CH bands

λ 4050 group in different comets will reveal differences which cannot be accounted for, except by assuming the presence of two emitting molecules. But, as far as we know, the comparisons made thus far have had only a superficial character and do not warrant any convincing conclusion.

CH_2 has often been considered as the parent-molecule for CH. The intensity gradients along the lines (i.e., the intensity changes with distance from center of molecules) may thus be fruitfully compared. As appears from Figure 3, the gradients are not identical for CH_2 and CH. Both molecules are concentrated close to the nucleus, but their lines extend differently from the nucleus. The lines of CH_2 fall off in intensity less abruptly than do those of CH. It may eventually turn out that CH_2 is actually not the parent-molecule for CH but that both result directly from a common parent, such as methane, or even from two different parent-molecules.

STRUCTURE WITHIN THE SWAN BANDS OF C_2

Attention has been called in previous papers[10] to emissions appearing within the Swan bands. Within the $\Delta v = +1$ sequence of Comet 1948I, lines are observed at the following wave lengths:

Between (4, 3) and (3, 2): λ 4689.7 (1) and λ 4695.4 (2?)
Between (3, 2) and (2, 1): λ 4705.0 (1–0) and λ 4708.4 (1–0)
Between (2, 1) and (1, 0): λ 4725.9 (2) and λ 4729.5 (1)

The separations in the last two doublets are practically the same, 3.4 A (or 15.4 cm^{-1}). Within the $\Delta v = 0$ sequence, two lines have been measured at λ 5146.2 (1) and λ 5151.4 (2). Within the $\Delta v = -1$ sequence, lines are observed at λ 5562.4 (1) and 5617.7 (1).

Certain of these lines agree quite well with features observed in Comet 1940c by Bobrovnikoff[10] and in Comet 1947n by Swings and Page,[8] for example, the doublet between (3, 2) and (2, 1). Others do not. The possible meaning of these emissions has already been discussed by Swings and Page.[8] It is imperative that "synthetic profiles" be drawn for the Swan bands, assuming a fluorescence mechanism. Yet certain lines, such as λ 4725.9, appear to rise so sharply above the background of (1, 0) that they do not seem to belong to C_2. One would rather think that another molecule is responsible for such lines.

As will be seen in the next section, additional unidentified lines are observed in the visual region. Some have the same intensity gradient as the emissions falling within the Swan bands. It is likely that an as yet unidentified molecular system is present in the region from λ 4600 to the red. The importance of laboratory work on such molecules as NH^+, CN^+, and C^+ cannot be overemphasized.

THE VISUAL REGION

On account of the strong solar spectrum appearing in the region of the nucleus, Comet 1948I is not favorable to the detection or investigation of faint nuclear emissions in the visual range. This appears clearly from Figure 1. Table 3 gives the measured emissions above λ 5100. The Swan bands (0, 0), (1, 1), (0, 1), (1, 2), and (2, 3) which are observed have not been included in the table. Most wave lengths are the mean values for the three spectrograms at distances $r = 0.73$, $r = 0.78$, and $r = 1.00$.

As has been stated by various observers,[5, 6, 7, 8] the a band of ammonia, presumably due to NH_2, does not seem able to explain all the emissions observed in the visual region. In particular, certain long lines may be related to the unidentified emissions within the Swan bands rather than to NH_2. No definite identification appears convincing through a systematic examination of likely molecules. The laboratory investigations on the a band have been reviewed and discussed by Swings, McKellar, and Minkowski.[8]

Ten years ago the red system of CN was often suggested for explaining certain emissions in the visual region. Once the fluorescence excitation of the violet system of CN be-

came proved,[22] and the low f-values of the vibrational transition of the red CN system ascertained,[23] the CN bands of the visual region were no longer considered. Indeed, the red CN bands of the visual region should not appear intensely in fluorescence. However, the recent observation[8] of intense bands in the nucleus of Comet 1947n and their probable attribution to the (2, 0) and (3, 1) transitions of the red system of CN have produced a

TABLE 3*

EMISSION LINES IN COMET 1948I; REGION $\lambda > 5300$

Comet 1948I		1947n	Earlier Measurements McD. and Mt. W.	Victoria Measurements	Lyon Measurements	Suggested Identification	Notes
λ	Int. and Length						
5357.9	1	51.6	55.3	.....	54.4	.....	
5430.7	3 sh	27.9	.....	27.7	.....	NH_2	
5446.3	2 sh	44.2	45.0	.....	49.7	.....	
5464.6	0 sh	66.2	.....	.....	.....	.....	1
5650	1 sh	.....	.....	.....	.....	.....	
5674.1	0 sh	79.0	.....	.....	.....	NH_2	
5694.1	0–1 sh	.....	87.1	94.6	96.3	NH_2	
5703.0	2 sh	02.2	01.5	04.0	08.2	NH_2	
5733.5	2 sh	32.5	31.2	31.4	.....	.....	
5743.0	0–1 sh	.....	39.6	41.4	42.7	NH_2	
5890.1	4	.....	.....	.....	.....	Na I	2
5896.6	2	.....	.....	.....	.....		
5978.2	5l	74.9	77.7	76.6	77.4	NH_2?	3
5996.5	4l	98.0	96.0	95.8	93.4	(NH_2?)	3
6018.6	1–2 sh	17.2	19.4	20.2	19.8	NH_2	
6097.8	2 sh	94.8	98.7	96.9	99.4	NH_2	
6111.1	1 sh	06.6	10.3	10.0	.....	NH_2	
6120.9	1 sh	18.0	20.9	20.9	.....	NH_2 plus $C_2(1, 3)$	4
6185.3	1 sh	86.5	.....	84.8	.....	NH_2 plus $C_2(0, 2)$	4
6210.6	1 sh	.....	.....	12.8	06.6	NH_2	
6297.7	10 sh	97.3	98.0	00.7	98.8	NH_2	5
6318.8	; sh	.....	.....	21.2	.....	NH_2	
6333.1	3–4 sh	29.5	33.2	35.2	29.4	NH_2	
6346.4	1	45.2	45.6	45.7	45.4	NH_2	
6361.3	1 sh	60.6	64.1	64.3	? 54	NH_2?	
6466.9	1	.....	.....	74.3	.....	.....	

* The columns list the following: first, the mean measured wave lengths; second, the intensities and estimates of the lengths of the lines ("sh" = short; "l" = long); third, the wave lengths obtained by Swings and Page (*Ap. J.*, **108**, 526, 1948); fourth, mean values of earlier measurements made at the McDonald and Mt. Wilson observatories; fifth, measurements made at Victoria in the spectra of Comet 1941 I and 1943 I (A. McKellar, *Ap. J.*, **98**, 142, 1943, and **99**, 162, 1944); and sixth, mean values obtained by J. Dufay for Comets 1936a, 1937h, 1937f, 1942g, and 1939d (*C.R.*, **222**, 51, 1946).

NOTES TO TABLE 3

1. This is not C_2 (4, 5), since (3, 4) is absent.
2. The Na emission is present only for $r = 0.73$ and $r = 0.78$; it is blended in the nuclear region by a short line, which remains present at larger heliocentric distances and is probably due to NH_2.
3. The NH_2 identification is not satisfactory; the lines are too long and too strong.
4. Minor contribution of C_2.
5. Often blended with night sky or twilight [*O* I] line; strong enhancement in the nuclear region is evidence for cometary emission.

[23] A. S. King and P. Swings, *Ap. J.*, **101**, 6, 1945. This paper concerns the (2, 0) band. The (0, 0) band at 1.05 μ is much stronger (see reference 8, n. 24).

renewed interest in the red system as a source of identification of cometary emissions. Its bands in the visual region should, like (2, 0) and (3, 1) and in contrast with the violet system, be concentrated near the nucleus. There is no reason for believing that the vibrational temperature of the red system of *CN* is as low as that of the blue system, since the excitation mechanisms are different. In fact, the identification of bands of the red system arising from $v' = 2$ and $v' = 3$ indicates that the vibrational temperature is higher for the red system than for the blue system. Hence it does not seem unreasonable to consider the possibility of transitions such as (4, 0) near λ 6200, (5, 1) near λ 6350, and (5, 0) near λ 5620. However, the identifications cannot proceed safely before synthetic profiles have been drawn for these bands. The infrared observations which were made with very low resolution revealed for the (2, 0) band a sharp maximum at λ 7906 and another shallower one near λ 7876. The red system has triple-headed bands, roughly equally spaced. The R_2 head of (2, 0) is at λ 7874, and the other two heads, R_1 and Q_1, are about 20 and 40 A to the red of R_2. With a resolution such as was used for Comet 1948I one may expect each vibrational transition to give several maxima. It is likely that some of the emissions in the visual region belong to this system. However, transitions corresponding to high vibrational levels, such as were often considered earlier, should not be retained. The fact that (3, 1) is fairly weak compared with (2, 0) indicates that the vibrational temperature of the red system, although higher than that of the blue system, is by no means very high. Such suggestions as were made by J. Dufay[6] thus appear unlikely. Pending the availability of synthetic profiles for the red *CN* bands, no tentative identification of *CN* has been entered into Table 3.

THE BAND SPECTRUM OF CO^+. I. FIRST NEGATIVE SYSTEM ($B^2\Sigma - X^2\Sigma$)

K. NARAHARI RAO
Yerkes Observatory
Received September 1, 1949

ABSTRACT

A comprehensive study was made of the first negative bands ($B^2\Sigma - X^2\Sigma$) of the CO^+ molecule. Revised values for the molecular constants of the two electronic states were obtained. The final results are summarized in Table 6.

A. INTRODUCTION

Three band systems are attributed to the CO^+ molecule. They are the so-called first negative carbon bands ($B^2\Sigma - X^2\Sigma$), the comet-tail bands ($A^2\Pi - X^2\Sigma$), and the Baldet-Johnson bands ($B^2\Sigma - A^2\Pi$). The relative positions of the electronic levels belonging to them are shown in Figure 1. This paper presents a study of the first negative bands. These bands have been known for a long time and have been studied by a number of investigators.[1] However, the accuracy of the molecular constants obtained thus far is

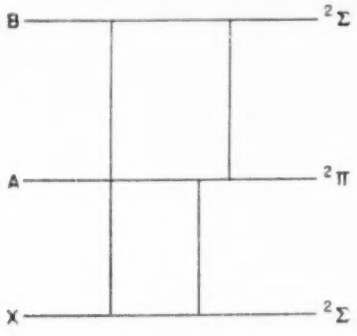

FIG. 1

rather disappointing. Therefore, it was considered desirable to reinvestigate these bands under good resolution, particularly because their lower state happens to be the ground state of the CO^+ molecule.

B. EXPERIMENTAL

The light-source used was a water-cooled discharge tube with a graphite hollow cathode. A ring of aluminum surrounding the graphite rod served as the anode. The tube was filled with a small amount of oxygen, which, under the action of the discharge, combined with the carbon, giving rise to carbon monoxide. A direct current of 400 mA and 600 volts between the electrodes gave rise to a very intense discharge inside the hollow. The first negative bands were photographed in the fourth order of a 21-foot grating

[1] W. Jevons, *Phil. Mag.*, **47**, 586, 1924; C. M. Blackburn, *Proc. Nat. Acad. America*, **11**, 28, 1925; R. C. Johnson, *Proc. R. Soc., London, A*, **108**, 343, 1925; R. Schmid, *Phys. Rev.*, **42**, 182, 1932; D. Coster, H. H. Brons, and H. Bulthuis, *Zs. f. Phys.*, **79**, 787, 1932; H. Biskamp, *Zs. f. Phys.*, **86**, 33, 1933; R. Schmid and L. Gerö, *Zs. f. Phys.*, **86**, 297, 1933; H. Bulthuis, Groningen diss., 1935; and L. H. Woods, *Phys. Rev.*, **63**, 431, 1943.

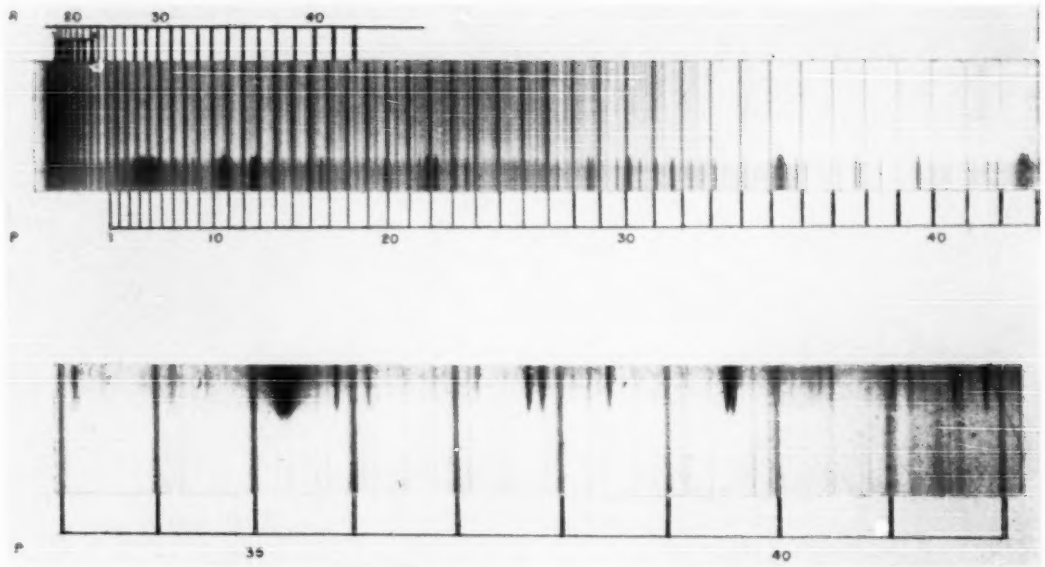

FIG. 2.—The (1, 4) band of the first negative system of CO^+

spectrograph with an exposure time of 4 hours. Figure 2 gives a reproduction of the (1, 4) band. The measurements and reductions of these bands were carried out in exactly the same manner as described in a previous investigation.[2]

C. ROTATIONAL STRUCTURE

For $^2\Sigma - {}^2\Sigma$ transitions the selection rule for the quantum number K of the total angular momentum apart from spin is $\Delta K = \pm 1$. Therefore, $^2\Sigma - {}^2\Sigma$ bands consist of two series of triple lines, one series corresponding to $\Delta K = +1$ (R branch) and the other to $\Delta K = -1$ (P branch). The P series consists of the sub-branches P_1, P_2, and ${}^PQ_2$, and the R series R_1, R_2, ${}^RQ_2$. The satellite branches Q_{12} and Q_{21} are, however, of negligible intensity except for the lowest values of K. So, for all practical purposes, we have a doublet P branch and a doublet R branch. This is indeed observed (see Fig. 2), except that the doublet splitting is resolved only for the higher K values. Table 1 gives the wave numbers of all the bands studied. The components of the doublets are given wherever measured.

For a $^2\Sigma$ state the rotational term values are given by

$$F_1(K) = B_v K(K+1) - D_v K^2(K+1)^2 + \ldots + \frac{\gamma}{2} K, \tag{1}$$

$$F_2(K) = B_v K(K+1) - D_v K^2(K+1)^2 + \ldots - \frac{\gamma}{2}(K+1) \tag{2}$$

where $F_1(K)$ refers to the components having $J = K + \frac{1}{2}$ and $F_2(K)$ to those with $J = K - \frac{1}{2}$,

$$B_v = B_e - \alpha(v+\tfrac{1}{2}) + \delta(v+\tfrac{1}{2})^2, \qquad B_e = \frac{h}{8\pi^2 c \mu r_e^2}, \tag{3}$$

$$D_v = D_e + \beta(v+\tfrac{1}{2}) + \ldots \tag{4}$$

where α, β, γ, and δ are constants.

The rotational constants were evaluated with the help of the combination differences

$$R_i(K-1) - P_i(K+1) = \Delta_2 F''(K), \tag{5}$$

$$R_i(K) - P_i(K) = \Delta_2 F'(K). \tag{6}$$

From the above relations it is easy to see that

$$\tfrac{1}{2}[\Delta_2 F_1(K) + \Delta_2 F_2(K)] = (4B_v - 6D_v)(K+\tfrac{1}{2}) - 8D_v(K+\tfrac{1}{2})^3. \tag{7}$$

Using standard graphical methods,[3] provisional B_v and D_v values were obtained from the observed $\Delta_2 F(K)$ values. In order to improve their accuracy, the following procedure was adopted. Combination differences of the type given below were formed:

$$\begin{aligned} R_i^{(0,0)}(K) - R_i^{(0,1)}(K) &= P_i^{(0,0)}(K) - P_i^{(0,1)}(K) \\ &= \Delta G''_{1/2} + (B''_1 - B''_0) K(K+1) - (D''_1 - D''_0) K^2(K+1)^2; \end{aligned} \tag{8}$$

$$\begin{aligned} R_i^{(1,0)}(K-1) - R_i^{(0,0)}(K-1) &= P_i^{(1,0)}(K+1) - P_i^{(0,0)}(K+1) \\ &= \Delta G'_{1/2} + (B'_1 - B'_0) K(K+1) - (D'_1 - D'_0) K^2(K+1)^2. \end{aligned} \tag{9}$$

[2] K. N. Rao, *Ap. J.*, **110**, 304, 1949.

[3] See, e.g., G. Herzberg, *Molecular Spectra and Molecular Structure*, Vol. 1: *Diatomic Molecules* (New York: Prentice-Hall Book Co., Inc., 1939), p. 198.

TABLE 1

Wave Numbers of Lines in the First Negative System of CO^+

K	(0, 0) Band		(0, 1) Band		(0, 2) Band		(0, 3) Band		(0, 4) Band	
	R	P	R	P	R	P	R	P	R	P
0	45636.91		43453.06		41299.55				37083.47	
1	640.18	45629.60	456.34	43445.66	302.81	41292.11		39168.81*	086.82	37075.95*
2	643.05	625.18	459.25	441.45	305.79	287.95		164.89	089.94	072.10
3	645.51	620.60	461.88	436.88	308.47	283.54		160.63	092.87	067.89
4	647.57	615.57	464.13	432.03	310.91	278.82		156.00	095.52*	063.48
5	649.32	610.10	466.03	426.79	313.01	273.77		151.19	098.06*	058.85
6		604.35	467.60	421.25	314.87	268.51		146.08	100.35*	054.00
7		598.22		415.44	316.36	262.91		140.81	102.46*	048.98
8		591.71		409.22	317.58	257.04		135.24	104.33*	043.68
9		584.88		402.72	318.69	250.89		129.40	105.94*	038.20
10		577.69		395.87		244.41		123.34	107.39*	032.50
11		570.09		388.69		237.66		116.99	108.57*	026.61
12	650.99	562.09		381.20		230.64		110.43	109.61*	020.50
13	649.86	553.77		373.35		223.28		103.57	110.35*	014.17
14	648.32	545.08	468.68	365.21		215.63		096.53		007.60
15	646.43	536.01	467.15	356.73	318.06	207.77		089.18		000.83
16	644.09	526.62	465.41	347.92	316.95	199.56	39198.99	081.57		36993.88
17	641.38	516.80	463.29	338.80	315.55	191.08	198.27	073.73		986.71
18	638.34	506.71	460.93	329.28	313.86	182.28	197.26	065.63		979.28
19	634.87	496.11	458.19	319.47	311.84	173.22	195.97	057.27	110.35*	971.67
20	630.97	485.23	455.14	309.32	309.50	163.82	194.44	048.77 048.60	109.61*	963.81
21	626.79	473.93	451.69	298.83	306.91	154.16	192.63	039.91 039.72	108.57*	955.73
22	622.21	462.32	447.99	288.11	304.01	144.20	190.54	030.79 030.60	107.39*	947.50
23	617.25	450.35	443.81	276.93	300.86 300.69	133.98 133.86	188.35 188.15	021.41 021.22	105.94*	938.93
24	611.80	437.96	439.42	265.51	297.35 297.19	123.44 123.34	185.74 185.55	011.77 011.59	104.33*	930.25
25	606.06	425.16	434.62	253.68	293.49 293.34	112.61 112.47	182.90 182.67	002.02 001.68	102.46* 102.10	921.35 921.19
26	600.03	412.04	429.45	241.52	289.40 289.15	101.50 101.33	179.73 179.49	38991.75 991.54	100.35* 100.02	
27	593.48	398.54	424.13 423.89	229.15 228.89	284.97 284.73	090.02 089.83	176.39 176.05	981.35 981.11	098.06* 097.67	
28	586.58	384.59	418.31 418.02	216.33 216.11	280.27 280.01	078.25 078.09	172.72 172.40	970.71 970.45	095.52* 095.07	
29	579.35	370.38	412.16 411.88	203.15 202.91	275.19 274.92	066.23 066.04	168.81* 168.42	959.79 959.53	092.58 092.19	
30	571.58	355.79	405.58 405.36	189.70 189.45	269.81 269.52	053.90 053.68	164.54 164.19	948.59 948.32	089.51 089.17	
31	563.57	340.76	398.78 398.41	175.86 175.64	264.14 263.81	041.23 041.03	160.03 159.66	937.17 936.82	085.83 085.56	
32	555.06	325.41	391.50 391.20	161.72 161.36	258.11 257.80	028.33 028.08	155.26 154.87	925.46 925.14		
33	546.32	309.64	383.93 383.55	147.21 146.91	251.81 251.39	015.06 014.84	150.22 149.84	913.49 913.14		
34	537.03	293.47	375.99 375.63	132.36 132.06	245.18 244.75	001.44 001.23	144.84 144.47	901.23 900.86		
35	527.51	276.98	367.67 367.35	117.13 116.83	238.24 237.66*	40987.62 987.37	139.26 138.88	888.70 888.34		
36		260.05	359.08 358.72	101.63 101.27		973.46 973.20	133.38 132.97	875.91 875.55		
37		242.73	350.02 349.63	085.77 085.40	223.28* 222.82	959.01 958.71	127.21 126.75	862.87 862.52		
38		224.89	340.66 340.33	069.48 069.14	215.63* 215.07	944.17 943.90	120.75 120.25	849.56 849.16		
39		206.87	330.88 330.48	052.92 052.53		929.12 928.76	113.99 113.52	835.93 835.55		
40		188.57	320.84 320.42	035.98 035.57		913.71 913.38	106.92 106.49	822.08 821.67		
41		169.59	310.40 309.88	018.63 018.28		897.97 897.67	099.63 099.14	807.90 807.51		
42				000.97 000.64		882.04 881.60	091.96 091.53	793.45 793.04		
43							084.03 083.54			
44				964.74 964.20			075.83 075.32			
45							067.40 066.90			
46							058.46 058.00			

* Blend.

TABLE 1—*Continued*

K	(1, 2) Band		(1, 3) Band		(1, 4) Band		(1, 5) Band	
	R	P	R	P	R	P	R	P
0	.....	.....	40855.65	.....	38762.79	.....	36700.26	.....
1	.....	.....	858.84	40848.34	766.08	38755.50	703.59	36693.03
2	.....	42967.14	861.71	844.18	769.04	751.43	706.57	689.03
3	.....	962.71	864.31	839.76	771.74	747.15	709.40	684.80
4	.....	957.76	866.58	834.98	774.15	742.54	711.95	680.39
5	.....	952.52	868.52	829.93	776.28	737.65	714.32	675.70
6	.....	946.91	870.18	824.56	778.16	732.50	716.43	670.80
7	.....	940.99	871.58	818.88	779.74	727.07	718.25	665.63
8	.....	934.67	872.58	812.86	781.08	721.44	719.91	660.26
9	.....	928.04	.....	806.58	.....	715.44	721.29	654.65
10	.....	921.02	.....	799.94	.....	709.29	722.43	648.80
11	42994.31	913.68	.....	793.00	.....	702.72	.....	642.71
12	993.52	906.00	.....	785.78	.....	695.95	.....	636.38
13	992.52	897.94	873.68	778.16	.....	688.90	.....	629.84
14	991.08	889.55	871.85	770.31	.....	681.56	.....	623.03
15	989.30	880.78	870.64	762.15	.....	673.95	.....	616.05
16	987.18	871.63	869.16	753.67	781.52	666.08	.....	608.76
17	984.67	862.18	867.29	744.85	780.34	657.91	.....	601.25
18	981.78	852.36	865.13	735.74	778.93	649.54	.....	593.50
19	978.57	842.20	862.65	726.30	777.18	640.82	722.07	585.54
20	974.97	831.67	859.81	716.56	775.11	631.79	721.84 720.76	577.33
21	971.13	820.79	856.71	706.49	772.79	622.52	720.53 719.25	568.87
22	966.66	809.59	853.22	696.08	770.13	612.96	719.08 717.47	560.18
23	962.14	798.11	849.44	685.39	767.23	603.18	717.23 715.45	551.35
24	961.90 957.08	797.92 786.15	845.28	674.33	764.02	593.01	715.21 713.20	551.22 542.17
25	956.88 951.69	785.89 773.81	840.93	663.07	760.51	582.63	712.94 710.69	541.99 532.75
26	951.45 945.88	773.52 761.16	840.75 836.18	662.94 651.40	756.74	572.00	710.40 707.92	532.56 523.13
27	945.59 939.78	760.88 748.14	835.96 831.04	651.27 639.42	752.66	561.01	707.61 704.84	522.93 513.19
28	939.50 933.27	747.90 734.81	830.81 825.62	639.27 627.10	748.43	549.91	704.56 701.61	512.97 503.06
29	932.99 926.40	734.48 721.02	825.36 819.81	626.94 614.48	748.19 743.74	549.68 538.38	701.29 698.06	502.81 492.67
30	926.06 919.10	720.75 706.92	819.53 813.74	614.30 601.52	743.49 738.80	538.16 526.63	697.73 694.23	492.45 482.05
31	918.84 911.49	706.61 692.44	813.38 807.28	601.34 588.27	738.52 733.52	526.37 514.60	693.94 690.18	481.80 471.13
32	911.16 903.50	692.11 677.61	806.85 800.44	588.06 574.68	733.28 727.99	514.35 502.19	689.84 685.86	470.90 460.01
33	903.15 895.06	677.26 662.41	.....	574.42 560.71	727.64 722.14	501.88 489.53	685.54 681.23	459.72 448.67
34	894.74 886.34	662.04 646.83	.....	560.46 546.45	721.70 715.93	489.27 476.54	680.96 676.40	448.36 437.01
35	885.93 877.16	646.51 630.89	.....	546.22 531.84	715.44 709.29	476.25 463.30	676.05 671.36	436.72 425.07
36	876.79 867.57	630.60 614.57	.....	531.56 516.93	702.72*	463.02 449.76	671.07	424.84
37	867.24 857.64	614.23 597.93	761.42	516.64 501.62	695.95	449.44 435.95		
38	857.30 847.29	597.57 580.84	761.04 752.64	501.39 486.04	695.29 688.30	435.58 421.80		
39	846.98 836.61	580.50 563.41	752.20 743.42	485.76 470.10	687.88 680.55	421.46 407.38		
40	836.20 825.95	563.06 545.59	743.04 733.76	469.82 453.83	680.20 672.57	407.00 392.67		
41	825.51 813.99	545.24 527.44	733.38 723.96	453.52 437.22	672.15 664.21	392.27 377.58		
42	813.63 802.15	527.06 508.84	723.46	436.91 420.21	663.75 655.62	377.20 362.24		
43	801.60 789.77	508.48	.....	419.95	655.10	361.86		
44	789.44 777.13	.....	.....	385.42				
45	776.67 763.97	.....	.....	384.98 367.42				
46	763.55 750.52	.....	.....	366.98				
	750.02							

TABLE 1—*Continued*

K	(2, 3) Band		(2, 4) Band		(2, 5) Band		(2, 6) Band	
	R	P	R	P	R	P	R	P
0	42482.20		40389.17				36294.47	
1	485.29	42474.97	392.27	40381.92		38319.71	297.67	36287.34
2	487.94	470.64	395.06	377.82		315.59	300.61	283.38
3	490.27	466.18	397.50	373.36		311.18	303.29	279.17
4	492.26	461.22	399.58	368.58		306.47	305.75	274.70
5	493.86	455.92	401.46	363.43		301.53	307.91	269.98
6		450.28		358.01		296.29	309.82	264.97
7		444.21		352.23		290.82	311.45	259.74
8		437.76		346.11		285.00	312.85	254.25
9		430.97		339.68		278.93	313.95	248.50
10		423.81				272.53		242.53
11		416.29		325.80		265.84		236.22
12		408.35		318.35		258.85		229.69
13	493.03	400.06		310.63	38344.46	251.55		222.89
14	491.19	391.45	402.18	310.44 302.49 302.28	343.75	243.96		215.89
15	488.98	382.36	400.56	294.03 293.82	342.72	236.09		208.57
16	486.46	372.97	398.74 398.56	285.28 285.06	341.35	227.89	314.67	200.97
17	483.54	363.19	396.48 396.30	276.33 276.00	339.72	219.43	313.58	193.17
18	480.18	353.01	393.87 393.64	266.71 266.45	337.78	210.64	312.31	185.09
19	476.48	342.47	390.90 390.69	256.89 256.61	335.53	201.58	310.81	176.78
20	472.35	331.55	387.54 387.30	246.71 246.49	332.99	192.20	308.98	168.17
21	467.91	320.27	383.84 383.61	236.27 236.02	330.14	182.54	307.05 306.84	159.36 159.25
22	462.99	308.56	379.85 379.58	225.44 225.21	327.00	172.56	304.70 304.49	150.27 150.12
23	457.76	296.53	375.43 375.21	214.34 214.05	323.53	162.26	302.12 301.90	140.86 140.72
24	452.07	284.12	370.72 370.50	202.78 202.54	319.71	151.69	299.23 299.02	131.20 131.06
25	446.05	271.27	365.66 365.42	190.96 190.71	315.59	140.93 140.69	296.11 295.88	121.32 121.11
26	439.63	258.12	360.19 359.90	178.71 178.51	311.18	129.75 129.52	292.67 292.45	111.13 110.94
27	432.83	244.50	354.44 354.18	166.16 165.95	306.47	118.20 117.96	288.99 288.74	100.69 100.44
28	425.54	230.57	348.30 348.04	153.32 153.08	301.53 301.22	106.46 106.20	285.05 284.80	089.98 089.73
29	417.94	216.20	341.76 341.45	140.11 139.86	296.29* 295.81	094.19 094.09	280.77 280.47	078.99 078.72
30	410.03	201.43		126.49 126.29	290.42 290.10	081.91 081.66	276.23 275.94	067.71 067.49
31	401.41	186.33	327.64 327.36	112.57 112.30	284.36 284.08	069.18 068.93	271.39 271.05	056.20 055.93
32	392.62	170.78	320.04 319.78	098.29 098.06	278.02 277.70	056.11 055.83	266.26 265.97	044.41 044.13
33	383.35	154.91	312.08 311.80	083.68 083.42	271.32 270.98	042.76 042.47	260.88 260.58	032.34 032.13
34		138.62	303.79 303.45	068.68 068.40	264.33 263.95	029.07 028.80	255.20 254.89	019.99 019.60
35		121.90	295.09 294.72	053.32 053.05	256.97 256.63	015.08 014.79	249.21 248.79	007.33 007.10
36		104.82	286.01 285.61	037.62 037.33	249.27 248.96	000.79 000.48		35994.45 994.14
37		087.35		021.55 021.23	241.27 240.90	37986.13 985.80		981.29 981.02
38		069.43		005.18 004.82	232.93 232.60	971.17 970.87		
39		051.24		39988.36 988.02	224.20 223.86	955.91 955.56		
40		032.54		971.20 970.87	215.18 214.85	940.31 939.97		
41		013.25		953.70 953.38	205.81 205.44	924.46 924.08		
42				935.80 935.46	196.10 195.74	908.14 907.74		
43					186.03 185.69	891.50 891.13		
44					175.56 175.17			
45					164.79 164.46			
46					153.80 153.29			
47					142.27 141.87			

TABLE 1—*Continued*

K	(3, 5) Band		(4, 7) Band	
	R	P	R	P
0	.....	.....	.....	.....
1	.....	39895.00	37398.50	37388.52
2	.....	890.92	401.19	384.52
3	.....	886.50	403.47	380.17
4	.....	881.66	405.43	375.46
5	.....	876.51	407.06	370.49
6	.....	871.02	408.39	365.13
7	.....	865.16	409.27	359.42
8	.....	858.90	.....	353.41
9	.....	852.28	.....	347.02
10	39916.54	845.37	.....	340.31
11	915.86	838.07	.....	333.26
12	915.01	830.42	408.88	325.87
13	913.74	822.39	407.83	318.14
14	912.13	814.00	406.33	310.06
15	910.14	805.27	404.52	301.64
16	907.77	.....	402.36	292.89
17	905.01	786.77	399.89	283.80
18	901.91	777.01	397.05	274.38
19	898.39	766.79	393.90 393.79	264.56
20	894.61 894.44	756.26	390.33 390.18	254.42
21	890.41 890.24	745.33	386.42 386.27	243.96
22	885.81 885.66	734.12	382.17 381.99	233.13
23	880.87 880.69	722.47	377.55 377.38	222.00
24	875.54 875.38	710.49	372.57 372.38	210.44
25	869.82 869.66	698.12	367.23 367.04	198.69 198.53
26	863.76 863.52	685.41	361.58 361.36	186.43 186.29
27	857.31 857.14	672.42 672.21	355.44 355.25	173.86 173.67
28	850.45 850.23	659.00 658.78	349.04 348.83	160.96 160.78
29	.....	645.11	342.30	147.65
	.....	644.96	342.05	147.49
30	835.65	630.93	335.07	134.09
	835.46	630.71	334.93	133.92
31	827.67	616.37	327.50	120.02
	827.42	616.12	327.26	119.83
32	819.22	601.40		
	818.95	601.18		
33	810.55	586.07		
	810.25	585.87		
34	801.33	570.41		
	801.03	570.14		
35	.....	554.30		
	.....	554.08		
36	.....	537.79		
	.....	537.52		
37	.....	520.97		
	.....	520.67		
38	.....	503.75		
	.....	503.47		
39	.....	486.21		
	.....	485.86		
40	.....	468.16		
	.....	467.85		

By plotting such differences against $K(K+1)$, straight lines result if the contributions of the terms in D are negligible. From their intercepts on the ordinate axes, $\Delta G_{v+1/2}$ can be obtained, and from their slopes, values for $(B_{v+1} - B_v)$. If the terms in D cannot be neglected, then for higher K values the points deviate from the straight lines $\Delta G_{v+1/2} \pm (B_{v+1} - B_v)K(K+1)$. From the extent of this deviation, $(D_{v+1} - D_v)$—that is, β—can be evaluated. It was, however, found that for the lower state there was no noticeable curvature in such plots when successive bands in the v'' progression were used. But, when $R_1^{(2,3)}(K) - R_1^{(2,6)}(K)$ was plotted against $K(K+1)$, the run of points indi-

cated a β'' of the order of 0.01×10^{-6}. Following the same method, a value of 0.22×10^{-6} was obtained for β'. From the provisional values for B_v and D_v the best values for each of the electronic states were chosen, and, with the ΔB and the ΔD values obtained in the above-described manner, the rotational constants for the other vibrational levels in the two electronic states were computed. For future reference these will be described as the ones derived in the second stage of evaluation.

The B values obtained above can be checked by the use of the following relation, whose validity is easily verified:

$$\tfrac{1}{2}[R(K-1)+P(K)]+(D'-D'')K^2(K^2+1)=\nu_0+(B'-B'')K^2. \quad (10)$$

With the values for D obtained earlier, the quantities given on the left were computed for all the bands studied and plotted against K^2. From the slopes of the straight lines that can be drawn through these points, $(B'-B'')$ values were derived. The B values obtained in the second stage were then adjusted in such a manner that no systematic difference existed between the $(B'-B'')$ values computed from them and the ones evaluated from relation (10). Table 2 summarizes the final results.

TABLE 2

ROTATIONAL CONSTANTS (Cm^{-1})

v	B_v PRESENT OBSERVATIONS		B_v BULTHUIS*		D_v PRESENT DATA	
	$B^1\Sigma$	$X^1\Sigma$	$B^1\Sigma$	$X^1\Sigma$	$B^1\Sigma$	$X^1\Sigma$†
0	1.7848_9	1.9677_3	1.780	1.965	$7.8_9\times10^{-6}$	$(6.3_4\times10^{-6})$
1	1.7546_0	1.9487_1	1.75	1.945	$8.0_8\times10^{-6}$	$(6.3_7\times10^{-6})$
2	1.7242_4	1.9296_0	1.71	1.926	$8.2_7\times10^{-6}$	$(6.3_4\times10^{-6})$
3	1.6940_6	1.9103_9	1.67	1.88	$8.5_8\times10^{-6}$	$6.3_5\times10^{-6}$
4	1.6636	1.8910_7	1.64	1.87	8.5×10^{-6}	$(6.4_0\times10^{-6})$
5	.....	1.8717_8	.....	1.86	.....	$(6.4_1\times10^{-6})$
6	.....	1.8524_4	.....	1.84	.....	$6.4_3\times10^{-6}$
7	.....	1.8328	.....	1.82	.....	$(6.4_3\times10^{-6})$

* Groningen diss., 1935.

† Values given in parentheses are estimates.

In Figure 3 $[\Delta_2F_1''(K)+\Delta_2F_2''(K)]/(2K+1)$ is plotted against $(K+\frac{1}{2})^2$ for the level with $v''=4$. The intercept of the straight line through these points on the ordinate axis gives $4B_4''$. According to the results obtained by Bulthuis, this would be at the place marked X in this diagram.

With the results summarized in Table 2, the following formulae for the rotational constants were obtained:

$$B_v'=1.7999_2-0.0302_5(v+\tfrac{1}{2}), \quad (11)$$

$$B_v''=1.9772_0-0.0189_6(v+\tfrac{1}{2})-0.00003_7(v+\tfrac{1}{2})^2, \quad (12)$$

$$D_v'=7.7_5\times10^{-6}+0.2_2\times10^{-6}(v+\tfrac{1}{2}), \quad (13)$$

$$D_v''=6.3_7\times10^{-6}+0.0_1\times10^{-6}(v+\tfrac{1}{2}). \quad (14)$$

The expressions for D agree well with those obtained from the theoretical formulae.[4]

[4] *Ibid.*, pp. 114–116.

D. VIBRATIONAL STRUCTURE

The separation between successive vibrational levels is represented by the relation

$$\Delta G_{v+1/2} = G(v+1) - G(v), \tag{15}$$

where the vibrational term values, $G(v)$, are given by

$$\Delta G(v) = \omega_e(v+\tfrac{1}{2}) - \omega_e x_e(v+\tfrac{1}{2})^2 + \omega_e y_e(v+\tfrac{1}{2})^3 \ldots \tag{16}$$

$$\omega_e x_e \ll \omega_e \quad \text{and} \quad \omega_e y_e \ll \omega_e x_e .$$

It has already been described in Section C how these $\Delta G_{v+2/1}$ values can be obtained from observations (see relations [8] and [9] above). The results are given in Table 3.

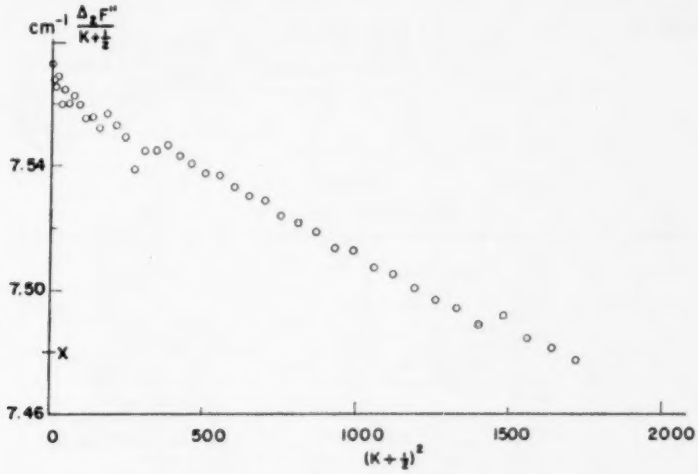

FIG. 3.— $\dfrac{\Delta_2 F_1''(K)+\Delta_2 F_2''(K)}{2K+1}$ against $(K+\frac{1}{2})^2$ for $v''=4$

TABLE 3

VIBRATIONAL QUANTA IN THE UPPER AND LOWER STATES

v	$\Delta G'_{v+1/2}(\mathrm{Cm}^{-1})$	$\Delta G''_{v+1/2}(\mathrm{Cm}^{-1})$
0	1679.40	2183.89
1	1626.50	2153.58
2	1575.57	2123.21
3		2092.93
4		2062.53
5		2032.16

With these data, the following formulae were derived for the vibrational term values for the upper and the lower electronic states:

$$G'(v) = 1743.18\,(v+\tfrac{1}{2}) - 27.927\,(v+\tfrac{1}{2})^2 + 0.3283\,(v+\tfrac{1}{2})^3, \quad (17)$$

$$G''(v) = 2214.24\,(v+\tfrac{1}{2}) - 15.164\,(v+\tfrac{1}{2})^2 - 0.0007\,(v+\tfrac{1}{2})^3. \quad (18)$$

The values of the origins of the bands obtained from the plots according to relation (10) are given in the Deslandres (Table 4).

TABLE 4

ORIGINS OF THE FIRST NEGATIVE SYSTEM OF CO^+ (CM^{-1})

v'	v''							
	0	1	2	3	4	5	6	7
0	45633.44	43449.62	41295.97	39172.76	37079.87	.....	.....	.....
1	.....	.....	42975.40	40852.15	38759.31	36696.77	.....	.....
2	.....	.....	.....	42478.75	40385.72	38223.19	36291.06	.....
3	.....	.....	.....	.....	.....	39898.85	.....	.....
4	.....	.....	.....	.....	.....	.....	.....	37392.19

TABLE 5

MOLECULAR CONSTANTS

	Upper State ($B^2\Sigma$)	Lower State ($X^2\Sigma$)
B_e	1.7999_2 cm^{-1}	1.9772_0 cm^{-1}
a_e	0.0302_6 cm^{-1}	0.0189_6 cm^{-1}
D_e	$7.7_8\times10^{-6}$ cm^{-1}	$6.3_7\times10^{-6}$ cm^{-1}
β_e	$0.2_2\times10^{-6}$ cm^{-1}	$0.0_1\times10^{-6}$ cm^{-1}
δ_e	.....	-0.00003_7 cm^{-1}
r_e	$1.1686_9\times10^{-8}$ cm	$1.1150_8\times10^{-8}$ cm
I_e	$15.546_6\times10^{-40}$ gm cm^2	$14.152_8\times10^{-40}$ gm cm^2
ω_e	1734.1_8 cm^{-1}	2214.2_4 cm^{-1}
$\omega_e x_e$	27.92_7 cm^{-1}	15.16_4 cm^{-1}
$\omega_e y_e$	0.328_8 cm^{-1}	-0.000_7 cm^{-1}
ν_e	45876.7_0 cm^{-1}	.....
ν_{00}	45633.5_2 cm^{-1}	.....

The molecular constants obtained in this investigation are summarized in Table 5.

The values for the internuclear distances and moments of inertia given in Table 5 were derived from the B values with the help of conversion factors based on DuMond's fundamental constants.[5]

E. SPIN DOUBLING IN THE $^2\Sigma$ STATES

L. H. Woods[6] was the first to study the spin splitting in the $^2\Sigma$ states of CO^+. From measurements of the first negative bands, she derived the absolute values of the differ-

[5] See G. Herzberg and K. N. Rao, *J. Chem. Phys.*, **17**, 1099, 1949.

[6] *Op. cit.*

ences of the spin-splitting coefficients for the upper and lower electronic states. The separations of the two components of the spin doublets are given by

$$\begin{aligned}\Delta\nu_P(K) &= P_1(K+\tfrac{1}{2}) - P_2(K-\tfrac{1}{2}) \\ &= (\gamma'-\gamma'')K - \tfrac{1}{2}(\gamma'+\gamma'');\end{aligned} \tag{19}$$

$$\begin{aligned}\Delta\nu_R(K) &= R_1(K+\tfrac{1}{2}) - R_2(K-\tfrac{1}{2}) \\ &= (\gamma'-\gamma'')K + \tfrac{1}{2}(3\gamma'-\gamma'').\end{aligned} \tag{20}$$

Following the procedure adopted by Woods, these separations were plotted against m, where for the P branch $\Delta\nu_P(K)$ was plotted against $m = K$ and for the R branch $-\Delta\nu_R(K)$ was plotted against $m = -(K+1)$. From the slopes of the straight lines through these points, the absolute values of $|\gamma' - \gamma''|$ were determined. The results are given in Table 6, along with the values obtained by Woods. Her values are systematically larger than those obtained in this investigation. In order to examine the cause for the discrepancy between the two sets of results given in Table 6, I measured the (1, 4) band

TABLE 6

DATA CONCERNING DOUBLET SPLITTING

Band (v', v'')	$\lvert\gamma'-\gamma''\rvert$	
	Present Investigation	Data of L. H. Woods
0, 1	0.009_2	0.0180
0, 2	$.008_1$	.0159
0, 3	$.010_3$	.0153
1, 2	$.009_3$	.0172
1, 3	$.008_4$	.0158
1, 4	$.010_0$	.0150
1, 5	$.009_2$	.0159
2, 4	$.009_0$	.0149
2, 5	$.009_0$	.0153
2, 6	$.008_8$	.0150
3, 5	0.007_9	0.0153

on the plate[7] from which Woods obtained her data. The $|\gamma_1' - \gamma_4''|$ value which I derived from these measurements is approximately half the value that she obtained. It would appear, therefore, that the discrepancy between Woods's results and those of the author is due to a difference in the method of evaluation or definition of γ not obvious from Woods's paper.

It is a pleasure to acknowledge my gratitude to Dr. G. Herzberg, under whose supervision this work was carried out, and to the government of India for the award of a Fellowship. Part of the computational work in this investigation was carried out at the National Research Council, Ottawa, Canada, during the winter months of 1949. My thanks are due to the officials of that institution for providing me with all the required facilities.

[7] My thanks are due to Professor R. S. Mulliken for allowing me to use the plates from which L. H. Woods made her evaluations.

THE DERIVATION OF VACUUM WAVE NUMBERS AND THE REDUCTION OF MEASURED WAVE LENGTHS TO STANDARD ATMOSPHERIC CONDITIONS

HAROLD D. BABCOCK
Mount Wilson and Palomar Observatories
Received September 1, 1949

ABSTRACT

Vacuum wave numbers derived from Barrell and Sears's data on the refractivity of air are systematically lower than those found from Kayser's *Schwingungszahlen*. The differences are nonuniform to an extent that requires consideration in dealing with precise wave lengths. Effects of water vapor are illustrated.

Tables are constructed from the data of Barrell and Sears for reducing wave lengths observed under nonstandard conditions to their values at 760 mm and 15° C. The new tables are compared with those of Meggers and Peters.

The *Tabelle der Schwingungszahlen* by H. Kayser[1] was based on measurements of the refractivity of air made by W. F. Meggers and C. G. Peters.[2] From the same measurements Meggers and Peters themselves derived tables to facilitate the reduction of wave lengths observed under nonstandard conditions to the values which they would have had under standard atmospheric conditions.

Studies of the refractivity of air by other observers have indicated that the results of Meggers and Peters are systematically too low. Kösters and Lampe,[3] Perard,[4] Paschen,[5] and H. Barrell and J. E. Sears[6] found accordant values of the refractivity differing from those of Meggers and Peters, and the shape of the dispersion-curve is also different. It will be sufficient to consider here only the results of the measurements by Barrell and Sears and to apply them to the problems indicated in the title of this paper.

I. VACUUM WAVE NUMBERS

A radiation of frequency ν_1, assumed constant, is associated with various wave lengths by the relation

$$\nu_1 = \frac{c}{\lambda_{1\,\mathrm{vac}}} = \frac{c}{\lambda_1 n_1} = \frac{c}{\lambda_1' n_1'},$$

where c is the velocity of light *in vacuo*, $\lambda_{1\,\mathrm{vac}}$ the wave length *in vacuo*, λ_1 and λ_1' wave lengths in any media whose indices of refraction for ν_1 are n_1 and n_1'. The vacuum wave number is conveniently computed as $1/\{\lambda_1 + \lambda_1(n_1 - 1)\}$.

Barrell and Sears summarized their extensive measurements in two similar equations, the first of which applies for dry air free of CO_2, and the second for ordinary air containing water vapor and 0.03 per cent by volume of CO_2. The second equation is appropriate here

$$(n-1)\times 10^6 = \left[0.378125 + \frac{0.0021414}{\lambda^2} + \frac{0.00001793}{\lambda^4}\right] \times p\left\{\frac{1 + (1.049 - 0.0157t)\,p10^{-6}}{1 + 0.003661t}\right\} - \left[0.0624 - \frac{0.000680}{\lambda^2}\right]\frac{f}{1 + 0.003661t},$$

[1] Leipzig, 1925; *Phys. Rev.*, **48**, 98, 1935.
[2] *Bur. Stand. Sci. Papers*, **14**, 697, 1918.
[3] *Phys. Zs.*, **35**, 223, 1934.
[4] *Travaux Bureau internat. poids et mesures*, **19**, 66, 1934.
[5] *Ann. d. Phys.*, **31**, 75, 1938.
[6] *Phil. Trans. R. Soc. London, A*, **238**, 1, 1939.

in which λ is in microns, p is in millimeters of mercury, t is in centigrade degrees, and f is the partial pressure of water vapor in millimeters of mercury.

From this equation with $p = 760$ mm and $t = 15°$, values of the dispersion factor (Table 1, second col.), the refractivity for dry air, half-saturated, and saturated air (third, fourth, and fifth cols.), and vacuum wave numbers have been computed. In the last column is the decimal part of the wave number as given by Kayser for dry air at 760 mm and 15°. Comparison of Kayser's values with those in the sixth column shows that the differences range from 0.003 to 0.028 cm^{-1}. Since wave lengths are most often meas-

TABLE 1

DISPERSION FACTOR, REFRACTIVITY, AND VACUUM WAVE NUMBER, 760 MM, 15° C

λ (A)	D DISP. FACTOR	$(n-1)\times 10^6$ RELATIVE HUMIDITY			VACUUM WAVE NUMBER RELATIVE HUMIDITY			
		Barrell and Sears			Barrell and Sears			Kayser
		0%	50%	100%	0%	50%	100%	0%
3000	0.404131	291.33	291.00	290.67	33323.625	.636	.647	.646
3250	.400006	288.36						
3500	.396801	286.05	285.71	285.37	28563.258	.268	.278	.286
3750	.394260	284.21						
4000	.392209	282.74	282.39	282.04	24992.933	.942	.951	.958
4250	.390520	281.52						
4500	.389138	280.52	280.17	279.82	22215.990	.998	6.006	6.011
4750	.387968	279.68						
5000	.386977	278.96	278.60	278.22	19994.423	.430	.437	.439
5250	.386130	278.35						
5500	.385400	277.83	277.47	277.11	18176.768	.775	.781	.781
5750	.384766	277.37						
6000	.384211	276.97	276.61	276.25	16662.052	.058	.064	.062
6250	.383725	276.62						
6500	.383293	276.31	275.94	275.57	15380.366	.371	.377	.373
6750	.382911	276.03						
7000	.382570	275.79	275.42	275.07	14281.776	.781	.786	.782
7250	.382264	275.57						
7500	.381989	275.37	275.00	274.63	13329.663	.668	.673	.668
7750	.381740	275.19						
8000	.381515	275.02	274.65	274.28	12496.565	.568	.571	.567
8500	.381123	274.74						
9000	.380796	274.51	274.14	273.77	11108.062	.066	.070	.065
9500	.380520	274.31						
10,000	0.380284	274.14	273.77	273.40	9972.628	.632	.636	.631

ured in ordinary air, it is interesting to compare Kayser's wave numbers with those in the seventh column. Smaller differences then appear, but they are still great enough to require consideration in utilizing fully the precision of the best wave lengths.

Barrell and Sears observed in the ranges, λλ 4358–6438, 10°–30°, and 720–800 mm, which in Tables 1 and 2 have been extended by extrapolation. The extension in wave length, especially to the ultraviolet, is possibly excessive, but, for temperature and pressure as applied in Table 2, it seems allowable.

With the aid of Table 1, vacuum-wave numbers obtained from Kayser's table may be expressed in terms of the more accurate data on refractivity, and the small effects of water vapor, amounting to roughly one part in three million for a change of 50 per cent in relative humidity, may be included.

H. D. Babcock and L. Herzberg, in their paper on certain bands of molecular oxygen,[7] derived wave numbers from the first equation of Barrell and Sears, instead of the second equation, quoted above, which we should have used. As a result, the differences which we found from Kayser's values are incorrect in absolute value. The more important relative values of the differences are, however, nearly the same as those obtainable from Table 1.

II. ADJUSTMENT OF WAVE LENGTHS FROM NONSTANDARD TO STANDARD ATMOSPHERIC CONDITIONS

From the relation noted above, $n_1\lambda_1 = n_1'\lambda_1' = \text{Constant}$, it is evident that $d\lambda = -\lambda(dn/n)$, and, for observations in air under ordinary conditions ($n < 1.0003$), it is sufficient to write $d\lambda = -\lambda dn$. Two wave lengths whose ratio is λ_2/λ_1 under standard conditions will be observed to have a ratio $\lambda_2(1 - \Delta n_2)/\lambda_1(1 - \Delta n_1)$ under some other conditions such that the respective changes in index are Δn_1, and Δn_2. If the reference standard, λ_1, is assumed to have its standard value under the nonstandard conditions, the derived wave length is $\lambda_2' = \lambda_2(1 - \Delta n_2 + \Delta n_1)$, and the correction that must be applied to λ_2' is $\lambda_2(\Delta n_2 - \Delta n_1)$.

A third wave length, λ_3, referred to λ_1 under the same nonstandard conditions as before, requires a correction $\lambda_3(\Delta n_3 - \Delta n_1)$. But, if λ_3 is measured from λ_2 as a standard, the correction is $\lambda_3(\Delta n_3 - \Delta n_2)$, and this is not equal to $\lambda_2(\Delta n_2 - \Delta n_1)$ *minus* $\lambda_3(\Delta n_3 - \Delta n_1)$. This means that tables for facilitating the adjustment of wave lengths to standard conditions should be designed for use with standards in any spectral region rather than with a single standard.

In Barrell and Sears's equation the final term, representing the effect of water vapor on the refractivity, may be ignored in the adjustment of wave lengths to standard conditions, except for wave lengths of highest accuracy observed under extreme conditions. The correction derived above, namely $\lambda_2(\Delta n_2 - \Delta n_1)$, may therefore be evaluated from the dispersion factors, D, in Table 1 and the density factors, which are obtained from the expression of Barrell and Sears:

$$p\left\{\frac{1 + (1.049 - 0.0157t)\,p \times 10^{-6}}{1 + 0.003661t}\right\}.$$

If δ_{obs} and δ_{st} are values of this density factor corresponding to the conditions of observation and to standard conditions, respectively, we find

$$\lambda_2(\Delta n_2 - \Delta n_1) = \lambda_2(D_2 - D_1)(\delta_{obs} - \delta_{st}) \times 10^{-6},$$

where subscripts 1 and 2 refer to data for λ_1 and λ_2, respectively. Table 2 shows the differences, $\delta_{obs} - \delta_{st}$, as computed for temperatures from 0° to 30° and for pressures from 600 to 780 mm. For example, the density factor at 760 mm and 15° is 720.88, and at 620 mm and 30° it is 558.84; the table shows the difference, −162.0.

In using Tables 1 and 2 it is necessary to remember only that subscript 1 is associated with the standard lines and subscript 2 with the lines that are being measured. The corrections are generally so small that the dispersion factors from Table 1 need be read only to four figures, and the density factors from Table 2 only to the nearest integer. Also the standards, as well as the wave lengths derived from them, may often be treated as a group instead of as individual lines.

Measurements made with large grating spectrographs at mountain observatories may be appreciably affected by the departure of the atmosphere from standard conditions. For example, overlapping orders of spectra may increase the available number of standards in a comparison spectrum, but it will then be unsafe to assume that the adopted

[7] "Fine Structure of the Red System of Atmospheric Oxygen Bands," *Mt. W. Contr.*, No. 750; *Ap. J.*, 108, 167, 1948.

wave lengths of all the standards on a plate may be assigned to their measured positions. An illustration is found in measurements, kindly supplied by Dr. W. S. Adams, of lines in the iron-arc comparison spectrum on a summer spectrogram (100-inch telescope, coudé spectrograph, second-order dispersion 3 A/mm). Among a larger number of well-known lines in the region of λ 4500, he measured eleven third-order arc lines, λλ 2953–3009. Assigning their standard wave lengths to the blue lines, he found the eleven ultraviolet lines to have wave lengths apparently 0.006 A, on the average, greater than their known values under standard conditions. But this apparent discrepancy is fully accounted for by noting that the average height of the barometer on Mount Wilson is 620 mm and that the summer temperature in the spectrograph is near 20°. From Tables

TABLE 2

CHANGE OF DENSITY FACTOR FROM ITS VALUE AT STANDARD CONDITIONS

$(\delta_{obs} - \delta_{st})$

p (Mm)	t						
	0°	5°	10°	15°	20°	25°	30°
600	−120.5	−131.3	−141.8	−151.8	−161.6	−171.0	−180.1
610	−110.5	−121.5	−132.1	−144.4	−152.2	−161.8	−171.0
620	−100.5	−111.7	−122.4	−132.9	−142.9	−152.6	−162.0
630	− 90.5	−101.9	−112.9	−123.4	−133.6	−143.5	−153.0
640	− 80.5	− 92.0	−103.1	−113.9	−124.3	−134.3	−144.0
650	− 70.4	− 82.2	− 93.5	−104.4	−115.0	−125.1	−135.0
660	− 60.4	− 72.3	− 83.8	− 94.9	−105.6	−116.0	−126.0
670	− 50.4	− 62.5	− 74.2	− 85.4	− 96.3	−106.8	−117.0
680	− 40.4	− 52.7	− 64.5	− 75.9	− 87.0	− 97.6	−108.0
690	− 30.4	− 42.8	− 54.8	− 61.4	− 77.6	− 88.5	− 99.0
700	− 20.4	− 33.0	− 45.2	− 56.9	− 68.3	− 79.3	− 90.0
710	− 10.4	− 23.2	− 35.5	− 47.4	− 59.0	− 70.1	− 80.9
720	− 0.3	− 13.3	− 25.9	− 38.0	− 49.6	− 60.9	− 71.9
730	+ 9.7	− 3.5	− 16.2	− 28.5	− 40.3	− 51.8	− 62.8
740	+ 19.7	+ 6.3	− 6.6	− 19.0	− 31.0	− 42.6	− 53.8
750	+ 29.7	+ 16.2	+ 3.1	− 9.5	− 21.7	− 33.4	− 44.8
760	+ 39.7	+ 26.0	+ 12.8	0.0	− 12.3	− 24.3	− 35.8
770	+ 49.7	+ 35.8	+ 22.4	+ 9.5	− 3.0	− 15.1	− 26.8
780	+ 59.8	+ 45.7	+ 32.1	+ 19.0	+ 6.3	− 5.9	− 17.8

1 and 2 we find the correction required for lines near λ 3000 when measured from standards near λ 4500 under the conditions 620 mm and 20° to be

$$-(0.4041-0.3891)\times 143\times 3000\times 10^{-6}=-0.0064\,\text{A}.$$

Under winter conditions the correction would have been about −0.004 A.

As a second example we derive the correction required for lines near λ 8000 when measured from standards near λ 4000 at 720 mm and 25°:

$$-(0.3815-0.3922)\times 61\times 8000\times 10^{-6}=+0.0052\,\text{A}.$$

Attention is directed to this example because it was solved incorrectly by Meggers and Peters when they illustrated the use of their tables. They obtained the result, +0.0028 A, by taking the algebraic difference of two separate corrections, i.e., for λ 4000 and for

λ 8000, each in terms of λ 6438, as equal to the correction of λ 8000 relative to λ 4000, a procedure which we found erroneous in an earlier paragraph. Used correctly, however, the data of Meggers and Peters lead to a correction, +0.0048 A, which differs from +0.0052 only because of the differences in refractivity employed in the two computations. To use the data of Meggers and Peters with secondary standards of wave length, take from their Table 5 the difference of the refractivity for the region measured *minus* the refractivity for the standards; multiply this difference by the nominal value of the wave length that is measured, by the density factor from their Table 3, and by 10^{-7}. In the present example this amounts to

$$-(2746.5-2817.1)\times 0.085\times 8000\times 10^{-7}=0.0048\,\text{A}\,.$$

Although the difference between 0.0052 and 0.0048 might often be ignored, such discrepancies may exceed 0.001 A under conditions commonly met.

While preparing this paper, I discovered an error which I committed in a recent paper on the ultraviolet solar spectrum.[8] The correction to standard conditions was made as +0.001 A, but it should have been −0.001 A. All wave lengths in Tables 1 and 3 of that paper should therefore be diminished by 0.002 A; the first line in Table 2 should read 2995–3133 A . . . − 0.0012 A, a new line should be interpolated after the first, reading 3133–3370 . . . (−0.0010)†, and the footnote concerning λλ 3133–3370 should be deleted.

CONCLUSIONS

The most reliable values of the refractivity of air lead to vacuum-wave numbers systematically smaller than those in Kayser's table, and the differences are nonuniform to an extent that requires consideration when the most accurate results are desired. Existing tables of term values[9] require small readjustments downward but may be used as they stand in conjunction with Kayser's table. Further determinations of the refractivity of air in the ultraviolet and infrared regions are needed. The tables of Meggers and Peters, when used for the reduction of measurements that are referred directly to the primary standard of wave length, give corrections slightly different from those now found; for use with secondary standards their data may be applied correctly by a modified procedure.

Some standards of wave length are considered to be reliable to about one part in fifty million; but, if observed in moist air, an uncertainty of 5 per cent in the relative humidity (at 760 mm and 30°) will introduce an uncertainty of one part in twelve million in the wave lengths.

[8] Babcock, Moore, and Coffeen, *Mt. W. Contr.*, No. 745; *Ap. J.*, **107**, 287, 1948.

[9] *Trans. I.A.U.*, **4**, 67, 1932.

PHOTOELECTRIC STUDIES. I. COLOR-LUMINOSITY ARRAY FOR MEMBERS OF THE HYADES CLUSTER*

OLIN J. EGGEN
Lick Observatory, University of California
Received July 25, 1949

ABSTRACT

Observations of 64 Hyades cluster stars have been made with photomultiplier photometers on the Washburn 15-inch and the Lick 12-inch refractors. The magnitudes and colors have been reduced to no atmosphere with the use of extinction factors determined each night. The dependence of the extinction factors upon the color of the star has also been determined nightly; the results for a typical night have been described to illustrate the procedure. The color system has a baseline slightly longer and shifted to the violet of the International System. Both the colors and the magnitudes have been reduced to the International System, Pg_p and C_p, by comparisons with the North Polar Sequence.

The observed magnitudes have been converted to absolute magnitudes by the use of an unpublished value for the convergent of the cluster, $A = 94°0$, $D = +7°6$, derived by R. E. Wilson. The resulting color-luminosity array, consisting of dwarf, bright-dwarf, subdwarf, and giant sequences, satisfies the observations of 52 of the 64 stars observed, within the uncertainties of the proper motions and colors. This result indicates that there is inappreciable "cosmical" dispersion in luminosity for the various sequences of the color-luminosity array. Of the remaining 12 stars, 9 are known, or probable, binaries, 2 stars populate an additional sequence to be described in a later paper, and 1 star is possibly a nonmember of the cluster. It is shown that the stars with high rotational velocities populate mainly the bright-dwarf sequence.

The present paper—the first of a series—is the result of an attempt to realize the advantages of the 1P21 photomultiplier for the precise measurement of magnitudes and colors of stars. This program was started in 1947 with the Washburn Observatory's 15-inch refractor, and it has been continued with the Lick Observatory's 12-inch refractor.

INSTALLATION

Since the Madison and Lick photometers, designed by Drs. A. E. Whitford and G. E. Kron,[1] respectively, are very similar, only the Lick installation will be described in detail. Figure 1 gives a general view of the instrument mounted on the 12-inch refractor. The optical column of the photometer contains the color filters, focal-plane diaphragm, dark slide, and a guiding eyepiece. The filter slide is 2 inches inside the focal plane. The focal-plane diaphragm has a diameter of 1.42 mm, which has been found to be the smallest possible to use and still clear all the light of a star. The multiplier is mounted in a cylindrical cavity turned in a solid piece of Duraluminum. The 90 volts per stage, required by the photomultiplier, are supplied by batteries mounted in a case permanently installed on the telescope tube. The signal received from the photomultiplier goes through a DC amplifier and records on an Esterline-Angus, 0–1 recording milliameter.

COLOR SYSTEMS

The color-sensitivity-curves of the photomultiplier with filters were determined at Madison and at Lick with quartz monochromators. The energy of the source was measured at each wave length with a thermocouple, and the response was corrected to constant energy. In Table 1 the column marked "Clear" gives the relative spectral response of the Madison cell, including the 15-inch objective. The columns marked "Blue" and "Yellow" for Madison contain the numbers under "Clear" multiplied by the appropriate

* *Contributions from the Lick Observatory*, Ser. II, No. 25.

[1] A more complete description of the photometer and amplifier may be found in two publications by G. E. Kron; *Lick Obs. Bull.*, **19**, 53, 1939 (No. 499), and *Electronics*, August, 1948.

transmissions of the two filters. The columns marked "Blue" and "Yellow" for Lick contain the relative spectral responses of the photomultiplier and 12-inch objective plus the blue and yellow filters, respectively. At Madison the blue filter was Schott BG1, 2 mm thick; the yellow was Schott GG7, 2 mm thick. At Lick the blue and yellow filters are, respectively, Corning 5330 and 3385, both of standard optical thickness.

TABLE 1

CONSTANT-ENERGY COLOR SENSITIVITIES OF PHOTOMULTIPLIER-FILTER COMBINATIONS

Wave Length	Madison			Lick	
	Clear	Blue	Yellow	Blue	Yellow
3700 A	1.10	1.04	.....	0.90	.....
3800	1.80	1.75	.....	1.88	.....
4000	2.33	2.22	.....	2.36	.....
4200	2.23	1.96	.....	2.14	.....
4400	2.15	1.33	0.01	1.89	.....
4600	2.08	0.83	0.08	1.39	.....
4800	1.90	0.19	0.60	0.80	1.16
5000	1.63	0.08	1.34	0.39	1.99
5200	1.38	.....	1.21	0.19	2.02
5400	1.10	.....	0.99	0.08	1.57
5600	0.73	.....	0.67	0.03	1.07
5800	0.43	.....	0.39	0.01	0.71
6000	0.23	.....	0.21	0.01	0.27
6200	0.12	.....	0.11	.....	0.08
6400	0.03	.....	0.03	.....	0.03

TABLE 2

PHOTOELECTRIC AND INTERNATIONAL EFFECTIVE WAVE LENGTHS FOR BLACK-BODY SOURCES

Temperature (° K)	Clear		Blue		Yellow		Y − B		
	P_e	P_g	P_e	P_g	P_e	P_y	P_e	P_g	
11,000	4420 A	4240 A	3980 A	4240 A	5260 A	5430 A	1280 A	1190 A	Madison
3,000	4950	4560	4250	4560	5370	5480	1120	920	Madison
11,000	.....	.....	4020	4240	5240	5430	1220	1190	Lick
3,000	.....	.....	4410	4560	5360	5480	950	920	Lick

Since the magnitudes and colors are to be reduced to the International System, an attempt has been made to derive the effective wave lengths of the two filter-multiplier combinations. Following F. H. Seares,[1] we have for either yellow or blue:

$$\lambda_e = \frac{\Sigma \lambda s y}{\Sigma s y}, \qquad (1)$$

where s is the sensitivity factor under "Blue" or "Yellow" in the present Table 1 and y is the relative energy of a black-body radiator, taken from Seares's Table 1. The resulting

[1] *Ap. J.*, **101**, 15, 1945; *Mt. W. Contr.*, No. 701.

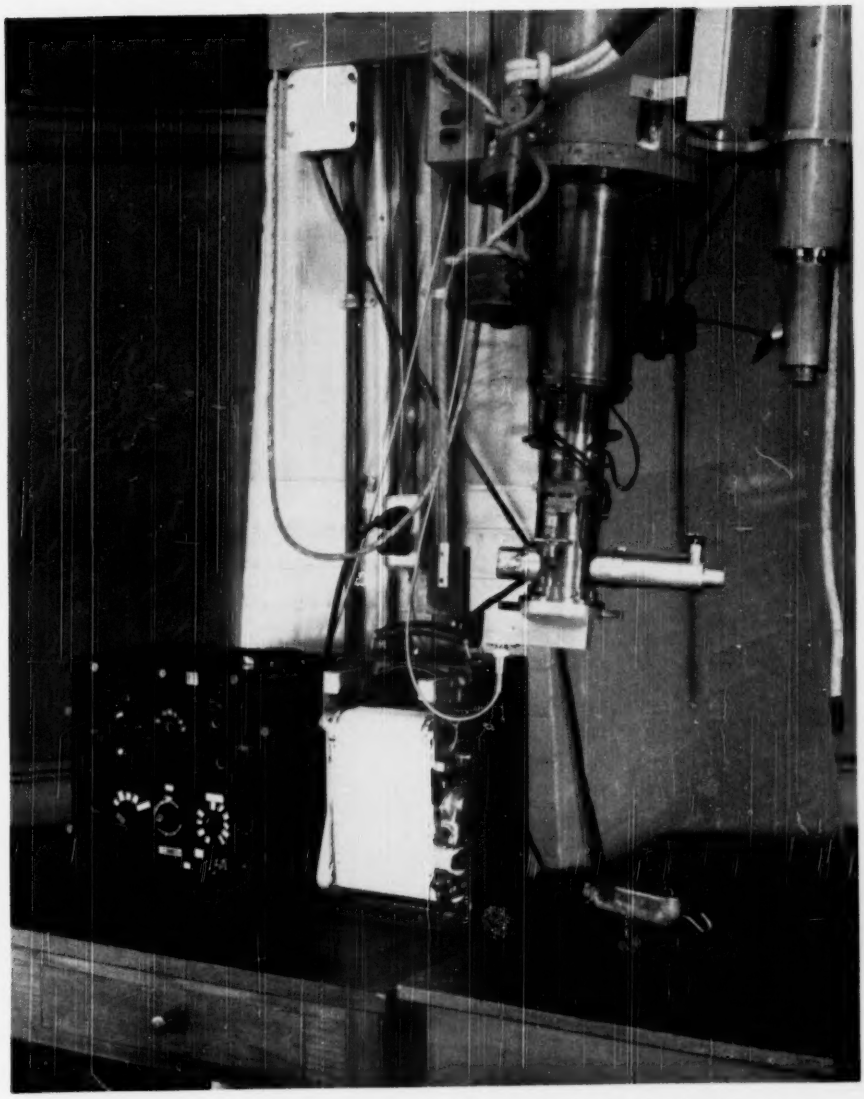

FIG. 1.—Photometer, amplifier, and recorder installation for the 12-inch refractor

photoelectric effective wave lengths and those for the International System from Seares's Table 3, both rounded off to 10 A, are given for two temperatures in the present Table 2. It should be noted that the effective wave lengths derived here are for no atmosphere; those for the International System include the extinction at the Mount Wilson pole.

Since the figures in Table 2 are based upon black bodies and are therefore largely theoretical, we have made the usual comparison with the stars of the North Polar Sequence.

TABLE 3

COLORS AND MAGNITUDES OF THE NORTH POLAR SEQUENCE

NPS	Pg_p	C_p	Pg_{int}	C_{int}	$C_{n,w}$	$Pg_p - Pg_{int}$
1	4.23	−0.07	4.40	+0.03	−0.07	−0.17
2	5.12	−0.09	5.23	−0.11	−0.11	− .11
3	5.72	+0.16	5.79	+0.18	+0.16	− .07
4	5.88	+0.14	5.92	+0.14	+0.13	− .04
5	6.46	+0.02	6.46	+0.03	+0.01	.00
2s	6.48	+0.26	6.47	+0.15	+0.24	+ .01
1r	6.61	+1.57	6.68	+1.53	+1.54	− .07
3s	6.66	+0.33	6.63	+0.23	+0.31	+ .03
6	7.11	+0.12	7.12	+0.06	+0.12	− .01
2r	7.89	+1.51	7.92	+1.57	+1.53	− .03
8	8.31	+0.25	8.30	+0.23	.....	+ .01
9	9.09	+0.20	8.94	+0.14	.....	+ .15
0	9.21	+0.17	9.13	+0.12	+0.16	+ .09
4r	9.28	+1.01	9.20	+1.02	+1.00	+ .08
11	9.83	+0.22	9.77	+0.20	.....	+ .06
12	10.13	+0.35	10.08	+0.31	.....	+ .05
4s	10.36	+0.47	10.31	+0.47	.....	+ .05
14	11.02	+0.45	10.93	+0.40	.....	+0.09

In Table 3 the columns labeled Pg_p and C_p are the mean magnitudes and colors computed from the relations

$$\left.\begin{aligned} C_p &= 0.90 + 0.80 C_M \\ &\pm 0.02 \quad \pm 0.01 \end{aligned}\right\} \text{Madison} \qquad (2a)$$

$$\left.\begin{aligned} Pg_p &= P e_M + 0.38 C_p \\ &\pm 0.01 \end{aligned}\right\} \text{Madison} \qquad (2b)$$

$$\left.\begin{aligned} C_p &= 1.16 + 0.89 C_L \\ &\pm 0.02 \quad \pm 0.01 \end{aligned}\right\} \text{Lick} \qquad (3a)$$

$$\left.\begin{aligned} Pg_p &= P e_L - 0.21 C_p \\ &\pm 0.01 \end{aligned}\right\} \text{Lick} \qquad (3b)$$

where the subscripts "M" and "L" refer to photoelectric magnitudes and colors observed at Madison and at Lick, respectively, and the uncertainties are expressed as probable errors. The column labeled "C_{int}" contains the International colors according to Seares and Joyner,[3] while the values for Pg_{int} are from the *Rome Report* of the International Astronomical Union[4] adjusted with the values of C_{int} in a manner suggested by Seares. The values of $C_{n,w}$ are the International colors determined by Stebbins and Whitford[5] with a photomultiplier photometer attached to the 60-inch reflector at Mount Wilson. The Madison magnitudes were determined independently of the colors through the use

[3] *Ap. J.*, **101**, 18, 1945; *Mt. W. Contr.*, No. 701.

[4] *Trans. I.A.U.*, **1**, 71, 1922.

[5] *Ap. J.*, **108**, 413, 1948; *Mt. W. Contr.*, No. 753.

of a third, "clear," deflection, whereas only two deflections, alternately through the blue and yellow filters, were taken at Lick; the Lick magnitudes were obtained from the blue deflections. Rewriting the expression (3*b*), we have

$$P e_L - P g_{int} = 0.21 C_g , \tag{3b'}$$

from which it is seen that the "blue" Lick magnitudes are to the violet of Pg_{int} by $0.21(Pg - Pv)$ or 220 A in the mean for black-body radiators of 11,000° and 3,000°. The corresponding value from Table 2 is $0.18(Pg - Pv)$. Similarly, rewriting expression (2*b*), we have

$$P e_M = P g_p - 0.38 C_p , \tag{2b'}$$

from which we find that the "clear" Madison magnitudes are $0.38(Pg - Pv)$ to the red of Pg_{int}. The corresponding value in Table 2 is $0.27(Pg - Pv)$. The agreement in both cases is satisfactory, considering the uncertainty in the black-body effective wave lengths arising from the lack of accurate data on the violet transmissions of both the 12- and the 15-inch objectives.

EXTINCTION

As already mentioned, the colors and magnitudes herein reported were reduced to no atmosphere, and the necessary reduction factors were determined each night. The dependence of these factors upon the color of the star was also determined nightly by choosing, as "extinction stars," two stars representing the extreme range of colors observed. The method used is best illustrated by an example. Figure 1 shows the logarithms of blue and yellow deflections, log d_b and log d_y, obtained January 27, 1949, for stars numbered 29 and 34 in Table 4, plotted against Air mass = sec z. Least-squares solutions, fitted to the plotted points, gave the following constants and coefficients, with accompanying probable errors:

$$\begin{aligned}
&\log d_b(34) = 1.016 - 0.130 \sec z \qquad \text{Zenith extinction} = 0^m.32 ; \\
&\qquad\qquad \pm 0.001 \quad \pm 0.001 \\
&\log d_y(34) = 0.565 - 0.070 \sec z \qquad \text{Zenith extinction} = 0^m.18 ; \\
&\qquad\qquad \pm 0.001 \quad \pm 0.001 \\
&\log d_b(29) = 0.855 - 0.113 \sec z , \qquad \text{Zenith extinction} = 0^m.28 ; \\
&\qquad\qquad \pm 0.001 \quad \pm 0.001 \\
&\log d_y(29) = 0.743 - 0.072 \sec z , \qquad \text{Zenith extinction} = 0^m.18 . \\
&\qquad\qquad \pm 0.001 \quad \pm 0.002
\end{aligned} \tag{4}$$

That the probable errors are of the right order can be seen from Figure 2. At no atmosphere the color, in magnitudes, of star No. 34 is $2.5(0.565 - 1.016) = -1.13$, and the color of No. 29 is $2.5(0.743 - 0.855) = -0.28$. Applying expression (3*a*), we find $C_p(34) = +0.15$ and $C_p(29) = +0.91$. The differences in the coefficients of sec z in expressions (4) show that the nearly universal practice of using the same photographic extinction for all colors can lead to serious errors. Since the present magnitudes were obtained from the blue deflections, the differential extinction effect at the zenith for stars 34 and 29 is 0.04 mag. on both P_e and C_L. If observed at the Lick pole, this effect would become 0.07 mag., which agrees with the figure determined theoretically by Seares[3] for the differential effect between A0 and K0 stars at the Mount Wilson pole. Since the coefficients of sec z for the yellow deflections rarely differ from star to star by more than is indicated in expressions (4), our practice has been to use the mean. For colors midway between the extremes of stars Nos. 29 and 34, the blue extinction was found by simple

interpolation; a few runs with three extinction stars amply proved the validity of this practice. Although observations of a dozen or more stars could be obtained during the time spent determining the extinction each night, rarely more than one hour, the increased accuracy in the slightly smaller output seemed well worth the time and effort.

THE OBSERVATIONS

The pioneer investigation of the Hyades cluster was published by Lewis Boss[6] in 1908. The succeeding researches are so numerous that no attempt will be made here to list them, since a summary of the work up to 1941 has been compiled by J. Ramberg.[7]

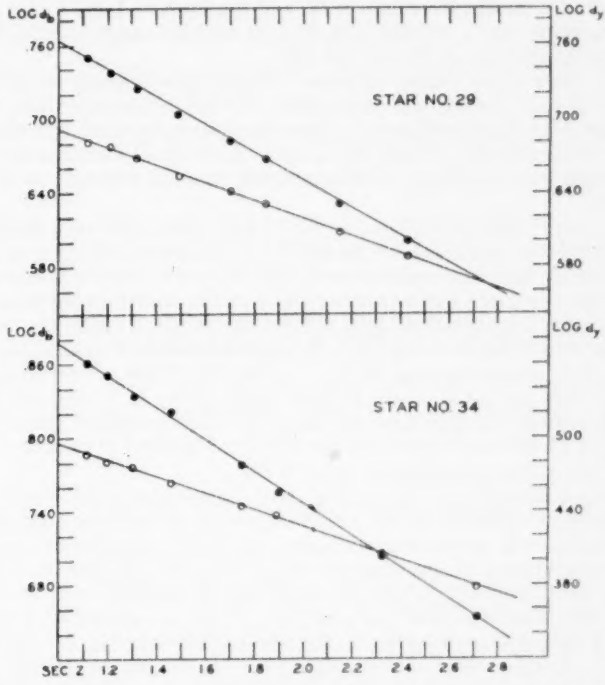

FIG. 2.—Extinction determination for stars Nos. 29 and 34 on January 27, 1949. The open circles represent the yellow deflections; the filled circles, the blue.

The most recently published derivation of the convergent point of the cluster is that of W. M. Smart.[8] However, Seares[9] has since shown that, by neglect of a regression error, the mean distance found by Smart may be too small by as much as 7 per cent. The present program of magnitudes and colors of the Hyades members was begun in 1947 to test the reality of the "cosmical dispersion" of the main sequence as defined by the cluster stars. The observing program has been confined to stars contained in a list of cluster members kindly supplied by Dr. R. E. Wilson of the Mount Wilson and Palomar observatories. The 1947–1948 observing season at Madison and the 1948–1949 winter season at Lick were unusually poor, so that only 64 stars, out of some 140 cluster members,

[6] *A.J.*, **26**, 31, 1908.
[7] *Stockholm Obs. Ann.*, Vol. **13**, 1941.
[8] *M.N.*, **99**, 168, 1939.
[9] *Ap. J.*, **102**, 323, 1945; *Mt. W. Contr.*, No. 716.

were observed. The distribution with magnitude of the stars observed, however, is satisfactory for the present purpose. Since the Hyades is the closest moving cluster, it has the greatest importance for establishing the zero point of absolute magnitudes, and it will therefore be kept on the observing program.

The baseline of the colors has been discussed above and is indicated in Table 2. The zero point of the magnitudes was established through observations of NPS 1 and 4 made at the beginning, middle, and end of each night. Stebbins and Whitford[10] have previously shown that the photographic-magnitude scale diverges from the photoelectric one by 0.2 mag. between magnitudes 5 and 9. This same effect is evident in the last column of Table 3. Therefore, in order to make the present magnitudes more comparable with the photographic results, the values of Pe_L and Pe_M for NPS 1 and 4 were fixed so as to bring the zero point into agreement with Pg_{int} at the mean magnitude of the 6 stars, NPS 4, 5, 2s, 3s, 6, and 8, or at $Pg_{int} = 5.9$–8.3.

A single Lick observation usually consisted of deflections through the yellow filter, the blue filter, and again through the yellow filter; the Madison observations included a "clear" deflection. The color systems were chosen to give nearly equal deflections in both the yellow and the blue for the reddest cluster stars observed. The average time spent on each star, per night, was 5 minutes. In all cases each star was observed on at least two different nights.

Measurable "clear" deflections at magnitude 13.5 are obtainable with the installation on the 12-inch refractor, but the use of the filters cuts this limit to photographic magnitude 12. This working limit has been arbitrarily lowered to 11.5, for, to maintain uniform accuracy, the time spent per star increases rapidly at the fainter magnitudes. Over the whole range in magnitude considered here, the average deviations from the mean do not exceed 0.01 mag., and residuals as large as 0.03 mag. are rare in both magnitude and color.

The results of the observations of 65 stars are listed in Table 4. The numbers in the first column are from the list of cluster members supplied by R. E. Wilson. The proper motions are taken from the *Boss General Catalogue*[11] when available, otherwise from a recent publication by Wilson.[12] For 4 stars not contained in either of these lists, the proper motions are taken from an earlier paper by Wilson.[13]

The most recent discussion of the photographic magnitudes in the Hyades region is that of E. Holmberg.[14] Table 5 contains the 39 stars common to Table 4 and Holmberg's lists. The prefixed A or B to the numbers in the second column of the table indicates in which of Holmberg's two catalogues the magnitudes are contained. For the stars brighter than 7.00 mag., Holmberg's catalogues give magnitudes determined by E. Hertszprung;[15] for the fainter stars the magnitudes are a mixture of determinations by Ramberg[7] and by Holmberg. Figure 3 shows graphically the relation between Pg_p and $Pg_p - Pg'(H)$, where $Pg'(H) = Pg(H) - 0^m18$. The correction of -0.18 mag. to Holmberg's magnitudes brings the two scales into agreement over the same magnitude range as was used in adjusting the Pg_p's to Pg_{int}.

Figure 4 shows a plot of Pg_p against C_p. The dispersion in magnitude, for a given color, is of the order to be expected from the differential in distance of the individual stars, caused by the depth of the cluster.

[10] *Ap. J.*, **87**, 237, 1938; *Mt. W. Contr.*, No. 586.

[11] Carnegie Institution of Washington, 1937.

[12] *Ap. J.*, **107**, 129, 1948; *Mt. W. Contr.*, No. 741.

[13] *A.J.*, **42**, 49, 1932.

[14] *Medd. Lund. Obs.*, Ser. II, No. 113, 1944.

[15] *A.N.*, **209**, 115, 1919.

TABLE 4

MEMBERS OF THE HYADES CLUSTER

No.	HD or BD	1950		Madison			Lick			Mean		Spectral Class		μ*	M_{pg_0}	$V_r \sin i$	Remarks
		α	δ	P_{gp}	C_p	n	P_{gp}	C_p	n	P_{gp}	C_p	Mt.W.	Y				
4	24357	3h50m3	+17° 11′	6.17	+0.25	3	6.17	+0.23	3	6.17	+0.24	F0	F4	0".151	+3.28	25	
6	25102	56.9	+10 11	6.64	+ .32	2	6.66	+ .34	2	6.65	+ .33	F3	F5	.171	+4.15	25	
7	+19°641	57.7	+20 14	9.16	+ .59	1	9.20	+ .58	2	9.19	+ .58	G2	G4	.154	+6.39	.....	
8	25202	3 57.9	+18 03	6.06	+ .25	2	6.06	+ .20	3	6.06	+ .22	F2	F4	.138	+3.06	100	
9	25570	4 01.2	+ 8 04	5.67	+ .27	2	5.64	+ .26	2	5.66	+ .265	F2	F4	.171	+3.22	0	
10	25825	03.3	+15 34	.....	.....	...	8.20	+ .43	2	8.20	+ .43	G2	.....	*.114*	+4.87	.....	
13	26345	07.8	+18 18	6.88	+ .30	2	6.87	+ .28	2	6.88	+ .29	F6	F6	.121	+3.76	0	
14	26462	08.7	+ 5 24	5.88	+ .25	2	5.90	+ .24	3	5.89	+ .24	F2	F4	.149	+3.25	0	45 Tau
15	26736	11.5	+23 29	8.47	+ .50	2	8.45	+ .50	2	8.46	+ .50	G4	.....	*.129*	+5.38	.....	
16	26737	11.5	+22 20	7.21	+ .32	2	7.19	+ .31	2	7.20	+ .315	F4	F5	.097	+3.54	.....	
17	26756	11.6	+14 30	8.92	+ .57	2	8.94	+ .56	2	8.93	+ .565	G5	.....	*.129*	+6.01	.....	
18	26767	11.7	+12 20	8.60	+ .53	2	.....	.....	...	8.60	+ .53	G3	.....	*.115*	+5.44	.....	
19	26784	11.8	+10 35	7.47	+ .40	2	7.49	+ .40	2	7.48	+ .40	F7	.....	*.125*	+4.52	.....	
20	26874	12.8	+20 42	8.39	+ .48	2	8.42	+ .48	2	8.40	+ .48	G6	G4	.115	+5.15	.....	
21	26911	12.9	+15 17	6.63	+ .28	3	6.63	+ .28	2	6.63	+ .28	F5	F5	.123	+3.61	25	48 Tau
23	27130	14.8	+16 48	8.90	+ .63	1	8.86	+ .61	1	8.88	+ .62	G6	.....	(.115)	+5.72	.....	†
24	27149	15.1	+18 07	7.96	+ .56	2	7.94	+ .57	1	7.95	+ .56	G4	.....	.116	+4.79	.....	†
25	27176	15.4	+21 28	5.76	+ .21	2	5.79	+ .22	2	5.78	+ .215	A8n	A8	.104	+2.33	25	51 Tau
29	27371	16.9	+15 31	4.59	+ .92	...	4.61	+ .92	..	4.60	+ .92	G8	G9	.121	+1.59	0	γ Tau
30	27383	17.0	+16 24	7.29	+ .43	1	7.29	+ .42	1	7.29	+ .425	F8	F9	.124	+4.34	0	55 Tau†
31	27397	17.1	+13 55	5.69	+ .20	3	5.69	+ .20	2	5.69	+ .20	F2	F3	.118	+2.66	75	57 Tau†
33	27429	17.5	+18 37	6.32	+ .26	2	6.32	+ .26	2	6.32	+ .26	F3	F3:	.118	+3.23	50	†
34	27459	17.8	+14 59	5.33	+ .15	...	5.32	+ .15	..	5.32	+ .15	A9n	F0	.113	+2.20	0	58 Tau
35	27483	18.1	+13 45	6.54	+ .33	3	6.50	+ .33	1	6.53	+ .33	F4	F6	.117	+3.50	0	†
38	27561	18.8	+14 18	6.82	+ .28	1	6.85	+ .29	2	6.84	+ .29	F6	F5	.120	+3.88	0	
39	27628	19.2	+13 58	5.85	+ .21	2	5.84	+ .19	2	5.84	+ .20	A4	A3p	.117	+2.82	0	60 Tau†
40	27685	19.9	+16 40	8.24	+ .54	2	8.28	+ .56	2	8.26	+ .55	G5	G4	.153	+5.80	.....	
41	27691	19.9	+14 56	7.38	+ .43	1	7.34	+ .44	2	7.35	+ .44	F9	.....	(.103)	+4.06	.....	†
42	+13°671	19.9	+14 08	.....	.....	...	10.68	+ .56	3	10.68	+ .56	G3	.....	*.107*	+7.48	.....	
43	27697	20.0	+17 26	4.68	+ .91	4	4.68	+ .91	4	4.68	+ .91	G9	K0	.114	+1.57	0	δ Tau
47	27749	20.5	+16 40	5.76	+0.22	3	5.80	+0.23	2	5.78	+0.225	A2	A1p	0 110	+2 62	0	63 Tau†

* The majority of the values for the proper motion are taken from the *Boss General Catalogue*. The italicized values are from a recent paper by R. E. Wilson, *Ap. J.*, **107**, 129, 1948; *Mt. W. Contr.*, No. 741. The four values in parentheses are taken from an earlier paper by Wilson (*A.J.*, **42**, 49, 1932).

† See notes to Table 4, p. 73.

TABLE 4—*Continued*

No.	HD or BD	1950		Madison			Lick			Mean		Spectral Class		π''	M_{Fp}	$V_r \sin i$	Remarks
		α	δ	P_{Fp}	C_p	n	P_{Fp}	C_p	n	P_{Fp}	C_p	Mt.W.	Y				
50	27819	4h21m.2	+17°20′	4.80	+0.10	3	4.84	+0.09	3	4.82	+0.095	A6n	A6	0″.120	+1.84	0	64 Tau
52	27836	21.3	+14.39				7.97	+0.46	2	7.97	+0.46	G1		*.106*	+4.77		
53	+17°.715	21.4	+17.53				10.65	+0.87	2	10.65	+0.87	K4		*.111*	+7.49		
56	27859	21.6	+16.46	8.13	+ .48	2	8.09	+0.49	2	8.11	+0.485	G0	G2	.120	+5.15		
57	27901	22.0	+18.56	6.23	+ .28	1	6.25	+0.27	2	6.25	+0.27	F0	F4	.117	+3.20	50	
59	27934	22.4	+22.11	4.14	+ .07	3	4.24	+0.09	3	4.19	+0.08	A4	A5	.111	+0.96	50	65 Tau
60	27946	22.4	+22.05	5.40	+ .20	3	5.38	+0.20	3	5.39	+0.20	A8n	A7	.125	+2.41	150	67 Tau
61	27962	22.6	+17.49	4.23	+ .01	2	4.24	+0.00	4	4.24	+0.00	A2	A1	.115	+1.18	0	68 Tau†
64	27990	22.9	+17.55				9.84	+0.81	3	9.84	+0.81	K0		*.098*	+6.44		†
66	28024	23.3	+22.42	4.34	+ .18	2	4.44	+0.18	3	4.38	+0.18	A6	F0	.118	+1.27	250	υ Tau
70	28052	23.5	+15.30	4.58	+ .18	1	4.62	+0.18	2	4.61	+0.18	A5n	F0	.116	+1.63	150	71 Tau
72	+13°.684	24.6	+14.09				11.45	+1.05	2	11.45	+1.05	K5		*.118*	+8.54		
74	+14°.699	24.9	+14.19				10.33	+0.86	3	10.33	+0.86	K2		(.102)	+7.11		
75	28226	25.0	+21.31	5.84	+ .22	2				5.84	+0.22	A6n	A5p	.106	+2.55	25	†
80	28305	25.7	+19.04	4.48	+ .95	3	4.47	+0.96	3	4.48	+0.955	G9	K0	.118	+1.50	0	ϵ Tau
81	28307	25.7	+15.51	4.75	+ .89	3	4.79	+0.90	1	4.76	+0.89	G8	G8	.109	+1.62	0	θ^1 Tau
82	28319	25.8	+15.46	3.46	+ .14	3	3.48	+0.15	4	3.47	+0.145	A6	A7	.108	+0.37	50	θ^2 Tau†
84	28355	26.0	+12.56				5.08	+0.15	2	5.08	+0.15	A5	A7	.112	+2.10	25	79 Tau
89	+17°.734	26.6	+17.47				9.63	+0.72	2	9.63	+0.72	G7		.116	+6.65		
90	+15°.634	26.7	+16.08				11.38	+1.03	3	11.38	+1.03	K5		*.097*	+8.37		
91	28462	27.1	+16.33				9.80	+0.75	2	9.80	+0.75	K0		*.109*	+6.72		
92	28485	27.3	+15.32				5.75	+0.25	2	5.75	+0.25	A8n	F0	.108	+2.68	−100	80 Tau†
94	28527	27.7	+16.05				4.84	+0.13	2	4.84	+0.13	A6	A6	.114	+1.88	0	
95	28545	27.8	+15.38				9.58	+0.73	2	9.58	+0.73	G8		*.098*	+6.30		
96	28546	27.8	+15.35	5.56	+ .16	1	5.57	+0.17	2	5.57	+0.17	A7	A5p	.108	+2.50	0	81 Tau
102	28677	29.0	+15.45	6.16	+ .23	1	6.19	+0.25	1	6.18	+0.23	F0n	F4	.108	+3.14	75	85 Tau
105	28805	30.2	+15.42				9.20	+0.64	2	9.20	+0.64	G7		(.102)	+6.04		
106	28878	30.8	+16.38				10.12	+0.80	2	10.12	+0.80	K0		*.105*	+7.02		
117	29388	35.4	+12.25				4.31	+0.09	2	4.31	+0.09	A5n	A6	.101	+1.28	0	90 Tau†
119	29488	36.4	+15.49				4.69	+0.10	2	4.69	+0.10	A5n	A7	.087	+1.30	50	92 Tau
138	31845	56.9	+15.51	7.06	+ .34	1	7.03	+0.34	1	7.04	+0.34	F6	F5	.094	+4.23		101 Tau
139	32301	5 00.1	+21.31	4.60	+ .09	1	4.65	+0.10	1	4.62	+0.095	A5n	A7	.080	+1.27	100	ι Tau
141	33254	06.6	+ 9.46	5.55	+0.16	2				5.55	+0.16	A5	A2p	0.066	+2.37	0	16 Ori†

NOTES TO TABLE 4

23. Spectroscopic binary; one spectrum; P = 5.61 days.
24. Variable velocity (Wilson, *Ap. J.*, **107**, 129, 1948; *Mt. W. Contr.*, No. 741).
30. ADS 3135.
31. Spectroscopic binary; one spectrum (Stillwell, *Pub. Dom. Ap. Obs. Victoria*, **7**, 337, 1945).
33. Two spectra (Wilson).
35. Two spectra (Wilson).
39. Metallic-line star.
41. ADS 3169, brighter star is spectroscopic binary with one spectrum; P = 4.00 days.
43. Metallic-line star.
47. Metallic-line star. Spectroscopic binary with one spectrum; P = 8.4 days.
61, 64. These two stars from ADS 3286.
75. Metallic-line star.
82. Spectroscopic binary with one spectrum; P = 140.7 days.
92. ADS 3264, brighter star is spectroscopic binary with one spectrum (Stillwell).
117. Spectroscopic binary with one spectrum (Stillwell).
141. Metallic-line star.

TABLE 5

COMPARISON OF Pg_p AND C_p WITH MAGNITUDES AND COLORS GIVEN BY HOLMBERG

No.	H	Pg_p	Pg(H)	C_p	C(H)	$Pg_p - Pg$(H)
82	A470	3.47	3.74	+0.14	+0.13	−0.27
61	B 77	4.24	4.44	+0.00	+0.11	− .20
117	B148	4.31	4.51	+0.09	+0.06	− .20
80	B 90	4.48	4.79	+0.96	+1.03	− .31
29	B 33	4.60	4.92	+0.92	+1.05	− .32
70	A262	4.61	4.89	+0.18	+0.20	− .28
43	B 58	4.68	4.95	+0.91	+0.92	− .27
119	B160	4.69	4.89	+0.10	+0.15	− .20
81	A462	4.76	4.99	+0.89	+0.89	− .23
50	B 64	4.82	5.02	+0.10	+0.11	− .20
94	A635	4.84	5.00	+0.13	−0.01	− .16
84	B 92	5.08	5.30	+0.16	+0.10	− .22
34	B 40	5.32	5.54	+0.15	+0.29	− .22
96	A648	5.57	5.80	+0.17	+0.21	− .23
31	B 37	5.69	5.92	+0.20	+0.38	− .23
92	A608	5.75	5.91	+0.25	+0.15	− .16
102	A765	6.18	6.38	+0.23	+0.24	− .20
57	B 72	6.25	6.34	+0.30	+0.16	− .09
33	B 38	6.32	6.41	+0.26	+0.18	− .09
21	B 9	6.63	6.71	+0.28	+0.29	− .08
30	B 34	7.29	7.40	+0.42	+0.40	− .11
41	A 28	7.35	7.54	+0.44	+0.37	− .19
24	B 18	7.95	8.16	+0.57	+0.47	− .21
52	A107	7.97	8.17	+0.46	+0.44	− .20
56	A120	8.11	8.41	+0.48	+0.54	− .30
23	B 14	8.88	9.10	+0.62	+0.66	− .22
17	B 6	8.93	9.15	+0.56	+0.56	− .22
105	A835	9.20	9.37	+0.64	+0.57	− .17
95	A640	9.58	9.73	+0.73	+0.69	− .15
89	B 96	9.63	9.65	+0.72	+0.62	− .02
91	A579	9.80	9.83	+0.75	+0.71	− .03
64	B 78	9.84	9.75	+0.81	+0.67	+ .09
106	A869	10.12	10.14	+0.80	+0.70	− .02
74	A389	10.33	10.28	+0.86	+0.73	+ .05
53	B 66	10.65	10.85	+0.87	+0.84	− .20
42	B 57	10.68	10.75	+0.56	+0.63	− .07
90	A542	11.38	11.36	+1.03	+0.85	+ .02
72	A356	11.45	11.57	+1.05	+1.00	−0.12

DISCUSSION

The photographic absolute magnitudes, M_{Pg_p}, in Table 4 have been computed from the individual parallaxes obtained from the expression

$$\pi = \frac{4.738\,\mu}{V \sin \lambda}.$$

The λ's were computed from a recently determined value for the convergent of the cluster, kindly communicated by R. E. Wilson in advance of publication:

$$A = 94\overset{\circ}{.}0\,, \qquad D = +7\overset{\circ}{.}6\,.$$

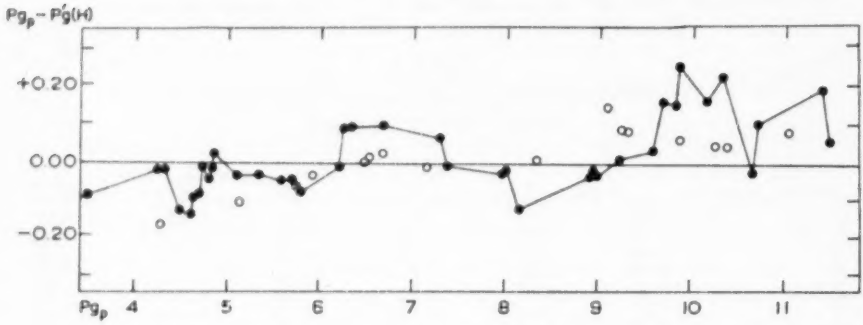

FIG. 3.—Comparison of Pg_p and Pg' (Holmberg). $Pg'(\mathrm{H}) = Pg(\mathrm{H}) - 0^{m}18$. The open circles represent the North Polar Sequence; $Pg_p - Pg_{int}$.

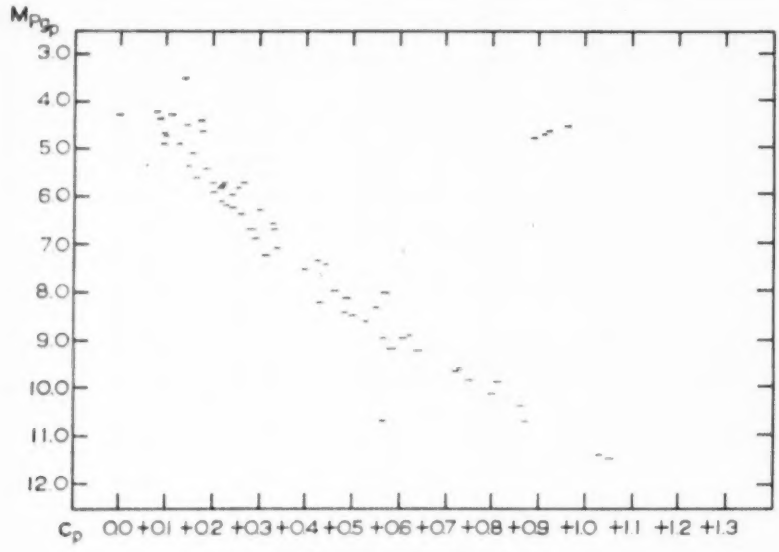

FIG. 4.—Observed magnitudes and colors

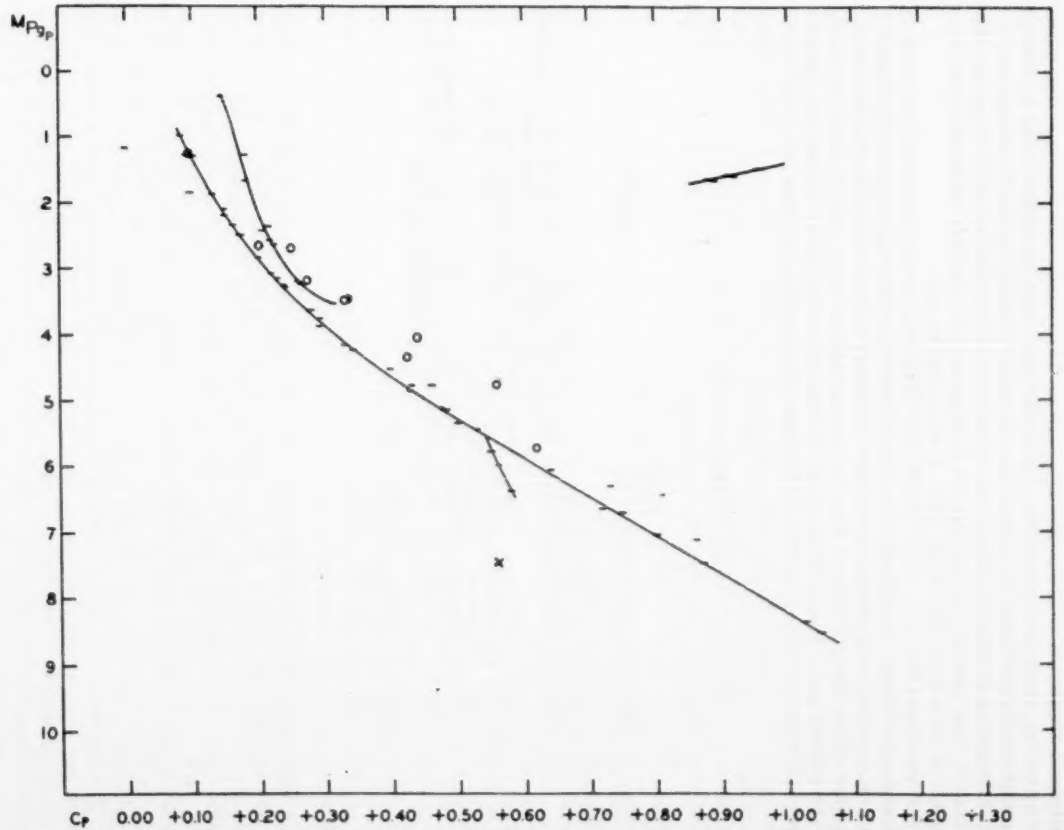

FIG. 5.—Color-luminosity array for the Hyades. The open circles represent known binaries; the cross indicates a possible nonmember.

A mean cluster velocity of 45.3 km/sec has been derived from Wilson's[12] radial velocities of the stars in the table. The resulting mean parallax for these stars is 0".0246 or a distance of 40.6 parsecs.

Figure 5 shows the color-luminosity array for the cluster. The length of the short, horizontal bar, representing each star, indicates the average deviation of the individual observations of color from the mean—in most cases 0.01 mag. or less. Stars known to be visual doubles, spectroscopic binaries with available orbits, or stars which show two sets of lines in their spectra are represented by open circles; one star which may not be a member of the cluster, No. 42 in Table 4, is marked by an *x*.

For stars bluer than $C_p = +0^m.30$ the color-luminosity array consists of two separate branches, one rising more steeply than the other with increasing blueness. We shall, for the present, refer to the steeper and redder of these two branches as the "bright-dwarf" sequence. Also, the continuous branch, extending from $C_p = +0.08$ to $C_p = +1.05$, will be referred to, in what follows, as the "dwarf sequence." More appropriate designations will be given in future papers of this series, when additional "fine structure" of the

TABLE 6

BRIGHT DWARFS

No.	M_{Pg}	C_p	Sp		Remarks
			W	Y	
82	0.37	+0.145	A6	A7	θ^2 Tau; Sp.B; 1 sp
66	1.27	+0.18	A6	F0	υ Tau; constant velocity (Stillwell, *Pub. Dom. Ap. Obs. Victoria*, **7**, 337, 1945)
70	1.63	+0.18	A5n	F0	71 Tau; variable velocity (Stillwell)
25	2.33	+0.215	A8n	A8	51 Tau; constant velocity (Stillwell)
60	2.41	+0.20	A8n	A7	67 Tau
75	2.55	+0.22	A6n	A5p	Metallic-line star; A5 K-line, F2 metallic lines
47	2.62	+0.225	A2	A1p	63 Tau; metallic-line star; A1 K-line, F5 IV = F0 II–III metallic lines
57	3.20	+0.27	F0	F4	
9	3.22	+0.265	F2	F4	
16	3.54	+0.315	F4	F5	

color-luminosity array will be described. The ten stars which lie on the bright-dwarf sequence are listed in Table 6. When the existence of this sequence first became evident from the Madison observations, Dr. W. W. Morgan classified the two brightest members, θ^2 and υ Tauri, as of spectral class A7–A8 and luminosity class III, or late A giants. In a later paper of this series, dealing with the stars in the solar region, it will be shown that the lower portion of the bright-dwarf sequence is populated by stars of luminosity class IV—the subgiants. Also in Table 6 are two stars contained in the Yerkes *Catalogue*[16] of metallic-line stars. The bright-dwarf sequence, thus, is evidently composed of A giants and F subgiants, with metallic-line stars representing the junction between them. It is known that the metallic-line spectra of the metallic-line stars in many cases match those of standard stars classified either as F0 III or F5 IV—a fact which is consistent with their intermediate position in the color-luminosity array. It should also be noted that two, less extreme, examples of metallic-line stars occur on the dwarf sequence. Their significance will be dealt with in a later paper.

The four red giants, γ, δ, θ^1, and ϵ Tauri, form a short segment of the giant sequence. The mean magnitude and color of these four stars are $M_{Pg} = +1^m.57$ and $C_p = +0.92$.

[16] Roman, Morgan, and Eggen, *Ap. J.*, **107**, 107, 1948.

We might compare these means with the observed magnitude and color of Pollux, the giant nearest the sun, with $P_{g_p} = +2.16$ and $C_p = +0.94$. If the stars are comparable, we arrive at a parallax of 0".076 for Pollux. The two trigonometric values quoted by Schlesinger[17] are 0".110 ± 0.011 (McCormick) and 0".062 ± 0.023 (Yale, Heliometer); the Mount Wilson spectroscopic value is 0".087.

Forty-nine of the 64 stars in Table 4 fall on one of the three sequences discussed above, within the uncertainties of the colors and the proper motions. The remaining 15 stars are discussed in the following paragraphs.

I. MULTIPLE SYSTEMS

The data for seven stars, which are known binaries, are given in Table 7. The data for the visual binaries have been summarized by Kuiper;[18] the double-lined binaries were found by Wilson.[12] The difference in visual magnitude for the first pair in the table is given by Kuiper as 2.28 mag. If we assume that the brighter component is a bright-dwarf with $M = +2^m80$ and $C_p = +0.13$, and that the fainter component lies on the dwarf sequence, with $M = +5^m50$ and $C_p = +0.54$, then the combined light would match the observed color and magnitude. In the same manner we can match the observed color and magnitude of star No. 30 with two dwarf components, $M = +4^m80$ with $C_p = +0.42$,

TABLE 7

KNOWN BINARIES

No.	M_{Pg_p}	C_p	Remarks
92	2.68	+0.25	ADS 3264; $=P$148.3 years; $\Delta m=2.28$ mag.
33	3.23	+0.26	Double lines
35	3.50	+0.33	Double lines
41	4.06	+0.44	ADS 3169; $P=487$ years; $\Delta m=1.37$ mag.; br. star is Sp.B., $P=4.00$ days
30	4.34	+0.425	ADS 3135; $P=88.9$ years; $\Delta m=1.12$ mag.
24	4.79	+0.56	Variable velocity
23	5.72	+0.62	Sp.B; $P=5.61$ days; 1 sp

and $M = +6^m00$ with $C_p = +0.61$. Star No. 41 lies 0.8 mag. above the dwarf sequence, but it is a triple system, with the brighter star of the visual binary also being a spectroscopic binary. The fainter component of star No. 23, a spectroscopic binary, can be predicted to be 1.2 mag. fainter than the brighter, a fact which would account for the presence of but a single spectrum in the integrated light of the system. Of the spectroscopic binaries found by Wilson—Nos. 24, 33, and 35—Nos. 24 and 35 evidently consist of nearly equally bright components. If the brighter component of No. 33 is a dwarf, then the fainter component must be more than 1 mag. fainter, and the appearance of two sets of lines in the spectrum is unexpected. However, as will be shown later, the bright-dwarf sequence for stars near the sun extends to the red of that shown in Figure 5 but maintains a nearly constant $M \sim +3^m7$, so that the double-lined binary, No. 33, probably consists of a dwarf and a bright dwarf of nearly equal M but of different C_p. Stars Nos. 64 and 95 may be undiscovered binaries; No. 95, however, is above the dwarf sequence by less than 0.4 mag., so that, if it is a binary, Wilson's failure to find double lines in the spectrum is to be expected; on the other hand, if the star is single, a correction of approximately +0".015 to the total proper motion would be necessary to place it on the dwarf sequence. Star No. 64 lies above the dwarf sequence by 0.7 mag., so that, if the star is double, the spectrum should show the lines of the fainter component. Only one set of

[17] *Catalogue of Trigonometric Parallaxes* (New Haven: Yale University Press, 1935).

[18] *Ap. J.*, **86**, 166, 1937.

lines, however, was seen by Wilson. This star is listed in Aitken's *Double Star Catalogue*,[19] ADS 3206, as a physical companion to star No. 61. The total proper motions for these two stars, which were used here to calculate the individual parallaxes, differ by 0".017.[20] If the two stars do form a physical system and if the total proper motion of the brighter star is the correct value, then it is necessary to increase the M of No. 64 by $\Delta M = 2.17\Delta\mu/\mu$, or by 0.34 mag. The star would then be but 0.35 mag. above the dwarf sequence, and, if it were a binary, two observable sets of lines would not be expected.

II. SUBDWARFS

The three stars, Nos. 7, 17, and 40 will be discussed more thoroughly in a succeeding paper concerning the subdwarfs near the sun. Unpublished observations of magnitude and color of the nearest subdwarfs have shown the existence of a well-defined subdwarf sequence which crosses the dwarf sequence at $C_p = +0.55$ and which is populated by both "high-velocity" and "low-velocity" stars. The Hyades stars, Nos. 7, 17, and 40, fall on this subdwarf sequence just below the cross-over point. We may compare star No. 7, the most extreme case of the three, with the high-velocity star μ Cassiopeiae as

Star	P_{Ep}	C_p	π	M_{Pop}
Hyades No. 7	9^{m}19	+0.58	0".0276	+6^{m}39
μ Cass	5.69	+0.58	0.130 ± .006	+6.26

in the accompanying tabulation. A comparison of the spectra of these two stars would be of interest; the luminosity criteria of the Yerkes *Atlas of Stellar Spectra*[21] places μ Cassiopeiae below the dwarf sequence.

III. MISCELLANEOUS

We have accounted for all but 3 of the 15 stars which lie off the dwarf, bright-dwarf, and giant sequences. Two of these stars, Nos. 50 and 51, will be shown in succeeding papers to be the lone representatives in the Hyades cluster of additional sequences populated more densely by such groups as the Pleiades and by the nucleus of the Ursa Major "cluster." For the present, we shall reject star No. 42 as possibly a nonmember of the cluster.

The HR diagram of the cluster, with spectral types determined at Yerkes[22] and Mount Wilson,[23] is shown in Figure 6. The metallic-line stars are indicated by crosses, the known binaries by open circles.

It is of interest to examine the distribution of the rotational velocity of the stars on the dwarf, bright-dwarf, and giant sequences of the color-luminosity array. The penultimate column of Table 4 contains the rotational velocities for some of the brighter stars in the cluster that have been determined by O. Struve.[24] These velocities are marked on a color-luminosity array in Figure 7. It is not possible to derive very definite conclusions from so few stars, but it does appear that the preponderance of high rotational velocities occurs on the bright-dwarf sequence. In this connection we might recall the results obtained by

[19] Carnegie Institution of Washington, 1932.

[20] In an earlier publication Wilson gives nearly equal values of μ for Nos. 61 and 64; 0".109 and 0".108, respectively (*Ap. J.*, **42**, 49, 1932).

[21] "Astrophysical Monographs," No. 4 (Chicago: University of Chicago Press, 1943).

[22] Morgan and Titus, *Ap. J.*, **92**, 256, 1940.

[23] *Ap. J.*, **107**, 129 1948; *Mt. W. Contr.*, No. 741. The spectral types for a few stars not already published were kindly supplied by Dr. R. E. Wilson.

[24] *Pop. Astr.*, **53**, 286, 1945.

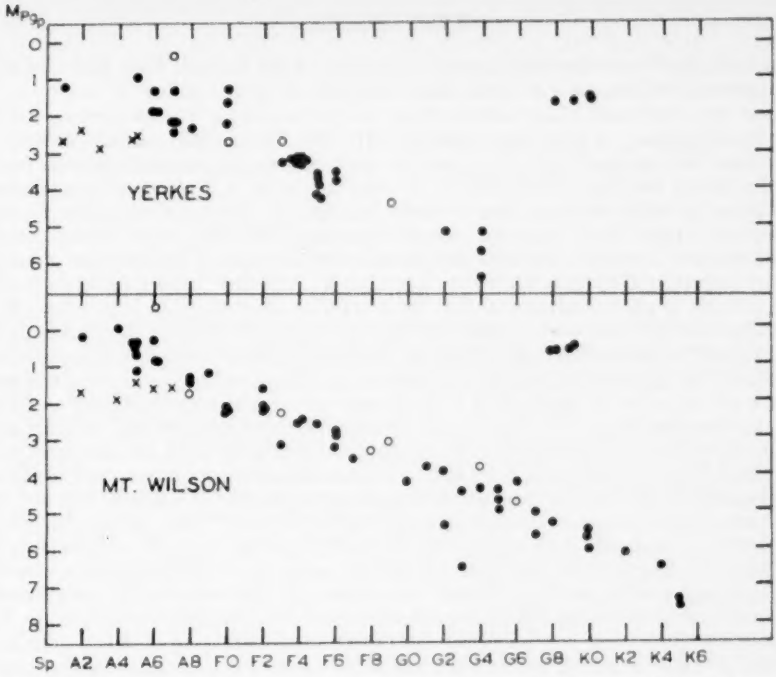

FIG. 6.—HR diagram for cluster members. The open circles indicate known binaries; the crosses, metallic-line stars.

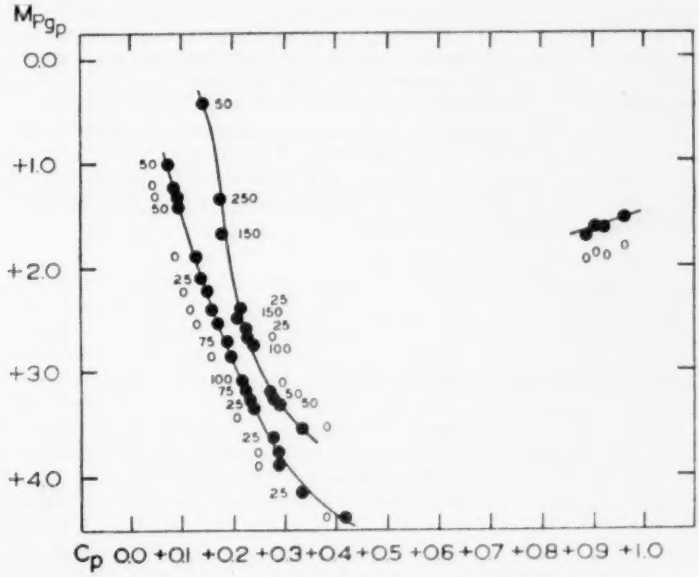

FIG. 7.—Rotational velocities, in km/sec, of the brighter Hyades

Adams and Joy[25] from the spectroscopic parallaxes of the A stars. They have described the appearance of the spectral lines, sharp or nebulous, by appending "s" or "n" to the spectral type, and have found differences in the luminosities of the two groups varying from about 1.5 mag. at A2 to near-equality at F0. This dispersion is comparable with the separation between the bright-dwarf and the dwarf sequences; however, whereas Adams and Joy found the sharp-lined stars to be more luminous, it is apparent from Figure 7 that the stars with nebulous lines or those having high rotational velocities populate mainly the bright-dwarf sequence. Struve[26] has suggested that rapid stellar rotation would produce a spurious absolute-magnitude effect because of the decrease in surface gravity caused by the centrifugal force. Emma T. R. Williams[27] subsequently concluded, from a study of color equivalents, that the n stars do show a higher level of ionization then they would if they had no rotation, thereby confirming Struve's suggestion. Later, J. A. Hynek[28] cast doubt on Miss Williams' results and, from theoretical considerations, computed that in the extreme case of an equatorial velocity of 250 km/sec the change in surface gravity of an A star is such as to change the total absorption of, say, λ 4226 of *Ca* I, by less than 5 per cent. In view of these conflicting considerations, it is probably safe to conclude that such a spurious absolute-magnitude effect is not involved in the separation found here between the dwarf and the bright-dwarf sequences, for the effect is just opposite to that which the cited investigations attempted to explain. Figure 7 may also have some bearing on the fact, pointed out by Struve,[29] that, unlike the smooth progression of mass and luminosity with advancing spectral type, the rotational velocities present a sharp cut-off near spectral class F2, or for $C_p \sim +0.25$. Again we are hindered by too few stars, but from Figure 7 it appears that this cut-off in the progression of rotational velocities occurs near the terminal point of the bright-dwarf sequence. It is possible, therefore, that, because both bright dwarfs and dwarfs were lumped together in the spectroscopic material, the cut-off resulted from a sudden diminution of the number of bright dwarfs, for the dwarf sequence contains relatively few rapidly rotating stars.

The observations discussed above were obtained, in part, under contract with the Office of Naval Research. It is a pleasure to acknowledge the sympathetic manner in which the Office of Naval Research, through its San Francisco representative, Dr. G. F. W. Mulders, supported this project. Although the observing program was planned and all observations were made by the author, the work is, in reality, the result of a joint effort with Drs. A. E. Whitford and G. E. Kron, without whose co-operation the design, construction, and maintenance of the photoelectric equipment would not have been possible. It is hardly necessary to add that this investigation—as, indeed, nearly all photoelectric photometry—owes much to the pioneering of Dr. Joel Stebbins, under whose tutelage I am privileged to continue.

[25] *Ap. J.*, **55**, 242, 1922; *Mt. W. Contr.*, No. 244.

[26] *Pop. Astr.*, **43**, 496, 1935.

[27] *Ap. J.*, **82**, 432, 1935.

[28] *Ap. J.*, **83**, 476, 1936.

[29] *Ap. J.*, **102**, 265, 1945; *Pop. Astr.*, **53**, 201, 1945.

PHOTOELECTRIC STUDIES. II. COLOR-LUMINOSITY ARRAY FOR MEMBERS OF THE PLEIADES CLUSTER*

OLIN J. EGGEN
Lick Observatory, University of California
Received October 5, 1949

ABSTRACT

Magnitudes and colors of 77 Pleiades stars have been determined with a photomultiplier photometer attached to the Lick Observatory 12-inch refractor. With the exception of known visual double stars and a few stars in congested regions, the 77 stars observed include all those which are certainly cluster members and brighter than photographic magnitude 11.0. On the basis of the deduced color-luminosity array the following results have been obtained:

1. In addition to the dwarf and bright-dwarf sequences common to the Hyades and Pleiades, the color-luminosity array for the Pleiades shows two additional sequences, designated here as the "blue-dwarf" and "bright blue-dwarf" sequences. Two stars in the Hyades, which were found to lie off the dwarf sequence, fall on the bright blue-dwarf sequence defined by the Pleiades. Of the near-by stars, Sirius falls on the blue-dwarf sequence. The available spectrophotometric data indicate that the separation between the blue-dwarfs and bright blue-dwarfs also appears in the spectra of the Pleiades stars; the hydrogen absorption in the bright blue-dwarfs is about 80 per cent of that in the blue-dwarfs.

2. The Pleiades do not populate the blue end of the dwarf sequence, as defined by the Hyades stars, brighter than $M = +2.6$, that is to say, above the intersection of the dwarf and blue-dwarf sequences. Also, the Pleiades do not contain bright-dwarfs with $M < +2.8$. It has previously been shown that at this point on the bright-dwarf sequence in the Hyades, the stars of luminosity class III (A giants) are separated from those of class IV (F subgiants) by the metallic-line stars. The lack of red giants in the Pleiades has been known for some time, but now it appears that the absence of giants also holds true among the early-type stars as well.

3. Where the bright-dwarf and bright blue-dwarf sequences join, or intersect, the dwarf sequence in the Pleiades, metallic-line stars appear to occur in the color-luminosity array of the Hyades. Pleiades stars occurring at these intersections may also be expected to be metallic-line stars.

4. Fitting the dwarf and bright-dwarf sequences of the Pleiades to those in the Hyades results in a modulus for the Pleiades of $m - M = 5.70$, or a parallax $\pi = 0''.0071$.

5. With the exception of two stars, one visual and one spectroscopic binary, the maximum deviation in magnitude of stars in areas A, B, and D from the various sequences amounts to 0.10 mag., which would be expected from the dispersion in distance due to the depth of the cluster, whose diameter is about 10 parsecs.

6. Appreciable reddening in the Pleiades is evident only in a small area surrounding Merope. A comparison of a highly reddened A0 star, for which $A_{Pg} = 1^m.45$, with two unobscured A0 stars, gives a ratio of total to selective absorption, $\chi = 4.7$.

7. Analysis of the available estimates of the rotational velocities of the cluster stars indicates that, as in the Hyades, the dwarf sequence contains relatively slowly rotating stars. The bright blue-dwarfs in both clusters also have small rotational velocities. The bright-dwarfs in the Hyades and the blue-dwarfs in the Pleiades are mostly in rapid rotation.

The first paper of this series,[1] hereafter referred to as "Paper I," gave the color-luminosity array for some of the Hyades stars. The present paper gives the results of a similar investigation of the Pleiades. The photometer and color system have been described in Paper I. All observations of the Pleiades, presented here in Table 1, were made with the Lick 12-inch refractor. A total of 213 observations of 77 stars is the basis for the present discussion. These 77 stars include all the known members of the cluster within 1° of Alcyone (25 Tauri) and brighter than photographic magnitude 11.0, with the exception of 10 stars consisting mainly of known binaries and stars in congested regions not resolvable with the 12-inch photometer. Also included are 6 stars which are more than 1° from Alcyone but which have been designated "very probable" members of the cluster by R. J. Trumpler.[2]

* *Contributions from the Lick Observatory*, Ser. II, No. 26.

[1] *Ap. J.*, **111**, 65, 1949.

[2] *Lick Obs. Bull.*, **10**, 110, 1921 (No. 333).

TABLE 1

COLORS AND MAGNITUDES OF PLEIADES STARS

Star No. (1)	1900									Spectral Class		
	Hertz. (2)	Tr. (3)	$\alpha - 3^h$ (4)	δ (5)	P_{kp} (6)	C_p (7)	Obs. (8)	MP_{up} (9)	Area (10)	M (11)	S (12)	$V_r \sin i$ (13)
1	8	R 11	56^m58^s	24°10′.5	$9^m.75$	$+0^m.37$	3	+4.00	B		F5	0
2	27	50	37 46	23 19.9	8.12	+ .24	2	+2.37	C	A8	A3	0
3	28	51	37 46	24 3.5	8.36	+ .17	3	+2.61	B	A7	A4	25
4	29	53	37 48	23 16.7	9.86	+ .37	3	+4.11	C		F5	
5	43	74	38 3	24 14.8	8.13	+ .12	2	+2.38	B	A4	A2	0
6	44	75	38 3	23 34.0	10.13	+ .41	3	+4.38	C		F5	
7	88	118	38 27	23 49.0	9.43	+ .34	3	+3.68	C		F5	
8	92	121	38 29	24 4.8	8.29	+ .185	2	+2.54	B	A7	A8	150
9	108	131	38 43	25 30.2	10.32	+ .40	3	+4.57	A		F8p	
10	117	139	38 51	23 58.5	5.24	− .155	3	−0.51	B	B8	B5	250
11	126	148	38 56	23 47.9	3.47	− .17	3	−2.28	C	B6	B5p	200
12	123	149	38 57	22 57.3	9.22	+ .26	3	+3.47	C		A8	0
13	133	153	38 59	24 7.1	10.79	+ .42	3	+5.04	B		F8	
14	145	163	39 10	23 23.3	9.25	+ .27	3	+3.51	C		F0	0
15	146	162	39 10	23 57.0	8.60	+ .20	2	+2.86	B	A5	A5	75
16	150	166	39 12	24 31.0	5.40	− .17	3	−0.35	A	B7	B8	150
17	156	170	39 15	24 9.2	4.05	− .18	3	−1.70	B	B6	B5	150
18	169	180	39 23	24 36.5	9.37	+ .37	2	+3.62	A		F2	0
19	187	195	39 30	23 43.3	8.10	+ .14	2	+2.35	C	A3	A2	100
20	206	208	39 37	24 9.0	8.71	+ .22	3	+2.96	B	A8	A6	50
21	213	213	39 39	23 46.2	10.51	+ .39	3	+4.76	C		G0	
22	216	215	39 41	24 1.4	7.18	+ .03	2	+1.43	B	A0	B9	0
23	219	217	39 42	24 18.9	10.18	+ .38	3	+4.43	A		F8	
24	227	223	39 44	23 58.6	9.72	+ .30	3	+3.97	B		F2	
25	242	231	39 52	24 3.3	3.66	− .16	3	−2.09	B	B7	B5	25
26	251	235	39 55	23 43.6	7.88	+ .07	2	+2.13	C	A3	A1	75
27	255	240	39 57	24 14.5	5.59	− .145	4	−0.16	A	B8	B8	150
28	265	247	40 5	24 12.9	6.28	− .12	2	+0.53	A	B9	B9	200
29	310		40 18	22 49.0	9.03	+ .47	3	+3.28	C		gF8	
30	298	270	40 15	23 1.7	10.68	+ .55	2	+4.93	C		G0	
31	323	286	40 23	23 38.2	3.98	− .14	3	−1.77	C	B6	B5	300
32	329	289	40 25	24 15.5	10.93	+ .49	4	+5.18	A		G0	
33	341	295	40 30	23 56.6	7.32	− .03	3	+1.57	B	A1	A0	50
34	371	311	40 39	23 18.8	8.31	+ .235	6	+2.56	C	A0	A0	50
35	385	324	40 42	23 28.6	10.74	+ .54	2	+4.99	C		G0	
36	388	327	40 43	23 47.8	9.70	+ .33	3	+3.95	C		F7	
37	396	331	40 46	22 48.0	9.68	+ .36	3	+3.93	C		F5	0
38	424	348	40 57	24 29.2	11.03	+ .51	3	+5.28	A		G0p	
39	428	350	40 58	23 16.4	11.08	+ .57	3	+5.33	C		F9	
40	436	354	41 02	24 12.6	6.69	− .09	3	+0.94	A	B9	B9	150
41	457	365	41 08	23 41.1	8.40	+ .165	3	+2.65	B	A8	A3	75
42	468	372	41 13	23 58.0	9.90	+ .33	3	+4.15	A		F2	
43	510	397	419 25	23 29.6	6.85	− .08	2	+1.10	B	A0	A0	150
44	513	399	41 26	24 16.7	7.86	+ .07	2	+2.11	A	A4	A2	100
45	520	402	41 28	23 36.3	7.10	− .06	1	+1.35	B	A0	B9	0
46	534	410	41 31	23 22.1	7.79	+ .05	2	+2.04	B	A3	A0	100
47	540	413	41 32	23 58.6	6.76	− .03		+1.01	A	A0	B9	0
48	542	414	42 32	23 47.8	2.65	− .175	4	−3.10	A	B7	B5p	250
49	620	448	41 56	23 38.0	10.30	+ .395	3	+4.55	B		F9	
50	681	486	42 10	23 50.0	9.75	+ .395	3	+4.00	A		F5	
51	693	493	42 16	24 0.6	8.50	+ .23	3	+2.75	A	A9	A7	100
52	695		42 17	24 54.4	9.37	+ .33	2	+3.62	A		F5	
53	708	500	42 21	23 19.8	10.62	+ .45	2	+4.87	B		F8	
54	722	506	42 26	23 6.8	5.20	− .17	3	−0.55	B	B8	B8	300
55	736	514	42 29	23 44.5	10.47	+0.41	3	+4.72	A		F9	

TABLE 1—*Continued*

Star	1900									Spectral Class		
(1)	Hertz. (2)	Tr. (3)	$\alpha - 3^h$ (4)	δ (5)	Pg_p (6)	C_p (7)	Obs. (8)	MPg_p (9)	Area (10)	M (11)	S (12)	$V_r \sin i$ (13)
56	742	518	42m33s	24° 2′.3	6m94	0m00	3	+1.19	A	A1	A0	50
57	760	530	42 39	23 9.7	10.88	+ .48	2	+5.13	B	...	G0	...
58	792	551	42 49	22 57.2	8.35	+ .19	2	+2.60	B	A6	A2	50
59	870	594	43 13	23 44.8	3.42	− .17	3	−2.33	A	B8	B8	250
60	878	602	43 13	23 49.9	4.93	− .14	4	−0.82	A	Pec.	B8p	...
61	885	607	43 16	23 34.9	8.19	+ .13	2	+2.44	A	A5	A2	100
62	891	613	43 19	24 5.4	7.49	− .02	1	+1.79	A	A2	A0	250
63	910	622	43 24	24 4.5	6.45	− .115	3	+0.75	A	B9	B9	25
64	924	629	43 29	23 56.5	7.97	+ .08	2	+2.27	A	A4	A2	75
65	948	651	43 37	23 4.5	9.47	+ .32	2	+3.72	B	...	F5	100
66	975	670	43 46	23 2.2	8.19	+ .125	2	+2.44	B	A4	A5	0
67	977	671	43 47	23 24.4	5.95	− .15	2	+0.20	A	B9	B8	250
68	996	688	43 59	24 2.7	7.50	− .02	2	+1.75	A	A2	A0	25
69	1069	742	44 30	24 11.5	7.45	− .01	1	+1.70	A	A2	...	...
70	1129	791	44 56	23 39.5	6.86	− .07	2	+1.11	A	A0	A0	50
71	1184	848	45 29	24 13.0	9.01	+ .24	3	+3.26	A	...	A8	75
72	...	S 37	35 28	23 9.9	9.41	+ .28	2	+3.66	D	...	...	...
73	...	S108	41 29	22 36.8	8.16	+ .13	3	+2.41	D	...	A1	...
74	...	S127	42 47	21 37.1	8.56	+ .235	2	+2.81	D	...	...	...
75	...	S137	43 18	22 18.2	7.68	+ .09	2	+1.93	D	...	...	75
76	...	S151X	44 18	25 4.6	9.93	+ .35	2	+4.18	D	...	...	...
77	...	S165	45 56	25 41.9	7.57	+0.08	2	+1.82	D	...	...	75

The bright Pleiades cluster stars form one of the most conspicuous groupings visible to the unaided eye. Partly for that reason the literature contains numerous investigations, all of which cannot be noted here. Instead, the reader is referred to a rather complete summary by L. Binnendijk.[3] E. Hertzsprung's extensive work on the proper motions of the stars within 1° of Alcyone culminated recently in his *Catalogue of 3259 Stars in the Pleiades*.[4] An earlier memoir by Hertzsprung delivered as the third *George Darwin Lecture*,[5] bears rereading by all who are interested in this famous group.

The photoelectric results for individual stars are given in Table 1. Column 1 contains the current number, which is introduced merely for convenience of reference in this paper. The numbers given these stars in the catalogues of Hertzsprung[4] and of Trumpler[2] are also listed in Table 1 in columns 2 and 3, respectively. Pg_p and C_p are the magnitudes and colors, on the International System, derived from the photoelectric measures by means of the formulae given in Paper I. With but three exceptions, each star was measured on at least two separate nights. The observed stars have been marked with their current numbers on a chart of the Pleiades reproduced in Figure 1. The spectral types in column 10 were kindly supplied by Dr. W. W. Morgan prior to publication; the types in column 11 are by A. Schwassmann.[6]

The most recent compilation of photographic magnitudes for the Pleiades stars has been published by Binnendijk.[3] The differences, $Pg_p - Pg'(B)$, where $Pg'(B) = Pg(B) - 0^m08$, are plotted against Pg_p in Figure 2. The correction of −0.08 mag. to Binnendijk's magnitudes brings the zero point of those magnitudes into agreement with Pg_p over the same range that Pg_p was adjusted to Pg_{int} in Paper I. It may be recalled, however, that

[3] *Leiden Ann.*, Vol. 19, Part 2, 1946.

[4] *Leiden Ann.*, Vol. 19, Part 1, 1947.

[5] *M.N.*, 89, 660, 1929.

[6] *Mitt. Hamburger Sternw.*, 6, 151, 1930.

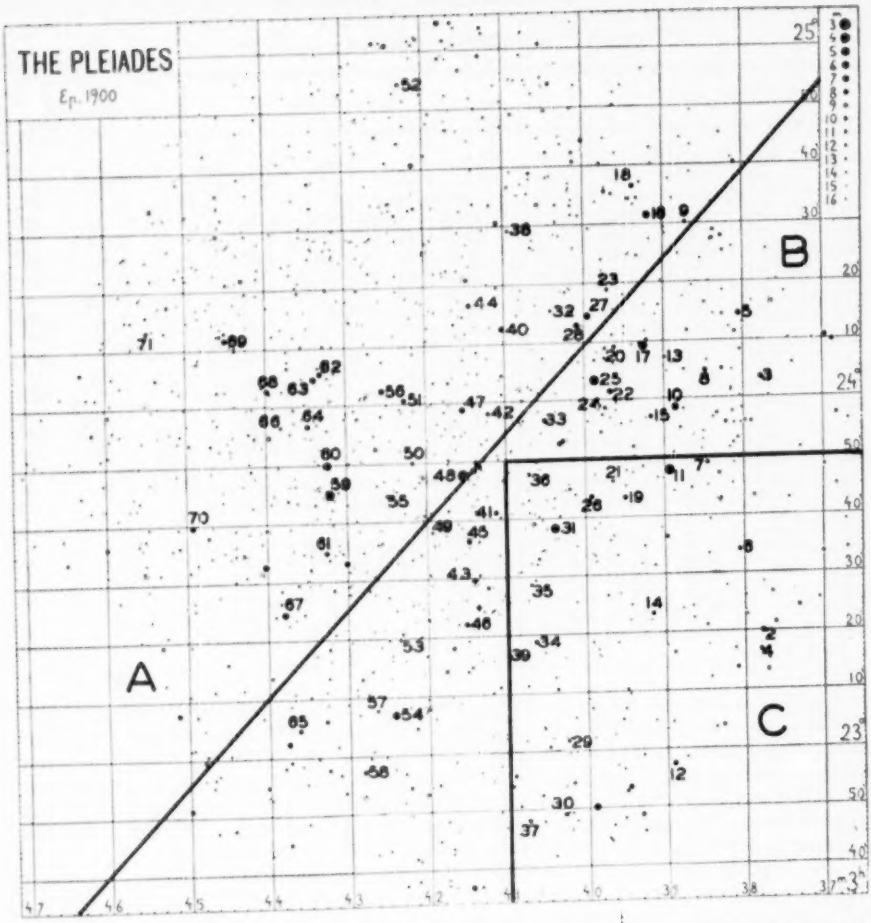

FIG. 1.—Region of the Pleiades from a chart by Hertzsprung. The numbers are those given the stars in Table 1, col. 1. The areas *A*, *B*, and *C* are explained in the text.

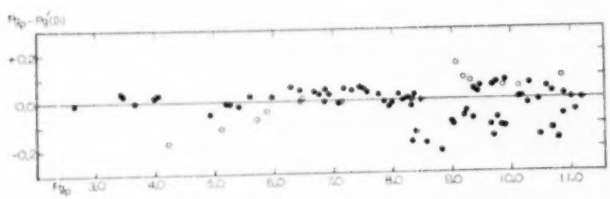

FIG. 2.—A comparison of Pg_p and Pg' (Binnendijk). $Pg'(B) = Pg(B) - 0^m08$. The open circles represent stars in the North Polar Sequence for which the ordinates are $Pg_p - Pg_{int}$ taken from Paper I.

Pg_p was adjusted to Pg_{int}: = 5^m9–8^m3. The purpose was, in view of the well-known divergence of photoelectric and photographic scales between magnitudes 5 and 9, to bring the apparent magnitudes of the Hyades stars, and therefore the absolute magnitudes also, into better agreement with previous work. If, instead of adjusting Pg_p to Pg_{int} over the range given above, we follow the convention of adjusting to a mean magnitude of 6.0 mag. in the North Polar Sequence, then we must add 0.07 mag. to Pg_p. Since we have subtracted 0.08 mag. from Binnendijk's magnitudes, we see that the zero point adopted by him is essentially that of the International System. The open circles plotted in Figure 2 indicate $Pg_p - Pg_{int}$ for the stars of the North Polar Sequence; these differences are taken from Paper I. It is rather surprising that Binnendijk's magnitudes do not show the scale divergence which we have come to expect when comparing photographic with photoelectric magnitudes and which is indicated by the stars of the North

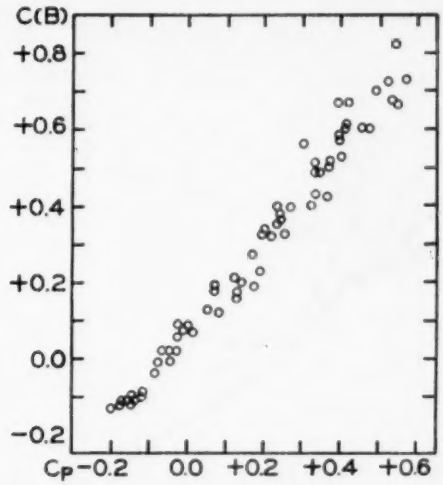

FIG. 3.—A comparison of the photoelectric colors, C_p, and those determined photographically by Binnendijk, $C(B)$.

Polar Sequence. A partial explanation may be that Binnendijk has weighted heavily the photoelectric magnitudes obtained by W. Calder.[7] Also puzzling is the apparent bifurcation in the scales at $Pg_p \sim 8^m5$ and reconvergence near $Pg_p \sim 11^m5$. This effect may be due to the heterogeneous origin of the magnitudes used by Binnendijk. In Figure 3, the values of C_p in Table 1 are plotted against the colors given by Binnendijk. Besides a zero-point correction of −0.07 mag., there appears to be a rather large scatter in the photographic colors as well as a divergence of scale.

In addition to the conspicuousness of the group, the Pleiades are also distinguished by the presence of an extensive nebulosity, which appears on long-exposure photographs. Several previous investigators have discussed the possible effect of this nebulosity on the apparent magnitudes and colors of the cluster stars. These investigations have provided evidence ranging from an inappreciable effect[8] to an average color excess for cluster stars

[7] *Harvard Ann.*, **105**, 453, 1936.

[8] Stebbins and Huffer, *Pub. Washburn Obs.*, **15**, 226, 1934; Stebbins and Whitford, *Mt. W. Contr.*, No. 712; *Ap. J.*, **102**, 324, 1945.

of about 0.16 mag.[9] Most of these investigations agree that the stars involved in the nebulosity surrounding Merope (25 Tauri) are, on the average, redder than the other cluster stars. To test for the effect of the nebulosity on the magnitudes and colors in the present material, the region within 1° of Alcyone has been divided into three areas, designated *A*, *B*, and *C* in Figure 1 and Table 1. The designation *D*, in column 9 of Table 1, indicates stars situated outside this region.

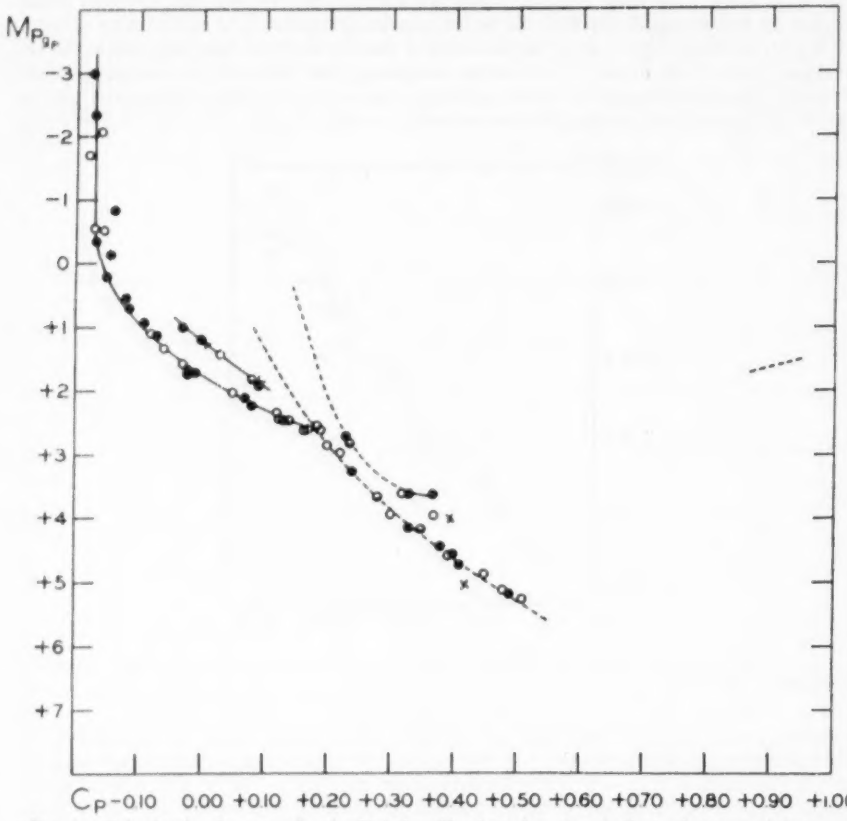

FIG. 4.—Color-luminosity array for the Pleiades. The dotted sections indicate that part of the array which is populated by the Hyades stars; the continuous sections represent the sequences added by the Pleiades stars. The filled, open, and half-filled circles represent stars in areas *A*, *B*, and *C* of Fig. 1, respectively. The two plus signs on the bright blue-dwarf sequence represent the only stars in the Hyades cluster that fall on this sequence. The cross lying above the dwarf sequence indicates the position of a visual binary; and that lying below, a possible nonmember.

Figure 4 contains the color-luminosity array for stars in areas *A*, *B*, and *D*, represented by filled, open, and half-filled circles, respectively. The absolute magnitudes were obtained from a modulus of $m - M = 5^m.75$ and the observed Pg_p. This value for the modulus was determined by fitting the dwarf sequence of the Pleiades to that for the Hyades obtained in Paper I. Figure 5 contains the HR diagrams constructed with the

[9] Seares and Joyner, *Ann. Rep. Mt. Wilson Obs.*, 1943–44, p. 8.

absolute magnitudes of Table 1 and the spectral types given by Morgan and by Schwassmann.

We may compare the parallax corresponding to the above modulus, 0.0071, with previous determinations listed in Table 2.

The value derived from the proper motions assumes that the observed motion is but a reflection of the solar motion. The two values obtained from the spectrum-magnitude relation resulted from a comparison of the HR diagram of the Pleiades with that obtained by H. N. Russell from four moving clusters—Hyades, Ursa Major group, 61 Cygni group, and the Scorpius-Centaurus cluster—and from trigonometric and spectro-

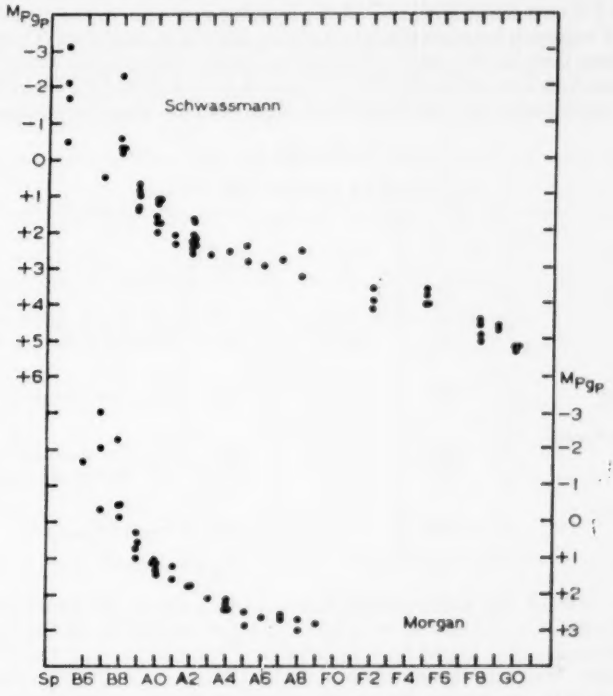

FIG. 5.—HR diagrams constructed from the spectral types by Morgan and by Schwassmann

scopic parallaxes of the near-by stars. Trumpler noted a systematic run in the moduli obtained for the various spectral classes from B5 to K5, with the largest deviations from the mean occurring for classes earlier than F5; inspection of Figure 4 indicates that such an effect might be expected. The presence, however, of this systematic run in the moduli derived from the various spectral classes, plus the fact that the parallaxes derived from the spectrum-magnitude relation are systematically smaller than those determined from geometrical methods, has led to the assumption that the stars in the Pleiades are fainter, intrinsically, for a given spectral type than the stars of, say, the Hyades.[10] The cause of this difficulty is apparent from Figure 4, where it appears that, although the Pleiades and the Hyades populate the dwarf sequence in common, the Pleiades includes an addi-

[10] See, e.g., Gratton, *Pub. Stockholm Obs.*, Vol. 13, No. 3, 1939.

tional sequence which joins the dwarf sequence at $C_p = +0^m19$. We shall, for the present, designate this new sequence as the "blue-dwarf" sequence.[11]

As is apparent from Figure 4, the Pleiades do not populate the dwarf sequence for $M < +2.6$, that is to say, above the intersection of the dwarf and the blue-dwarf sequences. It may be recalled from Paper I that the two stars, Hyades Nos. 50 and 61, fell to the left of the dwarf sequence; Hyades No. 61 is usually classified as the star with the earliest spectral type in that cluster. Figure 4 indicates that these two stars are the lone representatives in the Hyades of a sequence populated by five Pleiades stars. For convenience in future references we shall designate this sequence as the "bright blue-dwarf" sequence. The designations given here for the various sequences are indicated in Figure 6.

In Paper I it was found that two of the metallic-line stars in the Hyades lie on the bright-dwarf sequence between the late A giants and the F subgiants. There were, however, also three metallic-line stars which fell on the dwarf sequence. Two of these latter stars, Hyades Nos. 39 and 96, have an average $M = +2.66$ and $C_p = +0^m185$. It may be of some significance that the blue-dwarf sequence joins the dwarf sequence at $M \sim +2.6$, $C_p \sim +0^m19$. The third metallic-line star which lies on the dwarf sequence of the Hyades, Hyades No. 141, has $M = +2.37$ and $C_p = +0^m16$. From Figure 4 it appears that an extension of the bright blue-dwarf sequence would intersect the dwarf sequence near this point. We may, therefore, draw the tentative conclusion that the metallic-line stars occur in the color-luminosity array at the intersections, or junctions, of the various sequences. This apparent fact should be investigated spectroscopically; for, if true, it will have some bearing on theories of stellar composition and possibly of stellar evolution. We should expect the Pleiades stars lying near these intersections also to be metallic-line stars.

TABLE 2

PARALLAX OF THE PLEIADES CLUSTER

Method	π	p.e.	No. of Stars	Reference
Trigonometric:				
Pitman	0".017	±0".006	9	*Pub. A.A.S.*, **5**, 401, 1926
Alden	.009	±0.004	22	*McCormick Pub.*, **4**, 291, 1926
Proper-motion:				
Hertzsprung	.014		12	*A.N.*, **195**, 452, 1913
Spectrum-magnitude:				
Trumpler	.008		105	*Lick Obs. Bull.*, **10**, 117, 1921
Schwassmann	.006		122	*Mitt. Hamburger Sternw.*, **6**, 151, 1930
Color-magnitude:				
Eggen	0.0071		60	Present study

Figure 6 contains the color-luminosity array for the stars that are situated in area *C* of Figure 1. In Figure 4, which contains the stars in areas *A*, *B*, and *D*, we find no appreciable effect of the nebulosity on the colors; in Figure 6, however, most of the stars are evidently reddened. The most interesting case is star No. 34. This star has been classified A0 by Morgan and by Schwassmann, as well as by nearly all who have classified spectra of the Pleiades. A comparison of the magnitude and color of star No. 34 with four

[11] It is becoming increasingly evident that the present nomenclature, "dwarfs" and "giants," is wholly inadequate. Since future papers of this series, however, will give evidence of still further fine structure in the color-luminosity array, a revision of this unsatisfactory nomenclature is not, as yet, in order.

other cluster stars classified as A0 by Morgan and included in areas *A*, *B*, and *D* gives the accompanying tabulation.

Star No.	Sp(M)	P_{gp}	C_p	M	Obs.	Area	Sequence
47	A0	6^{m}76	−0^{m}03	+1.01	.....	A	Bright blue-dwarf
43	A0	6.85	− .08	+1.10	2	B	Blue-dwarf
70	A0	6.86	− .07	+1.11	2	A	Blue-dwarf
22	A0	7.18	+ .03	+1.43	2	B	Bright blue-dwarf
34	A0	8.31	+0.235	+2.56	6	C	(Blue-dwarf)

We see that both blue-dwarfs and bright blue-dwarfs have been classified A0. Although the mean absolute magnitudes of the two blue-dwarfs, Nos 43 and 70, and the pair of bright blue-dwarfs, Nos. 47 and 22, are nearly equal, the two bright blue-dwarfs average about 0.07 mag. redder than the blue-dwarfs. Before we can attempt a derivation of the

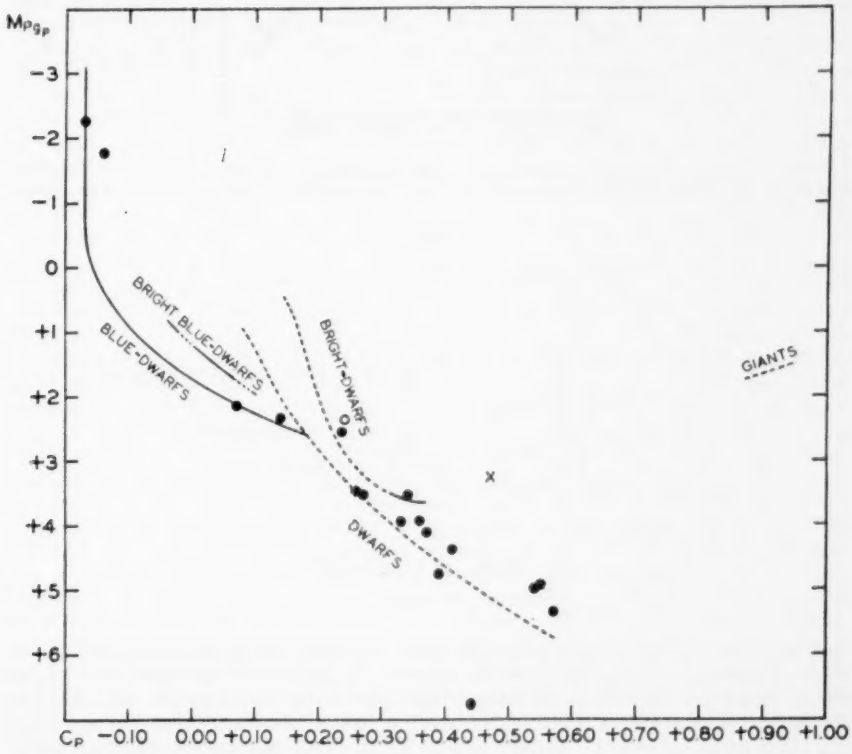

FIG. 6.—Effect of nebulosity on some stars in area *C* (see Fig. 1). The curves are taken from Fig. 4; the dotted sections represent that part of the color-luminosity array populated by Hyades stars, and the continuous sections represent those sequences added by the Pleiades stars. Filled circles deviating from the sequences probably represent obscured and reddened stars. The open circle indicates a spectroscopic binary; the cross a nonmember of the cluster. For convenience, the names given the various sequences in the text are repeated in the figure.

ratio of total to selective absorption from the observed magnitude and color of star No. 34, we must know to which of the two sequences of A0 stars it belongs. In Figure 7 the line intensities of $H\gamma$, derived by Lindblad and Stenquist,[12] are plotted against C_p for the stars in areas A and B. The three bright blue-dwarfs observed by them have been indicated with open circles; star No. 34 is represented by a cross. It appears that the absorption of $H\gamma$ in the bright blue-dwarfs is only about 80 per cent of that in the blue-dwarfs; a similar plot for $H\delta$ gives the same result. Furthermore, Figure 7 indicates that the sep-

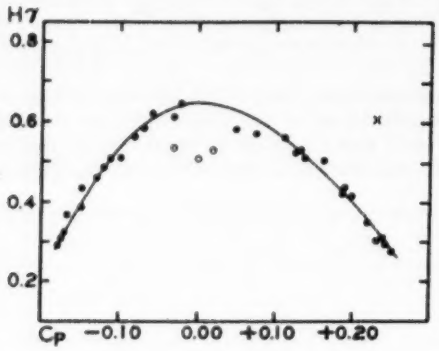

FIG. 7.—Photoelectric colors, C_p, and intensity of $H\gamma$ (Lindblad and Stenquist) for Pleiades stars. The filled circles indicate blue-dwarfs; the open circles bright blue-dwarfs; and the cross, star No. 34, a heavily reddened A0 star.

TABLE 3

RATIO OF TOTAL TO SELECTIVE ABSORPTION

Star No.	P_g	C_p	
43	6^m.85	−0^m.08	From Table 1 (blue-dwarfs)
70	6.86	−0.07	
Mean	6.86	−0.075	A0 unreddened
34	8.31	+0.235	A0 reddened
Diff.	1.45	+0.310	

$$\chi = A_{P_g}/E_{int} = 1.45/0.310 = 4.7$$

aration found here between the blue-dwarf and the bright blue-dwarf sequences is not an effect of hydrogen absorption upon the observed colors; for if that were the case, we should expect the bright blue-dwarfs to be the bluer of the two sequences. Because of its $H\gamma$ intensity, then, we may assume that star No. 34 is a blue-dwarf; from the $H\gamma$ intensity alone we would expect a normal color of about −0.05 mag., which is in good agreement with the value found below. With this assumption we compute the ratio of total to selective absorption, χ, as shown in Table 3.

The validity of the assumption that star No. 34 is a blue-dwarf could easily be tested

[12] *Stockholm Obs. Ann.*, Vol. 11, No. 12, 1943.

by intercomparing the spectra of these stars. The spectra of all three stars should be quite similar to that of Sirius, which is classified as A1V on the Yerkes system. Especially for this purpose, observations of the color and magnitude of Sirius have been obtained and may be compared with the corresponding data for stars Nos. 43 and 70 as given in the accompanying tabulation. The absolute magnitude given for Sirius was

Star	Pg_p	C_p	M
No. 43	6^m85	-0^m08	+1.10
No. 70	6.86	−0.07	+1.11
Mean	6.86	−0.075	+1.10
Sirius	−1.57	−0.07	+1.31

computed from the parallax given by Schlesinger,[13] $\pi = 0''.376$, which indicates that the star probably is a blue-dwarf. From the color of Sirius and the color-luminosity array of Figure 4 we compute a parallax of $0''.365$.

Returning to Figure 4, we see that, with but eight exceptions, the deviations of the Pleiades from the dwarf, bright-dwarf, blue-dwarf, and bright blue-dwarf sequences are all less than $\pm 0^m08$ in magnitude, or $\pm 0^m02$ in color. Since, as mentioned above, known binary systems have been avoided, these eight stars—Nos. 60, 27, 65, 50, 1, 57, 13, and 18—bear further investigation. Star No. 60 is Pleione (28 Tauri), a known shell-star variable in both light and spectrum; star No. 27, Asterope (21 Tauri), spectral class B8, may be a similar case. Binnendijk states that star No. 50 is a visual binary recently discovered by G. P. Kuiper; from its displacement above the dwarf sequence we can estimate that the difference in visual magnitude of the components is approximately 0.5 mag. Star No. 18 is one of only two stars, among 71 stars measured for radial velocity by Struve and Smith, for which the binary character "appears to be established with certainty because of the good accordance between the results of the two measurers."[14] Since star No. 18 stands 0.75 mag. above the dwarf sequence, we would expect two sets of lines to be visible in the spectrum if the departure from the dwarf sequence is due to its binary character. Since no mention of double lines was made by Struve and Smith, the star may represent an extension, in the Pleiades, of the faint end of the bright-dwarf sequence found in the Hyades. The same explanation may hold for star No. 2, in area *C*, shown with an open circle in Figure 6, which is included in the eight "suspected" spectroscopic binaries found by Struve and Smith; but in this case the situation is complicated by the fact that the star lies in the small area involved in the Merope nebulosity. This leaves the deviations of stars Nos. 65, 1, 57, and 13 unaccounted for, of which the first three are all above the dwarf sequence by 0.3 mag. and may be undiscovered binaries or may be involved in local patches of nebulosity. Star No. 13 is unique in that it falls below the dwarf sequence by 0.3 mag., and, since Pg_p and C_p for this star depend upon three observations which are consistent to within 0.01 mag. in both co-ordinates, the star possibly is not a member of the cluster; the radial velocity is not available. Eliminating the eight stars discussed above, we find the remaining stars show individual deviations from the mean color-luminosity array ranging up to $\pm 0^m08$—an amount which might be expected if the cluster were globular in form and if the tangential diameter of about 10 parsecs also represents the depth of the cluster.

In reference to Figure 6, we have already remarked on the heavily obscured star No. 34 and the suspected spectroscopic binary No. 2. The third outstanding deviation noted

[13] *General Catalogue of Stellar Parallaxes* (New Haven: Yale University Press, 1935).

[14] *Ap. J.*, **100**, 360, 1940.

in Figure 6 is star No. 30 with $M = +3.28$ and $C_p = +0^m47$. Although the star is situated in the Merope nebula, the deviation from the dwarf sequence is more than can be explained by this fact. Schwassmann classified the star as gF8, which would make it the sole giant member of the cluster. The star is not listed as a member by Trumpler, but, from the proper-motion data, it has been included by Hertzsprung. The star occurs in the catalogue of radial velocities by Struve and Smith, where it is unique in that it is the only star with a mean error in the velocity of less than ± 1 km/sec; this fact may indicate the difference, perhaps, of the character of the lines in this star as compared with the normal run of the Pleiades stars. The velocity from three plates is given as -4.0 ± 0.6 km/sec, whereas the mean velocity from all 31 stars of grade 1, which includes star No. 30, is given as $+5.15 \pm 0.99$ km/sec. We may assume from this evidence that the star probably is not a cluster member. Of the remaining 17 stars falling in area *C*, all but three show the effect of the nebulosity on the magnitudes and colors. Of these three stars —Nos. 11, 12, and 52—No. 11 lies near the boundary of area *C*, and Nos. 12 and 52 evidently are situated in rifts, or in front of, the Merope nebula. For the remaining obscured stars the only spectral types available are those by Schwassmann and by Gratton, neither of whose estimates are sufficiently accurate to use for testing the value of $\chi = 4.7$ derived above. A program is now in progress, with the Crossley reflector, to obtain photoelectric magnitudes and colors of stars in areas *A*, *B*, and *C* to photographic magnitude

TABLE 4

COMPARISON OF REDDENED AND UNREDDENED STARS

Star	Area	P_{Eg}	C_p	Obs.	Sp.	Star	Area	P_{Eg}	C_p	Sp.
29	C	10^m68	$+0^m55$	2	G0	53	B	10^m62	$+0^m45$	F8
35	C	10.74	+ .54	2	G0	32	B	10.93	+ .49	G0
39	C	11.08	+0.57	3	F9	38	A	11.03	+0.51	G0
Mean	....	10.83	+0.55	....	G0	Mean	....	10.86	+0.48	G0

15, and further discussion of the reddened stars in area *C* will be postponed until that program is finished. We might, however, call attention to the three faintest stars observed in area *C*—Nos. 29, 35, and 39. These three stars, of average spectral class G0, are compared, in Table 4, with three stars, also of average type G0, in the relatively clear areas, *A* and *B*. It appears that these three stars in area *C* are of a brightness to be expected for the mean spectral type, but they are nearly 0.1 mag. reddened relative to the corresponding stars in areas *A* and *B;* the spectral types given are by Schwassmann but are confirmed by Gratton. If we adopt the value for $\chi = 4.7$ derived above, determine the mean magnitude and color of these three stars in area *C* cleared of absorption, and assume that they are dwarfs, we obtain the results given in Table 5. When compared with three stars of the same mean magnitude in areas *A*, *B*, and *D*, we see that the mean corrected C_p is what we might expect, but there remains a discrepancy in the spectral types of nearly one whole class. A more complete investigation of this discrepancy must await the extension of the color-luminosity array to fainter magnitudes, but at present the following possibilities may be considered:

1. Stars Nos. 29, 35, and 39 form a small grouping situated nearer to the sun than the main cluster; this is a rather implausible assumption.

2. All three stars are binary systems, and the observed magnitudes are confused by both the obscuration and the presence of companion stars.

3. An inspection of Figure 1 shows that these three stars surround star No. 34, which was shown above to be affected by a total photographic absorption of 1.45 mag. and a selective absorption of +0.31 mag. Star No. 34 is evidently behind, or imbedded in, a

rather dense portion of the Merope nebula, whereas Nos. 29, 35, and 39 lie on or behind the edges of the same condensation. Several investigators[15] agree in giving the front of the Taurus cloud a distance of 140 parsecs, a radial extension of about 70 parsecs, and an average total absorption of approximately 2 mag. Since we place the Pleiades at a distance of 137 parsecs, it would appear that the Merope nebula is a section of the greater Taurus cloud which extends into the south-preceding portion of the Pleiades. It has been recently shown by W. S. Adams[16] that the Pleiades and its nebulosity are moving independently of each other, so we may assume that the juxtaposition in space is accidental. Since area *C* appears to be imbedded in nebulosity, we have reasonable grounds for expecting some interaction between the dwarf stars and the nebulosity such as that suggested by G. H. Herbig[17] for a group of isolated dwarfs imbedded in the Taurus cloud and characterized as T Tauri stars.[18] Herbig, however, found that the irregular variables in M8 and in the Orion nebula, for example, as a group are significantly different from those associated with the Taurus dark clouds. He concludes that, when highly luminous B stars are present, they collect all but the largest particles in the surrounding nebulosity and prevent near-by dwarf stars from being affected by particles of the correct size necessary to cause T Tauri characteristics. Merope, whose spectral class is estimated by Morgan as B6 and which has an $M = -1.77$, illuminates the nebulosity with which the

TABLE 5

COMPARISON OF REDDENED STARS, CLEARED OF ABSORPTION, WITH UNREDDENED STARS

Star	Area	P_{g_p} (Corr.)	C_p (Corr.)	Sp.	Star	Area	P_{g_p}	C_p	Sp.
29	C	9^m.41	+0^m.28	G0	72	D	9^m.41	+0^m.28	.....
35	C	9.56	+ .29	G0	24	B	9.72	+ .30	F2
39	C	10.09	+0.36	F9	42	A	9.90	+0.33	F2
Mean	.....	9.68	+0.31	G0	Mean	.....	9.68	+0.30	F2

stars under discussion are connected. Unlike the Orion nebula and M8, however, this nebulosity gives a pure reflection spectrum. Furthermore, Greenstein and Aller[19] have found that such dwarf A stars as HD 147009 and 147103, which illuminate bright reflection nebulae and which show a color excess of the same order of magnitude as Pleiades star No. 34, do not possess the usual peculiarities observed in either the T Tauri stars or the Orion nebular variables. They conclude that only faint dwarfs are affected by surrounding nebulosity. An attempt was made to test the constancy of stars Nos. 29, 35, and 39 and also of star No. 34, by comparing the Δm's between these stars and three unreddened stars, Nos. 32, 38, and 53, which are of nearly the same magnitude and color; these Δm's were obtained from the many existing series of photographic magnitudes of the Pleiades. But any variation which might be present is confounded with the large accidental errors in the magnitudes; the differences in magnitude between the comparison

[15] See, e.g., Pannekoek, *Proc. Kon. Akad. Amsterdam*, **23**, 707, 1920; and J. Ramberg, *Stockholm Obs. Ann.*, Vol. **13**, No. 9, 1941.

[16] *M. W. Contr.*, No. 760; *Ap. J.*, **109**, 354, 1949.

[17] *Pub. A.S.P.*, **60**, 257, 1948; and unpublished material.

[18] A. H. Joy, whose extensive investigation of the T Tauri variables first drew attention to these important stars, has reported the finding of several dwarf objects with T Tauri emission characteristics, which "show marked tendency to congregate in the neighborhood of areas of obscuration, usually on the periphery rather than in the centers of the dark regions" (*Pub. A.S.P.*, **58**, 244, 1946).

[19] *Pub. A.S.P.*, **59**, 141, 1947.

stars vary from one series to another by a greater amount than those between the stars to be tested. We are left, then, with the possibility that stars Nos. 29, 35, and 39 are raised above the main sequence, because of their connection with the nebulosity, through some other mechanism than simple absorption; but much additional material is needed before definite conclusions may be drawn. It is reasonable to expect, from what is now known concerning the T Tauri stars and dwarf M-type components with which some of them are physically connected, that when we push to fainter cluster stars in area *C*, T Tauri variables may be found.

Of the B stars which deviate from the color-luminosity array, we have already mentioned Pleione as a shell star known to vary in light and spectrum.[20] Asterope, No. 27, which lies in area *A*, shows a color excess of the same order as Pleione. This is rather surprising, since Asterope and Maia (No. 25) are the only two of the seven brightest stars for which bright hydrogen lines have not, at some time, been announced. It is possible, perhaps, that the star is obscured by a local patch of nebulosity, but star No. 28, which is less than 3′ south-following Asterope, appears to have a normal color. The only

TABLE 6

PLEIADES STARS OBSERVED WITH THE SIX-COLOR PHOTOMETER

No.	Pg_p	P_V	C_p	C'_p	Obs. (C'_p)
10	5^{m}24	5^{m}24	−0^{m}16	[−0^{m}14	2
11	3.47	.....	− .18	[− .20	1
16	5.40	5.43	− .18	[− .17	2
17	4.05	4.03	− .18	[− .19	3
25	3.66	.....	− .16	[− .16	1
27	5.59	5.58	− .13	[− .12	1
28	6.28	6.26	− .12	[− .13	1
31	3.98	3.92	− .14	[− .16	2
48	2.65	.....	− .18	[− .20	3
54	5.20	5.23	− .17	[− .17	1
59	3.42	.....	− .17	[− .18	2
60	4.93	4.94	−0.14	[−0.13	3

other discrepancy among the bright stars is Merope, which we have already shown to be involved in a nebulous region. A comparison of the results obtained by Stebbins and Whitford[21] for the 12 brightest Pleiades stars with the present results is given in Table 6. The values for P_V were derived from the deflections through the violet filter in the six-color photometry done by Stebbins and quoted by Binnendijk.[3] The values of C'_p are the International colors interpolated from the six colors. The value of Pg_V quoted for Pleione (No. 60) is derived from the measures of September 11, 1944; on August 23 and 24, 1943, Stebbins and Whitford found Pg_V = 5^{m}02 and 5^{m}04, respectively, or a mean of 5^{m}03, which indicates that the star was still recovering from the light-minimum started in 1938.[22] The light of the star has apparently remained constant from 1944 to 1949. The only difference greater than 0.03 mag. between Pg_p and P_V is 0.06 mag. for Merope (No. 31). To test for a possible light-variation in Merope, the seven stars, excluding Pleione, for which Pg_p, P_V, and Pe (Calder)[7] are available are listed in Table 7. Calder's photoelectric magnitudes have been adjusted to Pg_p for the 12 brightest stars. A small decrease in the light of Merope, in 1944, cannot be ruled out, but Calder's 1934 measures agree well enough with the present results, obtained in 1949.

[20] See, e.g., Struve and Swings, *Ap. J.*, **97**, 426, 1943.

[21] *Ap. J.*, **102**, 338, 1945.

[22] L. Binnendijk, *A.J.*, **54**, 117, 1949.

In the light of these results bearing on the Pleiades nebulosity, it is of interest to re-examine the six-color observations of the brighter Pleiades made by Stebbins and Whitford. Stars Nos. 11 and 17 have been classified B6 by Morgan, as has Merope, No. 31. The six-color observations of these three stars are given in Table 8.

From this comparison it would appear that the color excess given below for Merope, $E_{int} = +0.03$, is confirmed by the six-color observations and spectral types—that is, there exists a close correlation between the colors and the spectra. Since, however, B6 is the earliest spectral class present in the cluster, according to Morgan, and the brightest star, η Tauri (No. 48) is not included in this group, we need to examine the remaining unobscured bright stars for which six-color observations are available. The data are col-

TABLE 7

COMPARISON OF PHOTOELECTRIC MAGNITUDES FOR FIVE STARS

Star No.	1949 P_{Ep}	1944 P_V	1934 P_B (Calder)
31 (Merope)	3^{m}98	3^{m}92	3^{m}99
17	4.05	4.03	4.06
10	5.24	5.24	5.29
27	5.59	5.58	5.60
28	6.28	6.26	6.25

TABLE 8

SIX-COLOR OBSERVATIONS

Star No.	V	B	G	R	I	V−I	Obs.	M	C_p	Sp. (M)
11	−1.03	−0.49	−0.05	+0.54	+1.08	−2.11	1	−2.28	−0^{m}17	B6
17	−1.01	−0.48	−0.05	+0.52	+1.11	−2.12	3	−1.70	−0.18	B6
Mean	−1.02	−0.48	−0.05	+0.53	+1.10	−2.12	4	−1.99	−0.175	B6
Merope	−0.96	−0.46	−0.03	+0.49	+1.03	−1.99	2	−1.77	−0.14	B6

lected in Table 9. It is evident that Merope, at B6, agrees well enough in M and C_p, as well as in the run of the six colors, with the reddest of the B7 stars, No. 25; or, in other words, the small reddening apparent for star No. 25, in Figure 4, is confirmed by the six-color observations. The same is true of star No. 10, the reddest of the B8 stars on the V–I scale, which is also displaced from the mean color-luminosity array of Figure 4. Of the eight brightest stars in areas A and B, the brightest, $M = -3.10$, and the faintest but one, $M = -0.35$, are classified as of type B7, with the faintest but one, No. 16, being the bluest of the lot in V–I. Such a large range in luminosity within a spectral class should be evident in the spectroscopic luminosity criteria.

W. S. Adams'[16] recent investigation of the displacements and intensities of the interstellar lines in some of the brighter Pleiades stars has already been mentioned. It is of interest to compare the intensities of these lines with the deviations from the mean color-luminosity array. For this purpose the deviations may be expressed as color excesses, E_{int}, as shown in Table 10.

Adams has pointed out that the intensities of the molecular lines relative to the K line

are abnormally high for the Pleiades stars. P. W. Merrill[23] has suggested that there may be a difference in the place of origin of the K line and of the molecular lines, the K line arising from the absorption in the interstellar clouds between the Pleiades and the sun, while the molecular lines are produced in the clouds in the immediate vicinity of the Pleiades and subject to their radiation. Adams favors the view that all lines are produced in the same cloud, since the radial velocities derived from the K line and from the molecular lines agree, and he suggests that the molecular lines in the Pleiades stars may vary

TABLE 9

SIX-COLOR OBSERVATIONS

Star No.	V	B	G	R	I	V−I	Obs.	M	C_p	Sp. (M)
48	−1.00	−0.45	−0.05	+0.50	+1.01	−2.01	3	−3.10	−0^{m}175	B7
25	−0.96	−.46	−.05	+.51	+1.02	−1.98	1	−2.09	−.16	B7
16	−0.98	−0.46	−0.06	+0.52	+1.08	−2.06	2	−0.35	−0.17	B7
Means	−0.99	−0.46	−0.05	+0.51	+1.04	−2.03	6	−1.51	−0.17	B7
59	−0.97	−0.42	−0.05	+0.47	+1.00	−1.97	2	−2.33	−0.17	B8
10	−.93	−.44	−.05	+.49	+0.96	−1.89	3	−0.51	−.155	B8
27	−.92	−.44	−.06	+.50	+1.02	−1.94	1	−0.16	−.145	B8
67	−0.97	−0.46	−0.05	+0.50	+1.04	−2.01	1	+0.20	−0.15	B8
Means	−0.95	−0.44	−0.05	+0.49	+0.99	−1.94	7	−0.70	−0.155	B8

TABLE 10

COLOR EXCESSES AND INTERSTELLAR LINE INTENSITIES

Star No.	Star Name	C_p	E_{int}*	K	Intensity λ 3957	Intensity λ 4232
10	16 Tau	−0^{m}155	+0.015	2	2	3
11	17 Tau	−.17	.00	Tr	.....	Tr
17	19 Tau	−.18	−.01	2	Tr	2
25	20 Tau	−.16	+.01	4	2	4
27	21 Tau	−.145	+.025	1	Tr	2
31	23 Tau	−.14	+.03	Tr	1	3
48	25 Tau	−.175	−.005	1	.....	Tr
59	27 Tau	−0.17	0.00	2	.....	Tr

* Obtained by assuming a normal $C_p = -0.17$ for these stars, since Fig. 4 shows a near-vertical rise in this portion of the color-luminosity array.

in intensity. From the tabulation above, it appears that the relative intensity of K and λ 4232 is fairly constant for all but two of the stars, Nos. 31 and 59. No. 31, Merope, is the only bright star involved in the reddened area *C*, and the fact that K is present only as a "trace," while λ 4232 appears quite strong, would tend to confirm Adams' suggestion that the clouds absorbing K are the same ones that absorb the molecular lines when these clouds are close enough to a star to be stimulated by its radiation. Star No. 59, Atlas, appears quite normal in the color-luminosity array and in the run of the six colors, and the only suggestion of spectral peculiarity is a statement by Binnendijk,[3] who quotes

[23] *Pub. A.S.P.*, **58**, 354, 1946.

Kuiper, that "the peculiar spectrum of Atlas . . . shows that this bright star is situated above the main sequence."

In Paper I we were fortunate to have available for stars in the Hyades an extensive series of estimated rotational velocities by O. Struve, whose data permitted a limited analysis of the distribution of rapidly rotating stars in the color-luminosity array. A similar set of data for the Pleiades has been published by Struve and Smith.[14] In Figure 8 their estimates of the rotational velocities have been marked on the color-luminosity

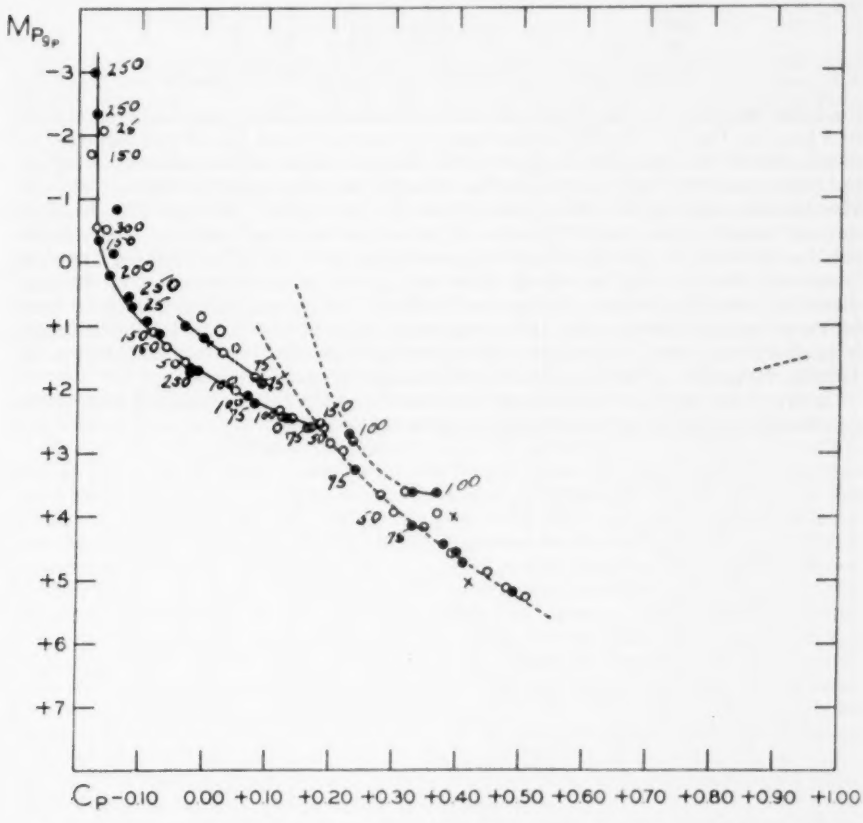

FIG. 8.—Rotational velocities (in km/sec) as estimated by Struve and Smith for the brighter Pleiades stars.

array for stars in areas *A*, *B*, and *D*; these values are also listed in the last column of Table 1. A few stars, in the more densely populated regions of the blue-dwarf sequence, have been omitted to avoid congestion in Figure 8; inclusion of these stars would have little effect on the average run of the velocities. We may recall that in Paper I it was shown that the stars with high velocities of rotation populated mainly the bright-dwarf sequence. This sequence is represented in the Pleiades by rather few stars, the rapidly

rotating stars in this group appear to populate the blue-dwarf sequence. Furthermore, for the blue-dwarf sequence, there appears, on the average, to be a dependence of rotational velocity upon absolute magnitude, as is evident in the accompanying tabulation. Here

$\overline{V_e \sin i}$	M (blue-dwarf)	No. of Stars
170 km/sec	−3 to −1	4
180	−1 to +1	5
130	+1 to +2	5
100	+2 to +2.5	4
60	+2.5 to +3.0	4

the mean velocities, for the magnitude intervals indicated above, have been rounded off to 5 km/sec. The five Pleiades stars which populate the bright blue-dwarf sequence, all of which lie in the luminosity range of +1 to +2, have rather slow velocities of rotation; the average is 30 km/sec, with three of the five stars showing negligible rotation. The two Hyades stars, Hyades Nos. 50 and 61 in Paper I, which fall on the bright blue-dwarf sequence, were both estimated by Struve to have zero rotational velocity, which makes this feature of the bright blue-dwarf sequence common to both the clusters. The rotational velocities for only four dwarf stars that fall below the intersection of the blue-dwarf and dwarf sequences have been estimated by Struve and Smith. The mean value for these four stars is 60 km/sec, in the luminosity range $M = +2.7$ to $+3.3$. The sample is small, but the mean is in good enough agreement with that for five dwarf stars in the Hyades, 50 km/sec, which are included in the same range in luminosity.

Many of the questions which have been raised and but briefly discussed here will be considered in more detail in succeeding papers of this series.

THE ILLUMINATION FROM THE SOLAR CRESCENT NEAR TOTALITY OF THE ECLIPSE OF MAY 20, 1947

R. A. RICHARDSON AND E. O. HULBURT
Naval Research Laboratory, Washington, D.C.
Received February 25, 1949

ABSTRACT

With a recording photocell of photopic spectral sensitivity, eleven measurements were made of the illumination from the solar crescent during the exposed outer one one-hundredth of the solar radius. From these the radial variation of emission near the edge of the solar disk was found to be approximately linear, decreasing from 0.48 to 0.36 at 99.0–99.9 per cent of the radius, with a slight trace of a shelf at about 99.6.

The Eclipse Expedition of the National Geographic Society and the United States Air Forces established its camp near Bocaiuva, Brazil, at an altitude of about 2200 feet above sea level in south latitude 17°12′.8 and west longitude 43°41′.3. Measurements were made of the illumination from the solar crescent near the times of second and third contacts of the May 20, 1947, eclipse, in order to provide data for the determination of the emission from the sun near the limb. The radial variation of emission near the edge of the solar disk was of interest in the physical theory of the sun's atmosphere. The measurements had not been planned in the original program of the expedition but were carried out with apparatus constructed and assembled after arrival at the Eclipse Camp. The experiment came about as the result of discussion with Dr. Harold A. Weaver and other members of the expedition, in which it became clear that, as far as was known, no crescent illumination measurements had been included in the plans of other expeditions.

The ratio e_r of the emission at a distance r from the center of the solar disk to the emission at the center has been well determined for r/r_1 from 0 to nearly 0.99 for various wave lengths in the optical spectrum by means of spectroscopic measurements on the uneclipsed sun;[1, 2] r_1 is the radius of the apparent solar disk. A portion of the data for e_r from Moll, Burger, and Van der Bilt (Fig. 6)[2] for wave lengths 450 and 550 $\mu\mu$ is plotted as ordinate in the two curves of Figure 1 against r/r_1 as abscissa. For r/r_1 from about 0.985 to unity, e_r may not be obtained reliably from the uneclipsed sun because of the boiling of the limb caused by atmospheric scintillation. However, as suggested by Julius,[3] e_r may be derived from measurements of the illumination from the crescents of the eclipsed sun near totality. Such observations were made by Ferwerda, Vitterdijk, and Wesselink[4] during the total eclipse of June 19, 1936. Certain of their data, in the form adjusted by Kopal,[5] for a wave-length band centering at 454 $\mu\mu$ are plotted as dots in Figure 1, in which the ordinates are J/J_0 and the abscissae are r/r_1; J is the total emission in the specified wave-length band from the crescent divided by its area and J_0 is the emission from the uneclipsed sun divided by the area of the solar disk; r is the distance from the center of the crescent to the center of the solar disk.

The radial emission function e_r may be derived from the crescent illumination values J/J_0 by rather intricate computation. Actually, e_r and J/J_0 approach equality as r/r_1 approaches 1 and are practically indistinguishable for $r/r_1 > 0.995$. Kopal[5] calculated e_r from the Dutch observations[4] of J/J_0; the e_r-curve which he obtained is given by the dotted curve of Figure 1 drawn among the dots. In the process he found that, when using the calibrations of the Dutch experimenters,[4] which they termed "rather rough," he ob-

[1] C. G. Abbot, F. E. Fowle, and L. B. Aldrich, *Ann. Ap. Obs. Smithsonian Institution*, **4**, 217, 1922.

[2] W. J. H. Moll, H. C. Burger, and J. Van der Bilt, *B.A.N.*, **3**, 83, 1925.

[3] *Ap. J.*, **23**, 312, 1906. [4] *B.A.N.*, **9**, 81, 1940. [5] *Ap. J.*, **105**, 60, 1946.

tained an e_r-curve about 61 per cent above that of Figure 1. Whereupon, he multiplied their observed values by 0.622 and obtained the dots of Figure 1 and the e_r-curve passing through the point $e_r = 0.271$ at $r/r_1 = 0.99$, which he considered to be well determined by the earlier measurements on the uneclipsed sun.

The values of J/J_0 obtained in the present experiments, the details of which are given below, are plotted in the circles and crosses of Figure 1. They refer to a spectral band with maximum at 550 $\mu\mu$ of the form of sunlight viewed with the light-adapted eye. The values of e_r, which correspond to them, differ from them by less than two-tenths of 1 per

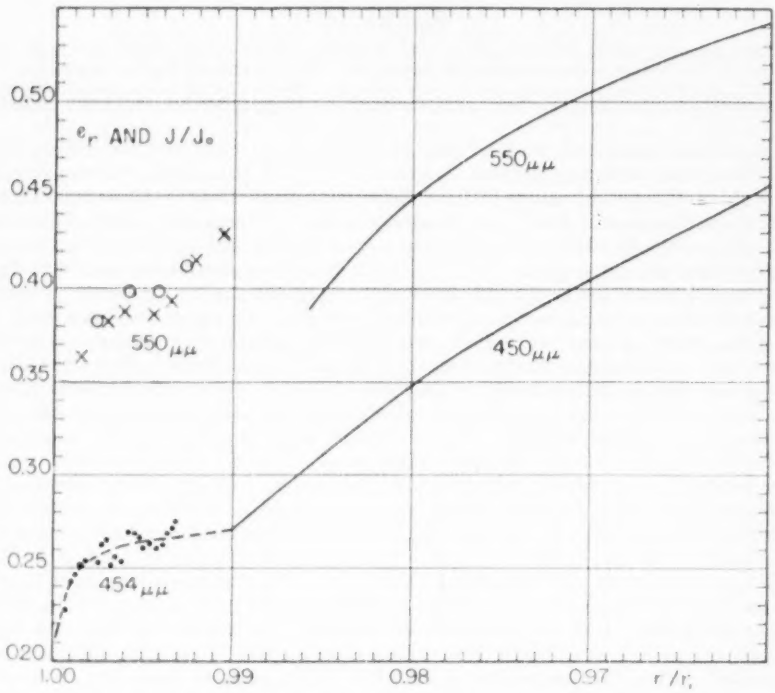

FIG. 1.—*Curves*, values of the radial brightness function e_r; *dots, circles, and crosses*, values of the relative crescent illumination per unit area J/J_0.

cent; the precise calculation of e_r from J/J_0 could be carried out after the manner of Kopal, but that has not been done here.

In the present experiments a Weston Photronic cell covered with a Viscor filter of greenish glass was mounted behind a hole 3.4 cm in diameter at the end of a tube 46 cm in length and 15 cm in diameter, blackened on the inside and covered at the far end with a diaphragm with a hole 1.5 cm in diameter; there were two other such diaphragms spaced equally along the tube. The spectral sensitivity of the Photronic cell with the Viscor filter was very close to that of the light-adapted eye, with the maximum at about 550 $\mu\mu$. The cell was connected to a microammeter; the microammeter was mounted on a panel together with a clock and was photographed with a camera. The instrument was calibrated by observing the deflection of the microammeter needle when the light from the uneclipsed sun, reduced by known amounts by neutral absorbing filters, passed through

the tube to the Photronic cell; at the same time the solar illumination was measured with a calibrated Macbeth illuminometer. It was found that the needle deflection was proportional to the illumination, for the low illuminations under consideration, and that 2.53 foot-candles caused a current of 1 microampere.

The tube was fixed in a position pointing at the sun during totality; its field of view of about 2° was so large that it did not have to be moved during the time that it was used. The other eclipse experiments of the present authors left eleven frames in the camera for the crescent illumination observations; seven frames were taken before second contact and four after third contact. The tube was covered in order that no light might fall on the cell during the earlier phases of the eclipse, the cover being removed about 10 seconds before the first frame was exposed. The data from the eleven frames are listed in the first three columns of Table 1, the first column being the frame number, the second column the G.C.T. of the observation (12 hours being omitted), and the third column the illumination at i foot-candles from the solar crescent. The times were probably correct

TABLE 1

CRESCENT ILLUMINATION VALUES

FRAME	G.C.T.		i (FT-C)	I (SEC)	δ (MINUTES OF ARC)	r/r_1	$\phi/\pi r_1^2$	J/J_0
	Minutes	Seconds						
1	33	59.4	15.2	43.9	0.29983	0.9905	0.00620	0.430
2	34	6.6	11.4	36.7	.25066	.9921	.00482	.415
3	.....	13.4	8.11	29.9	.20421	.9935	.00362	.393
4	.....	17.8	6.33	25.5	.17417	.9945	.00287	.387
5	.....	24.8	4.05	18.5	.12636	.9960	.00183	.388
6	.....	30.0	2.53	13.3	.09084	.9971	.00116	.383
7	.....	36.2	0.89	6.9	.04713	.9985	.00043	.363
33	38	44.8	1.92	11.1	.07493	.9976	.00088	.383
34	.....	53.6	4.56	19.9	.13433	.9958	.00201	.398
35	.....	1.0	7.10	27.3	.18428	.9942	.00313	.398
36	.....	8.0	10.14	34.3	0.23153	0.9927	0.00432	0.412

within ±0.3 second and the values of i within ±0.05 foot-candle, as far as reading the instruments was concerned; there may have been systematic errors. For example, the values of i may be a few per cent too great because of the 2° field around the sun, which included the illumination of the corona and 2° of the sky. During the 1937 eclipse Richtmyer[6] observed at Canton Island that the illumination of the corona and 5° of sky was about 0.02 foot-candle.

The position of the eclipse station was at south latitude 17°12′.8 and west longitude 43°41′.3; the predicted times of the second and third contacts, calculated from the *Eclipse Supplement* of the *American Ephemeris, 1947*, were $12^h34^m47^s$ and $12^h38^m37^s$, respectively. In Figure 2 the observed values of i are plotted in crosses for second contact and circles for third contact as ordinates against the times from the predicted respective contacts as abscissae; the frame numbers are written near the plotted points. Since the eclipse was closely, but not exactly, symmetrical at the two contacts, the two curves of Figure 2 should coincide to a close approximation. They did not do so; when the four third-contact points were shifted 7 seconds along the axis of abscissae, as shown by the circles with primed numbers, they fell on the curve of the second-contact observations within the accuracy of experiment. Since a clock error of as much as 0.3 second seemed

[6] *Nat. Geog. Soc. Solar Eclipse Tech. Papers*, No. 1, p. 10, 1939.

improbable, it appeared that the predicted contact times were all about 3.5 seconds slow.[7] Therefore, in order to bring the two curves into coincidence, the predicted contact times were each advanced 3.5 seconds. The time interval t from the advanced contact time was then determined for each observed i; the values of t are in the fourth column of Table 1.

It is convenient to introduce a parameter, δ, which is the length in minutes of arc of the exposed portion of the solar radius along the line of centers of the sun and moon. Computation, taking into account the augmented apparent lunar radius, showed that

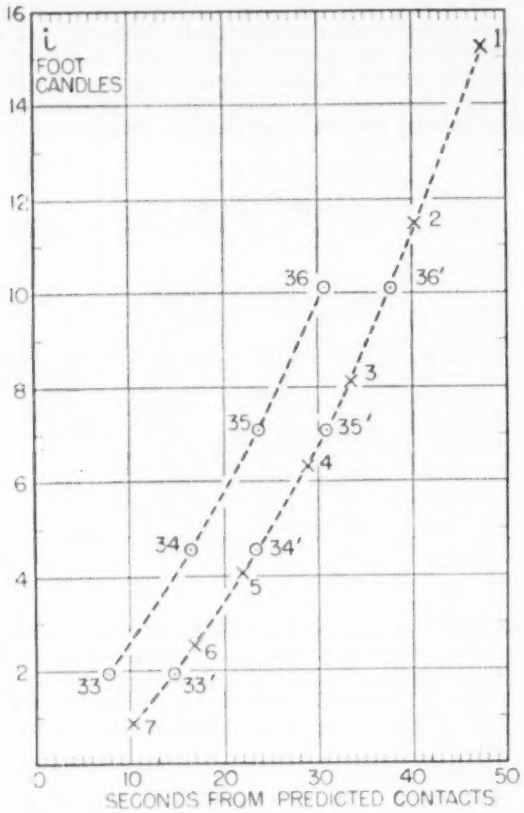

FIG. 2.—Observed values of the crescent illumination i; *crosses*, before second contact; *circles*, after third contact.

$\delta = 0.00067 5t$ and $0.00681t$ for the 60 seconds before second contact and after third contact, respectively.[8] The values of δ from these relations are in the fifth column of Table 1. The values of r/r_1 computed from $r/r_1 = 1 - \delta/2r_1$, with the apparent solar radius $r_1 = 15'.803$, are in the sixth column of Table 1.

[7] Dr. F. J. Heyden and Dr. L. C. McHugh carried out careful measurements of the contact times and found that the predicted contact times were slow by 3.68 ± 0.19 seconds.

[8] We are greatly indebted to Mrs. I. M. Lewis, astronomer of the Nautical Almanac Office, Naval Observatory, for the computations on which these values are based.

The area ϕ of the solar crescent is given by

$$\phi = (r_1^2 - r_2^2)\frac{\pi}{2} - x_1(r_1^2 - x_1^2)^{1/2} + x_2(r_2^2 - x_2^2)^{1/2} - r_1^2 \sin^{-1}\frac{x_1}{r_1} + r_2^2 \sin^{-1}\frac{x_2}{r_2}, \quad (1)$$

where

$$x_1 = \frac{r_1(r_2 - r_1) - (r_2 - r_1 + \delta/2)}{r_2 - r_1 - \delta},$$

$$x_2 = \frac{r_1(r_2 - r_1) - (r_2 - r_1 + \delta/2)}{r_2 - r_1 + \delta}.$$

The values of $\phi/\pi r_1^2$, the ratio of the area of the crescent to that of the solar disk, computed from equation (1), are in the seventh column of Table 1.[9]

From the definitions $J = i/\phi$ and $J_0 = i_0/\pi r_1^2$, where i_0 is the illumination of the uneclipsed sun, one has

$$\frac{J}{J_0} = \frac{i\pi r_1^2}{i_0\phi}. \quad (2)$$

The values of J/J_0 calculated from equation (2) with $i_0 = 5700$ foot-candles are in the eighth column of Table 1. The value $i_0 = 5700$ foot-candles was the result of many measurements made for the same solar altitude as that of the eclipse on preceding days when the sky was clear. During the crescent measurements the sun and corona were covered by a very thin cirrus veil, which did not change perceptibly during totality. Previous experience indicated that such a veil probably reduced i by an amount less than 10 per cent.

The values of J/J_0 from Table 1 are plotted in Figure 1 as ordinates against r/r_1 as abscissae; the crosses and circles refer to the crescents near second and third contacts, respectively. These, as has been said, are practically the same as the radial emission function, e_r. The values suggest a slightly less pronounced shelf in the e_r-curve for 550 $\mu\mu$ than that indicated by Kopal's analysis of the Dutch data for 454 $\mu\mu$. The observed J/J_0 values of both the Dutch and the present experiments point to a higher limb emission than that inferred from extrapolation of the e_r-curves of the uneclipsed sun. Whether the difference is real or will disappear with further work cannot be said at this time. It is apparent from Figure 1 that further measurements in several wave lengths covering the outer 2 per cent of the solar radius would be of value.

In conclusion, it is a pleasure to express to the National Geographic Society and the United States Air Forces our appreciation for the opportunity of being members of their Eclipse Expedition of 1947.

[9] These computations were kindly made by Mrs. Catherine Pinkston, of this laboratory.

A PHOTOGRAPHIC STUDY OF THE DRACONID METEOR SHOWER OF 1946*

LUIGI G. JACCHIA,† ZDENĚK KOPAL,† AND PETER M. MILLMAN‡

Received June 16, 1949

ABSTRACT

The present paper contains a discussion of 204 Draconid (Giacobinid) meteors photographed at North Bay, Ontario, Canada, during the night of October 9–10, 1946, and reduced at the Massachusetts Institute of Technology, Cambridge, Mass. The fundamental data pertaining to each individual meteor are assembled in Table 4.

The cosmic spread of the radiant turns out to be 6°.2, more than half of which is probably due to observational errors. This is much less than the spread of any of the other major showers investigated so far and, together with the fact that no Draconid meteors are observed except in the immediate neighborhood of the parent-comet, points to a relatively early stage of disintegration of the swarm.

The visual paths of the Draconid meteors proved to be of considerably shorter duration than those of most normal meteors and, considering their low geocentric velocity, were visible at abnormally great heights (between 90 and 98 km, on the average). The observed decelerations would point to masses which are, on the average, one hundred times smaller than those of other meteors of comparable brightness and geocentric velocity. All this indicates that the Draconid meteors are probably composed of "soft" material, which is more easily vaporized by friction in the earth's atmosphere than that of other meteor particles.

INTRODUCTION

In view of the prediction of a good Draconid (Giacobinid) meteor shower in October, 1946, plans were made at the Dominion Observatory, Ottawa, for an extensive photographic and visual coverage of these meteors. Only the direct photographic observations are discussed in detail in this paper. The results of the Canadian spectrographic and visual observations will be published elsewhere at an early date. In conformity with the general plan for future co-operation between the United States and Canada in programs of meteor photography, all the work of plate measurement and reduction has been carried out at the Center of Analysis of the Massachusetts Institute of Technology, Cambridge, Massachusetts.

OBSERVATIONAL PROGRAM

A synchronous motor and rotating shutter originally used by Thomson and Burland[1] in 1949 were remounted by Millman in 1946. Five cameras, two spectrographs and three direct cameras, were placed on the same mounting behind one rotating shutter. The shutter had ten vanes, the spacing between the vanes being half the width of the vanes (see Fig. 1). The shutter was rotated at 60 rpm by a Bodine synchronous motor, with shaft rotating 1800 rpm and a built-in worm reduction to give 60 rpm. A friction clamp was provided to take the strain on the shaft due to starting and stopping. The lenses were thus occulted ten times per second and were actually exposed to the sky for only one-third of the total exposure time. This feature is particularly valuable for meteor photography during a moonlit night when the bright sky tends to fog out the faint images. Heating coils back of the shutter prevented the accumulation of dew and frost on the lenses. Two views of the camera mounting appear in Figure 1.

* The measurements and reductions involved in this study were performed under contracts Nos. 8755 and 9169 with the Bureau of Ordnance of the U.S. Navy Department.

† Center of Analysis, Massachusetts Institute of Technology, and Harvard College Observatory, Cambridge, Mass.

‡ Dominion Observatory, Ottawa, Ontario, Canada.

[1] "Perseid Meteor Observations at Ottawa, August, 1940," *J.R.A.S. Canada*, **34**, 479, 1940.

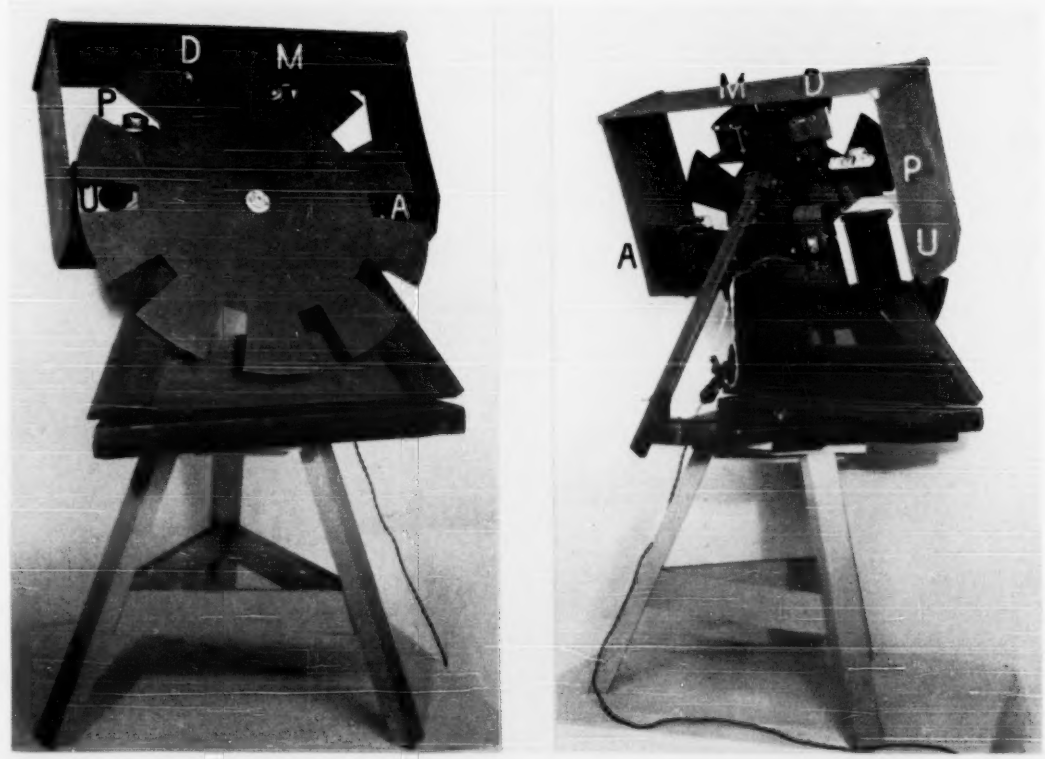

FIG. 1.—Two views of the camera mounting. Cameras A and U are spectrographs; cameras D, M, and P, direct cameras

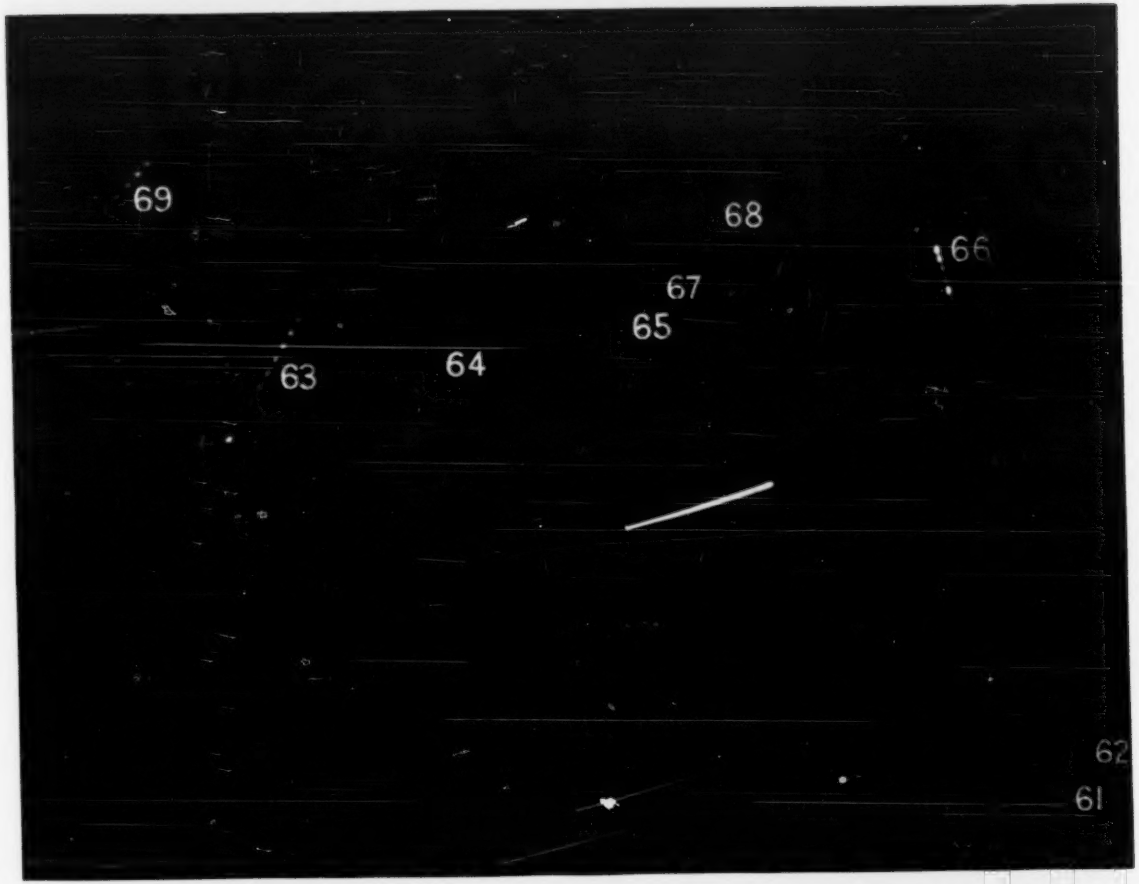

FIG. 2.—A portion of film No. D 738 with the positions of the meteor trails indicated by their serial numbers. Note the deterioration of star trails toward the end of the exposure.

The three direct cameras were adjusted so that their fields were adjoining with a small overlap. The total area of sky covered amounted to 4000 square degrees. The two spectrographs were directed to the central part of this area, their combined coverage being 3200 square degrees. Relevant data for the three direct cameras are listed in Table 1.

In addition to the equipment described above, it had been planned to make use of the 8- and 6-inch photographic telescopes at the Dominion Observatory, as well as several other smaller cameras. It had also been planned to operate a number of direct cameras without shutters at a station established at Rockland, Ontario. This would have given a base line 38 km in length, approximately at right angles to the azimuth of the radiant, and would have made possible the direct computation of height by triangulation measures alone.

Unfortunately, on October 9, the weather was very unfavorable over most of the eastern part of the North American continent. Rain and cloud conditions prevailed generally, and a check with several forecasting centers at noon gave no promise of any improvement in the weather in the Ottawa area for the next 12 hours. At 2:00 P.M. it was decided to attempt to move the cameras with the rotating shutter to a location where there was some hope of clear weather. In this emergency, contact was made with Air Marshal W. A.

TABLE 1

THE DIRECT METEOR CAMERAS

	Camera M	Camera P	Camera D
Model	Kodak Pupille	Kodak 35	Zeiss Ikon
Lens	Schneider Zenon	Anastigmat Special	Zeiss Tessar
Focal length	45 mm	50 mm	75 mm
Aperture ratio	$f/2.0$	$f/3.5$	$f/4.5$
Field	$47.^{\circ}4\times37.^{\circ}2$	$39.^{\circ}6\times27.^{\circ}0$	$42.^{\circ}0\times32.^{\circ}0$

Curtis, then Acting Chief of Air Staff for the Royal Canadian Air Force, and the situation was explained. A Dakota aircraft from Transport Command was immediately placed at the disposal of the Dominion Observatory party, with permission to fly to any airport where there seemed the best chance of good observing conditions. It was impossible to collect the equipment from Rockland in the time available; hence only the rotating shutter mounting and cameras and one of the graticules for visual observing were loaded in the aircraft. With a party of five meteor observers, the Dakota took off from Rockcliffe airport at 6:05 P.M. (1805 hrs.) E.S.T.

Making use of the best weather reports available, it was decided to fly northwest from Ottawa, with the intention of landing at Kapuskasing. However, the edge of the cloud bank was reached before arrival at North Bay, and, since several bright Draconids had already been sighted from the aircraft, a landing was made at North Bay at 1955 hours. The camera mounting was set up on the roof of the administration building of the airport, a few feet from the control tower, where 60-cycle a.c. power was available. Measures on large-scale maps from the Department of National Defence give this position at latitude 46°21′48″ N., longitude 79°25′00″ W., elevation 1225 feet above sea level. Exposures on all five cameras were commenced between 2025 and 2030 hours E.S.T. and were continued, with breaks only long enough for change of film, until 0029 hours, October 10. The speed of the rotating shutter was timed over 2-minute intervals with an accurate stop watch at both the beginning and the end of the period of observation. Any deviation from the assumed speed of 60 rpm was less than one part in five hundred. The sky was clear except for localized patches of thin cirrus haze during the first few minutes of observation and between 2300 and 2340 hours. The moon was within one day of full and only 100° from the radiant. This necessitated short exposures to avoid undue sky fog. The

average exposure time for the three direct cameras was 15 minutes, sixteen exposures on each camera being made in the 4-hour period of observation. Had it been practicable to use still shorter exposures, the photographic efficiency would have been higher. The emulsion used was Eastman Super XX roll film on cameras M and D and Super XX 35-mm film on camera P. The cameras were stationary, the center of the combined fields being kept near the radiant position by adjusting the mounting occasionally between exposures. Because of the danger of the camera shutters not functioning properly at the temperatures encountered, which varied from +40° to +35° F., the lenses were left open for cameras M and D and change of exposure was made by rolling the film to a new position. For camera P the shutter mechanism was coupled with the film wind, and hence the shutter was closed after each exposure. The times of the actual beginning and end of the

TABLE 2*

EXPOSURE DATA AND NUMBER OF METEORS PHOTOGRAPHED ON OCTOBER 10, 1946 (G.C.T.)

Film No.	Camera D			Camera M			Camera P		
	Beginning	End	No. of Meteors	Beginning	End	No. of Meteors	Beginning	End	No. of Meteors
731	1h27m0	1h46m9	3	1h26m6	1h47m1	3	1h26m8	1h47m0	0
732	1 46.9	2 04.0	0	1 47.1	2 03.9	1	1 47.0	2 04.2	0
733	2 04.0	2 18.5	3	2 03.9	2 18.4	1	2 04.2	2 18.4	1
734	2 18.5	2 33.7	3	2 18.4	2 33.6	1	2 18.4	2 33.6	0
735	2 33.7	2 49.0	17	2 33.6	2 48.8	4	2 33.6	2 48.9	1
736	2 49.0	3 05.5	5	2 48.8	3 05.5	4	2 48.9	3 05.5	1
737	3 06.6	3 18.4	6	3 06.4	3 18.3	3	3 06.5	3 18.6	1
738	3 18.4	3 35.1	17	3 18.3	3 34.9	14	3 18.6	3 35.2	3
739	3 35.1	3 46.6	17	3 34.9	3 46.8	12	3 35.2	3 46.7	3
740	3 46.6	3 59.6	29	3 46.8	3 59.4	19	3 46.7	3 59.5	6
741	3 59.6	4 13.6	12	3 59.4	4 13.4	4	3 59.5	4 13.5	1
742	4 13.6	4 26.2	8	4 13.4	4 26.0	0	4 13.5	4 26.1	0
743	4 26.2	4 41.3	2	4 26.0	4 41.2	0	4 26.1	4 41.2	0
744	4 41.3	4 56.0	0	4 41.2	4 56.0	1	4 41.2	4 56.0	0
745	4 56.9	5 11.9	3	4 56.7	5 11.8	0	4 56.8	5 11.8	0
746	5 11.9	5 28.6	0	5 11.8	5 28.6	0	5 11.8	5 28.6	0
Total of meteors			125			67			17

* 209 photographs of 206 different meteors; 204 Draconids; 2 non-Draconids.

exposures were only approximately recorded. Accurately timed star positions, for plate measurement, were impressed on the film by holding a large sheet of card in front of the whole mounting for a period of 10 seconds near the beginning and end of each exposure. This gave breaks in the diurnal star trails, and the centers of these breaks were timed with an error not greater than 2 seconds.

Because of the danger of low-lying fog at dawn and since the shower seemed to be over except for an occasional faint Draconid, the aircraft took off from North Bay at 0115 hours, October 10, and landed at Rockcliffe at 0245 hours. The films were developed immediately in Kodak developer DK 20, this fine-grain developer being used because it was desired to achieve high resolving power rather than image density. A search of the direct photographs revealed 207 trails of 204 different meteors, all but 2 meteors being Draconids. Later, two additional faint Draconid trails were found at M.I.T., making a total of 204 Draconid meteors photographed. The exposure data and the number of meteors recorded on each film are given in Table 2. A portion of film No. D 738 is reproduced in Figure 2, to illustrate the appearance of the photographed meteor trails.

FIG. 3.—The Mann machine for measurement of meteor plates. This photograph shows the front view of one of the five precision comparators designed and built by Mr. D. W. Mann, of Lincoln, Massachusetts, for our meteor program. Its main screw (*left to right*), driving the lower carriage, is 265 mm long and was found to be free from progressive or periodic errors exceeding 0.002 mm over its entire length, so that no screw corrections need to be applied to the measurements. The upper carriage, on which the plate is mounted, can be moved in a direction perpendicular to that of the main screw by another precision screw, 50 mm in length. The rectangular co-ordinates of any point over an area of 265 × 50 mm can, therefore, be determined at one setting to the instrumental precision of the order of 1μ, while rectangular co-ordinates over the entire field of 265 × 265 mm can be read off two additional scales, equipped with verniers permitting the position in both co-ordinates to be read to the nearest 0.02 mm. In addition, the plate on the upper carriage can be rotated (by hand or precise motion) in position angle, and the position read (by means of four verniers) to the nearest 10′ of arc. The microscope provides a magnification which can be varied between 5× and 30×.

Visual observations were carried out by Miriam S. Burland, M. M. Thomson, S. A. Mott, and Flying Officer E. R. Knox-Leet, and sporadically by P. M. Millman. All but one of this group were experienced meteor observers. The visual graticule was used on the runway near where the aircraft was parked, about 200 feet from the control tower. Counts and magnitude estimates were recorded for meteors observed in the field of the graticule, and an attempt was made to plot all the bright meteors appearing near the camera fields. Owing to the small size of the observing group and the high frequency of meteors at shower maximum, many were missed. From the visual records, 38 bright meteors which might possibly be identified with the photographic trails were listed. The subsequent plate measurement has confirmed the identification for 27 of these meteors, and visual magnitudes are hence available for these cases. The times of appearance within a few seconds are also available for most of these visually recorded meteors.

It may be noted here that, contrary to all predictions, the weather did clear at Ottawa in time for the latter part of the shower to be observed. There was still present, however, considerable cloud and haze, and this fact, combined with the bright moon, rendered the conditions for meteor photography in Ottawa much worse than those encountered at North Bay.

MEASUREMENTS OF THE PLATES

At M.I.T. the films received from Canada were mounted between thin glass plates, and two co-ordinate measures were made of both the meteor trails and the reference stars. At first, measurements were carried out on the historic Coast and Geodetic Survey measuring engine of the Harvard Observatory, designed in Victorian days with little regard for the comfort of the operator. Previously, at the inception of the Harvard–M.I.T. joint meteor program, a requirement for more adequate measuring facilities had become evident, and five modern plate comparators (see Fig. 3) were ordered from D. W. Mann, Inc., Lincoln, Massachusetts. These comparators were delivered to M.I.T. when the measurements of the Draconid films were already well under way. The use of the Coast and Geodetic Survey engine at the Harvard Observatory was then abandoned, and the Mann machines were used exclusively through the rest of the work. Several films measured earlier at Harvard were also remeasured on the Mann machines at M.I.T., without change of method, to make sure of the absence of any appreciable systematic errors between the two series of observations.

Rectangular co-ordinates x and y were, in general, measured for all visible time breaks on the star trails, as well as for all segments (and sometimes both segments and breaks) on the meteor trails. As a rule, four different observers measured each plate in succession, each taking at least three independent settings on every detail. It so happened that most films taken with cameras M and D buckled somewhat during exposures, probably because the film rollers loosened slightly and thus reduced tension on the film. Hence the star and meteor images, while perfectly sharp at the beginning of each exposure, grew progressively fuzzier as the film went out of focus toward the end of the exposure. Because of this effect, which also affected noticeably the apparent frequency distribution of observed meteors with time, the second (end) time break in the star trails was, as a rule, much inferior in definition to the first break and not infrequently altogether invisible. Whenever possible, therefore, we have referred all our measurements to the first time break. Only in the case of two sets of exposures (Nos. 738 and 742), where first time breaks were accidentally not impressed, the beginnings of the star trails, always less sharply defined than the breaks, were used as our reference points.

In the course of our measurements the whole field of each film was subdivided into a number of smaller areas for several reasons. It soon became apparent that linear relations between the measured and standard co-ordinates would be quite inaccurate over more than a small fraction of the field covered by each lens. The effects of refraction and of optical distortion were minimized by computing individual sets of linear plate constants for each selected area, using the time breaks on all star trails in the immediate vicinity of

each meteor or group of meteors. Moreover, measures have been made over a relatively small fraction of each field at a time for another important reason. It has been mentioned already that the films were mounted for measurement between two glass plates. These were sealed on the edges, without pressure, but not hermetically. Probably as a result of changing temperature and humidity, occasional and unpredictable "creeping" effects were observed on films left on the machine for several days. Such effects were not observed under similar conditions with plates when the photographic emulsion was coated on glass, so that the cause of this effect undoubtedly lies in the material of the film base. No practicable way of eliminating this film creep was found, other than by completing the measures in a short time so that the film did not have time to change by an appreciable amount. In general, we endeavored to complete all measurements of each selected area within a single day, so that the film would not have to stay in position overnight. If four measurers were to take their turns within a single day, the selected region could not be too large or rich. Sometimes, in spite of all possible precautions, a noticeable shift in position or orientation of a film between successive observers occurred, even within a few hours. In such cases the positions measured by one observer were reduced to the system of the other by means of linear transformations, the coefficients being determined from the given data by the method of least squares.

With such precautions, we have been able to subdivide each film into a moderate number of smaller areas, each characterized by its own system of linear plate constants, in which the O − C residuals for the mean positions of our reference stars are between 3 and 6 μ. This means that we have reached an accuracy attainable with measurements of similar objects on photographic emulsions coated on glass.

DETERMINATION OF THE RADIANT

PLATE CONSTANTS

In the computation of the plate constants we followed the method outlined by Whipple.[2]

Let the direction cosines for a point with celestial co-ordinates (α, δ) be

$$\lambda = \cos\delta \cos\alpha ,$$
$$\mu = \cos\delta \sin\alpha , \tag{1}$$
$$\nu = \sin\delta .$$

Let us now take two great circles through the plate center (λ_0, μ_0, ν_0), one coincident with the meridian of the right ascension through this point and the other perpendicular to it. The poles of these spherical co-ordinate axes will be given by

$$l_0 = -\sin\delta_0 \cos\alpha_0 , \qquad p_0 = -\sin\alpha_0 ;$$
$$m_0 = -\sin\delta_0 \sin\alpha_0 , \qquad q_0 = \cos\alpha_0 ; \tag{2}$$
$$n_0 = \cos\delta_0 , \qquad r_0 = 0 .$$

The gnomonic projection of the co-ordinates referred to this system upon a plane tangential to the celestial sphere at the plate center gives the so-called "standard co-ordinates" (ξ, η). For any point (λ, μ, ν) we shall have an angular distance σ from the plate center, computed by

$$\cos\sigma = \lambda\lambda_0 + \mu\mu_0 + \nu\nu_0 . \tag{3}$$

[2] "Photographic Meteor Studies. I," *Proc. Amer. Phil. Soc.*, **79**, 499, 1938.

Its standard co-ordinates will be given by

$$\xi = \frac{\lambda p_0 + \mu q_0}{\cos \sigma}, \qquad \eta = \frac{\lambda l_0 + \mu m_0 + \nu n_0}{\cos \sigma}. \tag{4}$$

The correlation between standard co-ordinates and observed rectangular co-ordinates (x, y) is taken to be linear, and the equations

$$x = a_x \xi + b_x \eta + c_x, \qquad y = a_y \xi + b_y \eta + c_y, \tag{5}$$

are the equations of condition for the least-squares computation of the plate constants $(a_x, b_x, c_x; a_y, b_y, c_y)$.

POLES OF THE TRAILS

From segment observations a straight-line equation $y = a + bx$ was determined graphically for each meteor trail. Using the plate constants, this equation was transformed into the corresponding equation $\eta = A + B\xi$ in the standard co-ordinate system, where

$$A = \frac{a + b c_x - c_y}{b_y - b b_x} \quad \text{and} \quad B = \frac{b a_x - a_y}{b_y - b b_x}. \tag{6}$$

The corresponding equation of a great circle in astronomical co-ordinates, $\alpha\lambda + \beta\mu + \gamma\nu = 0$, was then computed, using the co-ordinates of the plate center:

$$\alpha = A\lambda_0 + Bp_0 - l_0, \qquad \beta = A\mu_0 + Bq_0 - m_0, \qquad \gamma = A\nu_0 - n_0. \tag{7}$$

The direction cosines of the pole of the trail $(\lambda_p, \mu_p, \nu_p)$ are then given by

$$\lambda_p = \frac{\alpha}{\sqrt{\alpha^2 + \beta^2 + \gamma^2}}; \qquad \mu_p = \frac{\beta}{\sqrt{\alpha^2 + \beta^2 + \gamma^2}}; \qquad \nu_p = \frac{\gamma}{\sqrt{\alpha^2 + \beta^2 + \gamma^2}}. \tag{8}$$

THE RADIANT

To facilitate the plotting of the individual trails, or rather of their extension backward in the vicinity of the radiant, use was made of standard co-ordinates with the origin at $\alpha = 267°$, $\delta = +56°$ (1947.0). Let the direction cosines of this point be λ_r, μ_r, and ν_r and the auxiliary quantities l_r, m_r, n_r; p_r, q_r be defined in the same way as in equations (2). The meteor trail will intersect the ξ and the η axes at two points, whose distances from the origin of co-ordinates are given by

$$\Delta\xi = \frac{\lambda_p\lambda_r + \mu_p\mu_r + \nu_p\nu_r}{\lambda_p p_r + \mu_p q_r}; \qquad \Delta\eta = -\frac{\lambda_p\lambda_r + \mu_p\mu_r + \nu_p\nu_r}{\lambda_p l_r + \mu_p m_r + \nu_p n_r}. \tag{9}$$

Since the cameras were not driven, the individual radiant points of all the meteor trails on one exposure should define a curve on the film, which results from the composition of the proper motion of the apparent Draconid radiant and the diurnal motion of the sky. In reality, because of errors of observation and cosmic spread in the radiant, this curve will be a band, with the long side in the direction of the motion of the Draconid radiant on the film. Although the proper motion of the radiant is small compared to the diurnal motion of the sky, it is too large to be neglected on exposures averaging 15 minutes. This motion, computed on the assumption that the meteor particles followed exactly the orbit of Giacobini-Zinner's comet, gives an approximation closer than actually necessary in the reduction of the observations. We have combined the proper motion of the radiant, computed in this way, with the diurnal motion to obtain the apparent path of the radiant on the films.

COMPUTED RADIANT AND VELOCITIES

Cunningham's orbit of Giacobini-Zinner's comet, published in *Harvard Announcement Card* 775, has been the basis of our computations. The position of the earth was taken as at the time of maximum shower intensity, i.e., October 10.16, 1946, G.C.T., derived from the visual counts. The minimum distance of this point from the comet's orbit corresponds to a value of the eccentric anomaly $E = 3°20'14''.6$. We thus have the following position and velocity components for the earth and the meteors (equinox of 1946.0):

$$\text{Earth}\begin{cases} x_\oplus = 0.9585958\,, & x'_\oplus = -0.0050917\,, \\ y_\oplus = 0.2561784\,, & y'_\oplus = +0.0150917\,, \\ z_\oplus = 0.1111057\,, & z'_\oplus = +0.0065455\,, \end{cases} \qquad R_\oplus = 0.9984377\,;$$

$$\text{Meteors}\begin{cases} x_m = 0.9599673\,, & x'_m = -0.0041214\,, \\ y_m = 0.2568191\,, & y'_m = +0.0219461\,, \\ z_m = 0.1111543\,, & z'_m = -0.0030082\,, \end{cases} \qquad R_m = 0.9998485\,.$$

The relative velocity components and true radiant are given by

$$\left.\begin{array}{ll} x'_\oplus - x'_m = -0.0009703\,, & \lambda_{R_c} = -0.08224 \\ y'_\oplus - y'_m = -0.0068544\,, & \mu_{R_c} = -0.58097 \\ z'_\oplus - z'_m = -0.0095537\,, & \nu_{R_c} = +0.80976 \end{array}\right\} 1946.0\,.$$

The corresponding relative velocity between the earth and the meteors is 20.412 km/sec. This value, however, is considering the meteors at a distance of 0.9998485 A.U. from the sun. Since, instead, the actual distance was that of the earth, i.e., 0.9984377 A.U., the velocity should probably be corrected for the small difference. We have assumed for the geocentric velocity of the meteors before correction for zenith attraction the value $v = 20.433$ km/sec. This corresponds to a velocity of 23.257 km/sec after correction for zenith attraction up to a geocentric distance of 6440 km.

Since the observed position of the true radiant at October 10.16 differs by only 4°.5, or less than its probable error, from the computed position, we feel confident that the computed velocities are correct to at least one part in a thousand.

DETERMINATION OF THE INDIVIDUAL RADIANTS

An attempt was made to determine, whenever possible, individual radiants for each set of exposures. So, for example, all meteor trails on D 738, M 738, and P 738 were combined, and a radiant position was determined from their intersections. This was done in the following manner: The backward extension of the meteor trails was plotted in gnomonic projection, by means of its previously defined intercepts $\Delta\xi$ and $\Delta\eta$, on a transparent sheet of graph paper. A curve representing the apparent motion of the radiant, computed as described above, was drawn on the same scale on another sheet of graph paper, and the positions corresponding to the beginning and the end of the exposure, as well as those of the time breaks, were marked on it. This curve (a straight-line segment for all practical purposes) was placed beneath the meteor plot and, with the ξ and η axes respectively parallel to each other on the two sheets, was shifted until a position was found for which most trails intersected it within the exposure limits. Then the rectangular co-ordinates (ξ, η) of the position corresponding to the first time break were read off.

Owing to the progressive deterioration of images in the course of the exposure, meteors appeared, as a rule, more numerous in the first half of the exposure time. Eight radiant positions were determined in this manner.

For 27 meteors from the initial visual list of 38 the identification with photographic trails was firmly established. These meteors are in a preferred position with respect to the others photographed because the time of their appearance was recorded, and consequently the uncertainty resulting from the diurnal motion of the star field could be eliminated. They were divided into six groups, each of which yielded an excellent radiant position.

All the individual radiant determinations are collected in Table 3. Corrections were

TABLE 3

INDIVIDUAL RADIANT DETERMINATIONS

Sets of Exposures or Visual Meteor Groups	October 10 Average G.C.T. (Hours)	No. of Meteors	Apparent Radiant (1947.0)		True Radiant (1947.0)					
			α	δ	α	δ	t	Wt.	η	Wt.
731–732	1.501	7	266°500	55°048	261°765	54°039	−0.0024	1	+0.0007	4
735	2.583	19	267.235	55.822	261.988	54.143	− .0001	4	+ .0025	3
1	2.667	7	266.959	55.782	261.692	54.027	− .0032	3	+ .0005	4
736	2.833	9	267.257	56.057	261.923	54.205	− .0008	3	+ .0036	2
2	2.943	3	267.432	56.125	262.078	54.210	+ .0008	3	+ .0037	2
737	3.117	10	267.422	56.177	262.033	54.124	+ .0003	3	+ .0022	5
3	3.202	5	267.495	56.223	262.092	54.110	+ .0009	7	+ .0019	7
738	3.307	29	267.732	56.261	262.317	54.081	+ .0033	2	+ .0014	2
4	3.460	4	267.580	56.405	262.141	54.121	+ .0015	4	+ .0021	4
739	3.600	28	267.519	56.463	262.075	54.051	+ .0008	3	+ .0009	3
5	3.763	4	267.312	56.618	261.859	54.071	− .0014	4	+ .0012	7
740	3.800	42	267.511	56.692	262.055	54.130	+ .0006	4	+ .0023	5
741	4.050	9	267.324	56.773	261.898	54.004	− .0010	1	+ .0006	1
6	4.750	4	267.403	57.357	262.136	54.048	+0.0014	3	+0.0008	4

applied to each apparent radiant position for diurnal aberration and zenith attraction. The positions of the true radiant thus obtained are expressed both in equatorial co-ordinates (α, δ) and in standard co-ordinates (ξ, η), with origin at ($\alpha = 262°$, $\delta = +54°$; 1947.0).

A least-squares solution gives, for the true radiant, the following position and motion:

$$\left.\begin{aligned} \xi &= -0.0028\,(\pm 0.0013) + 0.00091\,(\pm 0.00040)\,t \\ \eta &= +0.0018\,(\pm 0.0007) - 0.00005\,(\pm 0.00022)\,t \end{aligned}\right\} (1947.0), \qquad (10)$$

where t is expressed in hours, G.C.T., October 10, 1946. In equatorial co-ordinates we have:

Time: October 10.16, 1946, G.C.T;

Position of the true radiant: (1947.0)
$$\begin{cases} \alpha = 262^{\circ}.07 \pm 0^{\circ}.13\,, \\ \delta = +54^{\circ}.09 \pm 0^{\circ}.04\,; \end{cases}$$

Daily motion of true radiant:
$$\begin{cases} \Delta\alpha = +2^{\circ}.1 \pm 0^{\circ}.9\,, \\ \Delta\delta = -0^{\circ}.1 \pm 0^{\circ}.4\,. \end{cases}$$

According to the least-squares solution, the motion of the true radiant is direct and amounts to $1^\circ.3 \pm 0^\circ.6$ per day. Although this figure looks very reasonable, its reality remains somewhat doubtful, since it exceeds its probable error by a factor of 2 only.

COMPUTATION OF THE INDIVIDUAL RADIANTS

Using the position and motion of the true radiant as derived from the least-squares solution, an ephemeris was prepared for the apparent radiant, and positions (ξ_0, η_0) and motions (ξ', η') in standard co-ordinates (with origin at $\alpha = 267^\circ$, $\delta = +56^\circ$, 1947.0) were derived for the instant t_0 of the first time break for each set of exposures. The proper motion of the apparent radiant had to be combined with the trailing velocity of the diurnal motion $(-[2\pi/T] \cos \delta$, where T = duration of the sidereal day) of stars at the radiant's declination, to represent the apparent motion of the radiant on the photographic films.

For the computation of the time of appearance of the meteors which were not observed visually, the system of standard co-ordinates was frozen at the time t_0, so that it did not take part in the rotation of the celestial sphere. Then, neglecting the curvature of the parallel of declination for the short time interval of the individual exposures, the instantaneous position of the radiant on the films at the time t was given with sufficient approximation by

$$\xi = \xi_0 + \xi' t - \frac{2\pi}{T} t \cos \delta$$
$$\eta = \eta_0 + \eta' t \,. \tag{11}$$

Eliminating t, the equation of the path of the radiant was obtained in the form

$$\eta = f + g\xi \,. \tag{12}$$

Each individual meteor trail had an equation of the form

$$\eta = \Delta\eta - \xi \tan \psi \,; \qquad \tan \psi = \frac{\Delta\eta}{\Delta\xi} \,. \tag{13}$$

We assumed that the radiant of each meteor trail was at its intersection with the locus of the radiants as given by equation (12), i.e., at the point whose co-ordinates were

$$\xi_R = \frac{\Delta\eta - f}{\tan \psi + g} \qquad \text{and} \qquad \eta_R = \frac{g\Delta\xi + f}{1 + g \cot \psi} \,. \tag{14}$$

This is equivalent to assuming that there was no cosmic spread in the radiant and no error in the observed direction of the meteor trail. All the spread was then due to diurnal motion, and the time of the meteor was given by

$$t_m = t_0 + \frac{\xi_R - \xi_0}{\xi' - (2\pi/T)\cos \delta} \,. \tag{15}$$

A different procedure was used for the 27 meteors whose time, t_m, was observed. For these meteors the positions $(\alpha_{R_0}, \delta_{R_0})$ of the apparent radiant were computed for the instant t_m. A correction $\Delta\alpha = \theta_0 - \theta_m$ (where θ_0 and θ_m are the sidereal equivalents of t_0 and t_m) was applied to the α of the computed radiant to account for diurnal motion, yielding the following apparent co-ordinates:

$$\alpha'_{R_0} = \alpha_{R_0} - \Delta\alpha$$
$$\delta'_{R_0} = \delta_{R_0} \,. \tag{16}$$

Standard co-ordinates (ξ_{R_0}, η_{R_0}) were computed for this point. The foot of the perpendicular from (ξ_{R_0}, η_{R_0}) to the meteor trail $(\eta = \Delta\eta - \xi \tan \psi)$ was assumed to be the radiant of the trail; its co-ordinates were:

$$\xi_R = \frac{\Delta\eta - \eta_{R_0} + \xi_{R_0} \cot \psi}{\tan \psi + \cot \psi}, \qquad (17)$$

$$\eta_R = \Delta\eta - \xi_R \tan \psi .$$

VELOCITIES

Once the radiant was established for each meteor trail, relative distances from the observer were computed by the methods used by Millman and Hoffleit[3] and Whipple.[4] The first segment was taken as origin for the distances. Whenever more than five segments were observed on the meteor trail, an equation of the form

$$d = a + bt + c\, e^{kt} \qquad (18)$$

was fitted by least squares to the observed relative distances, d. In this equation, b is the relative velocity comparable with the computed velocity v_∞ of the meteor after the geocentric velocity ($v = 20.433$ km/sec) has been corrected for zenith attraction and diurnal aberration. If v_∞ is expressed in kilometers per second, the ratio $K = v_\infty/b$ is the dimensional scale factor to reduce all computed relative distances into true distances, expressed in kilometers. A table of v_∞ computed for the duration of the shower follows.

G.C.T. (Hours)	v_∞ (Km/Sec)	G.C.T. (Hours)	v_∞ (Km/Sec)
1.5	23.105	3.5	23.079
2.0	23.095	4.0	23.080
2.5	23.086	4.5	23.084
3.0	23.081	5.0	23.090

Using these values of v_∞, K was computed for all the meteor trails where equation (18) could be written. As a check, K was also computed in a different way. The value obtained from the ratio v_∞/b was regarded as a first approximation and called K_1. At the center of the least-squares solution (time t_*), the value of the acceleration $\dot{v}$ then is, according to equation (18),

$$\dot{v}_* = K_1 h^2 c\, e^{kt_*} . \qquad (19)$$

From the computed value of v_∞ and $\dot{v}_*$ as given by equation (19), the velocity v_* at the time t_* was computed by

$$v_*^2 = v_\infty^2 - 33.2 \log_{10}(1 - 0.1019\, \dot{v}_0 \sec Z_R) , \qquad (20)$$

where Z_R is the zenith distance of the apparent radiant. Equation (20) is derived from Whipple's equation (16*a*) in "Photographic Meteor Studies. I."[2] The computed velocity v_* was then compared with the relative velocity $b + hce^{kt_*}$ from the least-squares solution, and the ratio $K_2 = v_*/(b + hce^{kt_*})$ was taken as a second approximation for K. From here on, the procedure was repeated until a satisfactory final value was reached for K.

[3] *Harvard Ann.*, **105**, 601, 1937.

[4] *Proc. Amer. Phil. Soc.*, **79**, 505, 1938.

There is usually a small nonsystematic difference between the values of K as determined from b and from the successive-approximation method. We have taken the arithmetic mean of the two as final for our computations of distances and heights.

For meteors of very short duration, showing four or five segments, no attempt was made to derive the deceleration. In such cases a linear equation of the type $d = a + bt$ was fitted by least squares to the observed values of d. The constant velocity b thus obtained was equated to $0.99\ V_\infty/K$ to obtain the scale factor K, experience having shown that 1 per cent is just about the average loss in velocity to be expected for shorter meteor paths at the observed height. No least-squares solutions were computed for meteors showing only three segments.

COMPUTATION OF HEIGHTS

The distance R_a from the observer to the point on the meteor path corresponding to the first segment is implicit in the scale factor K. If σ_a and σ_R are the angular distances from the optical film center of the first segment and of the radiant, respectively, we have

$$R_a = K \frac{\cos \sigma_R}{\cos \sigma_a}. \tag{21}$$

The height h_a of the point on the meteor trail corresponding to the first segment above the plane tangent to the earth's spheroid at the observing station is given by

$$h_a = R_a \cos Z_a , \tag{22}$$

where Z_a is the zenith distance of the first segment. The heights h_i of all other points on the meteor trail were computed from

$$h_i = h_a - D_i \cos Z_R , \tag{23}$$

where D_i is the distance in kilometers of point i from the point corresponding to the first segment. The distances R_i of all points other than the first segment were determined from h_i by $R_i = h_i \sec Z_i$. All the heights above the tangential plane were reduced to the heights above sea level by adding a correction $\Delta h_i = h_0 + (R_i \sin Z_i)^2/2r$, where h_0 ($= 0.373$ km) is the height above the sea level of the observing station and r is the radius of the earth.

PHOTOMETRY

The apparent panchromatic magnitudes of the meteor trails were estimated visually by comparison with neighboring star trails. Owing to the fact that the rotating shutter left the lens exposed only one-third of the time, the brightness of the star trails was reduced on the films by a factor of 3. Thus, neglecting reciprocity-law failure, a correction $+2.5 \log 3 = +1^m19$ must be applied to the apparent meteor magnitudes to account for this fact.

Only white stars (from B to F) were used to establish the magnitude scale, a star near the center of the field (declination δ_0) was selected as a standard, and all the other comparison stars (declination δ) were reduced to it by applying a correction $+2.5(\log \cos \delta - \log \cos \delta_0)$ to the catalogue magnitudes. The trailing velocity of the standard star on the film, in millimeters per second, is $v_s = (2\pi/T) f \cos \delta_0$, where T is the sidereal period of rotation of the earth and f the focal length of the camera in millimeters. If v_m is the velocity in millimeters per second of the meteor on the film, the velocity correction to be applied to the apparent meteor magnitudes is given by $-2.5 \log (v_m/v_s)$. Field correction and differential atmospheric extinction were minimized by using comparison stars in the immediate vicinity of each meteor trail. These corrections should generally be less than 0.1 mag. and were therefore disregarded.

TABLE 4

Fundamental Data

No.	Film	G.C.T. Comp.	G.C.T. Obs.	No. Segments	L'	Elong.	$\Delta\xi$	$\Delta\eta$	Δ	Cos Z_c
					s	°				
1	D731	1[b] 32.0		6	1.99	20.8	-0.0056	+0.0152		0.819
2	"	1 32.2		4	1.08	19.9	+0.0061	-0.0059		0.820
3	"	1 29.2		4	0.47	6.6	+0.0022	-0.0076		0.824
4	M731	1 32.7		6	1.97	13.7	+0.0455	-0.0124		0.819
5	"	(1 46.0)		4	1.13	16.6	-0.1119	-0.0234		0.799
6	"	1 33.2		4	2.05	34.7	-0.0153	-0.0553		0.819
7	M732	1 57.0		9	4.41	21.7	-0.0204	+0.0746		0.785
8	D733	2 7.6		6	1.52	17.4	-0.0040	+0.0118		0.770
9	"	2 4.5		6	1.22	11.9	+0.0046	-0.0109		0.775
10	M733	2 7.4		8	0.99	6.6	-0.0164	-0.0133		0.771
11	P733	2 14.2		5	3.91	27.0	-0.0106	+0.0069		0.761
12	D734	2 24.8		4	1.09	16.4	-0.0115	-0.1075		0.745
13	"	2 32.2		3	0.51	9.5	-0.0293	-0.1369		0.734
14	"	2 26.1		8	0.95	6.7	-0.0155	-0.0537		0.743
15	M734	2 26.5		5	2.06	29.6	-0.0136	-0.0262		0.743
16	D735	2 39.5		6	1.94	33.3	-0.0093	-0.0444		0.723
17	"	2 45.7	2[b] 43.0	6	3.50	33.3	-0.0246	-0.0358	0.292	0.714
18	"	2 42.6	2 42.0	9	5.48	32.6	-0.0184	-0.0183	0.048	0.719
19	"	2 42.3	2 40.5	9	4.50	29.0	-0.0167	-0.0316	0.208	0.719
20	"	2 40.8		4	1.35	30.9	-0.0117	+0.6389		0.721
21	"	2 42.1		4	1.29	28.2	-0.0147	+0.2320		0.720
22	"			3	too faint to be measured					
23	"	2 43.4		4	1.49	23.8	-0.0192	-0.0385		0.717
24	"	2 35.7	2 35.5	7	3.87	25.9	-0.0059	-0.0035	0.015	0.729
25	"	2 41.9		4	1.13	21.3	-0.0140	+0.0826		0.719
26	"	2 34.1		4	1.20	19.5	+0.0034	+0.0216		0.731
27	"	2 35.6		3	0.80	16.9	-0.0002	-0.0012		0.729
28	"	2 44.8		5	1.30	15.9	-0.0217	-0.1564		0.715
29	"	2 37.9		4	0.89	13.1	-0.0067	-0.0121		0.725
30	"	2 41.9	2 37.5	5	1.01	15.6	-0.0134	+0.0267	(0.574)	0.722
31	"	2 45.3		6	0.96	8.7	-0.0284	-0.0086		0.714
32a	"	(2 44.1)	2 46.0	7	0.97		(-0.0185)	(+0.0274)	(0.234)	0.715
32b	M735	2 45.8	2 46.0	13		4.3	-0.0230	+0.0136	0.142	0.712
33	"	2 38.9		(9)	0.47	2.0	-0.0099	-0.0101		0.724
34	"	2 39.3	2 35.7	13	3.38	16.0	-0.0140	-0.0062	0.230	0.727
35	"			1	only one segment					
36	P735	2 36.5		9	8.12	34.5	+0.0072	-0.0028		0.727
37	D736	2 56.0	2 55.7	6	2.29	33.6	-0.0113	-0.0949	0.048	0.698
38	"	2 51.2		4	2.01	31.7	-0.0002	-0.0003		0.705
39	"	2 50.3		6	1.02	12.3	+0.0027	-0.0062		0.707
40	"	2 57.3	2 56.2	9	1.65	8.5	-0.0139	-0.0208	0.122	0.700
41	"	——		6	2.56	20.0	+0.0270	-0.0029		0.700
42	M736	2 56.8	2 57.8	8	1.00	8.4	-0.0141	+0.0127	0.101	0.695
43	"	2 53.3		6	2.95	27.7	+0.0048	+0.0483		0.702
44	"	3 0.3		4	1.77	28.9	-0.0213	-0.2518		0.691
45	P736	2 59.6		3	2.28	36.3	-0.0232	+0.0088		0.692
46	D737	3 10.8		4	1.79	29.7	-0.0023	-0.0030		0.675
47	"	3 7.5		7	2.07	27.6	+0.0028	-0.0447		0.680
48	"	3 7.5	3 12.2	5	1.93	20.7	+0.0088	+0.0042	0.221	0.675
49	"	3 11.7	3 10.5	7	1.46	19.9	-0.0096	+0.0146	0.146	0.674
50	"	3 9.8		4	0.65	11.6	-0.0030	+0.0187		0.677
51	"	3 12.1		5	0.69	8.6	-0.0071	-0.0287		0.673
52	M737	3 10.3	3 10.9	7	0.30	3.7	-0.0056	+0.0103	0.077	0.675
53	"	3 15.5	3 15.2	9	3.23	18.8	-0.0170	+0.0071	0.034	0.668
54	"	3 12.3	3 11.6	12	3.53	29.3	-0.0045	-0.0043	0.116	0.672
55	D738	3 19.8		4	2.05	34.4	+0.0060	+0.0069		0.661

TABLE 4

Fundamental Data

No.	Film	G.C.T. Comp.	G.C.T. Obs.	No. Segments	L'	Elong.	$\Delta\xi$	$\Delta\eta$	Δ	Cos Z_0
56	EF38	3^h 26.4		6	2.°16	34.°1	+0.0124	+0.0434		0.651
57	"	3 25.3		10	3.64	31.2	+0.0103	+0.0466		0.652
58	"	3 17.6		4	2.03	29.3	+0.0113	+0.0119		0.664
59	"	3 21.8		5	1.45	29.6	+0.0032	+0.0576		0.658
60	"	3 21.6		5	1.51	27.7	+0.0027	+0.0762		0.658
61	"	3 28.8		4	1.17	25.9	+0.0190	+0.1195		0.647
62	"	3 21.0		4	1.12	24.6	+0.0011	+0.0118		0.659
63	"	3 31.9		13	4.39	17.4	+0.0156	+0.0105		0.642
64	"	3 26.5		3	0.78	16.9	+0.0078	+0.0078		0.650
65	"	3 28.2	3^h 27.9	8	1.90	14.9	+0.0141	+0.0214	0.047	0.648
66	"	3 28.7	3 28.4	11	2.29	13.5	+0.0189	+0.1440	0.045	0.647
67	"	3 18.3		4	0.79	12.8	+0.0071	+0.0157		0.663
68	"	3 28.7	3 31.6	4	0.83	13.5	+0.0161	+0.0314	0.328	0.645
69	"	3 24.1		6	1.82	16.2	+0.0075	+0.0029		0.654
70	"			5	too faint to be measured					
71	"			3	too faint to be measured					
72	MF38	3 25.0		6	1.60	13.6	+0.0637	+0.0080		0.653
73	"	3 22.1		6	0.24	2.5	+0.0031	+0.0025		0.657
74	"	(3 26.6)		3	0.30	6.4	+0.0870	+0.0123		0.651
75	"	3 25.4	3 22.5	9	1.06	9.6	+0.0488	+0.0088	0.105	0.657
76	"	(3 23.8)		6	0.78	10.5	+0.0051	+0.0002		0.653
77	"			3	only one segment measurable					
78	"			3	too faint to be measured					
79	"	3 22.2		7	0.99	10.1	+0.0038	+0.0027		0.657
80	"			38	sporadic					
81a	"	3 21.9		6	2.05	16.6	+0.0086	+0.0114		0.658
81b	EF38	3 22.1		6	"	"	+0.0082	+0.0109		0.657
82	MF38	3 24.4		5	1.16	12.1	+0.0117	+0.0419		0.654
83	"	3 22.3		5	1.09	13.4	+0.0051	+0.7828		0.657
84	"	3 18.8		4	1.20	17.0	+0.0042	+0.0301		0.663
85	"	3 29.9		4	1.32	28.5	+0.0149	+0.0141		0.645
86	EF38	3 27.3		5	2.44	21.0	+0.0741	+0.0089		0.649
87	"			2	too faint to be measured					
88	EF39	3 42.8		5	1.51	30.2	+0.0084	+0.0327		0.625
89	"	3 38.0		5	1.73	26.5	+0.0054	+0.0101		0.632
90	"	3 38.3		6	2.64	25.1	+0.0106	+0.0091		0.632
91	"	3 43.5		6	1.78	25.1	+0.0094	+0.0282		0.624
92	"			3	too faint to be measured					
93	"	3 39.7		5	1.05	28.3	+0.0061	+0.0245		0.630
94	"	3 38.1		7	2.23	21.7	+0.0045	+0.0098		0.632
95	"	3 41.2		5	2.31	25.6	+0.0171	+0.0071		0.627
96	"	3 36.3		3	0.99	21.0	+0.0022	+0.0088		0.635
97	"	3 40.9		6	1.16	14.3	+0.0030	+0.0089		0.628
98	"	3 36.9		4	0.83	14.2	+0.0086	+0.0145		0.634
99	"	3 41.3		6	1.14	12.8	+0.0034	+0.0084		0.627
100	"	(3 35.1)		5	0.88	15.3	+0.0078	+0.0309		0.638
101	"	3 41.2		12	2.09	13.0	+0.0089	+0.0504		0.627
102	"			3	too faint to be measured					
103	"	3 42.7		8	2.24	14.7	+0.0332	+0.0079		0.625
104	"	3 37.4		7	1.09	14.4	+0.0043	+0.0064		0.633
105	MF39	3 41.3		6	0.71	5.9	+0.0053	+0.0273		0.627
106	"	3 42.3		8	1.02	7.3	+0.0081	+0.0862		0.626
107	"			3	too faint to be measured					
108	"	3 36.5		6	1.03	11.2	+0.0089	+0.0170		0.635
109	"	3 44.4		7	1.45	13.6	+0.0081	+0.0133		0.622
110	"	3 39.3		8	2.91	18.9	+0.0004	+0.0098		0.632

TABLE 4

Fundamental Data

No.	Film	G.C.T. Comp.	G.C.T. Obs.	No. Segments	L'	Elong.	$\Delta\xi$	$\Delta\eta$	Δ	Cos Z_g
111	M739	3^h 43^{m}9		8	2.76	18.6	−0.0107	−0.3717		0.623
112	"	3 42.5	3^h 43^{m}0	8	1.88	17.3	+0.0002	+0.0002	0.043	0.625
113	"	3 40.3		6	1.57	19.7	+0.0019	+0.0027		0.629
114	"	3 46.2	3 45.7	4	2.39	27.4	+0.0175	+0.0054	0.018	0.620
115	"	3 37.4		7	2.33	21.1	+0.0056	+0.0149		0.634
116	"	(3 36.0)		5	1.08	33.2	+0.0320	+0.0162		0.638
117	P739	3 37.2		3	2.40	37.2	−0.0285	−0.0931		0.634
118	"	3 35.4		6	2.39	19.7	−0.0135	−0.0299		0.637
119	"			3	too faint to be measured					
120	D740	3 47.1		5	3.16	39.5	+0.0255	+0.0163		0.618
121	"	3 53.7		3	1.37	35.0	+0.0030	+0.0035		0.608
122	"	3 54.3		9	3.31	33.3	−0.0044	−0.0110		0.607
123	"	3 59.6		4	1.60	33.8	−0.0121	−0.0170		0.599
124	"			7	trail distorted owing to film motion					
125	"	3 49.2		9	3.07	28.6	+0.0072	+0.0184		0.615
126	"			3	too faint to be measured					
127	"	3 0.0		8	2.71	24.2	+0.0101	+0.0131		0.614
128	"	3 57.1		4	0.92	27.1	−0.0162	−32.35		0.603
129	"	3 49.7		3	0.75	25.5	+0.0014	+0.5890		0.614
130	"			2	too faint to be measured					
131	"	3 51.3		6	1.94	20.9	+0.0079	+0.0096		0.612
132	"	3 50.9		6	1.86	19.4	+0.0095	+0.0105		0.612
133	"	3 50.5		5	0.95	21.9	−0.0016	+0.0163		0.613
134	"	(3 46.3)	3^h 49^{m}0	10	3.83	21.6	+0.0445	+0.0143	0.081	0.616
135	"	3 52.5		5	1.30	17.4	+0.0022	+0.0037		0.610
136	"	3 50.4		12	2.87	16.0	+0.0041	+0.0115		0.613
137	"	3 50.3		10	2.26	16.9	+0.0031	+0.0125		0.613
138	"			3	too faint to be measured					
139	"	3 52.1		5	0.99	18.1	−0.0060	+0.0435		0.610
140	"	3 50.7		6	1.16	19.7	−0.0039	+0.0163		0.613
141	"	(3 50.0)		6	2.21	19.7	+0.1363	+0.0172		0.616
142	"			3	too faint to be measured					
143	"	3 50.5		3	0.56	12.9	+0.0148	+0.0118		0.613
144	"			3	too faint to be measured					
145	"			2	too faint to be measured					
146	"	3 55.4		6	0.83	9.5	−0.0028	−0.0039		0.605
147	"			3	too faint to be measured					
148	"			3	too faint to be measured					
149	M740	3 49.9		4	0.21	2.7	+0.0464	+0.0123		0.614
150	"			6	0.26	3.7	−0.0168	+0.0168		
151	"	——		5	0.13	1.6	−0.0087	+0.0061		
152	"	3 50.0	3 51.7	?	0.39	1.5	−0.0220	+0.0119	0.134	
153	"	(3 51.0)		7	0.34	3.3	+0.0748	+0.0046		0.609
154	"	(3 59.0)		5	0.41	5.5	−0.0998	+0.0187		0.600
155	P740	3 54.2		5	2.23	23.3	−0.0565	+0.0155		0.607
156	M740	3 53.9		7	1.09	8.8	−0.0174	+0.0263		0.608
157	"	3 50.3		8	0.85	7.9	+0.0333	+0.0122		0.613
158	"	3 47.8		5	0.69	11.5	+0.0196	+0.0170		0.617
159	"	3 51.0		4	1.84	22.1	−0.0056	+0.0099		0.614
160	"	3 50.3		9	1.61	11.9	+0.0111	+0.0124		0.613
161	"	3 56.3		5	0.88	13.8	+0.0044	+0.0032		0.604
162	"			3	too faint to be measured					
163	"	3 56.8		8	2.31	16.3	−0.0165	+0.2261		0.603
164	"	3 59.5		8	1.64	15.5	−0.0013	−0.0009		0.599
165	"	3 51.7		7	2.19	19.4	−0.0016	−0.0119		0.611

TABLE 4

Fundamental Data

No.	Film	G.C.T. Comp.	G.C.T. Obs.	No. Segments	L'	Elong.	$\Delta\xi$	$\Delta\eta$	Δ	Con Z_0
166	M740	3^h 50^{m}5		7	4.°14	28.°5	-0.0014	+0.0175		0.613
167	"	3 49.8		12	4.50	24.6	+0.0066	+0.0150		0.614
168	"			5	eporadic					
169	P740	3 50.7		6	5.87	41.0	-0.0268	+0.0126		0.613
170	"	3 50.7		10	8.27	34.9	-0.0162	+0.0129		0.613
171	"	3 54.0		9	7.63	34.3	-0.0267	+0.0193		0.607
172	"			4	too faint to be measured					
173	"	3 49.2		4	2.32	31.4	+0.0504	+0.0125		0.615
174	D741			3	too faint to be measured					
175	"	4 4.1		7	3.05	35.8	+0.0155	+0.0187		0.592
176	"	4 11.5		5	2.04	36.0	-0.0027	-0.0037		0.580
177				6	too faint to be measured					
178	"			5	too faint to be measured					
179	"	4 5.3		5	2.04	26.7	+0.0191	+0.0155		0.590
180	"	4 5.6		6	1.76	22.7	+0.0092	+0.0148		0.590
181	"	4 2.1		6	1.40	23.1	+0.0108	+0.0530		0.595
182	"	4 8.1		11	3.31	18.6	+0.0057	+0.0081		0.586
183	"	4 9.7		4	1.04	19.5	+0.0026	+0.0033		0.583
184	"	4 9.6		6	1.04	13.3	-0.0049	-0.0154		0.583
185	"	(4 6.6)		5	0.73	16.3	-0.0309	+0.0699		0.579
186	M741	(4 5.0)		6	0.43	5.8	+0.2451	+0.0158		0.591
187	"	(4 13.0)		6	0.58	7.1	+0.0212	+0.0081		0.576
188	"	4 7.6		9	1.18	8.4	+0.0053	+0.0080		0.586
189	"	4 4.7		8	1.64	15.3	+0.0229	+0.0173		0.591
190	P741			4	too faint to be measured					
191	D742	(4 22.0)		3	1.73	42.1	-0.0062	-0.0040		0.564
192	"	4 26.4		19	7.05	31.2	-0.0162	-0.0365		0.557
193	"	4 22.2		15	4.21	30.8	-0.0078	-0.0209		0.564
194	"	4 24.1		7	1.47	26.2	-0.0139	-0.0477		0.561
195	"	4 20.0	4^h 20^{m}5	7	1.96	24.5	-0.0001	-0.0002	0.041	0.567
196	"	4 18.1		3	1.08	23.6	+0.0155	+0.0136		0.570
197	"	4 17.1		11	1.80	12.9	-0.0014	-0.0158		0.572
198	"	(4 13.6)		5	0.78	11.4	+0.0352	+0.0267		0.580
199	D743	4 33.4	4 31.3	8	4.28	32.8	+0.0294	+0.0163	0.118	0.548
200	"	(4 38.3)		6	1.45	15.6	+0.0627	+0.0147		0.537
201	M744	4 49.2		7	2.44	22.9	-0.0092	-0.0785		0.523
202	D745	5 7.8	5 5.1	3	0.60	29.7	-0.0097	-0.0304	0.343	0.495
203	"	5 7.0		7	1.59	16.7	+0.0675	+0.0235	0.003	0.497
204	"	5 7.9		6	0.80	14.5	-0.0098	-0.0304		0.496
205	M736	3 0.9		6	2.71	30.5	-0.0256	-0.1683		0.690
206	D733	2 10.8		3	0.95	18.6	-0.0156	-0.1175		0.766

TABLE 4

Fundamental Data

No.	H_b	H_e	Pos. of Max. L	$R_{max.}$ c.	App. Max. Mag. m_p	$\int I\,dt$	$-2.5 \times \log \int I\,dt$	Vis. Mag.	Train	$\dot{v}_\infty$	p.e.	H_∞
1	101.0	91.7	0.4	142.7	-1.2	2.7	-1.1			-0.7	±2.1	96.3
2	106.9	101.2	0.3	169.2	-1.0	2.5	-1.0			—		
3	103.2	98.2	0.3	127.2	+0.3	0.4	+0.4			—		
4	97.8	88.5	0.8	95.5	-3.2	4.1	-1.5			—		
5	84.3	78.8	0.3	135.3	-2.8	8.1	-2.3			—		
6	93.8	88.3	0.7	141.2	-2.1	5.2	-1.8			—		
7	95.1	80.9	1.0	97.2	-3.4	5.5	-1.9			-1.0	±0.2	88.0
8	104.9	96.1	0.4	158.6	-0.9	2.7	-1.1			+1.0	±1.0	101.3
9	96.5	87.8	0.6	133.8	-1.6	2.2	-0.9			—		
10	92.4	86.8	0.4	120.0	-0.6	1.4	-0.4			-2.2	±2.0	87.1
11	91.1	83.2	0.5	91.1	-1.5	1.0	0.0			-5.8	±1.9	87.0
12	97.4	92.2	1.0	134.3	-0.4	0.8	+0.2			—		
13	92.2	88.9	0.5	124.9	-1.6	0.9	+0.1			—		
14	98.7	87.7	0.3	128.4	-0.2	0.9	+0.1			-3.2	±1.7	93.1
15	95.2	88.5	0.8	154.8	-5.9	86.1	-4.8			—		
16	103.5	97.0	1.0	174.7	-2.5	9.9	-2.5			—		
17	91.0	83.1	1.0	118.6	-2.6	4.3	-1.6	-1		-2.6	±0.8	87.0
18	100.2	87.2	0.8	122.2	-5.7	161.0	-5.5	-3	T	-1.5	±0.6	93.6
19	98.4	85.3	1.0	126.2	-3.0	7.8	-2.2	0		-0.4	±0.5	91.9
20	102.9	97.9	0.3	197.5	-2.0	4.9	-1.7			—		
21	103.3	98.3	0.3	193.9	-1.0	2.7	-1.1			—		
22	too faint to be measured											
23	103.8	98.9	0.7	143.0	-0.9	1.7	-0.6			—		
24	99.0	88.9	0.2	107.3	-1.5	3.0	-1.2	-1		+1.0	±0.7	94.0
25	103.5	98.2	0.0	183.8	-0.6	2.2	-0.8			—		
26	101.5	96.4	0.7	149.2	0.0	1.5	-0.4			—		
27	99.7	96.4	1.0	142.0	+0.1	0.9	+0.1			—		
28	96.0	89.4	0.1	140.6	-2.1	7.2	-2.1			—		
29	99.4	94.5	0.3	131.7	-1.4	1.7	-0.6			—		
30	102.3	95.6	0.5	173.3	-2.6	9.6	-2.5	-3		—		
31	106.3	98.1	0.0	121.7	-1.7	2.7	-1.1			-0.9	±1.0	102.2
32a	—	82.7	—	—	-4.0	—	—	-3	10^R	-1.5	±0.5	87.3
32b	104.0	—	—	—	—	—	—			+0.9	±0.4	94.3
33	—	—	0.1	(100.2)	-0.5	0.7	+0.4			-1.4	±1.4	67.2
34	94.4	74.1	0.2	158.8	-4.3	26.4	-3.6	-2		+0.9	±0.5	85.0
35	only one segment											
36	91.4	77.8	0.2	97.7	-1.4	2.2	-0.9			+1.2	±0.6	84.6
37	95.7	87.9	—	187.3	-3.1	22.1	-3.4	-2		-2.3	±5.4	92.1
38	100.1	95.3	0.0	141.1	-1.5	2.3	-0.9			—		
39	104.2	96.0	0.5	170.1	-1.0	3.0	-1.2			+4.9	±4.1	100.9
40	86.2	73.7	0.6	108.4	-3.0	5.0	-1.7	-1		-2.3	±0.5	79.9
41	103.3	94.7	0.8	106.1	-3.5	5.0	-1.7			—		
42	101.8	90.4	0.4	162.8	-5.7	173.6	-5.6	-3	T	+1.3	±1.3	96.2
43	97.0	90.0	0.4	121.3	-2.4	6.1	-2.0			-4.4	±1.2	93.1
44	103.5	98.8	0.3	142.7	-3.1	6.5	-2.0			—		
45	104.7	101.5	0.5	104.0	-2.1	1.3	-0.3			—		
46	102.4	97.8	0.5	146.9	-3.1	9.0	-2.4			—		
47	101.1	91.5	1.0	211.5	-0.9	5.9	-1.9			+1.0	±0.8	96.3
48	94.1	88.5	0.3	114.1	-1.5	1.8	-0.6	0		-5.9	±2.6	91.2
49	93.5	84.6	0.7	203.9	-3.9	28.5	-3.6	-1		-3.5	±0.7	88.9
50	82.7	78.7	0.5	135.5	-0.6	1.1	-0.1			-13.7	±4.5	80.7
51	87.3	81.8	0.3	130.8	-0.4	0.8	+0.2			-8.9	±0.6	84.5
52	92.5	83.4	0.2	126.4	-0.9	1.4	-0.4	0		-2.6	±1.8	87.8
53	94.0	82.9	0.5	111.5	-4.0	29.4	-3.7	-1		-5.3	±0.5	88.1
54	106.6	89.8	0.6	216.5	-2.4	22.8	-3.4	0		-1.4	±0.2	97.9
55	100.5	95.9	0.7	145.6	-2.2	3.9	-1.5			—		

TABLE 4

Fundamental Data

No.	H_b	H_e	Pos. of Max. I.	$R_{max.\ I.}$	App. Max. Mag. m_p	$\int I\,dt$	$-2.5 \times \log \int I\,dt$	Vis. Mag.	Train	v_∞	p.e.	H_∞
56	91.6	84.9	0.6	182.1	-2.6	7.6	-2.2			-7.1	±2.2	88.2
57	97.7	84.2	0.1	197.7	-2.2	15.0	-2.9			+2.0	±0.7	91.2
58	93.0	88.3	0.3	190.0	-1.2	1.9	-0.7			—		
59	103.1	97.0	0.3	226.7	-1.5	6.2	-2.0			—		
60	97.7	91.5	0.3	207.0	-0.6	2.7	-1.1			—		
61	102.6	98.0	—	197.6	-0.3	2.0:	-0.7:			—		
62	102.9	98.3	—	201.9	+0.3	1.0:	0.0:			—		
63	106.4	88.3	0.9	118.1	-4.0	35.7	-3.9			-0.8	±0.2	96.1
64	105.7	102.6	—	147.1	+0.2	0.5:	+0.7:			—		
65	96.5	86.8	0.5	139.6	-1.4	3.9	-1.5	0		-4.6	±0.6	91.4
66	98.7	83.7	0.5	156.4	-5.4	81.4	-4.8	-1		-0.4	±0.3	91.0
67	102.2	97.6	0.3	151.7	-1.2	2.0	-0.8			—		
68	98.3	93.8	1.0	145.6	-1.9	1.2	-0.2	0		—		
69	99.4	91.9	0.4	122.6	-3.8	11.4	-2.6			+0.4	±0.9	95.6
70	too faint to be measured											
71	too faint to be measured											
72	96.2	89.1	0.5	112.2	-3.2	6.6	-2.0			-3.5	±1.5	92.6
73			—	(150:)	-3.2	15:	-4.4			—		
74	87.9	84.9	1.0	148.0	-0.5	0.7	+0.4			—		
75	109.2	96.8	0.9	186.4	-6.0*	94.2	-4.9	0		+0.6	±1.1	103.0
76	98.3	91.0	0.4	178.4	-0.7	3.0	-1.2			—		
77	—	—	—	—	—	—	—			—		
78	too faint to be measured											
79	96.6	87.6	0.5	160.9	-0.7	1.8	-0.6			—		
80	sporadic											
81a	93.9	86.5	0.4	107.3	-4.4	13.1	-2.8			-1.4	±1.0	90.2
81b	92.0	84.9	0.4	103.3	—	—	—			-3.4	±1.4	88.4
82	92.4	86.5	0.7	121.1	-1.8	2.3	-0.9			—		
83	97.9	92.0	0.0	131.9	-2.3	5.1	-1.8			—		
84	94.9	90.3	0.3	130.3	-1.5	2.1	-0.8			—		
85	86.3	81.8	0.5	191.2	-3.4	10.6	-2.6			—		
86	83.1	77.7	1.0	87.6	-3.9	1.3	-0.3			-5.7	±2.0	80.3
87	too faint to be measured											
88	96.4	91.0	0.5	202.0	-1.0	2.6:	-1.0			—		
89	102.5	97.8	0.1	171.6	-0.9	2.6	-1.0			—		
90	—	—	—	—	-0.7	1.2:	-0.2:			—		
91	85.1	80.3	0.3	156.1	0.0	0.6:	+0.5:			-9.4	±3.9	81.9
92	too faint to be measured											
93	100.4	94.4	0.3	297.9	-2.9	35.6	-3.9			—		
94	94.3	85.6	0.7	153.0	-2.1	5.7	-1.9			-1.2	±1.0	89.9
95	104.0	98.1	—	(127.4)	-0.8	1.5:	-0.4:			—		
96	102.9	96.3	0.0	240.0	-1.3	4.9	-1.7			—		
97	92.3	85.9	0.5	150.4	0.0	1.0	0.0			-7.8	±0.8	89.0
98	99.3	95.0	0.3	154.4	+0.4	0.4:	+1.0:			—		
99	98.1	90.8	0.6	155.2	+0.4	1.0	0.0			+1.7	±2.3	94.5
100	102.7	96.7	0.3	202.9	-1.0	3.9	-1.5			—		
101	100.8	84.4	0.7	176.2	-2.7	14.5	-2.9			-0.1	±0.3	92.4
102	too faint to be measured											
103	104.1	94.1	0.8	123.3	-3.0	7.8	-2.2			+1.0	±0.9	98.5
104	95.1	86.7	0.4	200.5	-1.5	6.7	-2.1			-3.1	±0.7	90.8
105	83.6	76.3	0.6	120.5	-0.9	1.1	-0.1			—		
106	94.9	85.3	0.4	132.4	-2.4	7.4	-2.2			-3.0	±0.5	90.7
107	too faint to be measured											
108	100.6	93.2	0.6	152.2	-1.4	3.5	-1.4			+2.5	±5.1	97.7
109	98.7	89.9	0.5	159.5	-1.4	4.2	-1.6			+2.1	±2.7	94.3
110	95.4	85.2	0.9	117.8	-3.5	11.7	-2.7			+2.3	±1.1	90.5

TABLE 4

Fundamental Data

No.	H_0	H_e	Pos. of Max. L.	$H_{max.\ L.}$	App. Max. Mag.	$\int I\,dt$	$-2.5 \times \log \int I\,dt$	Via. Mag.	Train	$\dot{v}_e$	p.e.	H_e
					m							
111	94.6	84.7	0.9	120.8	−8.0*	260:	−6.0			+0.3	±1.5	89.6
112	100.7	90.8	0.7	182.8	−3.4	31.0	−1.2	0		−2.4	±1.1	94.9
113	97.4	90.4	0.6	166.3	−1.9	6.6	−2.1			−3.4	±1.8	93.8
114	—	—	1.0	—	−3.8	—	—	−2		—		
115	97.0	88.2	0.4	148.8	−2.7	8.3	−2.3			+1.6	±2.4	93.3
116	105.2	99.2	0.3	331.7	−1.8	18.6	−3.2			—		
117	99.6	96.7	0.0	102.8	−1.9	1.6	−0.5			—		
118	97.0	90.3	1.0	108.0	−1.6	0.9	+0.1			—		
119					too faint to be measured							
120	100.7	94.9	0.7	136.1	−2.9	7.5	−2.2			—		
121	102.3	99.4	0.0	170.1	−1.8	3.7	−1.4			—		
122	91.4	80.8	0.8	184.9	−4.1	55.7	−4.4			−2.7	±0.6	85.9
123	107.7	103.9	—	188.3	+0.1	—	—			—		
124					trail distorted owing to film motion							
125	100.9	89.2	0.5	192.1	−1.5	8.8	−2.4			+0.3	±0.6	95.0
126					too faint to be measured							
127	98.7	89.4	0.2	155.4	−2.5	7.1	−2.1			−4.6	±0.4	93.6
128	99.9	95.7	0.0	262.5	−2.1	10.3	−2.5			—		
129	93.2	90.2	1.0	225.2	−1.8	4.5	−1.6			—		
130					too faint to be measured							
131	97.7	90.6	0.8	145.7	−1.5	3.9	−1.5			+0.6	±1.0	94.2
132	94.9	88.0	0.6	140.7	−1.4	2.6	−1.0			−2.2	±1.4	91.4
133	108.2	102.5	0.1	253.3	−0.9	6.8	−2.1			—		
134	102.9	90.0	0.4	123.7	−3.5	19.9	−3.2	−1		−0.6	±0.4	97.0
135	96.2	90.5	0.2	160.1	−0.2	1.7	−0.6			—		
136	97.5	81.9	0.3	163.7	−1.6	8.5	−2.3			−0.8	±0.1	89.4
137	100.9	88.0	0.4	180.6	−2.5	19.7	−3.2			−0.4	±0.2	94.4
138					too faint to be measured							
139	96.8	91.0	0.3	214.0	−2.4	13.3	−2.8			—		
140	97.0	89.8	0.8	227.4	−1.9	10.2	−2.5			—		
141	92.2	86.0	0.3	113.0	−4.1	15.7	−3.0			−3.8	±1.2	89.5
142					too faint to be measured							
143	(108.1)	(105.2)	0.3	(160.7)	−0.9	1.6	−0.5			—		
144					too faint to be measured							
145					too faint to be measured							
146	93.9	87.5	0.3	146.8	−0.5	1.4	−0.4			−6.0	±0.8	90.7
147					too faint to be measured							
148					too faint to be measured							
149	—	—	—	—	+0.2	—	—			—		
150	—	—	—	—	−1.4	—	—			—		
151	—	—	—	—	−1.1	—	—			—		
152	—	—	—	—	—	—	—	−2	20*	—		
153	92.3	84.3	0.8	150.4	−0.9	2.4	−1.0			−4.1	±1.2	88.1
154	88.1	82.3	0.3	164.4	−0.7	1.4	−0.4			—		
155	87.9	83.3	0.5	97.5	−1.6	2.2	−0.9			−13.9	±2.2	85.4
156	102.0	93.5	0.5	137.9	−2.9	11.5	−2.7			+0.1	±1.9	97.7
157	101.1	91.0	0.4	175.0	−1.0	3.4	−1.3			—		
158	111.1	105.3	—	189.6	−0.1	1.7:	−0.6:			—		
159	93.9	89.6	0.7	111.1	−3.1	7.2	−2.1			—		
160	98.5	86.8	1.0	153.0	−3.4	12.5	−2.7			+6.0	±1.3	92.1
161	98.5	92.8	—	183.7	−1.9	9:	−2.4			—		
162					too faint to be measured							
163	90.8	81.9	0.7	118.2	−3.1	8.7	−2.3			−6.1	±1.7	86.9
164	88.6	79.8	0.5	169.6	−2.0	8.7	−2.3			−2.7	±2.3	83.5
165	93.5	85.9	0.5	130.9	−2.3	6.0	−1.9			−6.7	±1.1	89.5

TABLE 4

Fundamental Data

No.	H_b	H_e	Pos. of Max. L.	$H_{max.\ L}$	App. Max Mag. m_p	$\int I\,dt$	$-2.5 \times \log \int I\,dt$	Vis. Mag.	Train	$\dot{v}_e$	p.e.	H_e
166	89.5	80.9	0.6	110.5	−2.6	5.6	−1.9			+0.5	±3.3	85.2
167	98.5	83.1	0.4	143.7	−3.6	33.1	−3.8			+0.5	±0.7	89.5
168					sporadic							
169	91.9	85.1	0.4	91.7	−2.4	3.7	−1.4			−2.8	±0.4	87.8
170	98.6	86.3	0.4	96.0	−4.6	37.4	−3.9			−1.7	±1.0	92.2
171	96.0	84.9	0.3	93.6	−3.3	8.9	−2.4			−1.4	±1.1	91.1
172					too faint to be measured							
173	101.8	97.6	0.3	120.7	−2.4	2.3	−0.9			—		
174					too faint to be measured							
175	101.8	93.7	0.3	178.4	−2.0	7.5	−2.2			−1.7	±0.4	95.6
176	99.6	94.3	0.3	189.7	−1.2	4.2	−1.6			—		
177					too faint to be measured							
178					too faint to be measured							
179	98.8	93.4	0.7	144.1	−1.6	1.6	−0.4			—		
180	99.4	91.7	0.7	171.6	−1.5	1.3	−0.3			−6.4	±1.6	83.9
181	91.8	85.6	0.5	198.4	−0.7	2.0	−0.8			−5.5	±1.4	88.6
182	93.8	80.5	0.7	141.0	−2.2	6.9	−2.1			−1.2	±0.2	87.0
183	107.3	103.1	0.3	178.1	−0.6	1.4	−0.4			—		
184	98.8	92.0	0.5	177.4	−0.3	1.5	−0.4			−0.1	±1.2	95.4
185	99.9	94.4	0.8	250.5	−1.7	6.5	−2.0			—		
186	98.1	91.6	0.7	177.6	+0.1	1.0	0.0			—		
187	91.4	84.7	0.5	168.6	−0.9	1.9	−0.7			—		
188	96.2	85.2	1.0	146.0	−3.7	27.1	−3.6			—		
189	97.2	87.0	1.0	178.3	−3.2	11.6	−2.8			—		
190					too faint to be measured							
191	102.8	100.2	0.0	157.4	−2.4	6.4	−2.0			—		
192	89.5	66.3	0.8	182.8	−4.6	43.0	−4.1			−0.9	±0.2	77.5
193	109.2	90.6	0.5	247.8	−3.3	86.7	−4.8			−0.6	±0.1	99.9
194	101.6	94.8	0.5	236.3	−1.9	13.6	−2.8			—		
195	93.6	86.3	0.2	180.3	−1.5	7.3	−2.2	−1		−3.8	±1.3	89.8
196	93.5	90.8	0.5	146.0	−1.0	1.5	−0.4			—		
197	97.2	83.6	0.5	188.9	−5.4	112.9	−5.1	−1		—		
198	104.7	99.6	0.4	161.1	0.0	1.3	−0.3			−1.2	±4.8	102.1
199	96.3	87.5	0.3	140.1	−2.4	8.1	−2.3	−1		−0.7	±0.3	91.2
200	98.8	92.9	0.3	141.1	−1.9	2.9	−1.2			−3.3	±1.2	95.2
201	97.1	90.3	0.3	143.4	−5.1	41.9	−4.1			−3.5	±1.0	93.6
202	96.1	93.6	0.3	323.1	−2.9	14.1	−3.8	−1		—		
203	89.9	84.1	1.0	135.2	−1.7	3.2	−1.2	0		−1.2	±1.5	87.0
204	100.1	94.5	0.0	235.9	+0.1	2.6	−1.0			−4.4	±4.7	97.3
205	103.5	95.4	0.5	147.9	−2.5	5.7	−1.9			—		
206	87.7	84.1	0.3	137.6	−0.5	0.9	+0.1			—		

THE RESULTS

The most relevant data pertaining to each observed meteor are summarized in Table 4. The following is a brief explanation of the twenty-three columns which form the table.

1. Serial number of meteor.
2. Serial number of film.
3. Computed time of meteor. In a few cases the direction of the meteor trail near the radiant was nearly parallel to the trailing motion of the radiant, so that no reliable time could be computed. In such cases the time of the meteor was arbitrarily assigned on the basis of the meteor's photographic appearance (sharp images near the beginning of the exposure, fuzzy images toward the end). Such "assigned" times appear in parentheses.
4. Visually observed time, whenever the meteor was reliably identified with one on the visual list.
5. Number of segments visible on film.
6. Corrected trail length in degrees. This column gives the value of $L' = n/(n-1)\,L$, where n is the observed number of segments and L is the angular distance between the center of the first and the center of the last segment. In this manner it is assumed that the meteor appeared at the middle of the break preceding the first segment and disappeared at the middle of the break following the last segment.
7. Elongation, or angular distance between the first segment and the radiant.
8, 9. Intercepts $\Delta\xi$ and $\Delta\eta$ of the meteor trail on the ξ and η axes in gnomonic projection, as defined by equation (9). The center of projection is $\alpha = 267°$, $\delta = +56°$; 1947.0.
10. Minimum distance Δ of the projected meteor trail from the instantaneous mean apparent radiant, computed by $\sin \Delta = \lambda_p\lambda_{R_0} + \mu_p\mu_{R_0} + \nu_p\nu_{R_0}$. The subscript p refers to the pole of the trail, as defined by equation (8), and the subscript R_0 to the point whose co-ordinates are given by equation (16).
11. Cos Z_R, where Z_R is the angle between the meteor path and the vertical, i.e., the zenith distance of the apparent radiant.
12. Height of meteor above sea level in kilometers at the time of the first segment.
13. Height of meteor above sea level in kilometers at the time of the last segment.
14. Relative position of maximum light (first segment = 0, last segment = 1).
15. Distance of meteor at maximum light in kilometers.
16. Apparent panchromatic magnitude, m_p, at maximum light.
17. Integrated absolute luminosity $\int I dt$. I is taken to be 1 when the panchromatic absolute magnitude, reduced to a distance of 100 km, is zero. Time in seconds.
18. Integrated absolute magnitude, $-2.5 \log \int I dt$.
19. Visual magnitude, whenever observed.
20. Remarks on persistent train, whenever observed.
21. Acceleration, in kilometers per sec per sec, at center of meteor trail.
22. Probable error of acceleration.
23. Height $H_\bullet$ corresponding to the time $t_\bullet$ for which the acceleration was computed.

FREQUENCY OF METEORS

Table 5 gives the number of Draconid meteors photographed in 10-minute intervals. Where no accurately computed or observed time was available, the time assigned to the meteor was that of the middle of the film exposure. These values have been plotted in Figure 4. It is of interest to note that the final frequency-curve computed from all Canadian visual observations also shows drops in meteor rates just after 0300 and 0330 hours.

COSMIC SPREAD OF THE RADIANT

For the meteors for which the time was observed visually, it was possible to determine the distance Δ of the projected trails from the mean computed radiant. The individual values of Δ are given in Table 4, column 10. For meteor No. 30, Δ was rejected because too uncertain. This meteor trail, only 1° in length, had an elongation of 15° from the radiant and appeared in a film corner, in a region of badly distorted images with few comparison stars around it. For the remaining 26 meteors the average value of Δ is 0°.120 =

7.2. If this is considered as the average deviation of an error spread about a point radiant, then the probable error of this spread is 6.2. The comparable values for other showers, determined by Whipple on Harvard patrol plates, are: Taurids,[5] 17′; Geminids,[6] 13.5; Leonids,[7] 10′. In comparing these data with our value for the Draconids, it should be remembered that the observational errors are much smaller on the large-scale Harvard patrol plates and that errors in the visual time observations, occasionally recorded as amounting to 20 seconds or more, were reflected in the values of Δ for the Draconids, while no such error was present on the guided Harvard plates. It seems quite safe to say

TABLE 5

NUMBER OF METEORS PHOTOGRAPHED IN 10-MINUTE INTERVALS

Time Interval (G.C.T.)	No. of Meteors	Time Interval (G.C.T.)	No. of Meteors	Time Interval (G.C.T.)	No. of Meteors
$1^h 20^m$ to $1^h 29^m.9$	1	$2^h 40^m$ to $2^h 49^m.9$	12	$4^h 00^m$ to $4^h\ 9^m.9$	15
1 30 1 39.9	4	2 50 2 59.9	8	4 10 4 19.9	5
1 40 1 49.9	1	3 00 3 9.9	4	4 20 4 29.9	5
1 50 1 59.9	1	3 10 3 19.9	11	4 30 4 39.9	2
2 00 2 9.9	3	3 20 3 29.9	26	4 40 4 49.9	1
2 10 2 19.9	2	3 30 3 39.9	16	4 50 4 59.9	0
2 20 2 29.9	3	3 40 3 49.9	26	5 00 5 9.9	3
2 30 2 39.9	10	3 50 3 59.9	45	5 10 5 19.9	0

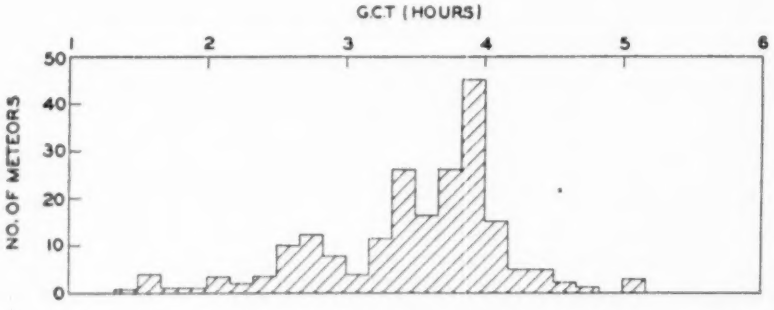

FIG. 4.—Frequency distribution of 204 Draconid meteors photographed at North Bay, Ontario, Canada, on the night of October 9, 1946.

that most of the observed spread of 6.2 for the Draconids was due to observational errors. The true cosmic spread was probably smaller than 2′ or 3′, i.e., much smaller than for the other major showers investigated by Whipple.

HEIGHTS

An anomalous feature of the Draconids is their great heights. On the average, they appeared at a height of 97.7 km and disapneared at 89.9 km, whereas a range from 90 to 70 km is normal for geocentric velocities between 20 and 25 km/sec. The frequency distribution of heights is listed in Table 6 and shown graphically in Figure 5.

The heights of disappearance are more scattered than are the heights of appearance. The average deviation from the mean height is ±4.45 km for the beginning points and

[5] *Proc. Amer. Phil. Soc.*, **83**, 738, 1940. [6] *Ibid.*, **91**, 198, 1947. [7] Unpublished.

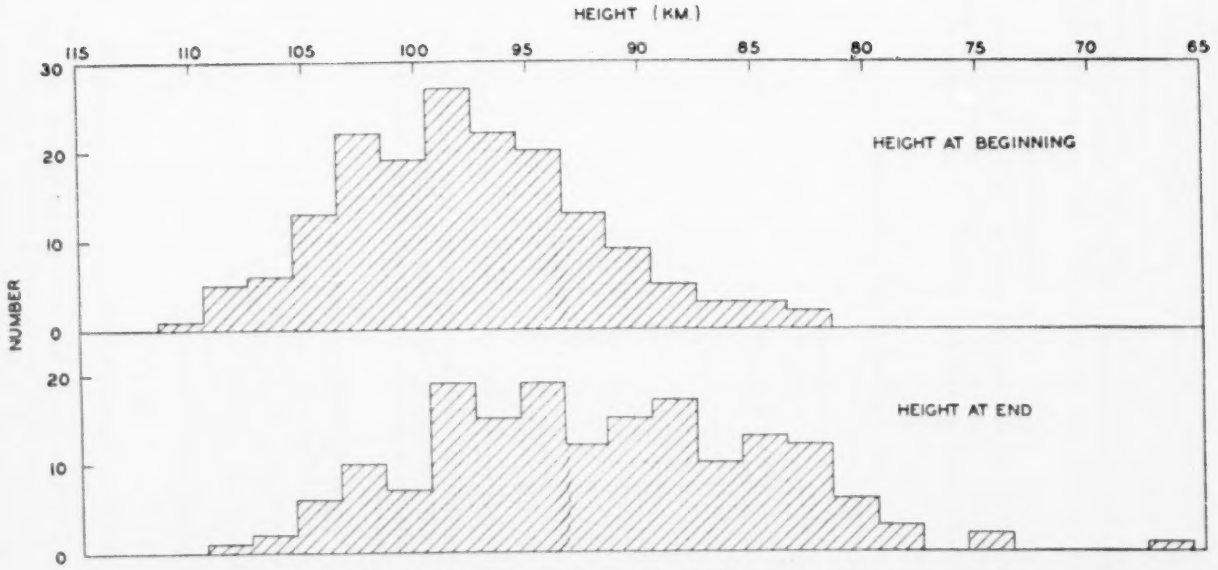

FIG. 5.—Distribution of heights at the beginning (*top*) and end (*bottom*) of observed meteor trails

± 5.31 for the endings. In other words, the meteors appeared at a fairly uniform height but penetrated to various depths in the atmosphere, according to their mass. That this was the case is shown by the correlation between the integrated light $\int I dt$, which—apart from a constant factor—is a measure of the initial mass, and the heights of appearance and disappearance (Table 7 and Fig. 6). As a rule, more massive meteors appeared at greater heights, and disappeared at lower heights, than did lighter meteors. The correlation is more pronounced for the heights of disappearance than for those of appearance. No systematic trend with time can be detected in the computed heights (see Fig. 7).

RELATIVE POSITION OF MAXIMUM LIGHT

The relative position of the brightest point on the trail is expressed by $(M - 1)/(n - 1)$, where M is the order number of the brightest segment and n the total number of segments observed. In computing the mean value of $(M - 1)/(n - 1)$, a number de-

TABLE 6

FREQUENCY DISTRIBUTION OF OBSERVED HEIGHTS

Height (Km)	No. of Meteors		Height (Km)	No. of Meteors	
	Beginning	End		Beginning	End
111–110	1	0	87–86	3	10
109–108	5	1	85–84	3	13
107–106	6	2	83–82	2	12
105–104	13	6	81–80	0	6
103–102	22	10	79–78	0	3
101–100	19	7	77–76	0	0
99– 98	27	19	75–74	0	2
97– 96	22	15	73–72	0	0
95– 94	20	19	71–70	0	0
93– 92	13	12	69–68	0	0
91– 90	9	15	67–66	0	1
89– 88	5	17			

rived from the length of the meteor trail expressed in segments, i.e., $(n - 1)$, was taken as the weight, so that the weighted mean is given by $[\Sigma(M - 1)]/[\Sigma(n - 1)]$. The mean for all meteors turns out to be 0.518, very close to the mid-point of the trail, as expected for low-velocity meteors.

APPARENT AND ABSOLUTE BRIGHTNESS

The frequency distribution of the apparent panchromatic magnitudes m_p at maximum brightness for 177 meteors is given in Table 8. The number of meteors with magnitude 0 and -1 at maximum is shown in parentheses because near the plate limit the count must necessarily be incomplete, owing to the different speeds of the cameras and the spread in angular velocity of the meteors. From -2 to -6 mag., the increase of the number of meteors with the magnitude is very nearly expressed by

$$\log_{10} n = 2.50 + 0.34\, m_p .$$

This corresponds to an increase by a factor of 2.2 per magnitude, not too different from the ratio 2.5 commonly found for meteor showers and also derived from the Canadian visual Draconid observations, soon to be published.

The apparent maximum brightness has only a relative statistical value, since it is affected by distance and by short-lived explosions on the trail. A better index of the dis-

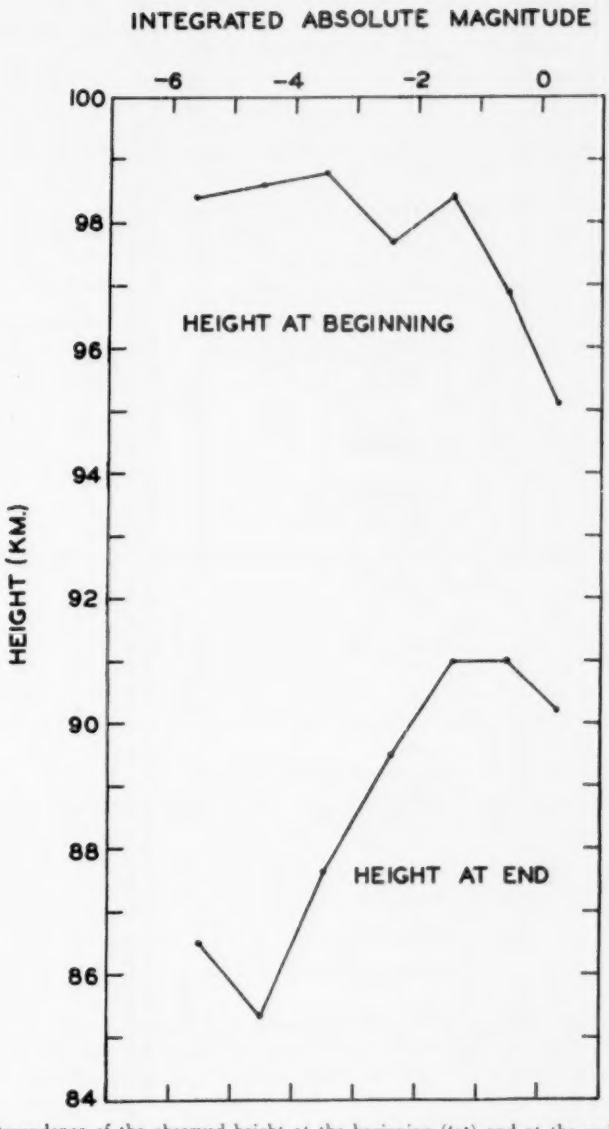

FIG. 6.—Dependence of the observed height at the beginning (*top*) and at the end (*bottom*) of a meteor on its integrated absolute magnitude.

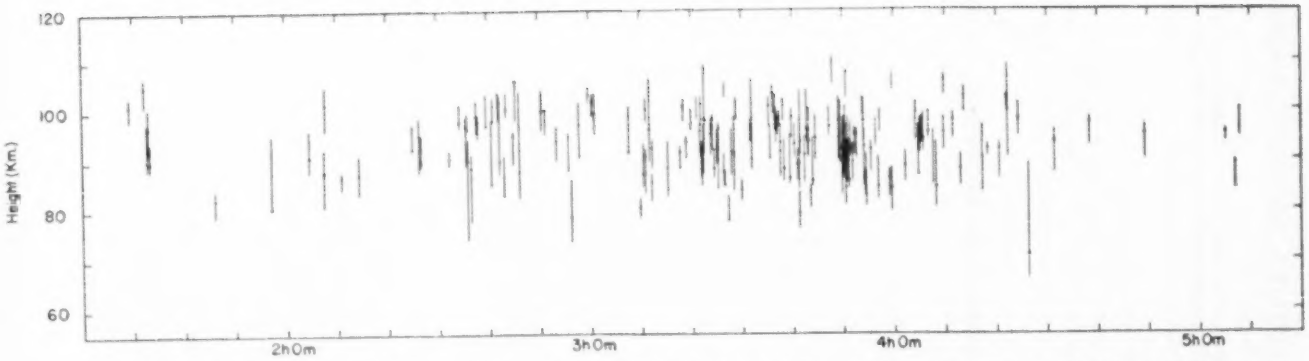

FIG. 7.—Heights of the observed Draconid meteors near the time of maximum frequency of the shower. Upper ends of the vertical lines correspond to the observed heights at the moment when the meteor first became visible; the lower ends correspond to the height at which the meteor disappeared. The heights at which the maximum light was attained are marked by a dot on each line.

tribution in size among the shower meteors is given by the integrated absolute magnitude $M_p = -2.5 \log \int I dt$, as defined earlier (see Table 9).

The increase of the number of meteors with absolute photographic magnitude is best expressed by the equation

$$\log_{10} n = 2.20 + 0.29 M_p ,$$

TABLE 7

INTEGRATED ABSOLUTE MAGNITUDES AND OBSERVED HEIGHTS

INTEGRATED ABSOLUTE MAGNITUDE ($-2.5 \log \int I dt$)			MEAN HEIGHT (KM)		NO. OF METEORS
Intervals		Mean	Beginning	End	
$+1^m.0$ to	$+0^m.1$	+0.3	95.1	90.2	13
0.0	−0.9	−0.5	96.9	91.0	44
−1.0	−1.9	−1.4	98.4	91.0	42
−2.0	−2.9	−2.4	97.7	89.5	45
−3.0	−3.9	−3.5	98.8	87.6	15
−4.0	−4.9	−4.5	98.6	85.3	8
−5.0	−6.0	−5.6	98.4	86.5	4

TABLE 8

DISTRIBUTION OF APPARENT PHOTOGRAPHIC MAGNITUDES AT MAXIMUM BRIGHTNESS

m_p	n	m_p	n	m_p	n
−8	1	−5	5	−2	52
−7	0	−4	16	−1	(46)
−6	4	−3	33	0	(20)

TABLE 9

DISTRIBUTION OF INTEGRATED ABSOLUTE PHOTOGRAPHIC MAGNITUDES

M_p	n	M_p	n	M_p	n
−6	3	−3	21	0	(33)
−5	5	−2	51	+1	(3)
−4	13	−1	42		

which gives a ratio of increase in numbers of 1.95 per magnitude. This number is considerably smaller than has generally been assumed for bright meteors in this magnitude range,[8] and the assumption of a constant value for this ratio is possibly not valid for the bright meteors. Certainly, the value found here could not be extended indefinitely to brighter meteors, as it leads to too great a mass for the Draconid shower.

[8] J. D. Williams, *A.J.*, **48**, 100, 1939; P. M. Millman, *J.R.A.S. Canada*, **29**, 210, 1935.

COMPARISON OF PANCHROMATIC AND VISUAL MAGNITUDES

Both visual and panchromatic magnitudes were available for 27 meteors. On the assumption that the recorded visual magnitude is that of maximum brightness, we obtain a mean value $m_p - m_v = -2^m0$. This value is, in all probability, larger than the true color index, since in several meteors the photographic maximum brightness is that of a short-lived burst, the effect of which was probably smoothed out in the visual observation. When the short bursts are eliminated, the difference between panchromatic and visual magnitudes becomes -1.4 mag. Millman and Hoffleit[9] found an index of -1.8 mag. for meteors recorded on blue-sensitive plates rather than the panchromatic emulsion of the present investigation. It should not be forgotten that, in our case, no correction was made for reciprocity-law failure.

LENGTHS OF THE TRAILS AND DURATIONS

The Draconid meteors were characterized by exceptionally short trails. The individual trail lengths, in degrees, are listed in column 6, Table 4, while column 7 in the same table gives the elongation, or angular distance, of the first segment from the radiant. The logarithmic mean of the ratio length/elongation is 0.09 for the Draconids, as compared with a logarithmic mean of 0.32 for double-station meteors photographed on Harvard AI plates.

This discrepancy is not due, as one might be led to suspect, to a greater abundance of fainter (i.e., shorter) meteors among the Draconids. The 27 brightest meteors give a logarithmic mean ratio of 0.12, while the ratio is less than 0.3 for all the Draconid meteors. Nor can a difference in the limiting magnitudes explain the discrepancy. For the three cameras used to photograph the Draconids, the panchromatic magnitude limit for the meteors was in the vicinity of 0; only for a few meteors quite close to the radiant, covered by the M camera, the limit was nearer to +1 mag. Near the center of the D films the Draconids had an average velocity of 4 mm/sec and a limiting magnitude of +0.2. The focal length of the Harvard AI camera is twice that of the D camera, so a meteor with a comparable angular velocity would move at 8 mm/sec on AI plates. Records show that, for a meteor moving with such a velocity, the limiting photographic (blue) magnitude near the center of an AI plate is approximately +0.6 on an average clear night. We must conclude, therefore, that the visible section of the path was much shorter for the Draconids than for most other meteors.

The same conclusion is reached if we consider the durations of the meteors. Table 10 shows the frequency distribution of the number of photographed segments for all those meteor trails for which panchromatic magnitudes were available. Averages of the mean apparent magnitudes and of the integrated panchromatic absolute magnitudes are given for each number of segments.

The average number of segments photographed per meteor was 6.3. Assuming that the meteor appeared 0.05 second before the center of the first segment and disappeared 0.05 second after the center of the last segment, we obtain a mean duration $\tau = 0^s73$. This is much less than the average duration of low-velocity meteors on Harvard patrol plates, especially if we consider the relatively low height of the apparent radiant above the horizon. Reducing the duration to that of a vertically incident meteor, we obtain $\tau \cos Z_R = 0^s44$, using for $\cos Z_R$ its average value of 0.61. In the Harvard patrol plates, meteors with a geocentric velocity of 23 km/sec give a mean "vertical" duration $\tau \cos Z_R = 1^s25$.

Lengths and durations of the Draconid meteors thus appear to have been shorter by a factor of 3 in comparison with other meteors.

[9] *Harvard Ann.*, 105, 623, 1947.

DECELERATIONS AND RELATED PROBLEMS

For most of the meteors the computed decelerations were smaller than, or comparable in magnitude to, their own probable errors. We accepted as significant only decelerations derived from at least five segments and exceeding their probable errors by a factor of more than 3. The 30 meteors with significant decelerations are listed in Table 11, which gives for each meteor, successively, (1) its serial number; (2) the height H_* in kilometers corresponding to the time, t_*, for which the deceleration was computed; (3) the integrated absolute luminosity $\int_{t_*}^{t_e} I dt$, defined in the same manner as in column 17, Table 4, but with the integration limited to the interval between t_* and the time of disappearance, t_e; (4) the velocity v_* at the time t_*, in kilometers per second; (5) the acceleration, $\dot{v}_*$ at the time t_*, in kilometers per sec per sec; (6) the probable error of the acceleration; (7 the number n of segments from which the acceleration was computed; (8) the weight of the

TABLE 10

FREQUENCY DISTRIBUTION OF OBSERVED DURATIONS

No. of Segments	No. of Meteors	Mean Apparent Mag. (Panchromatic)	Integrated Absolute Mag. (Panchromatic)
3	13	−0.8	−0.7
4	29	−0.8	−1.0
5	30	−1.0	−1.5
6	39	−1.0	−1.3
7	18	−1.3	−2.0
8	15	−1.6	−2.3
9	13	−1.8	−2.8
10	4	−2.3	−3.3
11	3	−2.0	−4.0
12	4	−1.4	−3.1
13	2	−2.0	−3.8
15	1	−2.0	−4.8
19	1	−1.9	−4.1

acceleration, in a scale from 1 to 3 based on the ratio acceleration/p.e. and the number of segments; (9) the logarithm of the air density ρ (in grams per cubic centimeter) at the height H_*, as computed from $\dot{v}_*$, v_*, and $\int_{t_*}^{t_e} I dt$; (10) the residual O − C of log ρ from the N.A.C.A. tentative standard density profile.[10] The atmosphere's density, ρ, was computed from the resistance equation

$$\dot{v} = -K_1 m^{-1/3} \rho v^2, \tag{24}$$

in which the mass m was assumed to be proportional to $\int_{t_*}^{t_e} (I/v^2) dt$. Since the observed range in v during a meteor trajectory is relatively small, we can replace v by v_* and write

$$\rho = -K \frac{\dot{v}_*}{v_*^3} \left[\int_{t_*}^{t_e} I dt \right]^{1/3} \tag{25}$$

[10] National Advisory Committee for Aeronautics, *Technical Note* No. 1200, 1947.

The scatter in the computed values of air density is too large (p.e. in log $\rho = \pm 0.24$, using the N.A.C.A. profile as a comparison standard) and the range in the observed heights is too small to attempt an analysis of density variation in the upper atmosphere on the basis of the data above.

For ordinary meteors and photographic magnitudes it was found[11] previously that the value log $K = 6.28$ gave computed values of ρ in statistical agreement with the N.A.C.A. density profile. For the Draconids, with panchromatic magnitudes, we find

TABLE 11

DECELERATIONS AND ATMOSPHERIC DENSITIES

No.	H_0	$\int_{t_0}^{t_e} I dt$	v_0	$\dot{v}_0$	p.e.	n	Wt.	log ρ (log K = 5.41)	O−C (From N.A.C.A.)
7	88.0	4.0	22.8	− 1.0	±0.2	9	1	−8.46	−0.67
11	87.0	0.36	21.1	− 5.8	1.9	6	1	−7.95	−0.23
17	87.0	2.9	22.1	− 2.6	0.8	6	1	−8.05	−0.33
40	79.9	3.3	22.2	− 2.3	0.5	9	1	−8.09	−0.82
43	93.1	2.6	21.5	− 4.4	1.2	6	1	−7.81	+0.28
49	88.9	21	21.8	− 3.5	0.7	7	2	−7.62	+0.22
51	84.5	0.35	20.2	− 8.9	0.6	5	1	−7.71	−0.15
53	88.1	14	21.2	− 5.3	0.5	9	2	−7.46	+0.33
54	97.9	12	22.5	− 1.4	0.2	12	3	−8.15	+0.21
56	88.2	4.8	20.6	− 7.1	2.2	6	1	−7.46	+0.34
63	96.1	25	22.7	− 0.8	0.2	8	2	−8.30	−0.04
65	91.4	1.7	21.3	− 4.6	0.6	7	2	−7.83	+0.16
97	89.0	0.55	19.7	− 7.8	0.8	6	2	−7.67	+0.18
104	90.8	3.6	21.8	− 3.1	0.7	7	1	−7.92	−0.03
106	90.7	2.9	21.8	− 3.1	0.5	8	2	−7.97	−0.02
122	85.9	49	21.9	− 2.7	0.6	9	2	−7.61	+0.04
127	93.6	1.6	21.2	− 4.6	0.4	6	1	−7.84	+0.28
136	89.4	3.4	22.7	− 0.8	0.2	12	1	−8.58	−0.71
141	89.5	2.9	21.5	− 3.8	1.2	5	1	−7.86	+0.02
146	90.7	0.59	20.8	− 6.0	0.8	6	1	−7.84	+0.11
155	85.4	1.1	19.0	−13.9	2.2	5	1	−7.26	+0.36
160	92.1	12.5	22.8	+ 6.0	1.3	8			
163	86.9	5.0	20.8	− 6.1	1.7	8	1	−7.52	+0.19
165	89.5	2.9	20.6	− 6.7	1.1	7	2	−7.55	+0.33
169	87.8	1.9	21.9	− 2.8	0.4	5	1	−8.08	−0.31
175	95.6	3.2	22.5	− 1.7	0.4	7	1	−8.26	−0.02
180	83.9	0.89	20.1	− 8.4	1.6	6	2	−7.59	−0.07
181	88.6	1.1	20.9	− 5.5	1.4	6	1	−7.80	+0.02
182	87.0	5.3	22.5	− 1.2	0.2	11	2	−8.33	−0.61
192	77.5	31	22.6	− 0.9	0.2	6	1	−8.20	−1.06
193	99.9	52	22.8	− 0.6	0.1	13	2	−8.31	+0.16
201	93.6	11	21.4	− 3.5	±1.0	7	1	−7.70	+0.42

that agreement with the N.A.C.A. profile is reached by using log $K = 5.41$. The difference between the two values of log K is 0.87, a truly extraordinary discrepancy in view of the fact that a difference of 1 mag. in the luminosity scale accounts for a difference of only 0.13 in log K.

It seems unreasonable to assume a correction of more than +1.5 mag. to reduce the panchromatic meteor magnitudes to photographic magnitudes; and that would still leave us with a discrepancy of 0.67 in log K or, in other words, with a difference of 5 mag.

[11] L. Jacchia, "Ballistics of the Upper Atmosphere," *H.C.O. and M.I.T. Technical Report*, No. 2, 1948 ("Harvard Reprints," Ser. II, No. 26).

in the luminosity scale. It appears, therefore, that *the Draconid meteors emitted at least one hundred times more luminous energy per unit mass than ordinary meteors do.*

If we consider this result along with the exceptionally short trajectories and abnormally great heights shown in previous sections, we come to the conclusion that *the Draconid meteors of October 10, 1946, were composed of "softer" material, more easily melted or vaporized than that of ordinary meteors.* An explanation of such a difference might be found, perhaps, in the age of the shower. Since no Draconid meteors are observed except in the immediate vicinity of the parent-comet, the shower appears to be of relatively recent origin. There is a possibility that "softer" material is present in great quantity in freshly disintegrated meteoric clusters of the cometary type but that most of this material is eliminated by sublimation or other processes as time goes on, leaving eventually to survive only ordinary stone meteoroids of the "harder" variety.

In conclusion, we should like to express our sincere thanks to Air Marshal W. A. Curtis, C.B., C.B.E., D.S.C., E.D., and to Group Captain D. A. R. Bradshaw, D.F.C., at Air Force Headquarters in Ottawa; to Air Commodore L. W. Wray, O.B.E., A.F.C., of the Air Transport Command, Rockcliffe; to the aircraft crew Squadron Leader W. O. Reeves, Flight Lieutenant T. A. R. Harris, and Flying Officer J. Thompson, D.F.C.; and to all others in the Royal Canadian Air Force who, by their prompt co-operation, made this research possible. We should also like to thank Mr. Lorne Hicks and his staff at the control tower of the North Bay Airport who, at very short notice, offered every assistance to make the observational program a success. Dr. D. A. MacLulich very kindly loaned us camera D for these observations.

The measurements and reductions involved in this study were performed at the Center of Analysis of the Massachusetts Institute of Technology under Contracts Nos. 8555 and 9169 with the Bureau of Ordnance of the U.S. Navy Department, as a part of a broad program of investigation of the physical properties of the upper atmosphere by means of meteor phenomena. The sincere thanks of the authors are due to Mrs. Mary H. Baker, Miss Virginia K. Brenton, Miss Jeannie R. B. Carmichael, Miss Nancy K. Rodier, and Mrs. Martha B. Shapley for the part that they took in the measurements of the photographic plates; and to Mr. Robert E. Briggs, Mr. Gilbert F. Davoren, Mrs. Beatrice R. Miller, Mrs. Laurelle B. Parrotta, and Miss Louise Richardson, who performed most of the tedious computational work involved in the reductions. Last, but not least, it is a pleasure to express our appreciation to Dr. Harlow Shapley, director of the Harvard College Observatory, for putting at our disposal all facilities needed for the successful completion of the work, and to Dr. Fred L. Whipple for stimulating discussions.

THE POYNTING-ROBERTSON EFFECT ON METEOR ORBITS

STANLEY P. WYATT, JR., AND FRED L. WHIPPLE
Harvard College Observatory
Received June 30, 1949

ABSTRACT

The Poynting-Robertson effect will operate to sweep small particles of the solar system into the sun at a cosmically rapid rate. Robertson derived an expression for the times of fall from initially circular orbits. Since, if other parameters are equal, the times are much less for orbits of high eccentricity, tables are given here to enable simple calculation of the times of fall in terms of the initial orbital elements, q and e, and particle radius and density. Total times of collapse are computed for several meteor showers.

Since there is a linear dependence of the time on particle radius, the material in showers should ultimately be dispersed so that larger particles move with greater orbital a and e than do the smaller ones. This leads to the possibility of observing the Poynting-Robertson effect in a given swarm by a correlation of the observed mean magnitude of meteors with the time while the earth transits the shower. Such a correlation is not detected for any shower definitively; an upper limit, therefore, is set for the age of showers, ranging from five million years for some to less than one hundred thousand years for the Geminids.

If some sporadic meteors had a common origin with the meteorites and asteroids, the operation of the Poynting-Robertson force requires that, for times of origin longer ago than the sixty million years suggested by Bauer, all material of radius less than 0.08 cm has been swept into the sun. Therefore, virtually no sporadic meteors fainter than the fifth magnitude can be arriving now on the earth unless they are cometary or interstellar in origin. For a time of three billion years the minimum radius is about 4 cm.

The tables given for computation of the times of orbital contraction are valid for any radiating body of known mass and radiation by means of a simple correction. The process of contraction is faster by a factor of about 100,000 for B stars than for the sun. But, conversely, the Poynting-Robertson effect due to the general radiation of a galaxy is entirely too small to affect appreciably the dynamics of interstellar dust.

In the early part of this century, J. H. Poynting[1] considered the effects of the absorption and subsequent re-emission of sunlight by small isolated particles in the solar system. His work was later modified by H. P. Robertson,[2] who used a precise relativistic treatment to establish, once and for all, the equations of motion for such particles to terms of the first order in the ratio of the velocity of the particle to that of light. While the process of absorption and re-emission produces no net force on a particle when one chooses to work with a stationary frame referred to the particle, it is found when the solar reference frame is used that there is introduced a resisting force on the particle which is proportional to its velocity. The retarding force exhibited in the equations of motion results in a slow secular decrease in semi-major axis and eccentricity of the orbit of any small body. Ultimately the body will fall into the sun.

Inasmuch as small meteoric material must be strongly affected by the Poynting-Robertson effect, it is of interest to find a method of calculating the time necessary, under given initial conditions, for such matter to be drawn into the sun. Robertson solved the problem for initially circular orbits. Since, however, for a given semi-major axis the time of fall is substantially less for highly eccentric orbits than for circular ones, we propose to develop here a method of computing the time numerically for the general case.

The assumptions in the development are as follows: (1) that the particles are spherical, with radius s, and of uniform density, ρ; (2) that they are somewhat larger than the critical limit where radiation pressure balances gravitational attraction ($s\rho > 5.72 \times 10^{-5}$ gm/cm^2) and large enough compared with the wave length of light so that diffraction effects are not appreciable; and (3) that the particles absorb all incident radiation from the sun over a cross-section πs^2 and re-emit this radiation isotropically at the same rate.

[1] *Phil. Trans. R. Soc. London, A*, **202**, 525, 1903.
[2] *M.N.*, **97**, 423, 1937.

The radial and perpendicular components of the equations of motion as found by Robertson are

$$\ddot{r} - r\dot{\theta}^2 = -\frac{\mu}{r^2} - \frac{2a\dot{r}}{r^2}, \tag{1}$$

and

$$\frac{1}{r}\frac{d}{dt}(r^2\dot{\theta}) = -\frac{a\dot{\theta}}{r^2}, \tag{2}$$

where $\mu = GM - ac$, the usual solar gravitational constant decreased by the outward-directed radiation pressure, and where

$$a = \frac{3E_\odot}{16\pi c^2 s\rho} = \frac{3.55 \times 10^{-8}}{s\rho}\ (\text{a.u.})^2/\text{year}.$$

We here denote by $E_\odot$ the total energy emitted by the sun per second, for which we have used the value 3.79×10^{33} erg/sec,[3] and by s and ρ the radius and density of the particle in question, expressed in c.g.s. units. It may be noticed at once that equation (2) integrates to

$$H = r^2\dot{\theta} = h - a\theta, \tag{3}$$

where H is the instantaneous value of the angular momentum and h is the initial value.

The secular perturbations for an osculating ellipse of semi-major axis a and eccentricity e have been calculated by Robertson and confirmed by us. For these two elements they are given by

$$\frac{da}{dt} = -\frac{a(2+3e^2)}{a(1-e^2)^{3/2}}, \tag{4}$$

$$\frac{de}{dt} = -\frac{5ae}{2a^2(1-e^2)^{1/2}}. \tag{5}$$

The only other secular change is the advance of perihelion, which is found by Robertson in the relativistic treatment to be

$$\frac{d\pi}{dt} = \frac{3G^{1/2}M^{1/2}\mu}{c^2a^{5/2}(1-e^2)}. \tag{6}$$

We now seek to find the long-term changes in these elements. It may first be noticed that the expression for perihelion advance is a maximum for large and dense bodies, where $\mu \cong GM$. For the cases in which we are interested, the rate of change is insignificant, amounting, for example, to 43″ per century for Mercury and less than this for small bodies of greater a and smaller e.

Of more interest are the changes in semi-major axis and eccentricity. If we deal with initially circular orbits, equation (4) is simplified and integrates to

$$t = \frac{a^2}{4a} = 7.0 \times 10^6 s\rho a^2 \text{ years}, \tag{7}$$

where t is the total time of fall for a particle of radius s cm, density ρ gm/cm³, at an initial distance of a astronomical units. This formula is due to Robertson. For the more general case of eccentric orbits we can at least find a readily integrable relation between a and e from division of equation (4) by equation (5). The result, after integration, is

$$a = \frac{Ce^{4/5}}{1-e^2}. \tag{8}$$

[3] Russell, Dugan, and Stewart, *Astronomy* (Boston: Ginn & Co., 1938), p. 534.

This relation is in contrast to the four-thirds power law found by Fessenkoff[4] for the nonrelativistic solution. The constant in equation (8) will hold at all times for any given particle, and, if we know a_0 and e_0 at any arbitrary time, it can be computed, once and for all, by solving for C:

$$C = a_0 e_0^{-4/5}(1 - e_0^2) . \tag{9}$$

From the earlier equations it is not possible to find a relation $a = a(t)$ that is independent of e. However, by substituting equation (8) in equation (5), one finds a relation involving only the eccentricity and time,

$$\frac{de}{dt} = -\frac{5a(1 - e^2)^{3/2}}{2C^2 e^{3/5}} .$$

Or

$$(t - t_0)_{\text{years}} = -\frac{2C^2}{5a}\int_{e_0}^{e} \frac{e^{3/5} de}{(1 - e^2)^{3/2}} = 1.13 \times 10^7 s\rho C^2 \int_{e}^{e_0} \frac{e^{3/5} de}{(1 - e^2)^{3/2}}, \quad e_0 > e , \tag{10}$$

where s and ρ are in c.g.s. units. The constant C^2 has the dimensions (A.U.)^2 and is evaluated from equation (9) by using the constants of the orbit. Then $(t - t_0)$ is given directly

TABLE 1

THE TIME INTEGRALS

e	$G(e_0)$	$(t-t_0)/10^7\, s\rho C^2$ years	e	$G(e_0)$	$(t-t_0)/10^7\, s\rho C^2$ years
0.00		0.704	0.78	0.771	4.10
.05	0.0052	0.778	.80	0.846	4.42
.10	.0158	0.858	.81	0.889	4.60
.15	.0305	0.946	.82	0.934	4.79
.20	.0489	1.04	.83	0.983	5.00
.25	.0710	1.15	.84	1.04	5.23
.30	.0969	1.27	.85	1.10	5.49
.35	.127	1.40	.86	1.16	5.77
.40	.162	1.55	.87	1.23	6.08
.45	.202	1.72	.88	1.32	6.43
.50	.249	1.92	.89	1.41	6.83
.55	.305	2.15	.90	1.51	7.29
.60	.370	2.42	.91	1.63	7.82
.62	.400	2.54	.92	1.78	8.45
.64	.432	2.68	.93	1.96	9.22
.66	.468	2.82	.94	2.17	10.17
.68	.506	2.98	.95	2.45	11.39
.70	.548	3.16	.96	2.82	13.06
.72	.595	3.36	.97	3.37	15.50
.74	.647	3.57	.98	4.30	19.60
0.76	0.705	3.82	0.99	6.37	28.89

in years. Although the integral cannot be found directly, the integrand is independent of the particle under consideration, and numerical integrations can be performed that will hold for all cases. We have tabulated in the second and fifth columns of Table 1 the function

$$G(e_0) = \int_0^{e_0} \frac{e^{3/5} de}{(1 - e^2)^{3/2}} \tag{11}$$

for interesting values of the eccentricity. Now, upon substitution of arbitrary particle radius, density, C^2, and the quantity tabulated in Table 1 for some initial eccentricity,

[4] *A. J. Soviet Union*, **23**, 366, 1946.

we can find the total time for the particle in question to spiral into the sun. For the time between any two nonzero eccentricities, one, of course, uses the difference between the corresponding tabular values.

For total times of fall to the sun from any initial eccentricity in terms of particle radius, density, and perihelion distance, the calculation can be made far simpler, although less general, by a reduction of equation (10). From equation (8), since

$$q = a\,(1 - e)\,,$$

we find

$$C^2 = q^2\,(1 + e)^2\,e^{-5/3}. \tag{12}$$

And thus, for total time of fall to the sun,

$$(t - t_0)_{\text{ years}} = 10^7\,s\,\rho\,q^2\left[\frac{1.13\,(1 + e_0)^2}{e_0^{5/3}}\int_0^{e_0}\frac{e^{3/3}\,d\,e}{(1 - e^2)^{3/2}}\right]. \tag{13}$$

We give in Table 1, third and sixth columns, the bracketed quantity in equation (13). For numerical results it is now required only to substitute for s and ρ in c.g.s. units and q in astronomical units. The latter quantity is directly available in most cometary and meteoric catalogues. It should be noted, however, that these results hold only for total time of spiraling into the sun and that the second and fifth columns of Table 1 should be used for the times between two arbitrary eccentricities.

Using the general relations for $a = a(e)$ and $q = q(e)$ in equations (8) and (12) in combination with that for $e = e(t)$, it is a straightforward matter graphically to relate semi-major axis or perihelion distance directly to the time. A calculation of $a(t)$ for various known meteor orbits shows a reasonably linear decrease of semi-major axis with the time to a given point, which depends on the value of C for the orbit in question, but averages about 1 A.U. Then the decrease in a is accelerated, and finally the particle falls into the sun in very short order. A plot of $q(t)$ shows a very slow decrease over most of the time but finally, also, a fast drop into the sun. The curves in Figure 1 show the nature of these relations for the Giacobinid and Leonid meteor showers.

The application of these results to small particles is interesting. As has been pointed out, the operation of the Poynting-Robertson drag should have been effective in sweeping out rather large volumes of the solar system in astronomically short times. For example, in the slowest case, that of bodies in circular orbits, we find that all particles of density 4 gm/cm^3, radius $\leq$ 1 cm, and initially within a sphere of radius of 1 A.U. centered on the sun, will fall into the sun in a period of 2.8×10^7 years.

We have selected several of the known meteor showers, and, using Yamamoto's[5] elements for the parent-comets (except for the parentless Geminid shower, where we have used Whipple's[6] elements for a photographed meteor), we have calculated the total time for these shower particles to fall into the sun. The results are shown in Table 2. The first four columns are self-explanatory; the fifth gives the constant C appearing in equation (8); the sixth gives the times of fall as computed from Table 1 in terms of particle radius and density; and the seventh gives, by way of comparison, the times as calculated from equation (7), assuming circular orbits. For example, a particle of radius 0.05 cm, corresponding to about a fifth-magnitude meteor, and of density 4 gm/cm^3 moving in the orbit of Halley's Comet would be drawn into the sun in about ten million years. It can be seen from the sixth column of Table 2 that the lifetimes of faint visual meteoric bodies in the well-known showers are relatively short astronomically.

We inquire now as to the possibility of observing the Poynting-Robertson effect during a meteor shower. From equation (10) it is evident that the times involved depend

[5] *Pub. Kwasan Obs.*, Vol. 1, No. 4, 1936.

[6] *Proc. Amer. Phil. Soc.*, Vol. 91, No. 2, 1947.

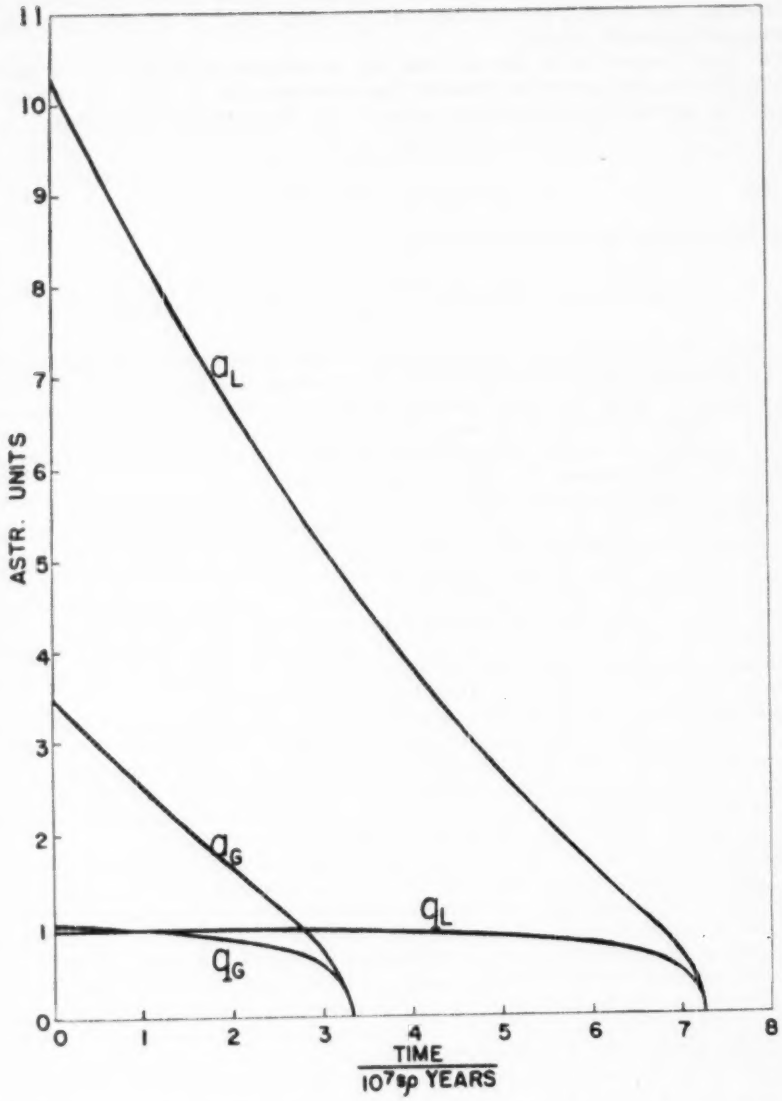

FIG. 1.—Semi-major axis and perihelion distance as functions of the time for two showers. Subscripts *L* refer to the Leonids and *G* to the Giacobinids. Times are reckoned from the present epoch.

linearly on the particle size and density. Let us make the simplifying assumptions, first, that the density of every meteoric particle is 4 gm/cm³ and, second, that a meteor shower originates as a uniformly dense swarm occupying an elliptical orbit with small circular cross-section in the plane normal to the velocity vector of the particles. If there is dispersion in the individual meteor radii, the smaller ones will be drawn toward the sun far faster than will their larger neighbors. At some time later, the cross-section of the swarm will be elongated in the radial direction relative to the sun, with the smaller particles orbiting closer to the sun. The conditions for observing this effect on earth are that the inclination of the shower shall be moderately low or retrograde and that enough time shall have elapsed since the formation of the shower for the various-sized particles to have been separated sufficiently for detection.

As an approximation to the orders of time involved in separating bright and faint particles for observation, we take all the above-listed showers with $i < 40°$ and assume

TABLE 2

TIMES OF FALL FOR SHOWER PARTICLES

Shower	Parent-Comet	a	e	C	$(t-t_0)/10^7 s\rho$ years	$(t-t_0)_{min}/10^7 s\rho$ years
Geminids	.....	1.396	0.900	0.289	0.143	1.4
Taurids	Encke	2.210	.8498	0.6995	0.605	3.4
Bielids	1852 III	3.5259	.75592	1.8902	2.79	8.7
Giacobinids	1933 III	3.520	.7160	2.241	3.32	8.7
Orionids?	Halley	17.96	.9673	1.186	5.10	230
Leonids	1866 I	10.325	.90542	2.0145	7.24	75
Perseids	1862 III	24.277	.96035	1.9491	12.2	410
Lyrids	1861 I	55.665	0.98346	1.8508	18.6	2200

TABLE 3

TIMES OF SEPARATION

Shower	Years	Shower	Years
Geminids	7×10^4	Bielids	2×10^6
Taurids	5×10^5	Leonids	3×10^6
Giacobinids	1×10^6	Orionids?	5×10^6

that all $i = 0°$, that the earth's orbit is circular, and that the perihelion advance of the shower is of no consequence. We now inquire how long it will take to separate fifth-magnitude meteors from those of magnitude -2, so that the earth will pass from one limit to the other in a period of 5 days. It should then be possible to observe a gradually changing mean magnitude over the period. The radii of such meteors are calculated separately for each shower. We take, as before, a density of 4 gm/cm³. We then apply to Watson's[7] values of mass, which were computed for meteors with velocity of 55 km/sec, a correction for the actual observed shower velocities listed by him.[8] This correction factor is calculated on the assumption that the kinetic energy of a meteor is proportional to its luminosity. The steps in the geometrical approximation applied are to solve for the present true anomaly of the intersection of earth and shower, to increase this by 5°, to find by equation (8) the new a and e satisfying the new true anomaly, and to integrate between the old and new eccentricities to determine the time. The results indicate the correct order of magnitude for the times of separation and are given in Table 3. Definitive correlations

[7] *Between the Planets* (Philadelphia: Blakiston Co., 1941), p. 115.

[8] *Ibid.*, p. 123.

of magnitude and time apparently are not found in observations of meteor showers. A shower may be of very recent origin so that the particles have not had time to become separated radially. Such may be the case with the Giacobinids. Among the older showers, where the magnitude effect should appear, those with orbits of low inclination and therefore favorable for observation of the effect are also most seriously affected by planetary perturbations. Since these perturbations are nonselective with respect to particle size but may be capable of dispersing the showers, the times given in Table 3 must be considered only as upper limits to the possible ages of the showers. It may be possible in the near future, by combining extensive data from visual, photographic, and electronic observations of meteor showers, to detect a systematic effect of the sort that we have outlined above.

Although meteor showers have in nearly all cases been identified with comets, the origin of sporadic meteors is not so clear. It is possible that some sporadic meteors have a common origin with the meteorites, which Harrison Brown and Claire Patterson[9] have shown to be planetary debris. It seems justified to make the unproved assumption that meteorites and asteroids are associated generically. Since the mean semi-major axis for the known asteroids is about 3 A.U., we may assume, in addition, that the parent-planet (or planets) of the meteorites disintegrated at about this distance from the sun. Particles

TABLE 4

TIMES OF FALL FOR ASTEROIDAL PARTICLES

q	q'	a	e	C	t
5	5	5	0.00	.....	70×10^7 s
3	3	3	.00	.....	25
3	5	4	.25	11.4	11
1	3	2	.50	2.60	1.9
1	5	3	0.67	2.31	2.9×10^7 s

thrown past the orbit of Jupiter, if not lost immediately to the solar system, would generally move in orbits with an apse near Jupiter's orbit. Hence most potential meteors from such a disrupted planet would have orbits lying entirely within that of Jupiter. The total times of fall to the sun for particles of density 4 gm/cm^3 in a few such orbits are given in Table 4. The column headings are, successively, perihelion distance, aphelion distance, semi-major axis (all in astronomical units), eccentricity, C as calculated from equation (9), and the time in years in terms of particle radius.

Let us consider, first, what sorts of particle will have been eliminated within the duration of the short cosmic time scale. The slowest bodies are those in a circular orbit at 5 A.U., and from Table 4 it is clear that all bodies of radius less than about 4 cm must have been swept into the sun within this time. Thus, for an assumed explosion 3×10^9 years ago, all meteoric bodies arriving on the earth from the asteroid belt must be very bright. However, if we assume a planetary breakup sixty million years ago, as suggested by Bauer,[10] it appears that all particles originating with the asteroids and of radius less than 0.08 cm must have been lost into the sun. It is probable, therefore, that the supply of sporadic material giving meteors fainter than about the fifth magnitude must be cometary or interstellar in origin, except possibly for a few stragglers from asteroidal collisions.

In considering the Poynting-Robertson effect in regions external to the solar system, the time for a body in a given orbit will be equal to that for the same body in the same orbit around the sun multiplied by the factor $E_\odot/E$, the ratio of the total energy per sec-

[9] *J. Geol.*, **56**, 85, 1948.

[10] *Phys. Rev.*, **74**, 501, 1948.

ond emitted by the sun to that emitted by the parent-star. In order to utilize the results given above, we must, of course, continue to express a and q in astronomical units. Near the large and hot B stars the times will be shorter than those near the sun by a factor of about 100,000, whereas for particles near M dwarfs the times will run approximately one hundred times as long.

The nucleus of the galaxy gives a negligibly small effect on the orbits of interstellar particles. What effect there is depends markedly on the co-ordinates of the particle concerned, since the net radiative flux vector due to the Milky Way will vary in magnitude and direction at each point of space because of the irregular distribution of bright clusters and overlying dark clouds. However, even for an idealized unobscured galaxy of absolute magnitude -15 and radius 1000 parsecs, where $E_\odot/E$ may be taken as about 10^{-8}, it is found that the time to spiral into the nucleus for a body of $s\rho \leqq 4$ is 10^{16} years for an initially circular orbit. And, although for highly eccentric orbits the times may be less by a factor of, say, 100, it is clear that the Poynting-Robertson effect has been of very little significance galactically. Its importance is restricted to small particles orbiting in the vicinity of individual stars.

ON THE INTEGRAL EQUATION GOVERNING THE DISTRIBUTION OF THE TRUE AND THE APPARENT ROTATIONAL VELOCITIES OF STARS

S. CHANDRASEKHAR AND G. MÜNCH
Yerkes Observatory
Received October 31, 1949

ABSTRACT

In this paper the integral equation governing the distribution of the true (v) and the apparent ($v \sin i$) rotational velocities of stars is reconsidered, with the object of suggesting the most suitable methods for analyzing observed frequency functions affected by a random orientation factor, $\sin i$, in the manner of the rotational velocities of stars. First, it is shown that there is a simple relation between the moments of the true and the observed frequency functions which enables us to pass from the moments of the one to the moments of the other. The mean and the mean square of the true rotational velocities of stars can therefore be determined directly from the corresponding means of the observed distribution of $v \sin i$. When it is felt that something more should be said about the true distribution of v than its mean and mean square, it is suggested that a comparison be made between the observed distribution and those derived from certain assumed forms of the true frequency function. Reasons are given for preferring this method to an inversion of the integral equation by a numerical procedure. The form

$$f(x) = \frac{1}{\sqrt{\pi}} \{ e^{-(x-x_1)^2} + e^{-(x+x_1)^2} \}$$

suggested by Elsa van Dien has therefore been considered in some detail, and a one-parameter family of frequency functions for $x \sin i$ has been derived.

The methods of analysis suggested in this paper have been applied to a rediscussion of the rotational velocities of stars.

1. *Introduction.*—A problem of some interest which arises in discussions relating to stellar rotation concerns the manner in which allowance must be made for the random orientation of the rotational axes of the stars in deriving the true distribution of the rotational velocities.[1] The precise nature of the problem encountered here is the following:

From a study of the line profiles of a rotating star we may deduce the value of $v \sin i$, where v denotes the equatorial rotational velocity of the star and i is the inclination of its axis of rotation to the line of sight. From the distribution of $v \sin i$ determined in this fashion for a homogeneous[2] group of stars, we wish to infer the true distribution of the rotational velocities v. It is apparent that an integral equation must govern the two distributions, and the problem is essentially one of solving this integral equation.

The same integral equation as that which governs the distribution of v and $v \sin i$ occurs also in other contexts: for example, in the discussion of the mass function of binary stars.[3] Again, the integral equation which governs the distribution of star images on a photograph of a globular cluster and the true space distribution of the stars in the cluster is also the same.[4] This paper is therefore devoted to an examination of this integral equation and to outlining suitable methods of analysis of observational data affected by random orientation in the manner of the rotational velocities of stars.

[1] Cf. O. Struve, *Pop. Astr.*, **53**, 202, 259, 1945; see esp. pp. 213 and 214.

[2] "Homogeneous" in the sense that selection has not operated for certain preferred orientations of the axis of rotation.

[3] Cf. G. P. Kuiper, *Pub. A.S.P.*, **47**, 15, 1935; see esp. pp. 32–36 and Fig. 2 on p. 32.

[4] Cf. S. Chandrasekhar, *Principles of Stellar Dynamics* (Chicago: University of Chicago Press, 1942), p. 233. Eq. (5.814) given on p. 233 becomes identical with the integral eq. (9) derived in § 2 of this paper, if eq. (5.814) is expressed in terms of the number of star images $2\pi v(x)x\,dx$ in a ring between x and $x + dx$ and the number of stars $4\pi r^2 N(r)\,dr$ in the cluster, in a spherical shell between r and $r + dr$, instead of $v(x)$ and $N(r)$.

2. *The basic integral equation.*—The problem which we wish to consider may be formulated in the following manner:

A parameter x occurs with a probability distribution governed by a frequency function $f(x)$ $(0 \leqslant x < \infty)$. The quantity

$$y = x \sin i \tag{1}$$

is observed where the probability of occurrence of the inclination i between i and $i + di$ is known to be $\sin i \, di$. It is required to relate the probability distribution of y with that of x.

Let $\phi(y)$ denote the frequency function of y. Then, from the definition of probability, it follows that $\phi(y)dy$ is the surface integral of $f(x) \sin i$ over the area included between the curves

$$y = x \sin i \qquad \text{and} \qquad y + dy = x \sin i \,, \tag{2}$$

in the (x, i)-plane (see Fig. 1). Thus

$$\phi(y)\, dy = \iint_{\Delta S} f(x) \sin i \, dx di \,, \tag{3}$$

where ΔS denotes the area shaded in Figure 1.

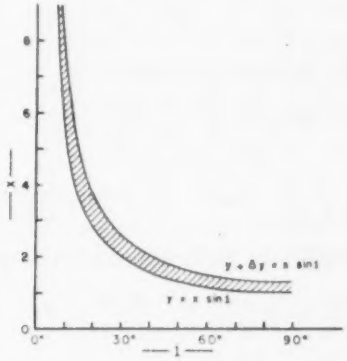

FIG. 1.—Illustrating the area in the (x, i) plane over which $f(x) \sin i$ must be integrated to give $\phi(y)dy$.

Now at a particular i, the height of the strip ΔS is given by

$$dx = \frac{dy}{\sin i} \,; \tag{4}$$

and, since y and dy are assigned, we can rewrite equation (3) in the form

$$\phi(y)\, dy = dy \int_{y = x \sin i} f(x)\, di \,, \tag{5}$$

where the integral is now extended along the curve $y = x \sin i$. Accordingly,

$$\phi(y) = \int_0^{\pi/2} f\left(\frac{y}{\sin i}\right) di \,. \tag{6}$$

Alternatively, we may also argue as follows:

At a particular x the width of the strip ΔS is

$$di = \frac{dy}{x \cos i}; \tag{7}$$

hence, we may also write

$$\phi(y)\, dy = dy \int_{y=x \sin i} f(x) \frac{\sin i}{x \cos i}\, dx, \tag{8}$$

where the integral is again extended along the curve $y = x \sin i$; using this equation of the curve to eliminate i in the integrand of equation (8), we obtain

$$\phi(y) = y \int_y^\infty \frac{f(x)}{x\,(x^2 - y^2)^{1/2}}\, dx. \tag{9}$$

This equation relating $\phi(y)$ and $f(x)$ is implicit in the papers of Struve on stellar rotation; and the equation occurs explicitly in Kuiper's paper to which we have already referred.[3]

It is, of course, clear that equations (6) and (9) are entirely equivalent.

3. *The formal solution of the integral equation.*—Equation (9) can be reduced to Abel's integral equation by the substitutions

$$y^2 = \frac{1}{\eta} \quad \text{and} \quad x^2 = \frac{1}{\xi}; \tag{10}$$

for, with these substitutions, equation (9) becomes

$$\Phi(\eta) = \int_0^\eta \frac{F(\xi)}{(\eta - \xi)^{1/2}}\, d\xi, \tag{11}$$

where

$$\Phi(\eta) \equiv \phi\left(\frac{1}{\sqrt{\eta}}\right) \quad \text{and} \quad F(\xi) \equiv \frac{1}{2\sqrt{\xi}} f\left(\frac{1}{\sqrt{\xi}}\right). \tag{12}$$

It is well known that the solution of Abel's equation (11) is given by

$$F(\xi) = \frac{1}{\pi} \frac{\partial}{\partial \xi} \int_0^\xi \frac{\Phi(\eta)}{(\xi - \eta)^{1/2}}\, d\eta. \tag{13}$$

In terms of the original variables the foregoing solution is equivalent to

$$f(x) = -\frac{2}{\pi} x^2 \frac{\partial}{\partial x} x \int_x^\infty \frac{\phi(y)}{y^2 (y^2 - x^2)^{1/2}}\, dy. \tag{14}$$

While equation (14) represents the formal solution of the problem, it is not of much practical use, since it requires differentiation and it is known that the differentiation of an observed frequency function can lead to results which are misleading unless the observations are of high precision. In practice it will therefore be advisable to use, as far as possible, only the moments of the observed frequency function, $\phi(y)$, and determine one or more parameters (such as the mean and the mean square deviation) of the true frequency function, $f(x)$. In any case, the form of the solution (14) emphasizes the fact that no artifice can really circumvent the necessity of differentiating the observed frequency function. Therefore, when the observed distribution is known in the form of a histogram (as is often the case) a numerical inversion of the integral equation (9) can hardly be expected to give trustworthy results.

4. *The relation between the moments of $\phi(y)$ and $f(x)$.*—We shall first show that there is a simple relation between the moments of $\phi(y)$ and $f(x)$.

Multiplying equation (9) by y^n and integrating over the range of y, we have

$$\int_0^\infty \phi(y)\, y^n dy = \int_0^\infty dy\; y^{n+1} \int_y^\infty dx\, \frac{f(x)}{x\,(x^2-y^2)^{1/2}}. \tag{15}$$

Inverting the order of the integration on the right-hand side, we obtain

$$\int_0^\infty \phi(y)\, y^n dy = \int_0^\infty \frac{dx}{x}\, f(x) \int_0^x dy\, \frac{y^{n+1}}{(x^2-y^2)^{1/2}}. \tag{16}$$

Now letting $y = tx$ in the integral over y, we have

$$\int_0^\infty \phi(y)\, y^n dy = \int_0^\infty f(x)\, x^n dx \int_0^1 \frac{t^{n+1}}{(1-t^2)^{1/2}}\, dt. \tag{17}$$

Hence

$$\overline{y^n} = \tfrac{1}{2}\sqrt{\pi}\, \frac{\Gamma\left(\frac{n}{2}+1\right)}{\Gamma\left(\frac{n}{2}+\frac{3}{2}\right)}\, \overline{x^n}. \tag{18}$$

In particular,

$$\bar{x} = \frac{4}{\pi}\,\bar{y}; \qquad \overline{x^2} = \frac{3}{2}\,\overline{y^2}; \qquad \overline{x^3} = \frac{16}{3\pi}\,\overline{y^3}. \tag{19}$$

It has been pointed out to us by Messrs. A. Brown, Su-Shu Huang, and D. Osterbrock that a relation of the form (18) also exists, when the relation (1) is replaced by the more general $y = x\psi(i)$, where $\psi(i)$ is an arbitrary integrable function of i; for, by multiplying the equation corresponding to (3) by y^n and integrating over the whole phase space we obtain the relation

$$\overline{y^n} = \overline{x^n} \int_0^{\pi/2} \psi^n(i)\, w(i)\, di\,, \tag{18'}$$

where $w(i)$ is the frequency function of i.

The mean, the mean square deviation, and the skewness of the true distribution $f(x)$ can therefore be derived from the moments of the apparent distribution $\phi(y)$ according to the following formulae:

$$\bar{x} = \frac{4}{\pi}\,\bar{y}; \qquad \overline{(x-\bar{x})^2} = 1.5\,\overline{y^2} - \frac{16}{\pi^2}\,\overline{y}^2,$$

and

$$\overline{(x-\bar{x})^3} = \frac{16}{3\pi}\,\overline{y^3} - \frac{18}{\pi}\,\overline{y^2}\,\overline{y} + \frac{128}{\pi^3}\,\overline{y}^3. \tag{20}$$

As an example of the application of the foregoing formulae we shall consider the recent results of A. Slettebak[5] on the rotational velocities of the Be stars. From his table of $v \sin i$ we find that

$$\overline{v \sin i} = 2.73\,; \qquad \overline{v^2 \sin^2 i} = 8.242\,; \qquad \text{and} \qquad \overline{v^3 \sin^3 i} = 26.356\,, \tag{21}$$

where a unit of velocity of 100 km/sec has been adopted. From equations (20) we now deduce that

$$\bar{v} = 3.48\,; \qquad \overline{(v-\bar{v})^2}^{1/2} = 0.50\,, \tag{22}$$

and

$$\overline{(v-\bar{v})^3} = -0.039\,.$$

The skewness of the true distribution is therefore negligible, and the mean (~350 km/sec) and the root mean square deviation (~50 km/sec) of the true distribution of the

[5] *Ap. J.*, **110**, 498, 1949; see esp. Table 2 of this paper.

rotational velocities of the Be stars are therefore determined with the same precision as these quantities are determined for the apparent distribution.

5. *Special forms of $f(x)$.*—When the frequency function $\phi(y)$ is not too well determined by the observations, then the mean and, to a less extent, the mean square are probably the only two quantities which can be determined with any degree of trustworthiness. Under these circumstances the formulae of the last section suffice to convert the mean and the mean square of observed frequency function into the corresponding means of the true frequency function, in which we are interested. However, in some cases it may be thought that $\phi(y)$ is well enough determined to say something more about $f(x)$ than its mean and mean square. In such cases attempts have been made in the literature to invert the integral equation (9) by a numerical procedure. But, as we have already indicated, such a procedure can be justified only in cases in which the observed frequency function can be differentiated with confidence. In all other cases it is preferable to assume a form for $f(x)$ involving one or more parameters and suggested by the physical nature of the quantity under discussion and to determine these parameters consist-

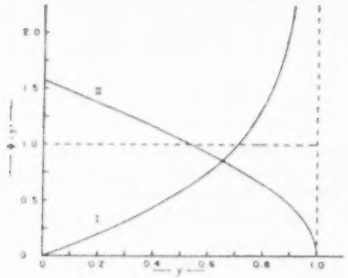

FIG. 2.—The frequency functions $\phi(y)$ derived from a δ-function centered at $x_1 = 1$ (curve *I*) and a uniform distribution of x in the interval $0 \leqslant x \leqslant 1$ (curve *II*). The same curves represent the function $\phi(y)$ for other values of x_1 if the abscissae are understood to mean y/x_1 and the ordinates $x_1\phi(x_1)$.

ently with the accuracy of the observational material. This latter procedure has the disadvantage that some form of $f(x)$ has to be assumed. Consequently, it entails a certain degree of arbitrariness; but it is inherent in the nature of the problem and cannot be avoided whenever the observed frequency function is not of a precision required for an unambiguous application of the solution given by equation (14).

In accordance with the remarks in the preceding paragraph, we shall consider certain special forms of $f(x)$ and derive the corresponding forms of $\phi(y)$.

The first form for $f(x)$ that we shall consider is when x takes only one value, say, x_1. Then

$$f(x) = \delta(x - x_1), \tag{23}$$

where δ denotes Dirac's δ-function. From equation (9) it now follows that

$$\begin{aligned} \phi(y;\, \delta_{x_1}) &= \frac{y}{x_1 (x_1^2 - y^2)^{1/2}} \qquad && y < x_1 \\ &= 0 && y > x_1 ; \end{aligned} \tag{24}$$

this distribution has therefore a singularity at $x = x_1$ (see Fig. 2).[6]

[6] The occurrence of this singularity makes the "reconstruction" of an observed $\phi(y)$ by superposing a number of distributions $\phi(y;\, \delta_{x_n})$ in the form

$$\phi(y) = \Sigma a_n \phi(y; \delta_{x_n})$$

a less valid procedure than it would be otherwise.

A second form of $f(x)$ which may be considered is the case in which all values of x less than a certain x_1 occur with equal probability. Then

$$f(x) = \frac{1}{x_1} \qquad x \leqslant x_1$$
$$= 0 \qquad x > x_1 . \tag{25}$$

For this form of $f(x)$, equation (9) leads to

$$\phi(y) = \frac{1}{x_1} \cos^{-1} \frac{y}{x_1} \qquad y \leqslant x_1$$
$$= 0 \qquad y > x_1 . \tag{26}$$

The nature of this distribution is also illustrated in Figure 2.

While cases (23) and (25) are sometimes useful, they do not provide the flexibility in the predicted forms of $\phi(y)$ which we should like to have for comparisons with observed frequency functions. A form for $f(x)$ which appears most suitable in the stellar contexts is the one suggested by Elsa van Dien,[7] namely,

$$f(x) = \frac{1}{\sqrt{\pi}} \{ e^{-(x-x_1)^2} + e^{-(x+x_1)^2} \} . \tag{27}$$

This form for $f(x)$ provides a family of frequency functions with two parameters. Also, for $x_1 = 0$, $f(x)$ represents a Gaussian distribution; and for x_1 large it is again, essentially, a Gaussian distribution; and between these two limits we have a family of "intermediate" distributions which are even.

For $f(x)$ given by equation (27) the first three moments are:

$$\bar{x} = \frac{1}{\sqrt{\pi}} e^{-x_1^2} + x_1 \Phi(x_1) ,$$
$$\overline{x^2} = x_1^2 + \tfrac{1}{2} , \tag{28}$$

and

$$\overline{x^3} = \frac{1}{\sqrt{\pi}} e^{-x_1^2} (1 + x_1^2) + (\tfrac{3}{2} + x_1^2)\, x_1 \Phi(x_1)$$

where

$$\Phi(x_1) = \frac{2}{\sqrt{\pi}} \int_0^{x_1} e^{-t^2} dt \tag{29}$$

is the error function. The numerical values of these moments are given in Table 1. The corresponding moments of y can be obtained in accordance with equation (19).

When $f(x)$ has the form (27), the equation for $\phi(y)$ becomes

$$\phi(y;\, x_1) = \frac{y}{\sqrt{\pi}} \int_y^\infty \frac{e^{-(x-x_1)^2} + e^{-(x+x_1)^2}}{x\,(x^2 - y^2)^{1/2}}\, dx , \tag{30}$$

or, alternatively,

$$\phi(y;\, x_1) = \frac{2y}{\sqrt{\pi}} e^{-x_1^2} \int_y^\infty \frac{e^{-x^2} \cosh 2xx_1}{x\,(x^2 - y^2)^{1/2}}\, dx . \tag{31}$$

In equations (30) and (31) we have emphasized the dependence of $\phi(y)$ on x_1 by including it as an argument.

It does not seem that the integral defining $\phi(y;\, x_1)$ can be reduced to known functions. However, it will appear from the discussion of this integral in §6 that we can get a fairly complete picture of $\phi(y;\, x_1)$ by considering its behavior for various ranges of its arguments.

[7] *J.R.A.S. Canada*, **42**, 249, 1948.

6. *The behavior of $\phi(y; x_1)$ for various ranges of its arguments.* (i) *The expansion of $\phi(y; x_1)$ in a power series in x_1.*—When $x_1 \leqslant 1$, we can obtain a rapidly convergent expansion for $\phi(y; x_1)$ by replacing $\cosh 2xx_1$ in equation (31) by its series and integrating term by term; thus,

$$\phi(y; x_1) = \frac{2}{\sqrt{\pi}} e^{-x_1^2} \sum_{n=0}^{\infty} \frac{(2x_1)^{2n}}{2n!} y \int_y^{\infty} \frac{e^{-x^2} x^{2n-1}}{(x^2 - y^2)^{1/2}} dx . \tag{32}$$

Letting

$$I_n(y) = y \int_y^{\infty} \frac{e^{-x^2} x^{2n-1}}{(x^2 - y^2)^{1/2}} dx , \tag{33}$$

we can rewrite equation (32) in the form

$$\phi(y; x_1) = \frac{2}{\sqrt{\pi}} e^{-x_1^2} \sum_{n=0}^{\infty} \frac{2^{2n}}{2n!} x_1^{2n} I_n(y) . \tag{34}$$

TABLE 1

CONSTANTS RELATING TO THE FREQUENCY FUNCTION

$$f(x) = \frac{1}{\sqrt{\pi}} [e^{-(x-x_1)^2} + e^{-(x+x_1)^2}]$$

x_1	x	x^2	x^3	$x/[2(x^2 - x_1^2)]^{1/2}$
0.0	0.5642	0.50	0.564	0.93593
0.1	0.5698	0.51	0.581	0.93598
0.2	0.5866	0.54	0.632	0.93719
0.3	0.6142	0.59	0.719	0.9418
0.4	0.6521	0.66	0.842	0.9518
0.5	0.6996	0.75	1.00	0.9693
0.6	0.7559	0.86	1.21	0.9951
0.7	0.8201	0.99	1.46	1.0292
0.8	0.8912	1.14	1.76	1.072
0.9	0.9682	1.31	2.11	1.122
1.0	1.0502	1.50	2.52	1.179
1.2	1.226	1.94	3.54	1.314
1.4	1.413	2.46	4.85	1.466
1.6	1.606	3.06	6.45	1.636
1.8	1.802	3.74	8.53	1.819
2.0	2.001	4.50	11.0	2.009
2.2	2.200	5.34	13.9	2.204
2.4	2.400	6.26	17.4	2.402
2.6	2.600	7.26	21.5	2.601
2.8	2.800	8.34	26.2	2.800
3.0	3.000	9.50	31.5	3.000

The integrals $I_n(y)$ $(n = 0, 1, \ldots)$ which occur in this expansion can all be expressed in terms of known functions in the following manner:

First, we may note that, with the substitution

$$x^2 = y^2 + u^2 , \tag{35}$$

I_n becomes

$$I_n = y\, e^{-y^2} \int_0^{\infty} e^{-u^2} (y^2 + u^2)^{n-1} du . \tag{36}$$

Next, we observe that the I_n's satisfy the recursion formula,

$$I_{n+1} = (n - \tfrac{1}{2} + y^2)\, I_n - (n-1)\, y^2 I_{n-1} \qquad (n = 1, \ldots) . \tag{37}$$

This formula can be derived by writing I_n in the form

$$I_n = y\int_y^\infty e^{-x^2}x^{2n-2}\frac{d}{dx}(x^2-y^2)^{1/2}dx \tag{38}$$

and integrating by parts; thus

$$\begin{aligned} I_n &= 2y\int_y^\infty e^{-x^2}x^{2n-2}(x^2-n+1)(x^2-y^2)^{1/2}dx \\ &= 2y\int_y^\infty \frac{e^{-x^2}}{(x^2-y^2)^{1/2}}x^{2n-2}[x^4-x^2(n-1+y^2)+(n-1)y^2]\,dx \\ &= 2[I_{n+1}-(n-1+y^2)I_n+(n-1)y^2I_{n-1}]; \end{aligned} \tag{39}$$

and this is equivalent to formula (37).

Using the recursion formula (37), we can reduce the evaluation of I_n to I_1 and I_0; and both these can be reduced to known functions. Thus (cf. eq. [36])

$$I_1 = y\,e^{-y^2}\int_0^\infty e^{-u^2}du = \tfrac{1}{2}\sqrt{\pi}\,e^{-y^2}y\,. \tag{40}$$

On the other hand,

$$I_0(y) = y\,e^{-y^2}\int_0^\infty \frac{e^{-u^2}}{y^2+u^2}\,du\,; \tag{41}$$

and we recognize I_0 as a standard integral which occurs in the theory of the line-absorption coefficient in stellar atmospheres;[8] and using known results we have

$$I_0(y) = \tfrac{1}{2}\pi[1-\Phi(y)]\,, \tag{42}$$

where $\Phi(y)$ denotes the error function (cf. eq. 29]).

All the integrals I_n can therefore be evaluated successively in terms of I_0 and I_1.

For purposes of practical calculation it is convenient to rewrite the expansion (34) in the form

$$\phi(y;\,x_1) = e^{-x_1^2}\sum_{n=0}^{\infty}F_n(y)\,x_1^{2n}\,, \tag{43}$$

where

$$F_n(y) = \frac{2^{2n+1}}{2n!\sqrt{\pi}}\,I_n(y)\,. \tag{44}$$

The functions $F_n(y)$ for $n = 0, \ldots, 6$, are tabulated (see Table 2). Using this table, we can evaluate $\phi(y;\,x_1)$ for all $x_1 \leqslant 1$ with entirely sufficient accuracy.

ii) *The expansion of $\phi(y;\,x_1)$ in a power series in y.*—An expansion of $\phi(y;\,x_1)$ in y analogous to the one in x_1 found in the preceding subsection can be obtained in the following manner:

First, using the relation

$$e^{-p^2} = \frac{2}{\sqrt{\pi}}\int_0^\infty e^{-u^2}\cos 2pu\,du\,, \tag{45}$$

[8] Cf. D. L. Harris, *Ap. J.*, **108**, 112, 1948. In Harris' notation

$$I_0(y) = \tfrac{1}{2}\pi\,e^{-y^2}H(y,0)\,;$$

and, according to equation (2) of his paper,

$$H(y,0) = \frac{2}{\sqrt{\pi}}e^{y^2}\int_y^\infty e^{-t^2}dt\,;$$

the result (42) quoted in the text follows from this.

we write

$$\frac{1}{\sqrt{\pi}}\left[e^{-(x-x_1)^2}+e^{-(x+x_1)^2}\right]=\frac{4}{\pi}\int_0^\infty e^{-u^2}\cos 2x_1u\cos 2xu\,du\,. \tag{46}$$

Then, inserting this expression in equation (30) and inverting the order of the integrations, we obtain

$$\phi(y;\,x_1)=\frac{4}{\pi}\int_0^\infty du\,e^{-u^2}\cos 2x_1u\int_y^\infty dx\,\frac{y\cos 2xu}{x\,(x^2-y^2)^{1/2}} \tag{47}$$

or, letting $x=yt$ in the integral over x, we have

$$\phi(y;\,x_1)=\frac{4}{\pi}\int_0^\infty du\,e^{-u^2}\cos 2x_1u\int_1^\infty dt\,\frac{\cos 2uyt}{t\,(t^2-1)^{1/2}}. \tag{48}$$

TABLE 2

THE FUNCTIONS $F_n(y)$ FOR $n=0, 1, \ldots, 6$

y	F_0	F_1	F_2	F_3	F_4	F_5	F_6
0.0	1.7725	0	0	0	0	0	0
0.2	1.3777	0.3843	0.0692	0.0135	0.0024	0.0004	0.000005
0.4	1.0131	.6817	.1500	.0283	.0049	.0008	.000010
0.6	0.7021	.8372	.2400	.0461	.0078	.0012	.000016
0.8	0.4571	.8437	.3206	.0675	.0112	.0017	.000022
1.0	0.2788	.7358	.3679	.0899	.0155	.0022	.000029
1.2	0.1590	.5686	.3677	.1078	.0202	.0030	.000037
1.4	0.08457	.39440	.32341	.11484	.02451	.00380	.000048
1.6	0.04192	.24738	.25232	.10844	.02689	.00460	.000061
1.8	0.01933	.14099	.17577	.09078	.02637	.00510	.000073
2.0	0.00829	.07326	.10989	.06756	.02300	.00509	.000081
2.2	0.00330	.03479	.06193	.04487	.01781	.00453	.000081
2.4	0.00122	.01513	.03156	.02668	.01228	.00359	.000073
2.6	0.000418	0.006028	0.014588	0.014255	0.007550	0.002525	0.000058

Now from the identity

$$J_0(z)=\frac{2}{\pi}\int_1^\infty\frac{\sin zt}{(t^2-1)^{1/2}}\,dt\,, \tag{49}$$

where $J_0(z)$ denotes the Bessel function of order zero, it follows that

$$\int_0^z J_0(z)\,dz=1-\frac{2}{\pi}\int_1^\infty\frac{\cos zt}{t\,(t^2-1)^{1/2}}\,dt\,. \tag{50}$$

Using this result in equation (48), we obtain (cf. eq. [45])

$$\phi(y;\,x_1)=\sqrt{\pi}\,e^{-x_1^2}-2\int_0^\infty e^{-u^2}\left\{\int_0^{2uy}J_0(z)\,dz\right\}\cos 2x_1u\,du\,. \tag{51}$$

We can now obtain an expansion of $\phi(y;\,x_1)$ as a power series in y by expanding the integral over the Bessel function in equation (51) as a power series in $2uy$. Thus, from the known series for $J_0(z)$ it follows that

$$\int_0^{2uy}J_0(z)\,dz=2\sum_{n=0}^\infty(-1)^n\frac{(uy)^{2n+1}}{(2n+1)\,(n!)^2}. \tag{52}$$

Therefore, defining

$$D_n(x_1)=\frac{2}{n!}\,e^{x_1^2}\int_0^\infty e^{-u^2}u^{2n+1}\cos 2x_1u\,du\,, \tag{53}$$

we can rewrite equation (51) in the form

$$\phi(y;\, x_1) = \sqrt{\pi}\, e^{-x_1^2}\left[1 - \frac{2}{\sqrt{\pi}} \sum_{n=0}^{\infty} (-1)^n \frac{D_n(x_1)}{(2n+1)\, n!}\, y^{2n+1}\right]. \tag{54}$$

The integrals $D_n(x_1)$ $(n = 0, 1, \ldots)$ which occur in this expansion can be reduced to the evaluation of D_0 by the use of the following recursion formulae, which are readily established by successive integration by parts:

$$(n+1)\, D_{n+1}(x_1) = (2n + \tfrac{3}{2} - x_1^2)\, D_n(x_1) - (n + \tfrac{1}{2})\, D_{n-1}(x_1)$$

and

$$D_n(x_1) = \left(1 - \frac{1}{n}\, x_1^2\right) D_{n-1}(x_1) + \frac{x_1}{2n}\, \frac{d D_{n-1}(x_1)}{d x_1} \qquad (n = 1,\ 2,\ \ldots). \tag{55}$$

By transformations similar to those used in the reduction of the integral which occurs in the theory of the line-absorption coefficient which combines Doppler effect and damping, we find that

$$D_0(x_1) = e^{x_1^2}\left\{1 - 2\, x_1\, e^{-x_1^2} \int_0^{x_1} e^{t^2} dt\right\}. \tag{56}$$

The expression on the right-hand side is simply related to a quantity which has been tabulated by Harris;[8] thus, in Harris' notation,

$$D_0(x_1) = -\tfrac{1}{2}\sqrt{\pi}\, e^{x_1^2} H_1(x_1). \tag{57}$$

Thus the functions D_n can all be evaluated. However, the series (54) does not extend the range of the expansion (43) by a large amount for $x_1 > 1$. Thus, for $x_1 = 1.5$, it is found that seven terms in the series (54) are required to evaluate ϕ at $y = 1.3$; for larger values of x_1 the range of y in which the series can be profitably used becomes less. Nevertheless, the series (54) does enable us to bridge the gap between the series (43) good for $x_1 \leqslant 1$ (and all y) and the asymptotic expansions found below for $x_1 > 2$.

iii) *An asymptotic expansion for $\phi(y; x_1)$ for x_1 large and $y < x_1$.*—When $x_1 > 2$, we can neglect the term in $e^{-(x+x_1)^2}$ in equation (30); the maximum error introduced by this is less than 2 per cent for $x_1 = 2$; and for larger values of x_1 the error introduced by this simplification decreases very rapidly—in fact, like $e^{-x_1^2}$! For $x_1 > 2$, we may therefore write

$$\phi(y;\, x_1) = \frac{y}{\sqrt{\pi}} \int_y^{\infty} \frac{e^{-(x-x_1)^2}}{x\,(x^2 - y^2)^{1/2}}\, dx \qquad (x_1 > 2). \tag{58}$$

With the substitution

$$x - x_1 = t, \tag{59}$$

equation (58) becomes

$$\phi(y;\, x_1) = \frac{y}{\sqrt{\pi}} \int_{-(x_1 - y)}^{\infty} \frac{e^{-t^2} dt}{(t + x_1)^{1/2}\,(t + x_1 + y)^{1/2}\,(t + x_1 - y)^{1/2}}. \tag{60}$$

Now let

$$y = a\, x_1 \qquad (a < 1). \tag{61}$$

Then

$$\phi(y;\, x_1) = \frac{y}{x_1 (x_1^2 - y^2)^{1/2}}\, \frac{1}{\sqrt{\pi}} \times \int_{-(1-a)x_1}^{\infty} \frac{e^{-t^2} dt}{(1 + t/x_1)^{1/2}\,[1 + t/x_1(1+a)]^{1/2}\,[1 + t/x_1(1-a)]^{1/2}}. \tag{62}$$

Now, if

$$(1 - a)\, x_1 > 2, \tag{63}$$

we may expand the denominator in formula (62) in a power series in $1/x_1$ and also extend the range of integration over t from $+\infty$ to $-\infty$. In this manner we shall obtain an asymptotic expansion valid for $x_1(1-a) \to \infty$. By the procedure indicated we find:

$$\phi(y; x_1) \simeq \frac{y}{x_1(x_1^2-y^2)^{1/2}} \frac{1}{\sqrt{\pi}} \int_{-\infty}^{\infty} e^{-t^2} \left\{ 1 - \frac{t}{x_1} \frac{2-a^2}{1-a^2} + \frac{t^2}{x_1^2} \frac{6-5a^2+2a^4}{2(1-a^2)^2} - \ldots \right\} dt, \tag{64}$$

or

$$\phi(y; x_1) \simeq \frac{y}{x_1(x_1^2-y^2)^{1/2}} \left\{ 1 + \frac{6y^4-5y^2x_1^2+2x_1^4}{4x_1^2(x_1^2-y^2)^2} + \ldots \right\}. \tag{65}$$

It will be noticed that the dominant term in the asymptotic expansion (65) is the contour for a δ-function in x centered at x_1; this is, of course, what we should have expected.

The expansion (65) is satisfactory for determining $\phi(y; x_1)$ for x_1 large and $y < x_1$; thus for $x_1 = 10$ it gives sufficient accuracy for $y < 8$.

iv) *An asymptotic expansion for* $\phi(x_1; x_1)$ *for* x_1 *large.*—The expansion found in the preceding section ceases to be valid when $y \to x_1$. However, for $y = x_1$ we can find a satisfactory expansion in the following manner:

For $y = x_1$ equation (58) is

$$\phi(x_1; x_1) = \frac{x_1}{\sqrt{\pi}} \int_{x_1}^{\infty} \frac{e^{-(x-x_1)^2}}{x(x^2-x_1^2)^{1/2}} dx. \tag{66}$$

Now let

$$(x-x_1)^2 = t. \tag{67}$$

Equation (66) becomes

$$\phi(x_1; x_1) = \frac{1}{(8\pi x_1)^{1/2}} \int_0^{\infty} \frac{e^{-t} dt}{t^{3/4}(1+\sqrt{t/x_1})(1+\sqrt{t/2x_1})^{1/2}}. \tag{68}$$

We can now obtain an asymptotic expansion for the integral on the right-hand side by expanding the denominator in a power series in $1/x_1$ and integrating term by term; thus

$$\phi(x_1; x_1) \simeq \frac{1}{(8\pi x_1)^{1/2}} \left[\Gamma(0.25) - \frac{5}{4x_1}\Gamma(0.75) + \frac{43}{32x_1^2}\Gamma(1.25) - \frac{177}{128x_1^3}\Gamma(1.75) + \frac{2867}{2048x_1^4}\Gamma(2.25) - \ldots \right], \tag{69}$$

or, inserting the values of the Γ-functions, we find

$$\phi(x_1; x_1) \simeq \frac{0.72320}{\sqrt{x_1}} \left\{ 1 - \frac{0.42249}{x_1} + \frac{0.33594}{x_1^2} - \frac{0.35053}{x_1^3} + \frac{0.43747}{x_1^4} - \ldots \right\}. \tag{70}$$

This series can be trusted to give the value of $\phi(x_1; x_1)$ with sufficient accuracy for $x_1 > 2$.

The values of $\phi(x_1; x_1)$ for $x_1 < 2$, determined in accordance with equation (70), are listed in Table 3.

v) *An asymptotic formula for* $\phi(y; x_1)$ *for* x_1 *large and* $y > x_1$.—When x_1 is large and $y > x_1$, we write

$$y = \beta x_1 \quad (\beta \gg 1) \qquad \text{and} \qquad t = x - y \tag{71}$$

in equation (58). We then find

$$\phi(y;\, x_1) = \frac{1}{(2\pi y)^{1/2}} \int_0^\infty \frac{\exp\{-[t^2 + 2(\beta-1)\, x_1 t + x_1^2 (\beta-1)^2]\}}{(1+t/\beta x_1)\,(1+t/2\beta x_1)^{1/2} t^{1/2}}\, dt. \quad (72)$$

When $\beta \gg 1$, the main contribution to the integral on the right-hand side comes from the neighborhood of $t = 0$. Accordingly, we may write

$$\phi(y;\, x_1) \simeq \frac{e^{-x_1^2(\beta-1)^2}}{(2\pi y)^{1/2}} \int_0^\infty e^{-2x(\beta-1)x_1 t}\, \frac{dt}{\sqrt{t}} \quad (73)$$

(x_1 large and $\beta \gg 1$).

TABLE 3

$\phi(x_1;\, x_1)$

x_1	$\phi(x_1;\, x_1)$	x_1	$\phi(x_1;\, x_1)$	x_1	$\phi(x_1;\, x_1)$	x_1	$\phi(x_1;\, x_1)$
2.0	0.4379	3.5	0.3485	5	0.2998	8	0.2434
2.5	.3995	4.0	.3296	6	.2768	9	.2306
3.0	0.3712	4.5	0.3136	7	0.2585	10	0.2197

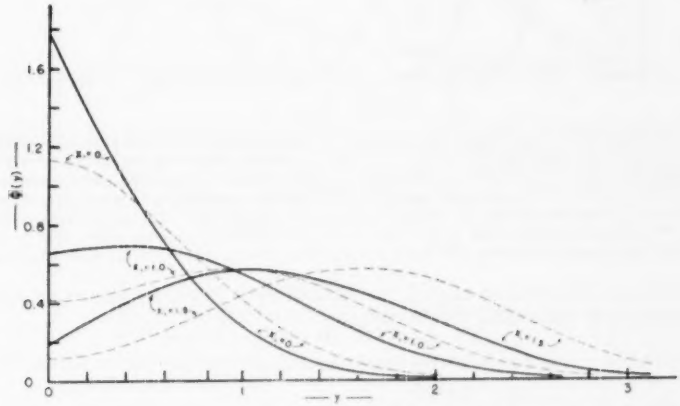

FIG. 3.—The frequency functions $\phi(y;\, x_1)$ (*full line curves*) derived from assumed distributions of x of the form given by equation (27) (*dashed curves*) for values of $x_1 \leqslant 1.5$. For $x_1 = 0$, $f(x)$ is Gaussian, and $\phi(y)$ is explicitly known; for $x_1 = 1.0$, $\phi(y)$ was derived from the expansion (43); for $x_1 = 1.5$ the the expansion (54) was used for $y \leqslant 1.3$; and, as the asymptotic form for large y (eq. [74]) is also known, the curve for $y > 1.3$ can be drawn without much ambiguity, since the area under the curve should be unity.

Hence

$$\phi(y;\, x_1) \simeq \frac{1}{2} \frac{e^{-(y-x_1)^2}}{\sqrt{y\,(y-x_1)}} \qquad (y \gg x_1). \quad (74)$$

7. *The one-parameter family of frequency functions* $\phi(y;\, x_1)$.—Using the various expansions for $\phi(y;\, x_1)$ obtained in §6, we can readily sketch the form of the frequency functions for various values of x_1. This is done in Figures 3 and 4.

8. *The true distribution of the rotational velocities of stars of different spectral types.*—We have already explained why, when we wish to say something more about the distribution of the rotational velocities of stars than its mean and mean square, it is preferable to compare the observed distribution of $v \sin i$ with that predicted on some assumed form of $f(v)$, instead of inverting the integral equation (9) by a numerical procedure. We shall now show that the particular form of $f(x)$ examined in the preceding sections allows us to represent the known observations on the rotational velocities of stars very satisfactorily.

Now, in order to make a comparison between an observed distribution of $v \sin i$ and the one-parameter family of frequency functions $\phi(y; x_1)$ derived in §§6 and 7, it is necessary that we determine *two* quantities from the observations, namely, (1) the *unit* in

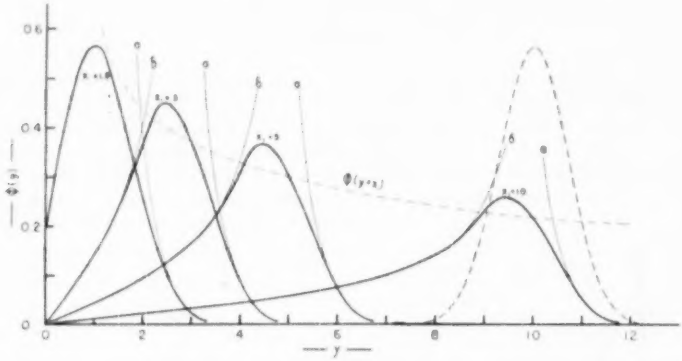

FIG. 4.—The frequency functions $\phi(y; x_1)$ (*heavy full-line curves*) derived from assumed distributions of x of the form given by equation (27) for $x_1 \geq 1.5$. In sketching the curves, use was made of the asymptotic expansion for $y < x_1$ (the curves marked δ), the expansion for $y \gg x_1$ (the curves marked a), and the value of $\phi(y; x_1)$ at $y = x_1$ given by equation (70) (*dashed curve*); these expansions, together with the condition that the area under the curve in each case should be unity, leave little ambiguity for drawing in the complete curves. For $x_1 \geq 2$ the frequency function $f(x)$ from which $\phi(y)$ is derived is, for all practical purposes, a Gaussian distribution centered at $x = x_1$ (the curve for $x_1 = 10$ is illustrated).

which x measures the velocity and (2) the parameter x_1 in the frequency function (30): for our assumption concerning $f(v)$ is, strictly,

$$f(v) = \frac{j}{\sqrt{\pi}} \left[e^{-j^2(v-v_1)^2} + e^{-j^2(v+v_1)^2} \right], \tag{75}$$

where $1/j$ is of the dimensions of a velocity. However, with the substitutions

$$j v = x \qquad \text{and} \qquad j v_1 = x_1, \tag{76}$$

the frequency function governing x reduces to $f(x)$ as we have defined it in equation (30).

Since the mean and (to a less extent) the mean square are probably the only two quantities which are determined with any precision, it appears that, in making comparisons between the observed distributions of $v \sin i$ and those derived from the function (75), we determine the parameters j and v_1 of the distribution in the following manner:

From the observed values of the mean and the mean square of $v \sin i$ we first determine the values of $\bar{v}$ and $\overline{v^2}$ according to the moment relations of §4 (eqs. [19] and [20]). From these mean values we next evaluate the quantity

$$\frac{\bar{v}}{[2(\overline{v^2} - \bar{v}^2)]^{1/2}}. \tag{77}$$

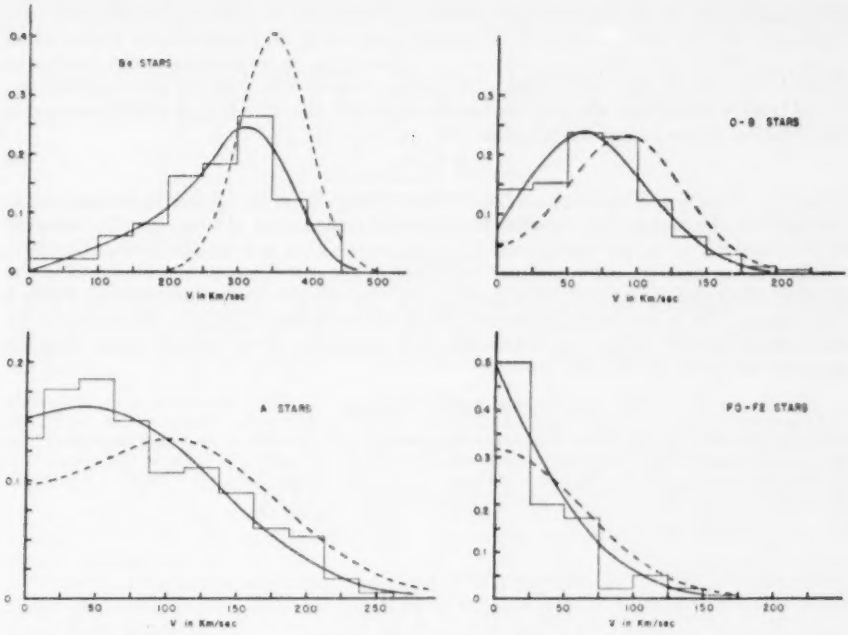

FIG. 5.—The comparison of the observed distributions of the rotational velocities of stars of different spectral types with those derived on the assumption of a true distribution of velocities of the form given by equation (75) and for values of the parameters listed in Table 4. In each case the observed distribution of $v \sin i$ is represented by the histogram, while the full-line curve represents the predicted distribution of $v \sin i$ for a true distribution of v given by the dashed curve.

TABLE 4

REDUCTION OF DATA ON ROTATIONAL VELOCITIES OF STARS OF DIFFERENT SPECTRAL TYPES

	Spectral Type			
	Be	O-B	A	F0-F2
$v \sin i$ (km/sec)	273	74	88	40
$v^2 \sin^2 i$ (km/sec)^2	82,420	7238	11,254	2978
v (km/sec)	348	94	112	51
v^2 (km/sec)^2	123,600	10,860	16,880	4470
$v/(2[v^2-v^2])^{1/2}$	4.90	1.47	1.20	0.82
x_1 computed	4.9	1.41	1.03	.....
x_1 adopted	5.0	1.5	1.0	0.0
j^{-1} (km/sec)	70	63	107	90

This quantity is clearly independent of the unit in which the velocity is measured; accordingly, for the distribution (75), it depends only on x_1 and assumes the values listed in the last column of Table 1 for the various values of x_1. Interpolating in this column of Table 1, we can therefore determine x_1 when the value of the quantity (77) has been deduced from observations. Once x_1 has been determined, the unit, $1/j$, in which x measures the velocity, follows from the relation

$$\bar{x} = j\bar{v} \ , \tag{78}$$

since $\bar{x}$ as a function of x_1 is known (eq. [28] and Table 1). With $1/j$ and x_1 determined in this fashion, the comparison between the observed distribution of $v \sin i$ and the member of the family $\phi(y; x_1)$ belonging to the derived value of x_1 is a straightforward matter.

The known data on the rotational velocities of the stars[9] have been analyzed in the manner described in the preceding paragraphs. The results are summarized in Table 4 and Figure 5. It is seen that the observations are represented entirely satisfactorily by the assumption (75) regarding the distribution of the rotational velocities and with the parameters listed in Table 4.

[9] For the Be stars we have used the results of Slettebak (*op. cit.*), while for the stars of the other spectral types we have used the data compiled by Struve (*op. cit.*, p. 259) and C. Westgate (*Ap. J.*, **77**, 141, 1933; **78**, 46, 1933; **79**, 357, 1934). Dr. Struve has pointed out to us that for the O and the B stars Miss Westgate's values for the rotational velocities may be too low; however, he believes that the relative distribution may be reliable. That Miss Westgate's rotational velocities for the O and the B stars are systematically too low would seem to be confirmed by Slettebak's work.

EXACT CURVES OF GROWTH FOR THE FORMATION OF ABSORPTION LINES ACCORDING TO THE MILNE-EDDINGTON MODEL
II. CENTER OF THE DISK

MARSHAL H. WRUBEL*
Yerkes Observatory
Received September 29, 1949

ABSTRACT

Curves of growth for absorption lines observed at the center of the disk have been computed to supplement the recently published curves for lines observed in the integrated flux. Six values of the damping from $\log a = -3.0$ to $\log a = -1.0$ and four values of $B^{(0)}/B^{(1)}$ from $\frac{1}{3}$ to $\frac{7}{3}$ have been considered. The computations are based upon Chandrasekhar's exact solution of the equation of transfer for the Milne-Eddington model and Hjerting's tabulation of the line-absorption coefficient.

GENERAL REMARKS

This paper is the second and concluding part of the computation of exact curves of growth for the Milne-Eddington model. The first part dealt with resonance absorption lines observed in the integrated flux.[1] The following curves are intended primarily for solar research, when observations may be made at the center of the stellar disk. The notation of Paper I is used throughout this paper, and most quantities defined there will not be redefined.

From S. Chandrasekhar's exact solution of the equation of transfer for the Milne-Eddington model[2] it follows that the ratio of the intensity at a point in the line to the continuous intensity is

$$r_\nu(\mu) = \frac{\lambda^{3/2}}{\mu + B^{(0)}/B^{(1)}}\, H(\mu)\left(\mu + \frac{B^{(0)}}{\lambda B^{(1)}} + \frac{1-\lambda}{2\lambda^{1/2}}\, a_1\right), \tag{1}$$

where μ is the cosine of the angle between the direction of observation and the normal. In this paper we are concerned with the center of the disk, where $\mu = 1$:

$$r_\nu(1) = \frac{\lambda^{3/2}}{1 + B^{(0)}/B^{(1)}}\, H(1)\left(1 + \frac{B^{(0)}}{\lambda B^{(1)}} + \frac{1-\lambda}{2\lambda^{1/2}}\, a_1\right). \tag{2}$$

Analogous to equation (9), Paper I, the quantity

$$\frac{W}{b} = \int_{-\infty}^{\infty} (1 - r_\nu)\, dv \tag{3}$$

is computed as a function of η_0. Six values of the damping from $\log a = -3.0$ to $\log a = -1.0$ were considered for $B^{(0)}/B^{(1)}$ equal to $\frac{1}{3}$, $\frac{2}{3}$, $\frac{1}{1}$, and $\frac{7}{3}$. The last two values of $B^{(0)}/B^{(1)}$ differ from those in Paper I for reasons described in the section on interpolation below.

The numerical computations were performed in exactly the same manner as those in Paper I. Hjerting's tables[3] were again used to determine λ as a function of v. The paragraph on "Construction of Tables" as it appears in Paper I fits the present case if $r_\nu(1)$ is substituted wherever R appears.

* National Research Council Postdoctoral Fellow, 1949–1950; now at the Princeton University Observatory.

[1] *Ap. J.*, **109**, 66, 1949 (hereafter referred to as "Paper I").

[2] *Ap. J.*, **106**, 145, 1947.

[3] *Ap. J.*, **88**, 508, 1938.

TABLE 1

log q_0	log q					
	−1.0	−1.4	−1.8	−2.2	−2.6	−3.0
	log W/b for $B^{(2)}/B^{(1)}=\frac{1}{3}$					
−2.8	−2.696	−2.696	−2.696	−2.696	−2.696	−2.696
−2.4	−2.297	−2.297	−2.297	−2.297	−2.297	−2.297
−2.0	−1.899	−1.899	−1.899	−1.899	−1.899	−1.899
−1.6	−1.503	−1.503	−1.503	−1.504	−1.504	−1.504
−1.2	−1.112	−1.112	−1.113	−1.113	−1.114	−1.114
−0.8	−0.733	−0.736	−0.737	−0.738	−0.738	−0.739
−0.4	−0.380	−0.388	−0.391	−0.392	−0.393	−0.393
0.0	−0.075	−0.089	−0.095	−0.098	−0.099	−0.100
+0.4	+0.171	+0.146	+0.135	+0.130	+0.129	+0.128
+0.8	+0.363	+0.324	+0.305	+0.297	+0.294	+0.293
+1.2	*+0.522*	+0.462	+0.432	+0.419	+0.414	+0.411
+1.6	+0.672	*+0.583*	+0.535	+0.513	+0.504	+0.500
+2.0	+0.828	+0.706	*+0.631*	+0.593	+0.576	+0.569
+2.4	+0.999	+0.846	+0.736	*+0.671*	+0.640	+0.626
+2.8	+1.182	+1.007	+0.862	+0.762	*+0.706*	+0.679
+3.2	+1.374	+1.186	+1.015	+0.877	+0.785	*+0.736*
+3.6	+1.570	+1.376	+1.189	+1.022	+0.891	+0.807
+4.0	+1.768	+1.571	+1.378	+1.193	+1.029	+0.904
+4.4	+1.967	+1.768	+1.571	+1.379	+1.196	+1.036
+4.8	+2.167	+1.967	+1.768	+1.572	+1.380	+1.199
+5.2	+2.367	+2.167	+1.967	+1.769	+1.572	+1.381
+5.6	+2.567	+2.367	+2.167	+1.967	+1.769	+1.573
+6.0	+2.767	+2.567	+2.367	+2.167	+1.967	+1.769
	log W/b for $B^{(2)}/B^{(1)}=\frac{2}{3}$					
−2.8	−2.771	−2.771	−2.771	−2.771	−2.771	−2.771
−2.4	−2.371	−2.371	−2.371	−2.371	−2.371	−2.371
−2.0	−1.973	−1.973	−1.973	−1.973	−1.973	−1.973
−1.6	−1.577	−1.577	−1.577	−1.578	−1.578	−1.578
−1.2	−1.186	−1.186	−1.187	−1.187	−1.188	−1.188
−0.8	−0.806	−0.809	−0.811	−0.812	−0.812	−0.812
−0.4	−0.452	−0.459	−0.462	−0.464	−0.465	−0.465
0.0	−0.143	−0.157	−0.163	−0.166	−0.167	−0.167
+0.4	+0.108	+0.084	+0.073	+0.068	+0.067	+0.066
+0.8	+0.306	+0.268	+0.250	+0.243	+0.240	+0.238
+1.2	*+0.471*	+0.413	+0.385	+0.372	+0.367	+0.365
+1.6	+0.624	*+0.539*	+0.494	+0.474	+0.465	+0.461
+2.0	+0.781	+0.665	*+0.594*	+0.559	+0.543	+0.537
+2.4	+0.951	+0.804	+0.700	*+0.640*	+0.612	+0.599
+2.8	+1.132	+0.962	+0.824	+0.731	*+0.680*	+0.656
+3.2	+1.322	+1.137	+0.972	+0.842	+0.758	*+0.713*
+3.6	+1.517	+1.324	+1.142	+0.982	+0.859	+0.782
+4.0	+1.714	+1.518	+1.326	+1.147	+0.991	+0.875
+4.4	+1.913	+1.714	+1.519	+1.328	+1.151	+1.000
+4.8	+2.113	+1.913	+1.715	+1.520	+1.330	+1.156
+5.2	+2.313	+2.113	+1.913	+1.715	+1.521	+1.332
+5.6	+2.513	+2.313	+2.113	+1.913	+1.716	+1.521
+6.0	+2.712	+2.513	+2.313	+2.113	+1.913	+1.716

TABLE 1—*Continued*

log η_0	log δ					
	−1.0	−1.4	−1.8	−2.2	−2.6	−3.0
	log W/b for $B^{(0)}/B^{(1)}=\frac{11}{9}$					
−2.8	−2.860	−2.860	−2.860	−2.860	−2.860	−2.860
−2.4	−2.461	−2.461	−2.462	−2.463	−2.463	−2.463
−2.0	−2.062	−2.062	−2.062	−2.063	−2.063	−2.063
−1.6	−1.666	−1.666	−1.666	−1.667	−1.667	−1.667
−1.2	−1.275	−1.275	−1.276	−1.276	−1.277	−1.277
−0.8	−0.894	−0.897	−0.899	−0.900	−0.900	−0.900
−0.4	−0.538	−0.545	−0.548	−0.549	−0.550	−0.550
0.0	−0.225	−0.238	−0.244	−0.246	−0.247	−0.248
+0.4	+0.033	+0.010	0.000	−0.004	−0.006	−0.007
+0.8	+0.240	+0.204	+0.187	+0.180	+0.177	+0.176
+1.2	*+0.412*	+0.358	+0.332	+0.320	+0.316	+0.314
+1.6	+0.570	*+0.491*	+0.449	+0.431	+0.423	+0.419
+2.0	+0.728	+0.619	*+0.554*	+0.522	+0.508	+0.502
+2.4	+0.896	+0.756	+0.661	*+0.607*	+0.582	+0.571
+2.8	+1.075	+0.911	+0.781	+0.697	*+0.652*	+0.631
+3.2	+1.263	+1.082	+0.924	+0.804	+0.729	*+0.689*
+3.6	+1.456	+1.266	+1.089	+0.937	+0.825	+0.757
+4.0	+1.653	+1.458	+1.269	+1.095	+0.949	+0.844
+4.4	+1.851	+1.654	+1.460	+1.272	+1.101	+0.960
+4.8	+2.051	+1.851	+1.654	+1.461	+1.275	+1.107
+5.2	+2.250	+2.051	+1.851	+1.655	+1.462	+1.278
+5.6	+2.450	+2.250	+2.051	+1.851	+1.655	+1.463
+6.0	+2.650	+2.450	+2.250	+2.051	+1.851	+1.656
	log W/b for $B^{(0)}/B^{(1)}=\frac{7}{8}$					
−2.8	−2.973	−2.973	−2.973	−2.973	−2.973	−2.973
−2.4	−2.573	−2.573	−2.573	−2.573	−2.573	−2.573
−2.0	−2.175	−2.175	−2.175	−2.175	−2.175	−2.175
−1.6	−1.779	−1.779	−1.779	−1.780	−1.780	−1.780
−1.2	−1.387	−1.387	−1.388	−1.388	−1.389	−1.389
−0.8	−1.004	−1.008	−1.009	−1.009	−1.010	−1.010
−0.4	−0.645	−0.651	−0.654	−0.655	−0.656	−0.656
0.0	−0.325	−0.337	−0.343	−0.345	−0.346	−0.346
+0.4	−0.057	−0.078	−0.087	−0.091	−0.093	−0.094
+0.8	+0.161	+0.128	+0.114	+0.107	+0.105	+0.103
+1.2	*+0.344*	+0.295	+0.271	+0.261	+0.257	+0.255
+1.6	+0.508	*+0.436*	+0.399	+0.383	+0.376	+0.373
+2.0	+0.668	+0.568	*+0.510*	+0.482	+0.470	+0.465
+2.4	+0.833	+0.704	+0.618	*+0.571*	+0.550	+0.540
+2.8	+1.009	+0.853	+0.735	+0.661	*+0.622*	+0.604
+3.2	+1.194	+1.019	+0.871	+0.763	+0.697	*+0.664*
+3.6	+1.386	+1.199	+1.028	+0.887	+0.787	+0.729
+4.0	+1.581	+1.388	+1.203	+1.037	+0.902	+0.810
+4.4	+1.779	+1.582	+1.390	+1.207	+1.045	+0.916
+4.8	+1.978	+1.779	+1.583	+1.392	+1.211	+1.053
+5.2	+2.178	+1.978	+1.779	+1.584	+1.394	+1.215
+5.6	+2.378	+2.178	+1.978	+1.779	+1.585	+1.396
+6.0	+2.578	+2.378	+2.178	+1.978	+1.779	+1.586

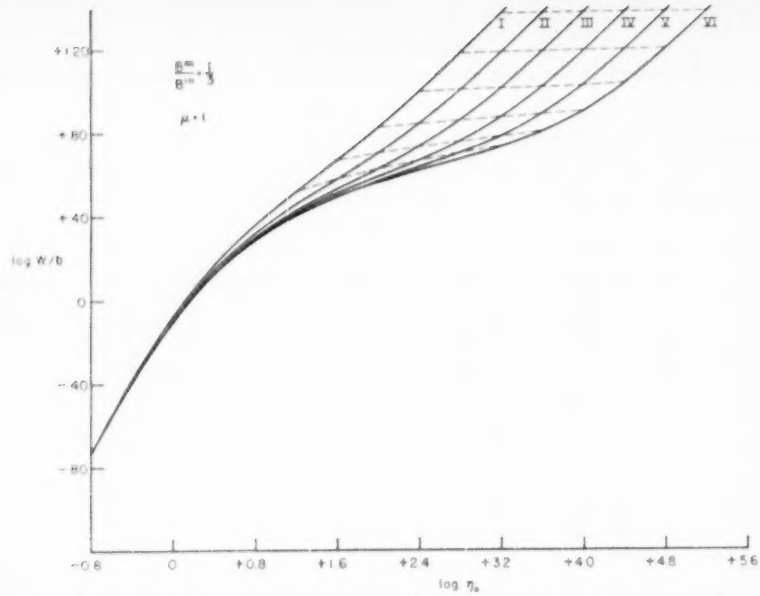

FIG. 1.—Theoretical curves of growth for $B^{(0)}/B^{(1)} = \frac{1}{3}$, $\mu = 1$: curve *I*, log $a = -1.0$; curve *II*, log $a = -1.4$; curve *III*, log $a = -1.8$; curve *IV*, log $a = -2.2$; curve *V*, log $a = -2.6$; curve *VI*, log $a = -3.0$.

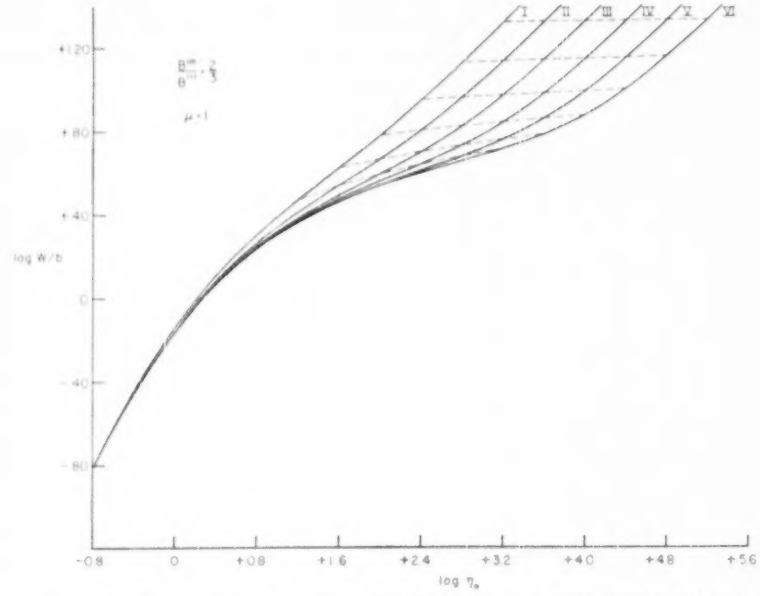

FIG. 2.—Theoretical curves of growth for $B^{(0)}/B^{(1)} = \frac{2}{3}$, $\mu = 1$; same notation as Fig. 1

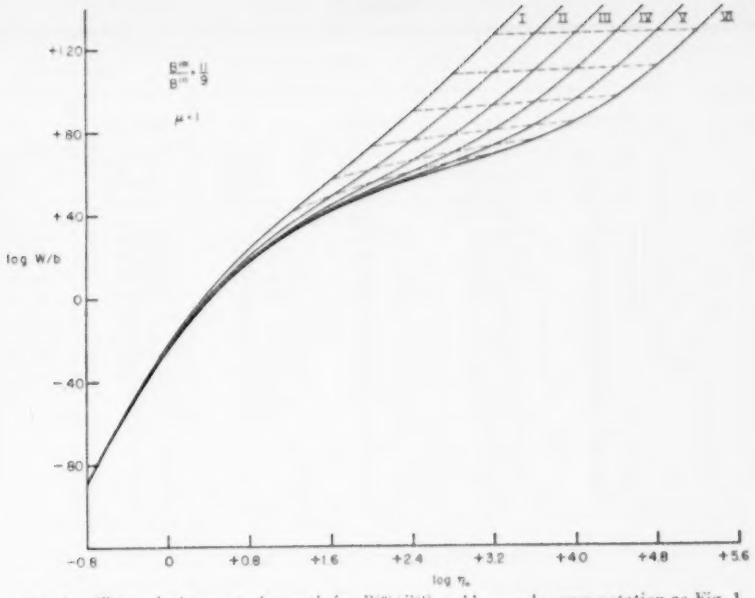

FIG. 3.—Theoretical curves of growth for $B^{(0)}/B^{(1)} = \frac{11}{9}$, $\mu = 1$: same notation as Fig. 1

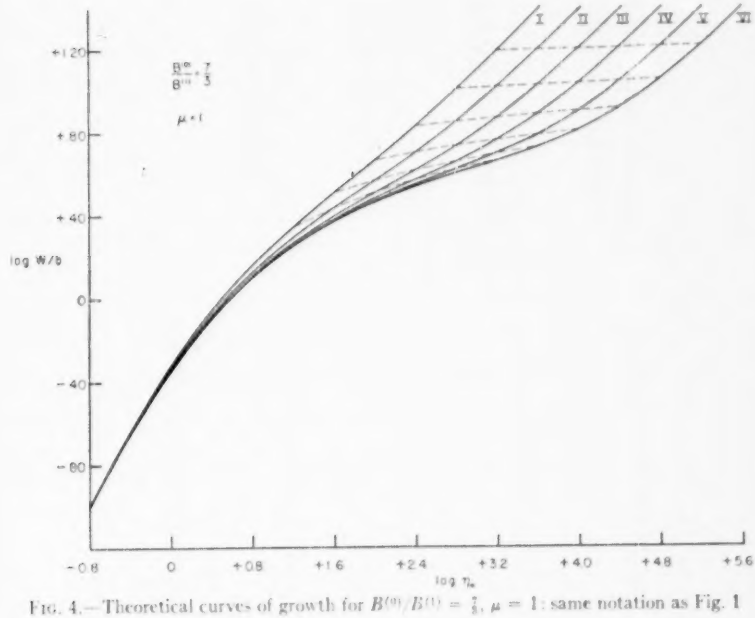

FIG. 4.—Theoretical curves of growth for $B^{(0)}/B^{(1)} = \frac{7}{5}$, $\mu = 1$: same notation as Fig. 1

TABLE 2

log η_0	log $a=-3.0$		log $a=-2.6$		log $a=-2.2$	
	$(W/b)_{2/3}$	$-D$	$(W/b)_{2/3}$	$-D$	$(W/b)_{2/3}$	$-D$
−0.8	0.1541	0.0282	0.1542	0.0283	0.1543	0.0283
−0.4	0.3430	0.0612	0.3431	0.0612	0.3438	0.0613
0.0	0.6801	0.1149	0.6811	0.1150	0.6827	0.1153
+0.4	1.163	0.179	1.166	0.179	1.170	0.180
+0.8	1.731	0.231	1.736	0.232	1.748	0.235
+1.2	2.319	0.260	2.330	0.262	2.358	0.267
+1.6	2.893	0.267	2.917	0.271	2.977	0.282
+2.0	3.442	0.262	3.495	0.271	3.623	0.293
+2.4	3.975	0.253	4.091	0.273	4.370	0.322
+2.8	4.526	0.253	4.782	0.298	5.379	0.401
+3.2	5.168	0.276	5.727	0.374	6.952	0.582
+3.6	6.058	0.349	7.230	0.551	9.589	0.938
+4.0	7.499	0.524	9.795	0.906	14.02	1.56
+4.4	9.997	0.877	14.16	1.53	.....	.....
+4.8	14.31	1.50	.....	.....	.....	.....
+5.2	21.50	2.54	.....	.....	.....	.....
+5.6	33.22	4.18	.....	.....	.....	.....
+6.0	52.04	6.76	.....	.....	.....	.....

log η_0	log $a=-1.8$		log $a=-1.4$		log $a=-1.0$	
	$(W/b)_{2/3}$	$-D$	$(W/b)_{2/3}$	$-D$	$(W/b)_{2/3}$	$-D$
−0.8	0.1545	0.0284	0.1551	0.0285	0.1562	0.0287
−0.4	0.3449	0.0614	0.3473	0.0619	0.3528	0.0633
0.0	0.6869	0.1162	0.6961	0.1183	0.7189	0.1231
+0.4	1.182	0.182	1.212	0.189	1.281	0.202
+0.8	1.779	0.240	1.852	0.254	2.023	0.286
+1.2	2.425	0.279	2.587	0.308	2.956	0.374
+1.6	3.121	0.307	3.462	0.366	4.205	0.492
+2.0	3.930	0.346	4.623	0.463	6.041	0.695
+2.4	5.010	0.431	6.361	0.654	8.923	1.055
+2.8	6.663	0.616	9.158	1.012	13.56	1.67
+3.2	9.376	0.973	13.72	1.63	20.99	2.68
+3.6	13.87	1.60	.....	.....	32.88	4.28
+4.0	.....	.....	.....	.....	51.81	6.83
+4.4	.....	.....	.....	.....	81.87	10.86
+4.8	.....	.....	.....	.....	129.7	17.3
+5.2	.....	.....	.....	.....	205.4	27.4
+5.6	.....	.....	.....	.....	325.5	43.4
+6.0	.....	.....	.....	.....	515.7	68.8

TABLE 3

Log W/b	Log a					
	−1.0	−1.4	−1.8	−2.2	−2.6	−3.0
	$\Delta \log \eta_0$ for $B^{(0)}/B^{(1)} = \frac{1}{9}$					
−0.8	+0.08	+0.08	+0.08	+0.08	+0.08	+0.08
−0.6	+ .08	+ .08	+ .08	+ .08	+ .08	+ .08
−0.4	+ .09	+ .09	+ .09	+ .09	+ .09	+ .09
−0.2	+ .09	+ .09	+ .10	+ .10	+ .10	+ .10
0.0	+ .10	+ .11	+ .11	+ .11	+ .11	+ .11
+0.2	+ .12	+ .13	+ .14	+ .14	+ .14	+ .14
+0.4	+ .13	+ .15	+ .16	+ .17	+ .18	+ .18
+0.6	+ .13	+ .14	+ .15	+ .17	+ .18	+ .20
+0.8	+ .11	+ .11	+ .11	+ .12	+ .12	+ .12
+1.0	+ .11	+ .11	+ .10	+ .10	+ .10	+ .10
+1.2	+ .11	+ .11	+ .11	+ .10	+ .10	+ .10
+1.4	+ .11	+ .11	+ .11	+ .11	+ .11	+ .11
+1.6	+ .11	+ .11	+ .11	+ .11	+ .11	+ .11
+1.8	+ .11	+ .11	+ .11	+ .11	+ .11	+ .11
+2.0	+0.11	+0.11	+0.11	+0.11	+0.11	+0.11
	$\Delta \log \eta_0$ for $B^{(0)}/B^{(1)} = \frac{1}{3}$					
−0.8	−0.10	−0.10	−0.10	−0.10	−0.10	−0.10
−0.6	− .10	− .10	− .10	− .10	− .10	− .10
−0.4	− .10	− .11	− .11	− .11	− .11	− .11
−0.2	− .12	− .12	− .12	− .12	− .12	− .12
0.0	− .13	− .13	− .14	− .14	− .14	− .14
+0.2	− .14	− .15	− .16	− .16	− .16	− .16
+0.4	− .15	− .16	− .17	− .18	− .18	− .19
+0.6	− .14	− .14	− .15	− .17	− .17	− .18
+0.8	− .13	− .13	− .13	− .13	− .13	− .13
+1.0	− .12	− .12	− .12	− .12	− .12	− .12
+1.2	− .12	− .12	− .12	− .12	− .12	− .12
+1.4	− .12	− .12	− .12	− .12	− .12	− .12
+1.6	− .12	− .12	− .12	− .12	− .12	− .12
+1.8	− .12	− .12	− .12	− .12	− .12	− .12
+2.0	−0.12	−0.12	−0.12	−0.12	−0.12	−0.12
	$\Delta \log \eta_0$ for $B^{(0)}/B^{(1)} = \frac{7}{9}$					
−0.8	−0.22	−0.22	−0.22	−0.22	−0.22	−0.22
−0.6	− .22	− .23	− .23	− .23	− .23	− .23
−0.4	− .24	− .24	− .24	− .24	− .24	− .24
−0.2	− .26	− .26	− .27	− .27	− .27	− .27
0.0	− .28	− .29	− .30	− .30	− .30	− .30
+0.2	− .30	− .32	− .33	− .34	− .34	− .34
+0.4	− .31	− .33	− .35	− .36	− .37	− .38
+0.6	− .29	− .30	− .31	− .33	− .35	− .37
+0.8	− .28	− .28	− .27	− .27	− .27	− .27
+1.0	− .27	− .27	− .26	− .26	− .26	− .25
+1.2	− .27	− .27	− .26	− .26	− .26	− .26
+1.4	− .27	− .26	− .26	− .26	− .26	− .26
+1.6	− .27	− .27	− .27	− .27	− .27	− .27
+1.8	− .27	− .27	− .27	− .27	− .27	− .27
+2.0	−0.27	−0.27	−0.27	−0.27	−0.27	−0.27

A comparison of these curves with those of Paper I shows that the $\mu = 1$ curves are shifted to the left with respect to the total flux-curves for the same value of $B^{(0)}/B^{(1)}$. This is not a simple lateral shift in which a constant $\Delta\eta_0$ is subtracted from each value of η_0 of the total flux-curve to give the corresponding curve for $\mu = 1$. Nor can one set of curves be constructed from the other by choosing a suitable value of m in equation (4), below. Neither method gives the true shape of the important transition region between $\eta_0 = 0.0$ and $\eta_0 = 2.4$.

Since these curves make use of an exact solution of the equation of transfer, they are free from *mathematical* approximations which have no physical counterpart. Differences between observations and these curves may therefore be considered as indicative of true *physical* factors to be investigated. For example, these curves apply, strictly speaking, only to resonance lines, and their application to other lines introduces an error difficult to estimate. Further, non-Maxwellian turbulent velocities in the atmosphere would introduce new terms in the absorption coefficient. Advances in the theory of turbulence should result in a method for taking these terms into account.

USE OF TABLES

Interpolation in log a for constant $B^{(0)}/B^{(1)}$.—For moderate values of η_0, interpolation for different values of the damping may easily be done directly across Table 1. For values of W/b lying below the value in italics, it is more convenient to interpolate along lines of constant $a\eta_0$. In Figures 1–4, which accompany the tables, the dotted lines are lines of constant $a\eta_0$.

Interpolation in $B^{(0)}/B^{(1)}$ *with log a and log* η_0 *constant.*—It follows directly from the form of r_ν that there is a constant difference between numerical values of W/b (not the logarithms) for the four values of $B^{(0)}/B^{(1)}$ tabulated, provided that log a and log η_0 are constant. In order to find W/b for intermediate values of $B^{(0)}/B^{(1)}$, it is necessary only to multiply this difference by a numerical factor m and add it to the initial value. Table 2 gives the value of W/b for $B^{(0)}/B^{(1)} = \frac{2}{3}$, as well as the difference, D; further,

$$\left(\frac{W}{b}\right)_{B^{(0)}/B^{(1)}} = \left(\frac{W}{b}\right)_{2/3} + mD\,, \tag{4}$$

$$m = \frac{4\,(B^{(0)}/B^{(1)} - 2/3)}{B^{(0)}/B^{(1)} + 1}\,. \tag{5}$$

It follows that m is -1, 1, and 2 for $B^{(0)}/B^{(1)}$ equal to $\frac{1}{3}$, $\frac{1}{9}^{1}$, and $\frac{2}{3}$, respectively. It was convenient in constructing these tables to compute curves for values of $B^{(0)}/B^{(1)}$ which corresponded to integral values of m. That is the reason $\frac{1}{9}^{1}$ and $\frac{2}{3}$ were used instead of $\frac{1}{3}$ and $\frac{1}{3}^{0}$. Curves for $\frac{1}{3}$ and $\frac{1}{3}^{0}$ can easily be constructed by using the above equations.

Reduction to a single curve of growth.—In order to compare data from different parts of the spectrum with a single curve of growth, it is necessary to be able to reduce all values of $B^{(0)}/B^{(1)}$ to a single value. If log W/b and log a are kept constant, a correction, Δ log η_0, may be added to η_0 to reduce all observations to a single curve for $B^{(0)}/B^{(1)} = \frac{2}{3}$. These corrections, obtained by interpolation in Table 1, are given in Table 3.

It is once again a pleasure to thank my wife for drawing the accompanying figures.

THE THERMODYNAMIC STRUCTURE OF THE OUTER SOLAR ATMOSPHERE. I. THE GENERAL METHOD OF ANALYSIS AND PRELIMINARY RESULTS*

RICHARD N. THOMAS
University of Utah†
Received September 15, 1949

ABSTRACT

The anomalous Balmer decrement in the solar flash spectrum is shown to result from self-absorption. The effect is analyzed numerically to obtain the population of the Balmer ground state as a function of height and thence an estimate of the kinetic temperature gradient. These results are combined with the Balmer emission decrement to obtain an estimate of the kinetic temperature, its gradient, and the electron density gradient.

I. INTRODUCTION: THE PROBLEM OF THE THERMODYNAMIC STRUCTURE OF THE OUTER SOLAR ATMOSPHERE

A value of the order of 10^{6}° K for the kinetic temperature of the solar corona seems conclusively established by several kinds of data.[1] The existence in the lower chromosphere of a value intermediate to the above and to the photospheric value seems equally well established observationally by Redman's measures of line profiles.[2] Thus one infers the presence of a kinetic temperature gradient that is positive outward. However, the observational results have as yet provided little in the way of a detailed description of the thermodynamic structure of the solar atmosphere in the region of the positive kinetic temperature gradient.

Several attempts have been made to provide a mechanism to explain the positive kinetic temperature gradient,[3] and thence to derive theoretically the detailed atmospheric structure that has not come directly from observations. Two difficulties have hindered these attempts. First, the numerical parameters characterizing the various suggested mechanisms are in each case only incompletely known from observations. Hence a certain incompleteness remains in the predictions made by each theory. Second, each of the suggested mechanisms has a certain amount of observational confirmation. Hence a detailed comparison of the theoretical predictions with the atmospheric structure becomes necessary for a choice between them. The essential difficulty lies in the fact that our customary models of stellar atmospheres are no longer adequate in these outer atmospheric regions, and we are at once attempting to learn just where they are inadequate (from an empirical study of the atmospheric structure) and to provide a new theoretical structure to take up where the old leaves off.

One of the above-mentioned attempts at providing a mechanism has been made by the present author.[4] The attempt led into a general question regarding the direction of departure of the physical state of the atmosphere from the predictions of the older models,

* Publication of this paper is supported by the University of Utah Research Fund.

† A part of the calculations in the present paper was performed while the author was a Frank B. Jewett Fellow at the Institute for Advanced Study.

[1] Edlén, *Ark. f. Mat. Astr. och Fys.*, Vol. **28B**, No. 1, 1941; Lyot, *M.N.*, **91**, 580, 1939; Grotrian, *Zs. f. Ap.*, **8**, 124, 1934.

[2] *M.N.*, **102**, 140, 1942.

[3] Bierman, *Zs. f. Ap.*, **25**, 161, 1948; Schwarzschild, *Ap. J.*, **107**, 1, 1948; Thomas, *Ap. J.*, **108**, 130, 1948; Miyamoto, *Pub. Astr. Soc. Japan*, **1**, 14, 1949.

[4] *Op. cit.*

independent of the mechanism. Quite apart from the detailed results of the investigation, one general conclusion holds, independent of all assumptions except that the kinetic temperature exceeds the effective temperature. (This assumption is the primary observational fact.) The general conclusion states that the population of any level will exceed that given by the Boltzmann distribution for the same kinetic temperature and electron density. Taking the observed values for these last two parameters, one finds that the optical depth in the Balmer series exceeds by a factor of 100 or so that obtained under the older models. Hence the self-absorption term in the hydrogen flash spectrum becomes more important than was realized earlier, and it was suggested that the Balmer decrement of the flash spectrum was no longer anomalous when the self-absorption term was included.

This realization that the hydrogen self-absorption cannot be legitimately neglected in many of the cases where it has been customary to do so provides a powerful tool for investigating the detailed atmospheric structure just mentioned; for a knowledge of the absorption as a function of height means a knowledge of the number of hydrogen atoms in the ground state of the Balmer series as a function of height. Therefore, in the present series of papers an attempt will be made to obtain the structure of the solar atmosphere from eclipse observations of the hydrogen flash spectrum. The present paper outlines the method and applies it to the 1932 eclipse. The results will be seen to justify confidence in the applicability of the method. Two points should be emphasized. First, while old data are to be reanalyzed, the results are quite independent of any of the modern theoretical attempts to explain the structure of the solar atmosphere. The analysis rests only upon the observation that the kinetic temperature rises in the atmosphere and that self-absorption is therefore likely to be important. The *amount* of self-absorption comes from the observations themselves and not from the theoretical structure which indicated that self-absorption might be present. The fact that the theoretical prediction of the amount of self-absorption[5] agrees satisfactorily with the observed value does not reflect an inclusion of the theory into the analysis for self-absorption. Second, the results rest only upon *relative* photometry in the region λλ 4000–3500. This fact might perhaps be put to use at the time of the next eclipse. It is surprising how little material on the Balmer lines exists in eclipse photometry. Restricting the spectral region to this limited range and attempting to obtain only relative intensities should materially simplify the lot of the eclipse observer who is attempting photometry.

II. SELF-ABSORPTION, THE NUMBER OF ABSORBING ATOMS, AND THE DENSITY-HEIGHT GRADIENT

The eclipse values refer to the emission along the line of sight and above a certain height. We may then write for the emission within a line (cf. eq. [57] of Paper III)

$$E_{n2}dv = C_1\varpi_n\nu_{n2}A_{n2}\int_h^\infty\int_{-\infty}^{\infty} b_n N_e^2 T_e^{-3/2}\, e^{X_n}\, e^{-N(y,\,x)a_{n2}} dy\, dx\, dv\,, \tag{1}$$

$$N(y,\,x) = C_2\int_y^\infty b_2 N_e^2 T_e^{-3/2}\, e^{X_2} dy\,, \tag{2}$$

where the C_i's are numerical constants and the other notation is standard. The Balmer decrement corresponds to a differentiation, or differencing, of equation (1) with respect to the quantum number n. We obtain

$$\frac{\Delta_n E_{n2}}{C_1} = (\ldots)\iint[\ldots]\left\{\frac{\Delta_n b_n}{b_n} + \frac{2X_n}{n} - \frac{3Na_{n2}}{n}\right\} + \Delta_n(\varpi_n\nu_{n2}A_{n2})\iint[\ldots] \tag{3}$$

$$\Delta_n \to f(n) - f(n+k)\,,$$

[5] Thomas, *Ap. J.*, **108**, 142, 1948; **109**, 480, 1949. Hereafter referred to as "Paper III."

since the absorption coefficient, a_{n2} varies as n^{-3} and where the brackets contain positive quantities whose specific expression is immediately obvious from equation (1). The inequality signs below each term indicate the effect of the term on the sign of the left-hand side of the equation. We see that only the third term—that coming from the self-absorption—gives a negative contribution. The result will assume significance in the discussion of Table 1.

We note that an integration of equation (1) must lead to some expression with the term $\varpi_n \nu_{n2} A_{n2}$ as a multiplicative factor. That is, we might expect equation (1) to become something like this:

$$E_{n2} = Kn^2 A_{n2} \nu_{n2}\, e^{X_n} b_n \,(\text{absorption})\,, \tag{1a}$$

and hence, differencing logarithmically, equation (3) to become something like this:

$$\Delta_n ln E_{n2} = \Delta_n ln\,(n^2 \nu_{n2} A_{n2}) + (X_n - X_{n+k}) + ln\,\frac{b_n}{b_{n+k}} + ln\,\frac{\text{abs}_n}{\text{abs}_{n+k}}\,, \tag{3a}$$

$$\overset{\vee}{0} \qquad \overset{\vee}{0} \qquad \overset{\vee}{0} \qquad \overset{\vee}{0} \qquad \overset{\wedge}{0}$$

where the last three factors now refer to properly weighted averages over the atmosphere. Effectively, the contribution to these terms comes from the lowest region observed and

TABLE 1

THE BALMER DECREMENT

n	C	O			
		670 Km	1500 Km	2330 Km	3170 Km
25–30	0.24	0.20			
20–25	.29	.23	0.30		
15–20	.37 (0.38)	.29	.32		
10–15	.53 (.54)	.31	.34	0.43	
10–13	0.34 (0.35)	0.13	0.14	0.24	0.29

that portion nearest the intersection of the line of sight with the solar radius orthogonal to it. In any event, if we now compare the observed Balmer decrement[6] with the predicted decrement, using the first term on the right-hand side of equation (3*a*) alone (which corresponds to the last term of eq. [3] alone), we obtain the results given in Table 1. The first column gives the two emission lines compared. The second column contains the logarithm of the relative intensities computed from the first term on the right of equation (3*a*) alone. That is, this column gives the value that one would observe were the atmosphere transparent to its own radiation and in thermodynamic equilibrium. The effect of the X_n term is small, and the result of including it is shown by the bracket value in the same column. The third to sixth columns contain the observed values of the logarithm of the intensity ratios. We note that in each case the observed value is less than the value of the second column but that the difference decreases as one progresses to the series head for a given height or to the greater height for a given pair of lines. This is the behavior to be expected of self-absorption. Further, we see from either the exact equation (3) or the "expected" equation (3*a*) that neither the departure from thermodynamic equilibrium (measured by the b_n) nor the effect of a bad guess at the kinetic temperature (reflected in the X_n) has the correct sign to bring about agreement between the second column and the third to the sixth columns. We have here, then, a quantitative verification of the suggestion that self-absorption effects are at the base of the apparent anomaly

[6] Menzel and Cillié, *Harvard Obs. Circ.*, **410**, 1935.

in the behavior of the Balmer decrement. Moreover, noting the behavior of the difference between computed (second col.) and observed decrement as a function of height, it would appear that Table 1 contains a numerical measure of the height decrement of the number of atoms in the ground state of the Balmer series. To obtain this numerical measure, one must have an explicit expression for the absorption term in equation (*3a*).

In Paper III, equation (60*b*), such an equation as (*3a*) was obtained under the assumption that the atmosphere was isothermal and that the b_n's were constant. This assumption, while certainly invalid in a strict sense, is, however, of some use in obtaining a preliminary estimate of the structure of the chromosphere, for reasons already mentioned above. Namely, most of the contribution to the observed emission comes from a rather small region near the base of the observed atmospheric sector. From equation (60*b*) of Paper III we then have, for the absorption term under this assumption,

$$\text{Absorption} = 1 + \Sigma(-1)^m \frac{(N_2 a_{n2})^m}{m!}(m+1)^{-3/2}\left(1 + \frac{m!}{2!\,(m-2)!}\,I_2 + \dots\right), \quad (4)$$

where N_2 is the number of atoms in the second level along the line of sight and

$$I_j = \frac{2}{\sqrt{\pi}}\int_0^\infty e^{-s^2} g^j(s^2)\,ds\,, \qquad g(s^2) = \frac{2}{\sqrt{\pi}}\int_0^s e^{-s^2} ds\,. \quad (5)$$

The terms involving the X_n and b_n in equation (*3a*) are certainly small, at least for $n > 10$; and so we introduce no error larger than that already allowed with the use of equation (*3a*) rather than (*3*) and constant b_n if we assume that the difference between the second

TABLE 2

THE POPULATION OF THE BALMER GROUND STATE

Height (km)	670	1500	2330	3170
$N_2 a_{n2}$	0.45	0.096	0.039	0.025
$N_2 \cdot 10^{-16}$	1.20	0.26	0.105	0.067
ln grad $N_2 \cdot 10^8$		−1.86	−1.07	−0.54

column and the third to sixth columns of Table 1 comes only from the absorption term. (We note, further, that any error acts to underestimate the absorption.) Further, by taking from Table 1 the top entry in each column,[7] we work in the region of quickest convergence of equation (4) and hence minimize any error as much as possible. (The procedure discards a great deal of useful data, of course.) Since equation (4) is a function only of the number of atoms along the line of sight that are in the Balmer ground state, equations (*3a*) and (4) coupled with Table 1 immediately give the number of atoms along the line of sight at any given level.

Table 2 contains the result of the solution for the self-absorption. The second row exhibits the value of the optical depth in H_{30} at the various heights, reduced from the particular optical depth computed from equation (6) for purposes of comparison. In the third row, N_2 is the number of atoms along the line of sight in the Balmer ground state. We note that the values exceed by a factor of 100 or so the values found earlier by Menzel and Cillié[6] in a specific application of the classical ideas of the chromospheric temperature to the earlier members of the Balmer series. Our higher value agrees with the predictions of Paper III. The logarithmic height gradient of the population of the ground state of the Balmer series is given in the fourth row.

[7] With the exception of the fourth column, where the second entry is used.

III. THE KINETIC TEMPERATURE GRADIENT

a) THE EMISSION HEIGHT GRADIENT AND ITS INTERPRETATION

It is instructive at this point to compare the method of the preceding section, whereby we obtained the height gradient of the number of atoms in the second quantum level, with the procedure customarily used to obtain the hydrogen density gradient in the chromosphere. The method of Section II has as its basis the determination of the absolute number of second-level hydrogen atoms at a particular atmospheric height. Only relative intensities of lines at the same height are used, and the effects of density and temperature gradient nearly cancel out of the computation. The information on height gradient comes from a comparison of the absolute numbers of second-level hydrogen atoms at two different heights. In the customary computations for the hydrogen density gradient, on the other hand, one compares relative intensities of lines at different heights. The more usual procedure is a null-balance technique,[8] i.e., one compares the heights at which the various hydrogen emission lines disappear. This last method has the advantage that it does not require the numerical measure of line intensities and that self-absorption effects are minimized. The disadvantage lies in the fact that, in general, observers do not obtain a continuous height-versus-spectrum record. The general application of the customary method then requires a comparison of measured line intensities at different heights.

If one obtained the intensity of the same line at different heights and put in the correction for differential self-absorption found in Section II, one would have a measure of the height gradient of the number of atoms in the upper level of the line. The measure would be essentially equivalent to that in Table 2 for the atoms in the second level. In the null method discussed above, the height gradient is a blend of the gradients in the two (or more) levels concerned. We see immediately that, even in an atmosphere of constant excitation state, the general method of comparison of line intensities and the null method would not give the same result; for the null method rests upon a knowledge of the relative numbers of atoms in the two excitation levels which is necessary to reduce to equivalent intensities. Hence the b_n ratio enters directly into the density gradient. That is, we compare the (higher) point in the atmosphere where the earlier Balmer line reaches the same intensity as the later Balmer line at a lower point. Since the b_n for the lower quantum level exceeds that for the higher, we must expect to traverse a greater difference in height for the points of equal intensity than we would, were all the b_n unity. Hence we expect to obtain a lower (apparent) density gradient from the null method than from either the method of comparing intensities of the same line or from the gradient of the population of the second level in Table 2. An example of the situation results from a comparison of the results of Wildt,[8] based on the null method; of Menzel and Cillié,[6] based on the intensities of the same line at different heights; and of our Table 2. Wildt obtains $0.92 \cdot 10^{-8}$ for the logarithmic emission gradient; Menzel and Cillié, $1.54 \cdot 10^{-8}$; and Table 2, $1.8 \cdot 10^{-8}$ (for comparable heights; units cm^{-1}). The value of Menzel and Cillié, incidentally, is that for the higher series members and is uncorrected for self-absorption effects.

We note further that it has been customary to identify the height gradient determined by either of the above methods with the height gradient of hydrogen. If the excitation state were constant with height, the identification would be valid. Constancy of excitation state, however, requires constancy of the factor (for given n):

$$b_n e^{\chi_n} N_e T_e^{-3/2} \qquad (6)$$

[8] Cf., e.g., Wildt, *Ap. J.*, **105**, 78, 1947.

(since the hydrogen is effectively all ionized in the region here under discussion). Without a more detailed model of the atmosphere, this assumption hardly seems justified.[9]

We then have the problem of separating the apparent gradient into the contribution from the gradient of hydrogen (electron density) and from the gradient of electron temperature. It is possible to form a rough estimate of the separation, again using only the data from the self-absorption solution but assuming the kinetic temperature known at one point.

b) THE KINETIC TEMPERATURE GRADIENT

We may represent the number of atoms in the second level as follows:

$$n_2 = K N_e^2 T_e^{-3/2} b_2 e^{X_2}; \tag{7}$$

and, differentiating logarithmically, we obtain

$$\frac{d\ln n_2}{dh} = \frac{d\ln N_e^2}{dh} - \frac{d\ln T_e}{dh}\left(\frac{3}{2} + X_2\right) + \frac{d\ln b_2}{dh}. \tag{8}$$

We note that the assumption of hydrostatic equilibrium seems justified for the solar chromosphere in the large. Then, since the hydrogen is effectively all ionized, we may write the equation of hydrostatic equilibrium in the following form:

$$0 = \frac{d\ln N_e^2}{dh} + 2\,\frac{d\ln T_e}{dh} + 2\,\frac{\mu m_H}{kT_e}\,g. \tag{9}$$

Solving for the kinetic temperature and electron density gradients, we have

$$\frac{dT_e}{dh} = 0.75 \cdot 10^{-4} + 0.76 \cdot 10^{4}\,\frac{d\ln b_2}{dh}, \tag{10}$$

$$\frac{d\ln N_e^2}{dh} = -1.3 \cdot 10^{-8} - 0.43\,\frac{d\ln b_2}{dh}, \tag{11}$$

where the values $T_e = 3.5 \cdot 10^4$, $N_e = 2 \cdot 10^{11}$, and the entry in Table 2 at the lowest height have been used. The quantity $d\ln b_2/dh$ cannot be accurately calculated until a model of the complete atmosphere is at hand. However, neglecting it gives a lower limit to the gradients (since its value is positive). An upper limit, based on substituting b_1 for b_2, can be set at about $5 \cdot 10^{-5}\text{cm}^{-1}$ for these conditions of temperature and density.[10] We may therefore conclude that the kinetic temperature gradient comes out positive, with a value roughly near $1\text{–}5 \cdot 10^{-4}$ deg/cm^{-1}, or corresponding to a rise of $10^5\text{–}5 \cdot 10^5$° K across the chromosphere. The corresponding electron density-gradient values are $1.3\text{–}3.5 \cdot 10^{-8}$ cm^{-1}.

Thus, we note that a first, crude analysis of the anomalous behavior of the flash-spectrum Balmer decrement in terms of self-absorption serves to predict not only a positive kinetic temperature gradient but one whose numerical value is roughly that required to reach the million-degree mark in the corona. Since these self-absorption effects in the chromospheric hydrogen emission lines have heretofore been neglected, it would seem that we now have an additional set of observational material for use in obtaining the thermodynamic structure of the solar atmosphere.

[9] We note, however, that we cannot completely discount the assumption from an observational standpoint. The observed relation between height of disappearance of emission line and relative effective number of emitting atoms (used in the null method) is nearly linear for the higher series members. This set of observations is a necessary condition for the validity of the excitation assumption, but not sufficient. Any satisfactory description of the solar atmosphere must comply with these observations. It may be, of course, that more careful determination of these relations will show a departure from linearity.

[10] From the data in Paper III.

In the foregoing no attempt has been made to combine the data from self-absorption with that from the more customary methods of analysis. It is fairly obvious that we have not used all the data obtained from the self-absorption effects, or used them completely properly. One has also been made aware, by the remarks of Section III*a*, of the incompleteness of the customary methods of analysis. The point of these remarks becomes clear when one notes that a combination of the self-absorption data with the emission height-gradient data calls for a comparison of the height gradients determined by the two methods. Consequently, any incompleteness in the two determinations appears one order more significant in their combination. With these remarks of caution as to the reliability of the result or conclusions to be drawn therefrom, we proceed finally to consider this combination of height gradients from self-absorption and from emission.

c) SIMULTANEOUS DETERMINATION OF KINETIC TEMPERATURE, KINETIC TEMPERATURE HEIGHT GRADIENT, AND ELECTRON DENSITY HEIGHT GRADIENT

We have already (Sec. III*a*) noted the difference between the density gradient of the later members of the Balmer series and that of atoms in the second quantum level. The observation was made earlier that they both exceeded the gradient from the null method. Now our attention goes to the observation that the gradient in the second quantum level exceeds that in the higher; the values, respectively, are $1.86 \cdot 10^{-8}$ and $1.54 \cdot 10^{-8}$. If we use the results of Table 2 to correct the last gradient for the effects of self-absorption, we find a correction of some 10 per cent and a gradient of $1.68 \cdot 10^{-8}$.

We can now write down equation (8) for levels n and 2. (Menzel gives his density-gradient result as pertaining to the higher-series members. The self-absorption correction is based on $n = 30$, where the emission gradient seems essentially the value given.) Numerical values are substituted, and the X_n term is dropped in the equation for n, as its value is negligible compared with X_2. We also repeat equation (9), using numerical values:

$$(n=2) \qquad -1.86 \cdot 10^{-8} = \frac{d\ln N_e^2}{dh} - \frac{d\ln T_e}{dh}(1.5 + 3.86 \cdot 10^4 T_e^{-1}) + \frac{d\ln b_2}{dh}; \tag{12}$$

$$(n) \qquad -1.68 \cdot 10^{-8} = \frac{d\ln N_e^2}{dh} - \frac{d\ln T_e}{dh}\,1.5 + \frac{d\ln b_n}{dh}; \tag{13}$$

$$(9) \qquad 0 = \frac{d\ln N_e^2}{dh} + \frac{d\ln T_e}{dh}\,2 + 3.04 \cdot 10^{-4} T_e^{-1}. \tag{14}$$

We now have three equations in the three desired unknowns: kinetic temperature, its gradient, and the electron density gradient. The final equation is quadratic in the kinetic temperature, and the smaller solution seems the correct one from physical considerations. If we use as an estimate of $d\ln b_2/dh$ the upper limit used in Section III*b* and neglect $d\ln b_n/dh$, we obtain a complex number for the value of the kinetic temperature. None of the quantities can be so far in error that their true value would compensate for this result. Therefore, we conclude that either the change in $\ln b_2$ is considerably short of the upper-limit estimate or it is nearly the same as the change in $\ln b_n$. A discussion of the more likely of these possibilities is futile until a more complete study of the behavior of the b_n over the atmosphere is made. For the present we simply base our estimate on the physical situation corresponding to the lower limit of expression (10); we ignore the b_n and b_2 terms. We obtain the following results:

$$T_e = 2.3 \cdot 10^4 \,^\circ\mathrm{K}\,; \qquad \frac{dT_e}{dh} = 0.4 \cdot 10^{-4}\ \mathrm{cm}^{-1}\ \mathrm{deg}\,; \qquad \frac{d\ln N_e^2}{dh} = -1.51 \cdot 10^{-8}\ \mathrm{cm}^{-1}\,. \tag{15}$$

Had we used the other solution of the quadratic equation in T_e, the results would have been

$$T_e = 8 \cdot 10^4 \,^\circ\mathrm{K}\,;$$

$$\frac{dT_e}{dh} = 1.3 \cdot 10^{-4} \text{ deg cm}^{-1}\,; \qquad \frac{d \ln N_e^2}{dh} = -1.12 \cdot 10^{-8} \text{ cm}^{-1} \tag{15'}$$

Each of the values in expression (15) is reasonable. The kinetic temperature is the most poorly determined quantity, yet its value lies within some 25 per cent of the 35,000° value determined by Redman[2] from line contours in roughly the same atmospheric region. As mentioned earlier, the gradients of the populations in the two quantum levels from which the results come have been determined only by a first-approximation method. Since the gradients differ only by 12 per cent of their value and the third significant figure is quite uncertain, we should perhaps be surprised that the derived kinetic temperature value lies as close to the supposed value as it does. Once again, however, we do not seek to draw specific numerical conclusions from the results of the present section. We observe only that, if this first rough analysis permits roughly reasonable results, we have every reason to expect that a more precise analysis based on the present general methods will provide much useful information about the general atmospheric structure.

IV. SUMMARY

We regard the present paper as a presentation and rough test of a method of attack on the thermodynamic structure of the outer solar atmosphere. The basis of the method lies in the observation that the anomalous part of the flash-spectrum Balmer decrement is, in reality, a measure of the hydrogen self-absorption in the solar atmosphere. The numerical amount of the anomaly permits one to obtain the absolute number of atoms in the ground state of the Balmer series at each atmospheric height for which eclipse observations exist. These data may be combined with the relative populations of the higher Balmer levels, obtained from the emission lines corrected for the effect of self-absorption, to derive numerical values of the kinetic temperature, kinetic temperature gradient, and electron density gradient. These preliminary results indicate that the method promises sufficient detail and accuracy to warrant a more precise study.

PROTON-PROTON REACTIONS IN RED DWARF STARS

LAWRENCE H. ALLER
Observatory, University of Michigan
Received September 17, 1949

ABSTRACT

The relative roles of the carbon cycle and of proton-proton reactions in red dwarf stars such as Krueger 60A and o_2 Eridani C are studied with the aid of models calculated by Schwarzschild and Keller, in which the heavy stuff is taken as the Russell mixture and as oxygen, respectively. The proportions of carbon-plus-nitrogen are taken as 0.08 and 0.15 for the RM and O models, respectively.

The lifetime of the carbon cycle, taken from recent work at the California Institute of Technology, is 10^6 years for $\rho = 80$ gm/cm^3, $T = 20{,}000{,}000°$ K, and hydrogen content $X = 0.35$. The adopted value of the Fermi constant is 1.13×10^{-4} sec^{-1}.

Our problem is to find a pair of X (hydrogen content) and Y (helium content) values that satisfy the mass-luminosity relation for the model and for which observed and calculated energy outputs are equal. For the Russell mixture, two solutions are possible. In one, 60–70 per cent of the energy comes from the carbon cycle, and the balance is supplied by the proton-proton reaction. In the second solution all the energy is contributed by the proton-proton reaction. For Krueger 60A, $X = 0.11$, $Y = 0.64$, $T_c = 15{,}400{,}000°$ K, with 60 per cent of the energy supplied by the carbon cycle; or, alternatively, $X = 0.34$, $Y = 0.64$, and $T_c = 10{,}700{,}000°$ K, with proton-proton reactions delivering all of the energy. Stellar models in which the heavy material is all oxygen are always too bright.

No emphasis can be placed on the actual X and Y values, since the opacity law assumed for the sun cannot apply in red dwarfs, nor are the models valid when energy generation occurs outside the convective core. If further work shows that the composition approaches that of the oxygen model, it may be necessary to assume a structure consisting of two zones of different molecular weight.

INTRODUCTION

During the last decade the carbon cycle has been fairly securely established as the source of energy in main-sequence stars similar to, or brighter than, the sun. Recent attempts have been made to construct models for giant and supergiant stars in which the energy is produced in a small dense core by the same means.[1] Kelvin contraction or the transmutation of deuterium, lithium, boron, or beryllium are inadequate as sources of energy for these stars.

The carbon cycle is capable also of explaining the luminosities of main-sequence stars fainter than the sun, e.g., Krueger 60 and o_2 Eridani C. For these objects, however, another process may play an important role—the proton-proton reaction.[2] Two protons are jammed together to form a deuteron with the ejection of a β-particle. The deuteron captures a proton to form He^3, which then combines with ordinary He^4 to form Be^7, which captures an electron to form Li^7, which, in turn, captures a proton and breaks down into two α-particles. We shall show that in the cooler stars there is a very good chance that proton-proton reactions may play a role comparable with that of the carbon cycle or may even supply the total energy output of the star.

NUCLEAR REACTIONS IN THE COOLER STARS

In the red dwarf stars the central temperatures lie in the range from ten million to sixteen million degrees, whereas the densities are probably between two hundred and a thousand times that of water.

The basic experimental data for the carbon cycle have recently been improved by a group of workers at the California Institute of Technology, where the cross-sections for

[1] Cf. A. Reiz, *Ann. d'ap.*, **10**, 301, 1947; G. Gamow and G. Keller, *Rev. Mod. Phys.*, **17**, 125, 1945; and R. S. Richardson and M. Schwarzschild, *Ap. J.*, **108**, 373, 1948.

[2] H. Bethe and C. L. Critchfield, *Phys. Rev.*, **54**, 248, 1938.

proton capture by C^{12}, C^{13}, and N^{14} have been measured for energies in the neighborhood of 90–130 keV. I am indebted to Professor Robert F. Christy, of the Kellogg Radiation Laboratory of the California Institute of Technology, for communicating the results to me in advance of publication. The accuracy of the measurement for C^{12} and N^{14} is probably around 30 per cent. The background count at 100 keV is troublesome, and it is unlikely that measurements can be made at lower energies. In particular, the range of proton energies of importance for stellar energy generation lies far below the experimentally attainable range. Therefore, one must extrapolate the cross-sections measured in the neighborhood of 100 keV to much lower energies by some device such as the Condon-Gamow-Gurney formula. The extrapolation appears to be a reasonably safe one.

The rate of capture of protons by N^{14} determines the lifetime of the process, since all other nuclei, C^{12}, C^{13}, etc., persist for much shorter periods of time. At a temperature of 20,000,000° K, a density of 80 gm/cm³, and a hydrogen content $X = 0.35$ (Bethe's "standard conditions"), the lifetime of N^{14} is 1×10^6 years. We shall adopt this figure for our present calculations.

The essential steps of the carbon cycle have been checked in the laboratory. On the other hand, no direct experimental verification of the fundamental step in the proton-proton reaction, ${}_1H^1 + {}_1H^1 \longrightarrow {}_2H^1 + \epsilon^+$, appears possible. For the cross-section of this reaction we must rely on the theoretical work of Bethe and Critchfield and on the theory of β-decay.

The probability of the collision of two protons and the penetration of their mutual potential barrier may be calculated accurately, since the force between two protons is well known from scattering experiments. In order for a deuteron to be formed, a positron must be emitted during the encounter. According to the Fermi theory of β-decay,[3] the probability of emission of a positron (per second) is

$$B = g f(W) |G|^2 , \tag{1}$$

where g, the so-called Fermi constant, is adopted from the discussion by Konopinski[3] as 1.13×10^{-4} sec^{-1}, $f(W)$ is a known function of the energy W of the emitted β-particle, and G is the matrix element of the nuclear transition. The value of G will depend upon the selection rules for the transition. The initial and final nuclei will each have a specific total angular momentum, J. According to the Fermi selection rules, only the transitions for which $\Delta J = 0$ are permitted, whereas the Gamow-Teller selection rules allow $\Delta J = \pm 1$, but forbid $J = 0$ to $J = 0$. Bethe and Critchfield adopted the Gamow-Teller rules and calculated G by an integration over the space co-ordinates of the two protons for a rectangular potential well. If the Fermi selection rules were valid, the probability would be smaller by a factor of 10^5, and the proton-proton reaction would be negligible as a source of energy generation. At one time it was thought that the astrophysical evidence favored the Fermi rules, but the arguments were inconclusive.[4] The recent discussion of all available data by A. M. Feingold and E. P. Wigner[5] indicates that at least some β-transitions occur with $\Delta J = \pm 1$. At present it seems most likely that the Gamow-Teller rules are obeyed and that the proton-proton reaction does play a role in the red dwarf stars.

MODELS FOR RED DWARF STARS

Precise calculations of the relative roles of the proton-proton reaction and of the carbon cycle in M dwarf stars cannot be made at the present time for lack of a suitable stellar model. Although our results will be of only qualitative significance, it would appear worth while to survey the problem of the red dwarf stars from the point of view of the energy

[3] Cf. E. J. Konopinski, *Rev. Mod. Phys.*, **15**, 209, 1943.

[4] R. E. Marshak and H. A. Bethe, *Phys. Rev.*, **57**, 69, 1940; E. Schatzman, *Ann. d'ap.*, **8**, 197, 1945; and *Ap. J.*, **107**, 110, 1948.

[5] "The Type of Interaction in the Theory of β-decay" (kindly supplied in advance of publication).

generation with the aid of an approximate model. In a preliminary approach to the problem we shall adopt the models calculated for the sun by M. Schwarzschild[6] and G. Keller[7] and apply appropriate homology transformations. We must emphasize that such a procedure can yield only qualitative results. For example, the interpolation formulae employed by Schwarzschild and by Keller for the opacity are valid only for the range of densities and temperatures in the sun. In the red dwarf stars the constants in the interpolation formula will be different. Furthermore, a single expression of the type $\kappa \sim \rho^n T^m$, where n and m are constant, will not be valid throughout the whole interior, and, for higher accuracy, resort must be had to formulae of the "broken-line" type as employed by Marjorie H. Harrison.[8] That is, in one part of the star $n = n_1$, $m = m_1$, and in another part $n = n_2$, $m = m_2$.

The recent work of Ralph E. Williamson and G. F. D. Duff[9] has emphasized the difficulties inherent in the construction of models for red dwarf stars. The opacity formulae differ considerably from those for the sun, and the density of the core is higher than the value predicted from the Schwarzschild and Keller models. Still further refinements eventually must be taken into account. For example, the thermal conductivity of the stellar material becomes important if the gas approaches degeneracy.

In the conventional model for a star such as the sun, an envelope in radiative equilibrium is fitted to a convective core. The eigenvalue of the solution gives one relation between the mass, radius, and luminosity of the star and its chemical composition, i.e., the mass-luminosity law. A different assumption about the opacity will give another form of the mass-luminosity law. Schwarzschild assumed that the heavy stuff, which is responsible for the opacity, is the Russell mixture. At the other extreme, Keller supposed that the heavy material consisted entirely of oxygen. Thus Keller's model is more transparent than Schwarzschild's, and the central temperatures are lower. Both have given mass-luminosity curves for their models. Our problem is to find a pair of hydrogen X and helium Y contents that produces a star that falls on the mass-luminosity-curve and for which the observed and calculated energy outputs are equal.

THE ENERGY-OUTPUT RELATIONSHIP

The law of energy generation is usually written in the form

$$\epsilon = \epsilon_0 \rho T^\nu, \tag{2}$$

where ρ is the density, T is the temperature, and ϵ_0 depends on the composition and the cross-sections for the processes involved.

Hence the luminosity of the star will be

$$L = 4\pi \int \epsilon_0 \rho^2 T^\nu r^2 dr, \tag{3}$$

where the integration is performed throughout the region where energy is produced—usually in the convective core of the star.

The exact law of energy generation by the carbon cycle is of the form[10]

$$\epsilon \sim \rho \tau^2 e^{-\tau}, \tag{4}$$

where

$$\tau = 42.7 \, (Z_1 Z_2)^{2/3} \left(\frac{A}{T}\right)^{1/3} \tag{5}$$

[6] *Ap. J.*, **104**, 203, 1946.

[7] (Thesis, Columbia University) "The Physical and Chemical Composition of the Sun."

[8] *Ap. J.*, **108**, 310, 1948.

[9] *M.N.*, **109**, 55, 1949.

[10] H. Bethe, *Phys. Rev.*, **55**, 434, 1939; *Ap. J.*, **92**, 118, 1940.

and Z_1 and Z_2 are the atomic numbers of the colliding nuclei and A is the atomic weight. Since N^{14} is the step of longest life, $Z_1 = 1$, $Z_2 = 7$, and $A = M_1M_2/(M_1+M_2) = \frac{14}{15}$ in atomic-weight units. We may employ equation (2), however, over a limited range of temperature, viz.,

$$\epsilon(\rho, T) = \frac{E}{M}\frac{A_{C+N}}{t_C^4}(1 - X - Y)\left(\frac{X}{0.35}\right)\left(\frac{\rho}{80}\right)\left(\frac{T}{1.5\times 10^7}\right)^{\nu}. \tag{6}$$

Here A_{C+N} is the fraction, by weight, of carbon-plus-nitrogen, among the heavy elements. For the Russell mixture and oxygen models I have adopted $A_{C+N} = 0.08$ and 0.15, respectively. The energy of the cycle, E, is 4.3×10^{-5} ergs per helium nucleus produced. The mass M of the average atom in the cycle is taken as 2.13×10^{-23} gm.

Now the lifetime of the cycle may be evaluated with the aid of equation (4). At $T = 15{,}000{,}000°$, $\rho = 80$, $X = 0.35$, $t_C^4 = 246$ million years. Actually, the lifetime will be shorter because at the higher densities the width of the potential barrier is cut down. We may estimate the acceleration from the calculations of Schatzman.[11] At a temperature of 15,000,000° and a density of 300 gm/cm³, the lifetime of a N^{14} nucleus is shortened by a factor of 1.7. For temperatures in the neighborhood of $1.5 \times 10^{7°}$ K, the exponent ν is approximately 22 for the carbon cycle.

Similarly, we find that for the proton-proton reaction we may write, to a high degree of accuracy,

$$\epsilon = 1.91\left(\frac{\rho}{100}\right)\left(\frac{X}{0.316}\right)^2\left(\frac{T}{15{,}000{,}000}\right)^4. \tag{7}$$

In stars for which the carbon cycle is operative, most of the energy is produced in the convective core, where the density ρ and temperature T follow the polytropic relations,

$$y = \frac{T}{T_c} \qquad \rho = \rho_c y^{1.5}, \qquad \frac{r}{r_f} = \frac{x}{x_f}, \tag{8}$$

where x and y are the polytropic variables and r_f is the radius of the convective core. From equations (3) and (6) we obtain

$$L_c = \frac{E}{M}\frac{A_{C+N}}{t_C^4}(1 - X - Y)\left(\frac{X}{0.35}\right)\left(\frac{\rho_c}{80}\right)\rho_c\left(\frac{T_c}{15{,}000{,}000}\right)^{\nu} 4\pi\frac{r_f^3}{x_4^3}\int y^{3+\nu}x^2dx \tag{9}$$

if the energy comes from the carbon cycle. If we extend the integration from $x = 0$ to $x = x_0$ (the value for which $y = 0$) we allow, to some degree, for the production of energy outside the convective core. The contribution of the region outside the convective core will be small, however, since ϵ depends on such a high power of the temperature.

Similarly, when the proton-proton reaction prevails, if the energy-producing region still can be regarded as an Emden polytrope of index $n = 1.5$, equations (3) and (7) will yield:

$$L_p = 1.91\left(\frac{X}{0.316}\right)^2\left(\frac{\rho_c}{100}\right)\rho_c\left(\frac{T_c}{15{,}000{,}000}\right)^4 4\pi\left(\frac{r_f}{x_f}\right)^3\int_0^{x_0} y^{n+3}x^2dx. \tag{10}$$

An application of equation (7) to a model of a typical red dwarf star shows that actually much of the energy is produced outside the convective core. This means that a star that derives its energy from the proton-proton reaction cannot be homologous to the sun, even if the opacity law is the same. In our first approximation we shall suppose that ρ and T obey the adiabatic relationship throughout the region of the star responsible for the energy generation.

[11] *J. de phys.*, Ser. 8, **9**, 46, 1948.

APPLICATIONS TO o_2 ERIDANI C AND KRUEGER 60A

These considerations have been applied to two stars, Krueger 60A and o_2 Eri C, whose masses, luminosities, and radii in terms of the corresponding quantities for the sun are taken from the work of Kuiper,[12] and shown in the accompanying tabulation.

	log M	log L	log R
Krueger 60A	−0.60	−1.77	−0.29
o_2 Eridani C	−0.70	−1.96	−0.37

The problem is to find a pair of X and Y values that will be consistent with the mass-luminosity-curve (eq. [10] of Schwarzschild's paper[6]), for stars built with the Russell mixture and for which the luminosity computed from equations (9) and (10) equals the observed luminosity, i.e.,

$$L_p + L_c = L_{\text{obs}} . \tag{11}$$

The results are given in Table 1. The second column gives the reaction, the fifth column the central temperature, and the sixth column the fraction of energy supplied by the proton-proton reactions. The condition (11) leads to two solutions. In one the hydrogen content is relatively low, and the star operates primarily on the carbon cycle. In the other the hydrogen content is larger, the central temperature is lower, and the star derives its energy almost exclusively from the proton-proton reaction.

TABLE 1

Star	Reaction	Hydrogen Content X	Helium Content Y	Central Temperature T_c	Fraction of Energy Supplied by p-p Reactions
Kr 60A	C-N+p-p	0.11	0.64	15.4×10^{6} K	0.40
	p-p	.34	.64	10.7	1.00
o_2 Eri C	C-N+p-p	.08	.76	15.0	0.35
	p-p	0.22	0.76	13.2	1.00

Several points are to be noted: (1) if the proton-proton reaction is forbidden, the stars may derive their energy entirely from the carbon cycle; (2) the hydrogen content will determine which of the two solutions will be appropriate for any given star; and (3) no emphasis is to be placed on the numerical values of X and Y, since these stars must be built on somewhat different models than those assumed.

For the oxygen models no solution is possible. Because of the large hydrogen contents required by the mass-luminosity relationship, the proton-proton reaction alone appears to generate too much energy.

In all probability the composition of the "heavy stuff" in the stars lies somewhere between the Russell mixture and pure oxygen. A rough estimate, based on what appears to be the most likely composition of the heavy material, suggests that no solution may be found at all, particularly if we accept the refinements suggested by Duff and Williamson. Instead of looking for mechanisms capable of explaining the luminosities of the red dwarf stars, we have the task of accounting for the fact that they are not brighter.

Since our knowledge of β-decay is probably on a more secure footing than our infor-

[12] *Ap. J.*, **88**, 486, 1938.

mation on the composition of stellar interiors, it is probably safer to seek a solution in terms of modifications of the model than in abandonment of the proton-proton reaction. If we suppose that the core of the star has a different composition than the radiative envelope, it should be possible to construct a model that will represent the red dwarf stars. Such a model has been considered by Ledoux[13] for the stars similar to the sun.

It is difficult to justify such a difference in composition for a red dwarf star, since changes in the hydrogen/helium ratio by the action of the energy-production mechanism should be very small in the presumed lifetime of the star, 3×10^9 years.

The next paper will describe a model for a red dwarf in which the energy generation occurs by the proton-proton reaction throughout the star. Refined data on the opacity, the effects of conduction, etc., will be included.

I want to express my thanks to Professor Christy, of the California Institute of Technology, for supplying me with the results on the target areas for the carbon cycle. I have had fruitful conversations with Dr. Williamson and Mr. Duff on the subject of the structure of red dwarf stars. I am indebted to Professor Hans Bethe for critical comments on the status of the stellar-opacity coefficient and the selection rules for β-decay. Finally, I should like to acknowledge that my interest in this problem was stimulated by the seminars and discussions by my former colleagues in the Indiana University physics department, particularly Professor Emil J. Konopinski.

[13] *Ap. J.*, **105**, 305, 1947; *Ann. d'ap.*, **11**, 174, 1948.

FURTHER STUDIES ON THE ORIGIN OF THE SOLAR SYSTEM

D. TER HAAR*
Purdue University, Lafayette, Indiana
Received August 31, 1949

ABSTRACT

This paper is a supplement to an earlier one on the same subject. The physical conditions in a gaseous disk around the sun, out of which the planetary system might have been formed, are considered, and the consequences of these conditions are studied.

I. INTRODUCTION

In a previous paper[1] we discussed in some detail the physical properties of a solar envelope in connection with Von Weizsäcker's ideas about the origin of the solar system.[2] The present paper covers the same ground as sections from the second, third, fifth, and sixth chapters of Paper A. The qualitative results are the same, but some quantitative results are slightly revised. The main reason for the present discussion is the fact that during the last two years the statistical theory of turbulence has made great progress through the work of Heisenberg[3] and Chandrasekhar.[4]

In Section II of the present paper we shall discuss the shape, density distribution, optical depth, and temperature distribution in the disk (cf. chap. ii, subsecs. A and C, of Paper A). In Section III we shall discuss the lifetime of the disk (Paper A, chap. iii, subsecs. A and B). In Section IV the masses and densities of the planets are discussed (Paper A, chap. v), and in Section V the satellite systems and the rotations of the planets (Paper A, chap. vi, subsec. C). In the appendix, finally, the formulae for the turbulent velocity and wave length of the largest eddy in the system are derived from an adaptation of Heisenberg's theory of turbulence.

II. PHYSICAL PROPERTIES OF THE SOLAR ENVELOPE

We shall assume in the following that the sun, during the whole development of the planetary system, has possessed the same properties as those shown at present, apart perhaps from its angular momentum. As was pointed out to me by Dr. Chandrasekhar, the question of the slow solar rotation is irrelevant to the present discussion, since the development of the planets and their satellites appears to be independent of the solar rotation. The question of the solar angular momentum is taken up in a separate paper.[5]

The radiation of the sun will be assumed to be a black-body radiation corresponding to 6000° K; and for the radius and mass of the sun we shall use 7×10^{10} cm and 2×10^{33} gm. The constitution of the gaseous envelope will be assumed to be about the same as the constitution of the sun, i.e., mainly hydrogen and helium, with about 1 per cent of carbon, nitrogen, and oxygen, and about one-hundredth of 1 per cent of metals.

The equations of motion in the envelope are

$$\text{grad } U + \frac{1}{\rho} \text{grad } p - \omega^2 \vec{s} = 0 , \qquad (1)$$

* This paper was written while the author was temporarily at Yerkes Observatory.

[1] D. ter Haar, *D. Kgl. Danske Vidensk. Selskab, Mat.-fys. Medd.*, Vol. **25**, No. 3, 1948. We quote this paper in the following as "Paper A," and shall as far as possible use the same notation.

[2] *Zs. f. Ap.*, **22**, 319, 1944.

[3] *Zs. f. Phys.*, **124**, 628, 1948.

[4] *Proc. R. Soc. London*, A, **200**, 20, 1949.

[5] D. ter Haar, *Ap. J.*, **110**, 321, 1949.

where U is the gravitational potential energy, ρ the density of the gas, p its pressure, ω its angular velocity, and $\vec{s}$ the vectorial distance from the axis of rotation, which we shall take as our z-axis.

For U we shall use

$$U = -\frac{\gamma M_0}{r}, \tag{2}$$

where γ is the gravitational constant, M_0 the solar mass (we neglect the gravitational action of the gaseous envelope), and r the distance from the center of the sun.

In order to get an expression for the pressure, we have to bear in mind that in the solar envelope the Reynolds number will be extremely large. The Reynolds number is defined by

$$Re = \frac{\rho v d}{\eta}, \tag{3}$$

where v is the average velocity, d a length of the order of the dimensions of the system, and η the coefficient of viscosity. Using $\rho = 10^{-10}$ gm/cm^3, $v = 10^5$ cm/sec, $d = 10$ A.U. $= 1.5 \times 10^{14}$ cm, $\eta = 10^{-2}$ poise, we have

$$Re = 10^{11}, \tag{4}$$

which means that we have to expect turbulent motion in the envelope. This involves the condition that the pressure will consist of two parts: gas and turbulent pressure:

$$p = p_g + p_{\text{turb}}. \tag{5}$$

Using, for the pressure, the gas kinetic formula,

$$p = \tfrac{1}{3} \rho v^2, \tag{6}$$

we see that the ratio of the two terms on the right-hand side of equation (5) is equal to the square of the ratio of the turbulent to the temperature velocity. Using for the turbulent velocity the expression from the appendix (eq. [A, 21]), we have

$$v_t = \vartheta v_{\text{orb}}, \tag{7}$$

where

$$\vartheta^2 = f \approx \tfrac{1}{3}$$

and

$$v_{\text{orb}} = \left[\frac{\gamma M_0}{r}\right]^{1/2} \tag{8}$$

is the orbital velocity in a Kepler orbit.

For the temperature in the disk, we shall find (eq. [29], below)

$$T = \nu a r^{-1/2}, \qquad a = 400^\circ \text{ K A.U.}^{1/2}, \tag{9}$$

where ν is a numerical factor ranging from 0.9 for $r = 0.4$ A.U. to 0.1 for r larger than 5 A.U.

Combining equations (6), (7), (8), and (9), we find for the ratio p_g/p_{turb}:

$$\frac{p_g}{p_{\text{turb}}} = \left[\frac{v_g}{v_{\text{turb}}}\right]^2 = \chi r^{1/2}, \tag{10}$$

where

$$\chi = \frac{\nu a k}{\vartheta^2 \gamma M_0 m} \sim 0.002 \text{ A.U.}^{-1/2} \tag{11}$$

(k = Boltzmann's constant; m = mass of a proton). Since $r^{1/2}$ varies only between 0.6 and 6.5 in the solar system, it follows that p_{turb} is always at least a hundred times larger than p_g, and we shall neglect p_g in the following in order to simplify the calculations.

For the pressure we now have

$$p = p_{\text{turb}} = \tfrac{1}{3}\vartheta^2 \rho \frac{\gamma M_0}{r}. \tag{12}$$

Substituting expression (12) in equation (1) and introducing

$$\sigma = \log\left(\frac{\rho}{\rho_0}\right), \tag{13}$$[6]

we find that equation (1) is equivalent to

$$\frac{\vartheta^2}{3}\frac{\partial \sigma}{\partial z} = \left[-\frac{1}{r^2} + \frac{\vartheta^2}{3}\frac{1}{r^2}\right] z, \tag{14}$$

$$\frac{\vartheta^2}{3}\frac{\partial \sigma}{\partial s} = \left[\frac{r\omega^2}{\gamma M_0} - \frac{1}{r^2} + \frac{\vartheta^2}{3}\frac{1}{r^2}\right] s. \tag{15}$$

Equation (14) can be integrated and gives

$$\sigma = \left(1 - \frac{3}{\vartheta^2}\right)\log r + \psi(s), \tag{16}$$

where ψ has to be determined from equation (15), which, after the substitution of equation (16), has the form

$$\frac{d\psi}{ds} = \frac{3}{\vartheta^2}\frac{\omega^2}{\gamma M_0}\, r\, s. \tag{17}$$

Since ψ has to be independent of z, ω^2 has to be of the form

$$\omega^2 = \mu^2(s)\frac{\gamma M_0}{s^3}\frac{s}{r}. \tag{18}$$

Since the pressure gradient is everywhere small as compared to the gravitational force, we may, in the first approximation, neglect grad p in equation (1), and we have

$$\frac{\partial U}{\partial s} = \omega^2 s \qquad \text{or} \qquad \omega^2 = \frac{\gamma M_0}{r^3}. \tag{19}$$[7]

Since a dissipation of the disk will result in a steep density gradient, and therefore in a steep pressure gradient, we might introduce this artificially by putting

$$\mu^2 = 1 - \beta s, \tag{20}$$

where β will be determined by demanding a maximum planetary mass in the neighborhood of $s = 5$ A.U. (cf. Paper A, p. 29).

From equations (13), (16), (17), (18), and (20), we now get, for the density,

$$\rho = \rho_0 \frac{r}{r_0}\left(\frac{s}{r}\right)^{\kappa} e^{-\kappa\beta s}, \tag{21}$$

where

$$\kappa = \frac{3}{\vartheta^2} = 10. \tag{22}$$

[6] This σ is slightly different from the σ introduced at this point in Paper A.

[7] Cf. eq. (8).

The "height" of the disk, or, better, the distance over which the density is decreased by a factor 2, is given by

$$\frac{h}{r} \cong \left[\frac{2 \log 2}{\kappa}\right]^{1/2} \approx 0.4 . \tag{23}$$

The density in the equatorial plane is given by

$$\rho(s) = \rho_m \frac{s}{s_m} e^{1-(s/s_m)}, \tag{24}$$

where the maximum density, ρ_m, is attained for $s = s_m$; s_m is given by

$$s_m = \frac{1}{\kappa\beta} . \tag{25}$$

In the following, we shall use

$$\frac{\rho_m}{m} = 10^{14} \text{ at cm}^{-3}, \qquad \rho_m \sim 10^{-10} \text{ gm cm}^{-3} \qquad s_m = 3 \times 10^{13} \text{ cm}, \tag{26}$$

corresponding to a total mass of the disk of

$$M = \int \rho d V \cong \int 2\pi h s d s \rho(s) \sim 0.1 M_0 . \tag{27}$$

The optical depth in the disk will be given by

$$\tau(s) = \int^s \delta \frac{\rho(s)}{m} d s , \tag{28}$$

where δ will be the cross-section for Rayleigh scattering (cf. Paper A, p. 32; $\delta = 10^{-27}$ cm^2), and $\rho(s)$ the density given by equation (24). It must be remarked here that the calculation of the optical depth in Paper A was far from satisfactory.

The temperature in the disk will now be given by

$$T(s) = a s^{-1/2} e^{-\tau(s)/4}, \tag{29}$$

since the energy received from the sun will be proportional to $e^{-\tau}/s^2$ and the emitted energy proportional to T^4. We normalize the temperature to 6000° K at the surface of the

TABLE 1

	Planet							
	Mercury	Venus	Earth	Mars	Jupiter	Saturn	Uranus	Neptune
τ	0.16	0.40	0.72	1.39	6	8	8	8
T (° K)	600	420	330	230	40	20	15	10

sun, so that $a = 400°$ K A.U.$^{1/2}$; using equation (28) for the optical depth $\tau(s)$, we get the results of Table 1, which give the optical depth and temperature for distances corresponding to the mean distances of the planets from the sun. It must be remarked here that equation (29) presupposes negligible ionization in the disk, which is probably correct, as was shown in Paper A.

III. LIFETIME OF THE DISK

The total energy content of the disk will be of the order of

$$E_0 = \frac{\gamma M_0 M}{r_1}, \tag{30}$$

where r_1 is of the order of magnitude of a few astronomical units. The dissipation in the disk is completely governed by turbulent dissipation. Heisenberg[3] gives, for the dissipation per cubic centimeter per second,

$$\delta E \sim \rho \frac{v_t^3}{\lambda}, \tag{31}$$

where λ is the wave length of the largest eddy and is given by (see eqs. (A, 24) and (A, 25))

$$\lambda = \alpha s, \qquad \alpha = 0.618. \tag{32}$$

Integrating expression (31) over the disk and using equations (7), (8), (23), (24), and (32), we get

$$\frac{dE}{dt} = \int \delta E d V \sim 10^{-3} M \left(\frac{\gamma M_0}{s_m}\right)^{3/2} \frac{1}{s_m}, \tag{33}$$

and for the lifetime of the disk we obtain

$$\tau = E_0 \left[\frac{dE}{dt}\right]^{-1} \sim 100 \left[2\pi s_m \left(\frac{\gamma M_0}{s_m}\right)^{-1/2}\right] \sim 1000 \text{ years}. \tag{34}[4]$$

This lifetime is of the same order of magnitude as the one given by equation (5.4) in Paper A, and it is much smaller than t_{cr} (eq. [5.5] in Paper A), i.e., the time necessary to build up bodies of the mass of the planets. Again the conclusion seems inevitable that either equation (34) gives an underestimate of the lifetime of the disk by a factor perhaps as large as 10^6, because a regular system of vortices decreased the dissipation of energy by that amount; or the condensation into planets started at a time when there still was a strong interaction between the solar envelope and the surrounding interstellar gas, so that the dissipation process was counteracted by a replenishing of matter from the surrounding interstellar medium.

[4] It is interesting to compare the result obtained here with Von Weizsäcker's estimate of the lifetime in his paper on general cosmogony (*Zs. f. Ap.*, **24**, 181, 1947). He gives in that paper for the lifetime the expression

$$\tau' = \frac{R^2}{r v_t \lambda},$$

where R is the outer radius of the system and r the radius of the central condensation. For E_0 we can roughly write in Von Weizsäcker's notation

$$E_0 \sim \frac{v_{orb}^2 MR}{r},$$

and, for dE/dt,

$$\frac{dE}{dt} \sim \delta E \times \text{vol.} \sim \frac{M v_t^3}{\lambda} \sim \frac{M \lambda v_{orb}^2 v_t}{R^2}$$

($v_t \sim [\lambda/R] v_{orb}$), so that we get Von Weizsäcker's formula.

IV. MASSES AND DENSITIES OF THE PLANETS

In view of the fact that we have a slightly different density distribution than was used in Paper A, we have to repeat the calculation of the masses of the different planets. We can again use equation (5.3) of Paper A:

$$M_n = A\,\Delta_n \rho\,(r_n)\, r_n^3\,, \tag{35}$$

where M_n and r_n are the mass and the mean distance of the planet from the sun, A a constant, and Δ_n the fraction of the gas taking part in the condensation process. As was shown in Paper A, only metallic compounds can take part in the condensation process in the region of the inner planets, but practically all compounds can take part in the condensation process leading to the outer planets. One might fear that the slightly different temperatures would upset these considerations. However, the density in the envelope is now slightly smaller. Using the temperatures given in Table 1 and $\rho/m = 10^{10}$ atoms/cm^3 (as was remarked in Paper A; the result is rather insensitive to changes in density), we find that Table 5.I of Paper A must now be replaced here by Table 2, giving the critical

TABLE 2

	Planet							
	Mercury	Venus	Earth	Mars	Jupiter	Saturn	Uranus	Neptune
T (° K)	600	420	330	230	40	20	15	10
χ	45	30	23	16	3	2	1	1

sublimation heats χ in calories per mole for the regions where the different planets are now situated.

As was remarked in Paper A, the difference in condensation processes in the two regions has two consequences: (*a*) fewer condensation nuclei will be formed in the inner regions, and they will consist mainly of metal and rock, while the condensation products in the outer regions will be more numerous and will be water droplets, etc.; and (*b*) the condensation in the inner regions will proceed more slowly than in the outer regions; in the outer regions gravitational capture may have played a role but not in the inner regions. Altogether, we assumed in Paper A and we shall here again assume that Δ_n is one hundred times larger in the outer regions than in the inner regions. This, then, also makes l_{cr} (see eq. [5.5] in Paper A) one hundred times larger in the inner than in the outer regions. For $\rho\,(r_n)$ in equation (35), we can use equation (24). Normalizing all quantities to unity for $r_n = 1$ A.U., we have

$$\frac{M_n}{M_e} = \frac{\Delta_n}{\Delta_e}\left[\frac{r_n}{r_e}\right]^4 \times 10^{-0.22(r_n - r_e)}\,, \tag{36}$$

where the subscript e denotes the earth and where all distances are expressed in A.U. The final results are collected in Table 3, which should replace Table 5.II in Paper A.

The agreement between the calculated and the observed masses is slightly worse than that obtained in Paper A. It might be profitable to examine whether the processes discussed by Von Weizsäcker in a recent paper[9] would give a better agreement. He shows that there is a tendency during the dissipation process to produce a void in the middle of the disk. This void might correspond to the fact that the calculated masses for Mars, Jupiter, Saturn, and Uranus in Table 3 are so much larger than the observed masses.

It was stated in Paper A that it was possible to understand the densities of the planets

[9] *Zs. f. Naturforsch.*, **3a**, 524, 1948.

from the condensation process. It turns out that there are indeed strong arguments in favor of the idea that the inner planets are all built up out of the same material, while the outer planets contain large amounts of hydrogen and helium. Dr. H. S. Brown has kindly informed me that a model of Jupiter consisting of hydrogen only is able to account for the observed density. That the differences in density in the series of the inner planets may well be due to the differences in pressure in their interior can easily be seen as follows. In order to get a rough estimate of the influence of the pressure on the density, we have to remember that the pressure is nearly constant over most of the interior and, in first approximation, is given by

$$p \approx \frac{\gamma M \rho}{R}, \tag{37}$$

where R is the radius, M the mass, and ρ the mean density of the planet. We might now ask what will be the density of, say, *Fe* and *Ba* at these high pressures. Using Jensen's figures[10] for these densities, we see that these densities vary just as the observed densities in the series of the inner planets (see Table 4): the density variations can, in

TABLE 3

Planet	Δ_m/Δ_e	ρ_m/ρ_e	r_m/r_e	M_{calc}/M_e	M_{obs}/M_e
Mercury	1	0.5	0.4	0.035	0.05
Venus	1	0.8	0.7	0.3	0.8
Earth	1	1	1	1	1
Mars	1	1.2	1.5	4	0.1
Jupiter	100	0.6	5	8000	318
Saturn	100	0.1	10	10,000	95
Uranus	100	2×10^{-3}	19	1600	15
Neptune	100	2×10^{-3}	30	40	17
Pluto	100	2×10^{-7}	39	1.3	0.9

TABLE 4*

Planet	Pressure (Atm.)	$\rho_{Fe}/(\rho_{Fe})_{p=p_e}$	$\rho_{Ba}/(\rho_{Ba})_{p=p_e}$	ρ_{calc}/ρ_e
Mercury	2×10^6	0.74	0.46	0.69
Venus	2×10^6	0.93	0.94	0.89
Earth	3×10^6	1	1	1
Mars	4×10^5	0.77	0.56	0.73

* All densities are normalized with respect to the earth.

first approximation, be understood as due to the differences in central pressure. Of course, a rigorous calculation should take into account a possible stratification of the matter, and a variation of pressure and density through the planet.[11]

V. THE SATELLITE SYSTEMS; ROTATION OF THE PLANETS

Since the lifetime of the planetary envelopes (as given by eq. [34]) is even smaller than the lifetime of the planetary disk, while the dimensions of the satellites are about the same as those of the smaller planets, we have to accept the theory that the satellites were already formed (at any rate, practically formed) when the planets got their envelopes. We should like to give the following picture of the formation of the satellite systems. In

[10] *Zs. f. Phys.*, **111**, 373, 1938.

[11] After this paper was written Dr. H. S. Brown informed me that he has submitted to the *Astrophysical Journal* a paper treating these matters in a more rigorous manner.

the original "roller-bearing" rings of the planetary disk, many condensation products were formed. The larger ones became planets, and they collected a large envelope around them. These extended atmospheres were able to catch smaller condensation products—the "regular" satellites (for a discussion of the difference between the "regular" and the "irregular" satellites see Paper A). Owing to the capture and subsequent loss of hydrogen, the orbits of these "regular" satellites were ironed out into circular orbits. The "irregular" satellites were captured outside the envelope, and the ironing-out did not take place to such an extent. Regular systems of vortices in the planetary envelopes might possibly account for regularities in the sequences of the mean distances of the satellites from the primaries.

We should like to finish this paper with a brief discussion of the rotational periods of the planets.[12] There seems to be no reason to believe that the condensation products had acquired a large angular momentum before the period of the gravitational capture started. However, during the period of gravitational capture, the envelope will rotate *directly* around the planet (compare the discussion in Paper A and in Von Weizsäcker's paper[2]). The rotational velocities will again, in first approximation, be given by Kepler's third law. Matter condensing onto the planet will therefore, in general, possess angular momentum. If the exchange between the condensing matter and the extended envelope were perfect, this matter should have a rotational velocity corresponding to a Kepler velocity at the surface of the growing planet. However, the exchange will probably not be perfect, and in the following we shall, rather arbitrarily, assume, as the upper and lower limit of the angular momentum obtained by the planet from the condensing material, $\frac{3}{4}$ and 0.15 of the angular momentum corresponding to a perfect exchange.

Neglecting factors of the order of magnitude 1, the angular momentum per unit mass of matter condensing on a planet of mass m and radius r will be

$$\delta\Theta = \zeta \sqrt{(\gamma m r)}\,, \tag{38}$$

where ζ is the exchange factor, lying between 0.5 and 0.1. The total increase of angular momentum per unit of time will be given by

$$\frac{d\Theta}{dt} = \zeta \sqrt{(\gamma m r)}\,\frac{dm}{dt}\,, \tag{39}$$

from which follows

$$\frac{d\Theta}{dm} = \zeta \sqrt{(\gamma m r)}\,. \tag{40}$$

Equation (40) can be integrated and gives

$$\Theta = \tfrac{2}{5}\zeta\,[M \sqrt{(\gamma M R)} - M_{cr} \sqrt{(\gamma M_{cr} R_{cr})}\,]\,, \tag{41}$$

where M_{cr} and R_{cr} are the mass and radius of the planet at the moment that the gravitational capture started to be important and where we have assumed that $\Theta = 0$ for $R = R_{cr}$. Since, for the inner planets, R is about equal to R_{cr}, we should indeed expect a low angular momentum, as has been found. For the earth, with the largest R of the four inner planets, the angular momentum is the largest.

For the outer planets, we can neglect the last term, and for the period we get

$$T = \frac{4\pi}{3\zeta}\left(\frac{R^3}{\gamma M}\right)^{1/2} = \frac{2}{3\zeta}\,T_{\text{Kepler}}\,. \tag{42}[13]$$

[12] Although our results are about the same as those obtained by Hoyle (*M.N.*, **106**, 406, 1947), the processes considered are different. Hoyle does not consider the influence of the extended envelope on the final angular momentum.

[13] If the exchange is perfect and if matter is condensing isotropically, ζ will be equal to $\frac{2}{5}$, giving $T = T_{\text{Kepler}}$ as expected.

In Table 5 we have collected T, calculated with $\zeta = 0.5$ and $\zeta = 0.1$, and the observed T for the four outer planets and for the sun.

It is seen that, for the four outer planets, T_{obs} lies between the two limits given in the second and third columns. It is perhaps not irrelevant that Neptune, which probably obtained quite an appreciable fraction of its mass during the last stages of the disk, when the matter was streaming out of the system, has a relatively low angular momentum.

TABLE 5

Planet	T_{calc} (Hours)		T_{obs}
	$\zeta = 0.5$	$\zeta = 0.1$	
Jupiter	4	20	10 hours
Saturn	5	25	10 hours
Uranus	4	20	11 hours
Neptune	3	17	16 hours
Sun	4	20	25 days

It is also seen from Table 5 that the sun's angular momentum definitely suggests a problem. As we remarked before, this problem lies outside the scope of the present paper and will be discussed elsewhere.[5]

I should like to express my sincere thanks to Professor S. Chandrasekhar for many helpful discussions.

APPENDIX

The Scale of Turbulence in a Differentially Rotating Gaseous Medium

S. CHANDRASEKHAR AND D. TER HAAR

In this appendix we shall show how, by an adaptation of Heisenberg's recent elementary theory of turbulence, we can determine the scale of turbulence.[14]

Heisenberg's theory is based on the following expression for the rate of transfer of energy (ϵ_k) from all eddies with wave numbers less than a given k to all wave numbers exceeding this k:

$$\epsilon_k = 2\rho\left\{\nu + \kappa\int_k^\infty \frac{dk}{k^{3/2}}\sqrt{F(k)}\right\}\int_0^k F(k)\,k^2 dk\,, \tag{A, 1}$$

where $F(k)$ denotes the spectrum of turbulence, ν the coefficient of kinematic viscosity, and κ is a numerical constant of order unity.

For the case of fully developed stationary turbulence, when ϵ_k is constant and the Reynolds number is infinite, the solution of equation (A, 1) is given by the Kolmogoroff spectrum,

$$\begin{aligned} F(k) &= F(k_0)\left(\frac{k_0}{k}\right)^{5/3} && k \geq k_0 \\ &= 0 && k < k_0\,. \end{aligned} \tag{A, 2}$$

[14] We shall follow the development of Heisenberg's theory given by one of us: S. Chandrasekhar, *Proc. R. Soc. London*, A, **200**, 20, 1949. This paper will be referred to as "*op. cit.*" in the rest of the appendix.

It will be noticed that this expression for the spectrum involves two constants of integration, k_0 and $F(k_0)$. The reason for the appearance of *two* constants in the solution is the following: In considering stationary turbulence, without reference to the external agency maintaining the turbulence, we must assume the size of the largest eddies to which the energy will be principally communicated and the energy in the system in the form of turbulence as given: the former is related to the occurrence of a smallest wave number k_0, below which the statistical theory cannot be extended, and the latter is related to $F(k_0)$:

$$\tfrac{1}{2}\overline{v^2} = \int_0^\infty F(k)\,dk = F(k_0)\int_{k_0}^\infty \left(\frac{k_0}{k}\right)^{5/3} dk \qquad \text{(A, 3)}$$

or

$$\overline{v^2} = 3F(k_0)\,k_0\,. \qquad \text{(A, 4)}$$

It is clear that if we can specify, in some way, the manner in which the external agency is maintaining stationary turbulence, we shall be able to eliminate one of the two constants which appear in the theory: i.e., in effect, determine the *scale* of turbulence given by $\lambda = 2\pi/k_0$. We shall show how in a differentially rotating gaseous medium of the type contemplated in the paper (cf. eq. [8]) we can determine this λ.

When there is differential rotation, eddies which are absorbed in a particular place arrive from regions which are separated from it by distances of the order of their mean free path. Consequently, if we picture turbulence in terms of eddies traversing a certain mean distance, l, with a mean velocity, v, before they are reabsorbed in the medium, we can write, for the energy (per unit volume) communicated at any place by this constant flow of eddies from regions with different mean motions, the expression

$$\tfrac{1}{2}\zeta\,\frac{d}{ds}\left(l v\,\frac{dV^2}{ds}\right), \qquad \text{(A, 5)}$$

where V represents the mean mass velocity at s and ζ is a factor of order unity.[15]

When we analyze turbulence into eddies with various wave numbers, we need an expression analogous to (A, 5) which will give the energy communicated by this mechanism to eddies with wave numbers between k and k_0; for we may then equate this to ϵ_k/ρ. If $l(k, k_0)$ and $v(k, k_0)$ denote the mean free path and the velocity appropriate to eddies in the wave-number interval (k, k_0), we may write

$$\epsilon_k = \tfrac{1}{2}\zeta\rho\left|\frac{d}{ds}\left[l(k, k_0)\,v(k, k_0)\,\frac{dV^2}{ds}\right]\right|. \qquad \text{(A, 6)}$$

We must now express equation (A, 6) in terms of the spectrum. Arguing in a manner similar to Heisenberg's in his elementary theory (cf. *op. cit.*), we can write

$$\epsilon_k = \tfrac{1}{2}\zeta\kappa\rho\left|\frac{d^2V^2}{ds^2}\right|\int_{k_0}^k \frac{dk}{k^{3/2}}\sqrt{F(k)}\,. \qquad \text{(A, 7)}$$

Combining equations (A, 1) and (A, 7), we have

$$\beta\int_{k_0}^k \frac{dk}{k^{3/2}}\sqrt{F(k)} = \left\{\frac{\nu}{\kappa} + \int_k^\infty \frac{dk}{k^{3/2}}\sqrt{F(k)}\right\}\int_{k_0}^k F(k)\,k^2 dk\,, \qquad \text{(A, 8)}$$

where

$$\beta = \tfrac{1}{2}\zeta\left|\frac{d^2V^2}{ds^2}\right|. \qquad \text{(A, 9)}$$

[15] The energy transported is only the turbulent energy, so that one would expect v^2 instead of V^2 in expression (A, 5). However, the two are proportional to each other (cf. e.g. [A, 21], below).

Differentiating equation (A, 8) with respect to k and rearranging the terms, we obtain

$$\frac{\nu}{\kappa}+\int_k^\infty \frac{dk}{k^{3/2}}\sqrt{F(k)}-\frac{1}{k^2\sqrt{F(k)}\,k^3}\left[\beta+\int_{k_0}^k F(k)\,k^2dk\right]=0\,. \qquad \text{(A, 10)}$$

If we now let (cf. *op. cit.*, eq. [9])

$$g=k^3F(k) \qquad \text{and} \qquad y=\beta+\int_{k_0}^k F(k)\,k^2dk\,, \qquad \text{(A, 11)}$$

equation (A, 10) becomes equivalent to the pair of equations

$$\frac{\nu}{\kappa}+\int_y^\infty \frac{dy}{k^2\sqrt{g}}-\frac{y}{k^2\sqrt{g}}=0 \qquad \text{(A, 12)}$$

and

$$\frac{dk}{dy}=\frac{k}{g}. \qquad \text{(A, 13)}$$

But these are identical with equations (11) and (12) of *op. cit.* Accordingly, for fully developed turbulence we may write (*op. cit.*, eqs. [15] and [16])

$$g=\tfrac{4}{3}y \qquad \text{and} \qquad k=\alpha y^{3/4}\,, \qquad \text{(A, 14)}$$

where α is a constant. But the constant α is not an arbitrary one, as in the theory of stationary turbulence; for, according to equation (A, 11),

$$y=\beta \qquad \text{when} \qquad k=k_0\,. \qquad \text{(A, 15)}$$

Hence

$$k_0=\alpha\beta^{3/4}\,. \qquad \text{(A, 16)}$$

This is the new relation which determines the scale of turbulence.

Returning to equations (A, 11) and (A, 14), we have

$$\begin{aligned} F(k) &= \frac{4}{3\alpha^{4/3}}\frac{1}{k^{5/3}} && k\geqslant k \\ &= 0 && k<k_0\,, \end{aligned} \qquad \text{(A, 17)}$$

which is the Kolmogoroff spectrum.

If we write this Kolmogoroff spectrum in the standard form (A, 2), we have the relations

$$F(k_0)\,k_0^{5/3}=\tfrac{4}{3}\alpha^{-4/3}\,; \qquad k_0^{4/3}=\beta\alpha^{4/3} \qquad \text{(A, 18)}$$

and

$$\overline{v^2}=3F(k_0)\,k_0\,.$$

These relations can be combined alternatively in the form

$$\overline{v^2}=4\beta k_0^{-2}\,; \qquad F(k_0)\,k_0^2=\tfrac{4}{3}\beta\,; \qquad k_0=\alpha\beta^{3/4}\,. \qquad \text{(A, 19)}$$

The first of equations (A, 19) gives us the turbulent velocity at any point of the system, as soon as β is known. The second one gives us the size of the largest eddy at any point, if the energy density is given.

For the case considered in the paper (cf. eq. [8])

$$V^2=\frac{\gamma M_0}{s} \qquad \text{and} \qquad \beta=\zeta\frac{\gamma M_0}{s^3}, \qquad \text{(A, 20)}$$

where we have written s instead of r to emphasize that we are essentially dealing with a two-dimensional system.

The energy in the system will be determined by the gravitational field. We may therefore write

$$\overline{v^2} = 3F(k_0)\, k_0 = fV^2 = f\frac{\gamma M_0}{s}, \tag{A, 21}$$

where f is a numerical factor which we may expect to be of the order of $\frac{1}{3}$. We also have (cf. the second of eqs. [A, 19])

$$F(k_0)\, k_0^3 = \tfrac{4}{3}\zeta\frac{\gamma M_0}{s^3}. \tag{A, 22}$$

Combining equations (A, 21) and (A, 22), we get

$$k_0 = 2\left(\frac{\zeta}{f}\right)^{1/2}\frac{1}{s}. \tag{A, 23}$$

Hence

$$\lambda = \frac{2\pi}{k_0} = \pi\left(\frac{f}{\zeta}\right)^{1/2} s = a\, s\ (\text{say}). \tag{A, 24}$$

Equation (A, 24) was assumed without proof by Von Weizsäcker[9] and in Paper A.

The numerical factor a (which we expect to be of the order of unity) can be determined empirically in the following manner. From equation (A, 24) the Titius-Bode law is an immediate consequence, and the best agreement between the observed and calculated mean distances of the planets from the sun is obtained for

$$a = 0.618. \tag{A, 25}[16]$$

[16] The derivation of eq. (A, 25) is simple and runs along the lines of chap. iii, subsec. D, of Paper A.

NOTES

THE SPECTROSCOPIC BINARY CPD−61°669

Among the southern objects with variable radial velocity listed in Moore's *Fourth Catalogue of Spectroscopic Binary Stars*[1] and for which no orbit has been thus far determined, CPD−61°669[2] seemed very promising. Neubauer had taken four plates of the star at the former Lick Observatory Station in Santiago, Chile, which enabled him to announce[3] that the radial velocity of −61°669 is variable, with a range of about 200 km/sec; a further remark was that probably two spectra were present on the secured plates.[4]

In order to determine the period of the velocity variation and the orbital elements, the star was placed on the spectrographic program of the 154-cm reflecting telescope at Bosque Alegre. Forty-one measurable plates, all on Eastman 103*a*-O emulsion, were obtained; one in December, 1946, and the rest in November and December, 1948, and January, March, and April, 1949. The equivalent slit-width was either 0.6 or 0.9 A; only for the 1946 spectrogram was it 1.5 A. The spectrograph used was the Wood-grating one which gives a dispersion of about 42 A/mm.

THE PERIOD

The distribution of the radial velocities derived from our 1948 and 1949 spectrograms suggested a preliminary period of 2.97 days for the variation in velocity. This preliminary period was further improved by taking into account the radial velocity from the plate secured in 1946. Since its value fell near maximum positive velocity, a decision had to be made as to whether the point belonged to the ascending or to the descending branch of the velocity-curve. Each case corresponds to a different improved period, namely, 2.9703 and 2.9723 days, respectively, and, in fact, to a slightly different plot of the measurements. The velocity-curve suggested by the plot corresponding to the period of 2.9723 days was smoother, and only for this reason was this value adopted. Consequently, our phases have been computed with 2.9723 days as the period, the origin being arbitrarily chosen at JD 2432000.0 (June 28.5, 1946). The last figure of our period might be in error.

The way in which the observations are distributed rules out the possibility of periods smaller than 1 day and between 1 and 2 days.

THE SPECTRUM

The spectrum of CPD−61°669, on our plates, is of type B3, according to the criterion indicated by Morgan, Keenan, and Kellman in their *Atlas of Stellar Spectra;* the lines are sharp, and interstellar *Ca* II is present. Our classification is in agreement with the one given for the star in the *Henry Draper Catalogue.*

The Balmer series is seen up to *H*16. At around maximum negative velocity, the *H* lines look somewhat shallower and shaded toward the red; but our plates do not distinctly show double lines at any phase of the cycle of velocity variation. At around maxi-

[1] *Lick Obs. Bull.*, No. 483, p. 31, 1936.

[2] $\alpha = 6^h30^m7$; $\delta = -61°50'$ (1950.0). CD − 61°1394 = 63 G. Pictoris = BS 2410 = L. 2377 = HD 46792 (Sp. B3).

[3] *Pub. A.S.P.*, **42**, 235, 1930.

[4] *Pub. Lick Obs.*, **18**, 56, 1932. The dispersion of Neubauer's spectrograms is 37 A/mm at $H\gamma$.

mum positive velocity the *H* lines give the impression of being sharper and perhaps stronger than at those phases which correspond to the maximum velocity of approach.

The *Mg* II 4481 line shows changes in intensity which seem to have no relation to the variation of velocity. The intensity of *Mg* II 4481 relative to *He* I 4471 varies from about ½ to about 0.

THE RADIAL VELOCITIES

The lines measured for the determination of radial velocities were those of *H*, *He* I, *Ca* II, and *Mg* II in the interval λλ 3797–4482. No systematic variation between the

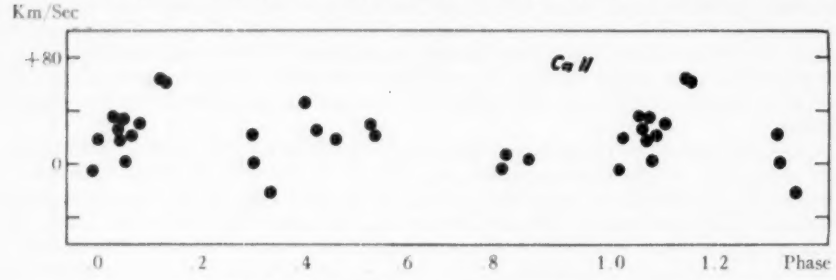

FIG. 1.—Radial-velocity measurements for *Ca* II

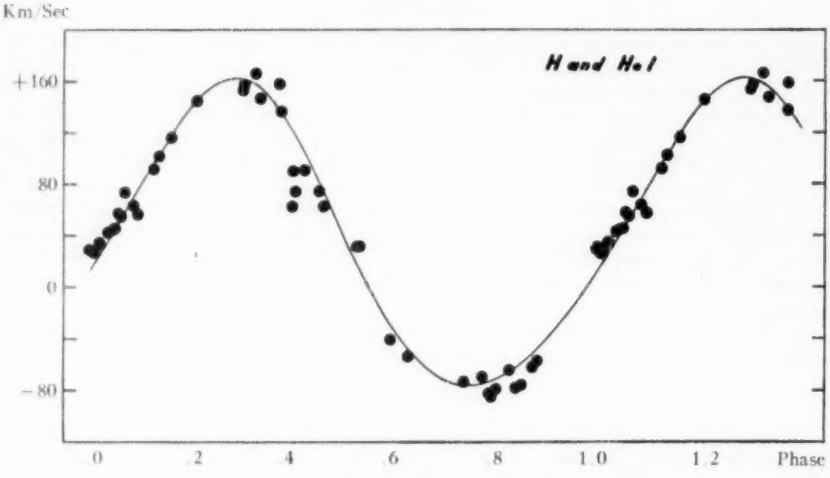

FIG. 2.—Radial velocity-curve from lines of *H* and *He* I

different elements was noticed, except, of course, for the interstellar *Ca* II H and K lines. Therefore, only one plot was considered for the stellar lines, namely, the one which results from taking, for each plate, the mean of the radial velocities from *H*, *He* I, and *Mg* II. The plot for the interstellar lines is shown in Figure 1; the one for the stellar lines in Figure 2. Table 1 gives the numerical values.

Orbital elements were derived by applying the methods of Lehmann-Filhés and of Wilsing-Russell, and the mean of both results was adopted as the elements of the system. They are shown in Table 2.

TABLE 1

RADIAL VELOCITIES OF CPD −61°669

DATE	U.T.	PHASE* (PERIOD)	RADIAL VELOCITIES (KM/SEC)				
			H	*He* I	*Mg* II	*Ca* II	All Lines except *Ca* II
1948 Dec. 18	1:54	0.000	+ 32	+ 25	.....	− 5	+ 29
18	2:28	.008	+ 37	+ 18	+ 18	+ 19	+ 27
18	3:30	.023	+ 35	+ 36	+ 31	.....	+ 35
18	11:35	.038	+ 43	+ 40	+ 60	+36	+ 43
18	5:04	.045	+ 41	+ 49	.....	+26	+ 45
18	5:35	.052	+ 37	+ 57	.....	+17	+ 46
18	6:03	.058	+ 60	+ 56	.....	+34	+ 58
21	5:44	.063	+ 56	+ 54	.....	+ 2	+ 55
21	6:22	.072	+ 67	+ 87	.....	+21	+ 74
1949 Jan. 11	2:50	.088	+ 38	+ 80	+ 95	+30	+ 64
11	3:24	.097	+ 52	+ 63	.....	.....	+ 57
14	5:02	.128	+ 93	+111	+ 83	+64	+ 92
14	5:51	.139	+ 97	+110	.....	+61	+102
29	4:17	.164	+113	+119	+128	.....	+116
29	7:42	.212	+137	+150	+163	.....	+145
March 27	1:20	.303	+153	+153	.....	+22	+153
27	1:56	.306	+156	+159	+154	+ 1	+157
April 13	23:06	.329	+165	+167	.....	.....	+166
14	0:09	.339	+157	+134	+166	−21	+147
1946 Dec. 10	2:14	.376	+136	+138	.....	.....	+137
1949 April 14	2:50	.377	+155	+160	+166	.....	+158
1948 Dec. 19	6:30	.401	+ 57	+ 70	.....	.....	+ 63
1949 Jan. 12	1:15	.402	+ 88	+ 92	.....	+46	+ 90
1948 Dec. 19	6:58	.407	+ 61	+ 92	.....	.....	+ 74
1949 Jan. 12	2:54	.425	+ 82	+101	.....	+25	+ 91
30	1:00	.454	+ 74	+ 78	.....	.....	+ 75
30	1:36	.463	+ 75	+ 54	+ 42	+19	+ 63
27	6:55	.528	+ 37	+ 26	+ 35	+30	+ 32
27	7:28	.536	+ 31	+ 33	.....	+21	+ 32
1948 Nov. 17	3:35	.594	− 42	− 34	.....	.....	− 41
26	4:02	.628	− 60	− 48	.....	.....	− 54
Dec. 20	6:31	.738	− 67	− 85	.....	.....	− 73
1949 Jan. 28	0:42	.777	− 69	− 72	.....	− 4	− 70
28	1:25	.787	− 74	− 96	.....	+ 7	− 83
31	1:06	.792	− 86	− 89	− 79	.....	− 86
31	1:46	.802	− 77	− 81	.....	.....	− 79
13	7:38	.828	− 52	− 88	.....	+ 3	− 64
28	5:18	.842	− 79	− 81	− 65	.....	− 78
28	6:00	.851	− 77	− 75	.....	.....	− 76
28	7:39	.875	− 52	− 73	.....	.....	− 62
28	8:18	0.884	− 51	− 64	.....	.....	− 57

* The origin of the phases was arbitrarily taken at JD 2432000.0.

TABLE 2

ORBITAL ELEMENTS OF CPD −61°669

P =	2.9723 days	T = 0.380 P (origin arbitrarily taken at JD 2432000.0)	
γ = +	34 km/sec		
K =	119 km/sec	$a \sin i$ = 4.8 × 10^6 km	
e =	0.10	$f(m)$ = 0.50 ⊙	
ω =	39°		

DISCUSSION

The velocity-curve which corresponds to the derived orbital elements is drawn in Figure 2. It represents the measured radial velocities quite well, except for the group of points at about phase 0.4 *P*. Its existence led us to think that perhaps we are in the presence of the same phenomenon as that encountered in some eclipsing stars of early spectral type, such as AU Monocerotis.[8] The differences described above in the appearance of the *H* lines seem to give some support to the idea, but the evidence is not quite conclusive. The star probably deserves attention from photoelectric observers.

Mr. Julio Albarracín assisted in the reduction of some of the plates.

J. SAHADE
J. LANDI DESSY

OBSERVATORIO ASTRONÓMICO
CÓRDOBA, ARGENTINA
July 20, 1949

SPECTROGRAPHIC OBSERVATIONS OF THE ECLIPSING VARIABLE UX MONOCEROTIS AT BOSQUE ALEGRE

At the suggestion of Dr. O. Struve, the eclipsing star UX Monocerotis was included in the spectrographic program of the 154-cm reflecting telescope at Bosque Alegre during December, 1946, and February and March, 1947. The spectrographic equipment was not suitable for the phases of eclipse with a series of reasonably short exposure times; furthermore, the observations at maximum had to be of rather long exposure. Hence, our observations are not sufficient for a detailed study of this remarkable system. However, since they give a general picture of the changes in the spectrum during the month preceding Struve's[9] own observations, it was decided to publish the results. They are presented in Table 1. The spectrograms were taken on Eastman 103*a*-O emulsion with equivalent slit-widths of 1.5 or 1.8 A. The dispersion used was about 42 A/mm.

I am indebted to Mr. Julio Albarracín for checking the reduction of the plates. It is a pleasure to record my indebtedness to Mr. Martín Dartaget who allowed me to share part of his observing time during December, 1946, for the taking of some of the plates of UX Monocerotis.

JORGE SAHADE

OBSERVATORIO ASTRONÓMICO
CÓRDOBA, ARGENTINA
August 11, 1949

[8] Sahade and Cesco, *Ap. J.*, **101**, 235, 1945; *McDonald Contr.*, No. 106.

[9] *Ap. J.*, **106**, 255, 1947; *McDonald Contr.*, No. 138.

TABLE 1

RADIAL VELOCITIES OF UX MONOCEROTIS

DATE	U.T.	EXPOSURE TIME (MINUTES)	PHASE (DAYS)	RADIAL VELOCITIES (KM/SEC)				REMARKS*
				Ca II	*H*	*Ca* I	*Fe* I	
1946 Dec. 17	3:36	116	0.030		− 37	+ 32	+ 46	Underexposed; secondary present; red emission at *Hβ*
17	6:22	205	0.145		− 18	+ 9	+ 27	Secondary present; red emission at *Hβ*
23	5:27	212	0.203	− 78	− 69	+ 43	+ 14	Red emission at *Hβ*, *Hγ*, *Hδ*
1947 Feb. 9	3:04	131	0.866	−118	−129 + 35			*Ca* II K, sharp core; *H* double (*v*<*r*); no emission
1946 Dec. 6	6:21	136	0.954	−107	− 54	+ 3	+ 68	No emission
24	7:09	112	1.273	−147	−186		+ 75	No emission
1947 Feb. 10	1:52	120	1.816	−265	−295 + 85			*H* double (*v*>*r*); red em. at *Hβ*
10	4:00	115	1.905	−234	−258 +135			*Ca* II K, there might be a sharp violet comp.; *H* double (*v*>*r*); red em. at *Hβ*
1946 Dec. 7	5:11	60	1.905	−209	−212		+113	Underexposed; red em. at *Hβ*?
13	4:54	137	1.989	−118	−349 + 96		+ 84	*H* double (*v*>*r*); no emission
25	3:57	134	2.140	− 67	−160 + 60		− 35	*H* double (*v*<*r*); no emission
25	6:30	160	2.246	− 20	−325 + 60			*H* double (*v*<*r*); no emission
1947 Feb. 11	1:28	117	2.800	−126 + 10	−148			*Ca* II K double; *H* broad and shallow; no emission
11	4:25	90	2.923	−109	−128	− 4		Somewhat underexposed
1946 Dec. 14	4:14	135	2.961	−113	−134	− 26		Sharp lines; no emission
14	6:54	154	3.072	−147	−172		+ 23	No emission
26	3:12	125	3.109	−111	−136		− 68	Lines broad and deep; no emission
26	5:21	120	3.198	−175	−117	+ 1		Lines broad and deep; no emission
26	7:17	100	3.279	− 92	−108			Lines broad and deep; no emission
1947 Feb. 12	1:12	142	3.789	+ 6	− 80 +135			Underexposed; *H* double
1946 Dec. 15	3:43	92	3.940	+ 62	− 71 + 99	− 61		*H* double and shallow (*v*=*r*); no emission
15	5:22	93	4.008	+ 86	− 43 +138			*Ca* II K probably double; *H* double (*v*=*r*); no emission
15	7:12	115	4.085	+ 10	− 97 +177			Sharp red component to *Ca* II K?; *H* double (*v*=*r*); no emission
27	3:18	165	4.113	+ 58		−113		*H* absent or extremely weak; no emission
21	6:52	120	4.166	+124				*H* absent or extremely weak; no emission
1947 March 14	0:12	91	4.224					Underexposed; *H* absent or extremely weak
Feb. 7	2:36	137	4.751	+ 71 +194	− 82		−146	*H* weak; red em. at *Hβ*
13	1:14	116	4.790	+ 84				Underexposed
1946 Dec. 16	3:48	90	4.943	+104	+ 90			*H* weak; no emission
16	5:45	130	5.024	+ 91	+ 24			No emission
22	6:45	120	5.161	+ 28 +146	0			Red emission at *Hβ*

* "*r*" means red component; "*v*" means violet component. The phases have been computed from the light-elements given in Schneller's *Katalog* for 1941: Principal Minimum = JD 2418602.84 + 5.906604*E*.

THE RADIAL VELOCITIES OF CPD−63°896

The Be star CPD−63°896[1] shows an absorption spectrum corresponding to the spectral type B8 and single and central emission of *H*. Changes in intensity are shown by the *H* emission, as well as by *Mg* II 4481 relative to *He* I 4471. On our spectrograms the ratio of the intensities of these two absorption lines varies from about 6 to about 0.2.

Previous spectrographic observations were made at the former station of the Lick Observatory in Santiago, Chile, and, from the three spectrograms obtained, Neubauer[2] detected a variation in velocity of the order of 68 km/sec.

The star is included in the Lick *Catalogue of Radial Velocities*[3] and in Moore's *Fourth Catalogue of Spectroscopic Binary Stars*.[4] In the former we find the indication "E +18, 2 sp.?" and the remark: "The hydrogen lines have central emission lines, the position of which, as well as that of the absorption components, is variable."

TABLE 1

RADIAL VELOCITIES OF CPD−63°896

Date	U.T.	Radial Velocities (Km/Sec)		Date	U.T.	Radial Velocities (Km/Sec)	
		Emission	From Absorption except *Ca* II			Emission	From Absorption except *Ca* II
1946 Dec. 6	7:46	.....	+25	1947 Oct. 23	8:10	+26	+33
15	2:22	+19	+36	Dec. 2	3:46	+28	.....
16	2:25	+28	+37	2	7:48	+34	+42
17	1:58	+38	+38	3	3:33	+24	+28
18	2:28	+45	+37	12	7:40	+28	+34
23	1:23	+28	+33	1948 Nov. 28	7:26	+32	+34
23	2:09	+20	+31	28	7:51	+35	+30
23	2:55	+26	+17	Dec. 17	6:04	+14	+25
25	2:03	+12	+28	17	6:39	+23	+27
26	1:29	+30	+24	19	7:33	+26	+27
27	1:13	+35	+35	1949 March 26	4:09	+30	+29
28	4:48	+30	.....	27	3:06	+32	+41
1947 Feb. 7	0:40	+28	.....	April 16	0:49	+23	+22
10	0:19	+31	+26	July 15	22:40	+36	+17
11	0:00	+25	+27				

The present observations were made with the Wood grating spectrograph attached to the 154-cm reflecting telescope at Bosque Alegre, which gives a dispersion of about 42 A/mm. Eastman 103*a*-O emulsion was used and an equivalent slit-width, which, for most of the plates, was either 0.8 or 1.2 A.

Radial velocities were derived by measuring the stellar lines within the wave-length interval λλ 3720–4862, and the individual results are tabulated in Table 1. They do not show a variation in velocity of the order of the one previously found. The dispersion of our results is probably not significant, and, in the case of the *H* emission, they follow a

[1] $\alpha = 8^h7^m8$; $\delta = -63°39'$ (1950.0). CD−63°386 = BS 3217 (6.38 mag.) = HD 68423 (Sp. B8).

[2] *Pub. A.S.P.*, **42**, 235, 1930. The dispersion of the Chile spectrograms is 37 A/mm at $H\gamma$.

[3] *Pub. Lick Obs.*, **18**, 70, 1932.

[4] *Lick Obs. Bull.*, No. 483, p. 32, 1936.

Gaussian distribution. The mean values of the radial velocities from our spectrograms are as follows:

H emission:	+28.1 ± 1.3 (m.e.) km/sec	(28 plates)
H absorption:	+29.2 ± 2.5	(20 plates)
He I absorption:	+28.7 ± 3.0	(24 plates)
Mg II absorption:	+26.9 ± 3.0	(21 plates)
All absorption:	+30.1 ± 1.3	(26 plates)
Interstellar *Ca* II:	+24.0 ± 3.3	(10 plates)

Mr. Julio Albarracín assisted in some of the computations.

JORGE SAHADE
JORGE LANDI DESSY

OBSERVATORIO ASTRONÓMICO
CÓRDOBA, ARGENTINA
October 25, 1949

THE SPECTRUM OF NOVA SCUTI 1949

The spectrum of Nova Scuti 1949 was recorded on six nights, August 6–14, with the 4° objective prism attached to the Burrell telescope. An additional plate was secured with the 2° prism on August 30. Since the star during this period was fainter than 8.3 photovisual magnitude, it was thought advisable to report the changes in its spectrum in spite of the obvious observational limitations. The dispersion is 283 A/mm at $H\gamma$ and about 1800 A/mm at 8400 A with the 4° prism, and about twice these values with the 2° prism. For this reason the features recorded have been assigned only approximate wave lengths, and the identification in a number of cases is uncertain.

In all, nineteen plates of various Eastman emulsions were used; some had more than one exposure, and for some plates filters were used to diminish the fogging action of the bright full moon. A summary of all the features observed is given in Table 1. The asterisk following the number in the first column indicates that the wave length is given according to the best identification. The estimate of intensity is given in the last column. Features just visible in at least two spectra are designated by 1 and the strong emission line *O* I λ 8446 by 50. In the case of the absorption features the designation 50 is given to the atmospheric A band.

The magnitude of the nova was estimated from the spectra plates. No trace of the nova spectrum appeared on a blue plate taken on July 29.18 U.T., which shows spectra of stars as faint as the star HD 175662 (m_{pv} = 10.3). From August 6 to August 11 the continuum of the nova appeared like a K2 star of about 8.3 mag., when all spectral regions up to λ 8700 are taken into account. This value is probably also near the photovisual one. Actually, during this period the nova, from the appearance of its spectrum, was between the magnitudes of HD 175376 and HD 175518. On August 14 its magnitude was 9.1 and on August 30 it was 10.1. The strong emission features at $H\alpha$ and in the infrared portion contributed a great deal to the total brightness, especially at the later stages.

On August 6.2 (U.T.) the spectrum from the ultraviolet to $H\alpha$ showed mostly absorption characteristics. A faint emission line appeared to the red side of the strong absorption H line, as well as to the red of the K line. On August 10.1 (U.T.) and later, the emission features were predominant, especially the hydrogen lines, H and K, and lines in the region between λ 4500 and λ 4600. All these features are listed in Table 1. No detailed description will be given of the part of the spectrum which is readily observed with slit spectrographs of higher dispersion.

The description of the infrared region from $H\alpha$ up to λ 8700 is as follows: Kodak Spectroscopic I-N emulsion was used. In the first section of the spectrum up to the telluric a

band (λ 7240), densities are generally a little low, owing to the lack of sensitivity of the emulsion. The wave lengths of the band refer to mean values, as appear in our spectra. On August 6.2 the following absorption features were present: λ 6660 and the atmospheric bands at λ 6867 (B), λ 7240 (a), λ 7615 (A). The band at λ 8125 appears to be partly due to the telluric H_2O absorption in this region. Likewise, the B band appears to be blended with a stellar feature, since its position was at λ 6950, while on all other nights it appeared at λ 6890. This is supported by the appearance of a faint emission feature at λ 6950 in later spectra. The emission features were very inconspicuous or invisible on

TABLE 1

WAVE LENGTHS AND IDENTIFICATIONS

λ	Identification		Int.	λ	Identification		Int.
	Emission Lines				Emission Lines		
3690	3685	*Ti* II	1	6380	6374	*Si* II	2
3734*		*H* 13	1	6563*		*Hα*	20
3750*		*H* 12	2	6690	6678	*He* I	2
3771*		*H* 11	2	6760			2
3780			2	6805			2
3798*		*H* 10	2	6890			2
3816	3814	*He* II	2	6950			2
3835*		*H* 9	3	7000	7002	*O* I	2
3859	3863	Various	2	7070	7065	*He* I	2
3889*		*H* 8	3	7130			3
3900	3900–3913	*Ti* II	3	7270	7254	*O* I	3
3934*		*Ca* II	5	7425			3
3969		*Ca* II	5	7500			5
3995*		*Fe* II	1	7535			3
4025*		*Fe* II	2	7773*		*O* I	15
4069*		Various	2	7940	7947–52	*O* I	5
4102*		*Hδ*	6	8050			5
4143*		*He* I	1	8216*		*N* I	4
4176*		*Fe* II	3	8260			3
4233*		*Fe* II	3	8446*		*O* I	50
				8630	8662	*Ca* II	4
4290*		*Fe* II	3				
4340*		*Hγ*	8				
4146* 4447*		*Fe* II	4		Absorption Lines		
4500* 4600*		*Fe* II	7	3922	3934	*Ca* II	10
				3957	3969	*Ca* II	10
4640	4629	*Fe* II	2	4280	4285–95	*Ti* II	4
4710			2	4324	4340	*Hγ*	3
4861*		*Hβ*	15	4760	4762–76	*C* I	3
4940	4924	*Fe* II	4	4841	4861	*Hβ*	2
5016	5018	*Fe* II	4	5760			1
5175	5169	*Fe* II	3	6360	6371	*Si* II	1
5205	5198	*Fe* II	3	6470			3
5300	5276–5317	*Fe* II	3	6660			4
5360	5365	*Fe* II	3	6867*		B band	5
5590			2	6950		Blend B	5
5800			3	7240*		a band	8
5900	5896	*Na* I	3	7615*		A band	50
6010			2	8125			4
6140	6156–58	*O* I	3				

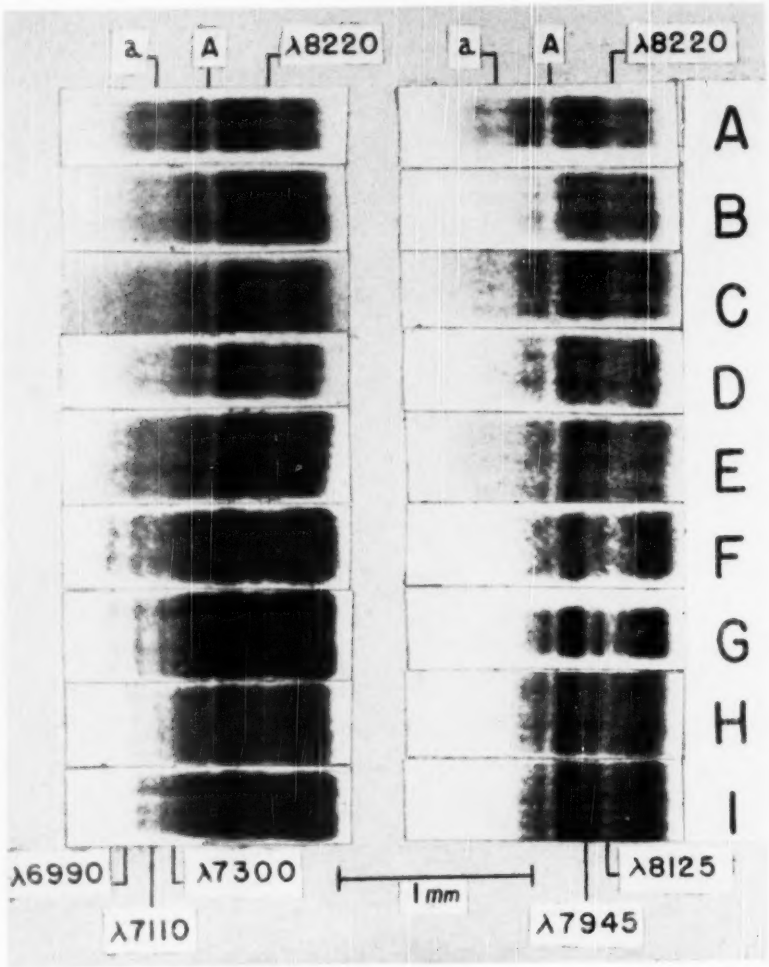

FIG. 1.—The set to the left shows strongly exposed spectra to bring out features between λ 6880 and the atmospheric A band. The spectra of the following stars are shown: *A*, HD 155102 (A2); *B*, HD 4373 (K2); *C*, HD 182040 (C1); *D (right)*, HD 5223 (C2); *D (left)*, HD 156074 (C2); *E*, HD 223392 (C3); *F*, RY Dra (C4); *G*, RX Peg (C5); *H*, UX Dra (C7); *I*, WZ Cas (C9).

August 6.2. Two lines at λ 7940 and λ 8050 are shown in the spectrum, while the presence of the oxygen line at λ 7773 is very doubtful.

On August 7.1 the two lines λ 7940 and λ 8050 were a little stronger than λ 7773, which was, however, growing rapidly. The oxygen line at λ 8446 was then the strongest feature in this spectral region, and it remained so thereafter. Other emission lines at λ 8216 and λ 8260 were suspected. In the region between *Hα* and the A band, the strongest emission feature was λ 7500 with another strong line at λ 7425, and at times the faint line at λ 7535 appeared. Another well-defined line appeared at about λ 7130 and a somewhat fainter one at λ 7070. Additional emission lines observed are listed in Table 1.

On August 11.1 the oxygen emission line at λ 8446 was two or three times as strong as the near-by continuum. The width of λ 8446 is about 60 A, and it was denser in the direction of the extreme infrared. This was the strongest line in the spectrum and was followed in density by *Hα* and the line λ 7773. The emission at λ 8216 is clearly visible, as well as λλ 7940, 8050, and 8260. Near the end of the spectrum a well-marked line at λ 8630 appears. The continuum between λ 8446 and λ 8700 is very dense, owing perhaps to the presence of the hydrogen Paschen series. The same appearance held also on the following nights (August 13.1 and 14.1) and, as far as can be judged, as late as August 30.1.

It is a pleasure to thank Dr. J. J. Nassau, who suggested this study, which was undertaken during my brief residence at the Warner and Swasey Observatory.

ATTILIO COLACEVICH

WARNER AND SWASEY OBSERVATORY
CASE INSTITUTE OF TECHNOLOGY
September 1, 1949

NOTE ON THE SPECTRAL CLASSIFICATION OF CARBON STARS IN THE INFRARED

Spectra of twenty-three standard carbon stars were taken with the 4° objective prism attached to the Burrell telescope, using Kodak Spectroscopic I-N plates and a No. 89 Wratter filter. The observed spectral region is from λ 6880 to λ 8700. The standard stars are those given by Keenan and Morgan;[1] spectra for additional stars taken previously under the same conditions were also available.

Enlargements of some typical spectra are shown in Figure 1. For comparison purposes the spectra of an A2 star (*A*) and a K2 star (*B*) are given. The set of strongly exposed spectra to the left shows features between λ 6880 and the atmospheric A band, while the set on the right shows the region between the A band and λ 8700.

All the absorption bands appearing in these spectra are listed in Table 1 according to their mean wave lengths. The second column gives the estimated intensities; intensity 1 refers to the weakest band relative to intensity 10 for the A band. The estimated widths in angstroms of the bands are given in the third column; the intensities and widths are those observed in the spectrum of a C5 star.

All bands with the exception of the telluric bands are due to *CN* and have been verified on slit spectra kindly furnished to us by Dr. P. C. Keenan; their vibrational numbers are included in Table 1.

From an examination of the available spectra we may draw the following conclusions with respect to the spectral classification of carbon stars: In the spectra of early-type stars and C0 stars (Fig. 1) the only features visible are the telluric bands listed in Table 1.

[1] *Ap. J.*, **94**, 501, 1941.

The *CN* band at λ 7945 appears in spectra of class C1 and later. In C4 and later spectra the strengthening of the cyanogen creates the appearance of emission-like features which assist in the classification. In C1 and C2 spectra, in addition to the appearance of λ 7945 already mentioned, the bands at λ 8125 and λ 8320 appear. These bands produce the emission-like features at λλ 7770, 8010, and 8220. The first of these is the strongest and widest. In overexposed spectra of class C3 the enhancement of the bands at λ 6990 and λ 7110 gives rise to the emission-like feature at λ 7070.

The spectrum of the carbon star appears fully developed at class C4. The bands λλ 7945, 8125, and 8320 are strong, and in underexposed spectra the region between the emission-like features at λ 7770 and λλ 8450–8650 seems to be completely clear of absorp-

TABLE 1

BANDS IN CARBON STARS IN INFRARED

λ	Int.	Width	Assignment	λ	Int.	Width	Assignment
6990*	5	100	(3–0)	7945*	8	70	(2–0)
7110*	8	150	(4–1)	8125*	12	80	(3–1)
7240	8	250	a band (H_2O)	8220	5	250	Tell. (H_2O)
7300*	3	50	(5–2)	8320*	5	80	(4–2)
7460*	1	70	(6–3)	8540*	1	60	(5–3)
7615	10	80	A band (O_2)				

* Due to *CN*.

TABLE 2

NEW CARBON STARS IN CYGNUS

Star	R.A.	Dec.	Sp.	Star	R.A.	Dec.	Sp.
1	19h45m6	+38° 24′	C4–C6	10	19h59m2	+35° 22′	C4–C6
2	19 46.4	+36 33	C4–C6	11	19 59.2	+36 50	C3
3	19 50.7	+35 42	C4–C6	12	19 59.8	+37 17	C7–C9
4	19 55.2	+37 28	C3	13	20 00.5	+37 27	C4–C6
5	19 56.3	+36 17	C3	14	20 01.9	+39 56	C4–C6
6	19 56.6	+36 04	C7–C9	15	20 03.3	+36 23	C4–C6
7	19 57.0	+38 31	C3	16	20 04.2	+38 21	C1–C2
8	19 57.2	+35 57	C7–C9	17	20 04.3	+37 50	C7–C9
9	19 58.1	+39 49	C4–C6	18	20 05.8	+39 27	C4–C6

tion. In spectra of moderate exposure the emission features at λ 8010 and λ 8220 are well marked, as well as the feature at λ 7390 (Fig. 1). In overexposed spectra the region between λ 6880 and the A band is also available for classification. The growth of the bands brings out two strong emission-like features near the A band at λ 7390 and λ 7540, and three fainter ones at λλ 6900, 7070, and 7320.

For stars of class C7 and later the intrinsic reddening of these stars assists in the classification, as the emission-like feature at λ 6900 is lost, owing to the weakness of this spectral region.

On the basis of these criteria it is possible to place the carbon stars in the following four groups: C1–C2, C3, C4–C6, and C7–C9. The greatest uncertainty is in the first of these groups.

An application of these criteria was made to a plate of 34-minute exposure, taken June 16, 1947, in connection with the survey of M stars by Nassau and van Albada.[3]

[3] *Ap. J.*, **109**, 391, 1949.

The circular field of 21 square degrees has its center at R.A. = 20^{00} and Dec. = $+38°$ (1950). Stars of 13.5 infrared magnitude and brighter were examined. In all, twenty-two carbon stars were discovered, of which four were already listed in the previous survey of 2.2 square degrees.[2] Since carbon stars are usually variable, we conclude that there is in this region in Cygnus a minimum of one such star per square degree to the limit reached by the survey. Table 2 gives the 1855 co-ordinates and spectral groups of the eighteen new carbon stars.

J. J. Nassau
A. Colacevich*

Warner and Swasey Observatory
Case Institute of Technology
October 7, 1949

THE SPECTRUM OF THE LIGHT OF THE NIGHT SKY DURING THE RECENT SUNSPOT MAXIMUM

A few spectrograms of the light of the night sky were obtained at Hyderabad, India, during the recent sunspot maximum, in order to see whether any deviations from the normal could be noticed. The spectrograph employed in this investigation contained a single dense flint prism of the constant-deviation type, with the camera lens working at $f/4.0$ and the collimator of 14 inches focal length. The instrument had a mean dispersion of 120 A/mm in the 5200 A region. The comparison spectrum used is from a mercury arc. All the exposing was done on clear moonless nights with a slit width of 0.4 mm and the collimator pointed in a southeasterly direction at an altitude of 25°. The exposures were started $2\frac{1}{2}$ hours after sunset and stopped 2 hours before sunrise; consequently, there could not have been any interference due to twilight or dawn. Two exposures of the order of 100 hours each were made on Kodak Super Panchro Press plates during the months of March and April, 1947. The plates were measured by means of a comparator while minute details of band structure were studied from the microphotometric records. A number of fine details can be discerned from the microphotometric records, but these are not visible to the unaided eye on the plates. Most of the peaks measured from the microphotometric records coincide, however, with the large number of radiations discovered by Cabannes and Dufay,[1] and thus the possibility of their presence due to photographic emulsion irregularities may be ruled out. Table 1 gives a list of the prominent lines seen visually along with the relative intensities. The intensities measured by Babcock[2] are also listed in the table.

TABLE 1

Wave Length (Angstroms)	Intensity (Author)	Intensity (Babcock)	Wave Length (Angstroms)	Intensity (Author)	Intensity (Babcock)
6364	40	10	5443	5	
6300	60	40	5405	3	
5963	2	0	5233	2	
5893	30	7–45	4886	2	2
5775	10	0	4760	3	
5755	20		4475	5	
5730	23		4354	8	
5699	8		4277	5	
5577	150	100			

* Visiting professor from the Naples Observatory.

[1] *C.R.*, **198**, 306, 1934.

[2] *Pub. A.S.P.*, **51**, 47, 1939.

Figure 1 shows the microphotometric record of one of the spectrograms obtained. The usual predominant features, viz., the forbidden transitions of [*O* I], 5577, 6300, and 6364 A, as well as the D lines of *Na* I are very distinct, the intensity of the sodium lines being somewhat less than that of the red oxygen line. This might be expected from the work of Babcock; for, according to him, the sodium lines are very weak relative to the rest of the spectrum in summer. A broad band of intensity nearly equal to the D lines of sodium can be seen in the region near 5700 A. Four components at wave lengths 5699, 5730, 5755, and 5775 A can be easily seen. This band may be glimpsed on a few reproductions of spectrograms obtained by Cabannes and Dufay as well as Babcock but is totally absent on those taken by Slipher.[3] An observed doublet of appreciable intensity at wave lengths 5405 and 5443 A is, however, extraordinarily weak on the spectrograms of Elvey, Swings, and Linke,[4] as well as Babcock's, while it cannot be detected at all on reproductions of Slipher's spectra.

Four bands observed at 5405, 5442, 5755, and 5963 A are in coincidence with the members of the first positive system of nitrogen. Of these, 5405, 5442, and 5755 A are very intense, being members of the intense bands found on either side of the green auroral line. Among them, 5442 and 5755 A are also found in active nitrogen. The Vegard-Kap-

FIG. 1.—Microphotometric record of night-sky spectrogram

lan system as well as the second positive system of nitrogen are not quite conspicuous on these spectrograms, which merely show a broad continuum in the blue and violet with a few lines of appreciable intensity.

The possibility that the large intensity of the two broad bands found on either side of the green auroral line may have originated from auroral activity may be ruled out because of the low geomagnetic latitude (8°) of Hyderabad, together with the large azimuth of the direction in which the collimator was pointed. It is interesting to note that the spectrograms of the McDonald investigators, as well as Babcock's, which showed the bands faintly, were taken in 1939, when sunspot numbers were a minimum. The enhanced intensity may probably be due to the intense solar activity during the recent sunspot maximum.

It is a pleasure to acknowledge indebtedness to Dr. J. C. Kameswara Rav for his keen interest and encouragement; to Sir C. V. Raman for having kindly provided facilities for obtaining the microphotometric records; and to Dr. Fred L. Whipple for helpful criticism.

M. K. VAINU BAPPU

HARVARD COLLEGE OBSERVATORY
March 27, 1949

[3] *M.N.*, **93**, 657, 1933.

[4] *Ap. J.*, **93**, 337, 1941.

A HIGH-TEMPERATURE MODEL ATMOSPHERE*

The temperatures of the early-type stars are not well known because the methods of color temperature are not conclusive for these stars and the excitation or ionization temperature scales rest upon somewhat shaky extrapolations; consequently, another determination of the temperature of an early-type atmosphere is of value. The method of model atmospheres offers a powerful tool for doing this; for, once an acceptable model atmosphere has been obtained, the integrated net flux emerging from it may be calculated. By definition the integrated net flux determines the effective temperature of the atmosphere. This temperature will be the effective temperature of the spectral type corresponding to the model atmosphere. The method of model atmospheres has the further advantage that the actual variation of the physical properties of a stellar atmosphere are incorporated into the computations.

The procedure is the following for a model characterized by a given boundary temperature, T_0, and surface gravity, g. First, a structure which is in mechanical equilibrium is obtained by integrating the differential equation of mechanical equilibrium. Then the net flux in this atmosphere is calculated at a number of optical depths. If this flux is constant with depth, we can say that the model represents a *real* stellar atmosphere in radiative equilibrium. The parameters of the model are varied until such a real atmosphere is obtained. The spectral type of the model atmosphere is then obtained by comparing computed relative line intensities with the observed values in spectra of suitable type. The effective temperature of the model atmosphere, and hence of the similar observed spectral type, follows from the computed integrated flux.

The equation for mechanical equilibrium in a stellar atmosphere is

$$\frac{dp_g}{d\tau} = \frac{g}{\bar{\kappa}+\sigma} - \frac{dp_r}{d\tau}, \tag{1}$$

where p_g is the gas pressure, p_r is the radiation pressure, $\bar{\kappa}$ is a mean absorption coefficient, and σ is the coefficient of electron scattering which is independent of wave length. The term in the radiation pressure depends upon the unknown radiation field; however, for a first approximation we can replace $dp_r/d\tau$ by its value in a gray atmosphere. We shall use a Chandrasekhar-type mean absorption coefficient. Then it follows[1] that

$$\frac{dp_g}{d\tau} = \frac{g}{\bar{\kappa}+\sigma} - \frac{\sigma_R}{c} T_e^4, \tag{2}$$

where σ_R is the radiation constant, 5.67×10^{-5} erg/cm^2/sec. For all atmospheres with $T_e > 20{,}000°$ the term in T_e is not negligible and must be included. It is not sufficient to define a

$$g_{\text{eff}} = g - (\bar{\kappa}+\sigma)\frac{dp_r}{d\tau}$$

and then proceed as though g_{eff} were constant with depth.

Equation (2) was integrated to give the structure of the atmosphere in the radiative zone. The following assumptions were made:

$$T_0 = 25{,}200°, \qquad \log g = 4.200,$$

$$T^4 = T_0^4\left(1+\tfrac{3}{2}\tau\right); \qquad \text{hence } T_e = 30{,}000°,$$

$$H{:}He = 85{:}15 \text{ by number},$$

and the opacity comes from H, He, and He^+ and from electron scattering.

* The details of the methods used and the results obtained will be presented in a forthcoming publication of the Copenhagen University Observatory.

[1] A. B. Underhill, *M.N.* (in press).

At about $\tau = 2.00$ the model becomes unstable with regard to convection. The model was continued to greater depths by integrating the expression which gives the adiabatic gradient for a mixture of radiation and ionizable gas.[2] The effect of a nonzero radiation pressure is to reduce the adiabatic gradient from the value given by Unsöld's well-known formula or from the table of entropy values given by Unsöld in a recent paper.[3]

When a model in mechanical equilibrium had been obtained, the net flux was calculated in detail at several optical depths by a method of representative points and weights due to Strömgren.[4] This method is equivalent to solving the Schwarzschild integral equation at each wave length studied for the case of scattering and absorption. Throughout the calculations, care was taken to evaluate the necessary absorption coefficients and ionization equilibria in detail; the flux was calculated at 23 wave lengths between λ 228 and λ 8204. The results of these calculations are given in Table 1. We see that the integrated flux is satisfactorily constant with depth and that the mean value is 33.29×10^{12} erg/cm²/sec.

TABLE 1

THE INTEGRATED FLUX IN ERG/CM²/SEC

τ	F (Erg/Cm²/Sec)	Departure from Mean (Per Cent)
0.00	32.72×10^{12}	−1.7
0.10	32.67	−1.9
0.60	33.27	+0.0
1.00	34.49	+3.6

From the definition of effective temperature,

$$\pi F = \sigma_R T_e^4 ,$$

we find that T_e is 36,800°. This value is somewhat higher than that estimated above, but this fact does not vitiate the computations, for it turns out that the actual $dp_r/d\tau$ is very close to the gray-body value. The success of this model and of the present method of including the effects of the radiation pressure is a recommendation for the use of the Chandrasekhar mean-absorption coefficient.

The emergent monochromatic flux is plotted in Figure 1. The quantity F_ν is plotted against $1/\lambda$. Also plotted is B_ν (36,800°). The considerable deficiency of radiation in the region $\lambda < 912$ A and the large excess of radiation to the red of the Lyman limit are the most spectacular results. It is evident that the emergent flux of an O- or B-type star is not closely that of a black body at the effective temperature of the star.

The next thing is to estimate the spectral type of the model. From the electron density we can show, using the Teller-Inglis[5] formula, that the hydrogen Balmer series should break off at about $n = 15$; consequently, the model, if it is type O9 to B2, is of luminosity class V. The computed Balmer jump is of the order of magnitude of that observed by Barbier and Chalonge[6] for B0 stars. However, this criterion is not very exact, for there is some question as to how much the observations are affected by the blended higher members of the Balmer series, whereas all such blanketing effects are neglected in the computations. A more exact spectral classification can be made by calculating the rela-

[2] *Ibid.*

[3] *Zs. f. Ap.*, **25**, 11, 1948.

[4] *A.J.*, **53**, 107, 1947.

[5] *Ap. J.*, **90**, 439, 1939.

[6] *Ann. d'ap.*, **4**, 30, 1941.

tive strengths of the line pairs *C* II λ 4267/*C* III λ 4187 and *Si* III λ 4820/*Si* IV λ 4089. By computing the equivalent widths of these lines in detail, we find the results in Table 2. We assume that the lines are formed in absorption and that the relative abundances of silicon and carbon to hydrogen are those found by Unsöld[7] in the atmosphere of τ Sco.

It seems most likely that the spectral type of the model atmosphere is a little later than O9 V but definitely earlier than B0 V—say, O9.5 V. The absolute values of the computed equivalent widths suggest that the real relative abundances of carbon, silicon, and hydrogen are nearly the assumed abundances.

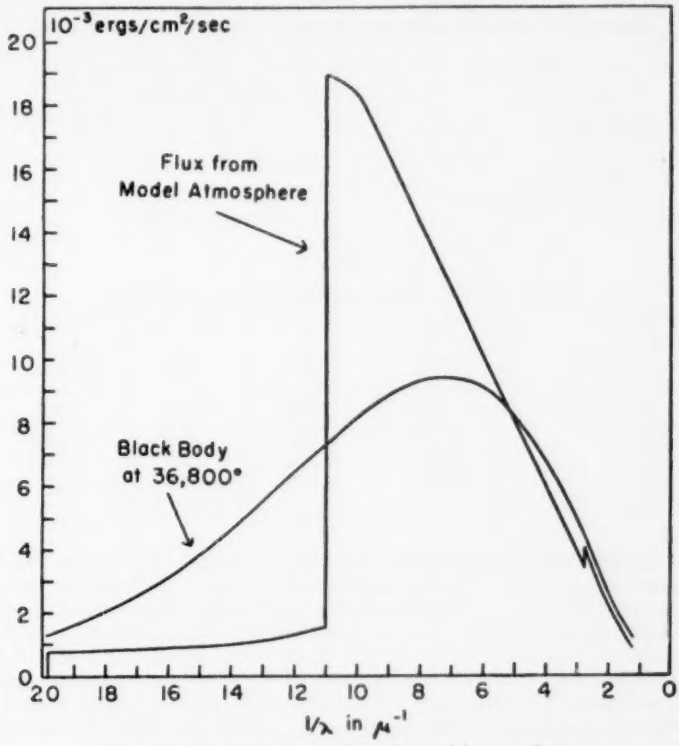

FIG. 1.—The flux emergent from the model atmosphere

The effective temperature, 36,800°, found for O9.5 V stars is rather higher than the temperature estimated by Kuiper[8] from the ionization temperature scale or by Petrie[9] from the excitation temperature scale. However, a detailed study of the structure of the model atmosphere, as revealed by the present computations, shows that such a result is to be expected and is, indeed, mostly due to the large emergent flux in the region $912 < \lambda < 1500$ A. The detailed computations also show nicely that the core of a line is formed at high levels in the atmosphere, $\tau \sim 0.05$, whereas the wings will be formed at depths up to $\tau \sim 1.50$. In view of this result, it is difficult to visualize what is represented by

[7] *Zs. f. Ap.*, 21, 22, 1941.

[8] *Ap. J.*, 88, 439, 1938.

[9] *Pub. Dom. Ap. Obs. Victoria*, Vol. 7, No. 21, 1947.

the layer at one temperature and pressure which is commonly used in simplified theories of line formation and which underlies the concepts of ionization and excitation temperature.

The limb darkening of the stellar atmosphere may be readily computed, since we have obtained the monochromatic source function as a function of optical depth from the computations for the net flux. We get the results given in Table 3. Here the darkening

TABLE 2

LINE RATIOS FOR SPECTRAL CLASSIFICATION

Ratio	Calculated	τ Sco B0 V (Unsöld)*	10 Lac O9 V (Aller)†
C II/C III	1.17	1.77	0.91
Si III/*Si* IV	0.25	0.41	~ 0

* *Zs. f. Ap.*, **21**, 22, 1941.
† *Ap. J.*, **104**, 347, 1946.

TABLE 3

THE LIMB DARKENING OF THE MODEL ATMOSPHERE

$\cos \vartheta$	λ 6251	λ 4234	λ 1006	Pure Scattering
1.00	1.000	1.000	1.000	1.000
0.50	0.892	0.845	0.663	0.688
0.20	0.777	0.726	0.438	0.490
0.05	0.688	0.574	0.373	0.380
0.00	0.561	0.476	0.338	0.331

at λ 6251 corresponds to that expected for visual-red wave lengths; that at λ 4234 to that expected at photographic wave lengths; and that at λ 1006 to that from a dominantly electron-scattering (isotropic scattering) atmosphere. In the last column is given the theoretical limb darkening[10] for an atmosphere scattering according to Rayleigh's phase function. At λ 6251, I_ν (0, 0°) is 1.57×10^{-3} erg/cm²/sec; at λ 4234 it is 3.17×10^{-3} erg/cm²/sec; and at λ 1006 it is 24.69×10^{-3} erg/cm²/sec. If an expression of the form $1 - u + u \cos \vartheta$ is fitted to the computed results by the method of least squares, we find that the coefficient of limb darkening, u, is 0.35 at λ 6251, 0.44 at λ 4234, 0.67 at λ 1006, and 0.65 for the case of Rayleigh scattering.

ANNE B. UNDERHILL*

COPENHAGEN UNIVERSITY OBSERVATORY
September 17, 1947

[10] S. Chandrasekhar, *Ap. J.*, **105**, 435, 1947.

* Fellow of the National Research Council.

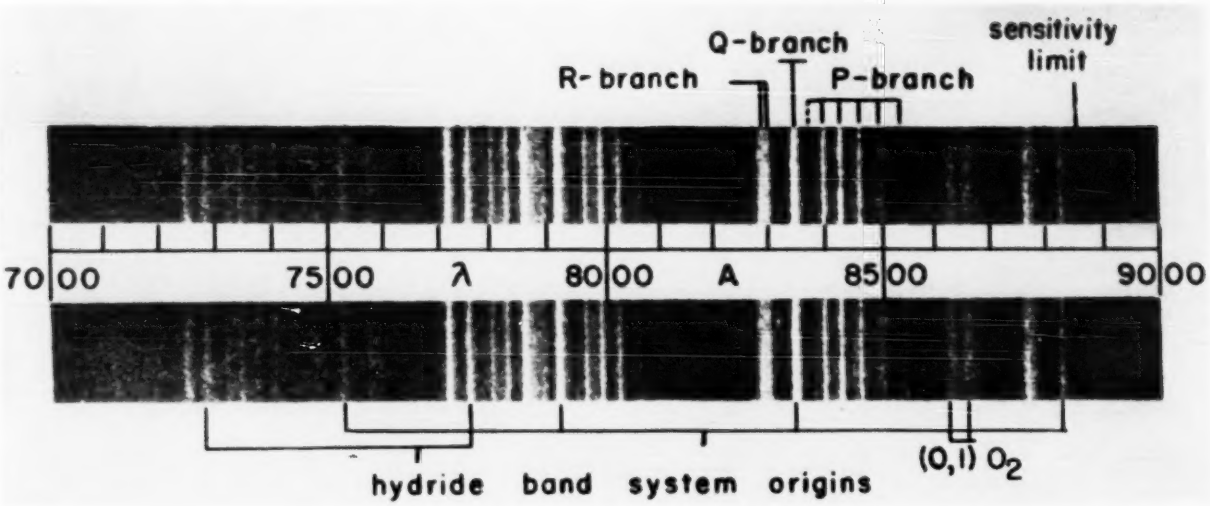

FIG. 1.—The infrared spectrum of the night sky

HYDRIDE EMISSION BANDS IN THE SPECTRUM OF THE NIGHT SKY

Recent spectra of the light of the night sky obtained at the Yerkes Observatory have resolved the rotational structure of the intense unidentified emission bands in the infrared. Spectra obtained by Meinel[1] at the Lick Observatory with a similar spectrograph, but with lower resolution, showed the presence of a large number of intense radiations with complex structure between 7200 A and the limit of the plate sensitivity at 8900 A. From these earlier spectra it was possible to identify only the P and R branches of the (0, 1) transition of the atmospheric system of O_2 near 8640 A.[2] The remaining radiations could not be attributed to any known system of O_2, N_2, NO, CO, CN, CO_2, or H_2O. A new spectrograph, used in the present investigation, was subsequently constructed which has a dispersion of 247 A/mm in the first order and a photographic resolution of approximately 10 μ. This instrument has provided excellent spectra of the night sky, showing clearly the rotational structure of the unidentified bands. Figure 1 is of an exposure of 12.0 hours on a hypersensitized Eastman I-N emulsion with a projected slit-width of 21 μ.

The rotational structure shows conclusively that the bands can be produced only by a hydride molecule. Preliminary values of B'_v and B''_v for the 8347 A band are 13 and 16 cm^{-1}, respectively, with the most likely J-numbering scheme. These values of B limit consideration to the OH molecule. The values of B'_v and B''_v depend on the v-numbering of the vibrational levels and will rest upon the full analysis of the band system.

The fact that these bands are very intense and are resolved by a dispersion of 247 A/mm indicates that it would be entirely possible to observe them with a higher dispersion. An attempt is being made to use the McDonald 50 A/mm, $f/2.5$ grating spectrograph to obtain resolution of the R and Q branches of the 8347 A band. A complete report on the analysis of the new hydride band system will appear later. This investigation is being sponsored by the Office of Naval Research.

A. B. MEINEL

LICK AND YERKES OBSERVATORIES
January 19, 1950

[1] *Pub. A.S.P.*, **60**, 357, 1948.

[2] A. B. Meinel, *Trans. Amer. Geophys. Union*, February, 1950 (in press).

THE OBSERVATORY

FOUNDED 1877

* * *

A Magazine presenting current developments in Astronomy by means of Articles, Correspondence, Notes on discoveries and Reviews of important astronomical books. The papers read at the Meetings (Astronomical & Geophysical) of the Royal Astronomical Society and the discussions which follow are also fully reported.

* * *

Annual subscription for 6 issues, post free, 15/- should be sent to

The Editors, ROYAL OBSERVATORY

Greenwich, London S.E., 10

The
FACE
of the
MOON

BY RALPH B. BALDWIN

An answer, in terms of the meteorite theory, to the question of how the moon came to exist in its present form.

The study of the moon—a mirror for the study of the earth.

256 pages. 6½"×9½". Illustrated. $5.00.

THE UNIVERSITY OF CHICAGO PRESS

POPULAR ASTRONOMY

A magazine now in its fifty-eighth year, devoted to the elementary aspects of Astronomy and allied sciences.

Published monthly, except July and September.

Yearly subscription rates: Domestic $4.00; Canadian $4.25; Foreign $4.50 (U.S. dollars).

Address

POPULAR ASTRONOMY

CARLETON COLLEGE

NORTHFIELD, MINNESOTA, U.S.A.

ASTROPHYSICAL MONOGRAPHS

Sponsored by the Editors of the Astrophysical Journal

PRINCIPLES OF STELLAR DYNAMICS

By S. CHANDRASEKHAR

In this monograph the dynamical methods of interpreting the motions in the galaxy, spiral nebulae, and star clusters are developed from a coherent point of view. "This book should exert a profound influence on the future developments in the field of galactic dynamics. I can recommend its study unreservedly to newcomers in the field and to those who already have a passing acquaintance with its problems. The experts can profit from reading it."—BART J. BOK, in *Science*. 1942. $5.00

SPECTRA OF LONG-PERIOD VARIABLE STARS

By PAUL W. MERRILL

This monograph is devoted largely to the observational side of the subject, but some discussion of the physical significance of various spectral features is included. A brief introduction and a historical chapter are inserted for the benefit of the reader who is not a specialist in stellar spectra. "To one wishing an intimate view of our present knowledge of the spectra of long-period variable stars, whether he be a student, astronomer, physicist, or chemist, the present monograph is recommended."—J. H. MOORE in *Astronomical Society of the Pacific*. 1940. *Paper*, $2.50

THE MASSES OF THE STARS, WITH A GENERAL CATALOGUE OF DYNAMICAL PARALLAXES

By HENRY NORRIS RUSSELL *and* CHARLOTTE E. MOORE

"Astrophysicists will be grateful to the authors for so thorough an examination of available knowledge. . . . We may be permitted to congratulate the senior author on this magnificent outgrowth from an idea which germinated in his mind thirty years ago."—PROFESSOR A. S. EDDINGTON, *The Observatory* (England). 1940. *Paper*, $4.50

THE DISTRIBUTION OF THE STARS IN SPACE

By BART J. BOK

". . . an extremely important contribution to the field of galactic structure, invaluable alike to both students and research workers in the field."—*Science*. The large number and variety of researches carried out in this field during the past fifteen years are discussed critically in this study with clarity and dispatch. 1937. *Paper*, $2.50

THE UNIVERSITY OF CHICAGO PRESS